Solitons and Radiation in Nonintegrable Systems

Oliver Francis Oxtoby

Thesis Presented for the Degree of
Doctor of Philosophy in Applied Mathematics

UNIVERSITY OF CAPE TOWN

August 2007

To my father,

who has been talking fondly about my PhD for just about as long as I can remember!

To my mother, who kept the balance.

You have both been very important to me.

ABSTRACT

In this thesis we investigate solitons in nonintegrable nonlinear evolution equations, with particular reference to their radiation. First we study the effects of damping and driving on the kink of ϕ^4 theory. Our investigation includes the effects of radiation for the first time, and as a result we discover a new feature, namely a resonance between the driving and the wobbling mode at its natural oscillating frequency. We show that this resonance is unique in that the driving transfers energy to the translational mode of the kink as well as to its oscillatory mode. We also show that the wobbling kink does not behave chaotically for small oscillating amplitudes.

Continuing the theme of radiation from solitary waves, we study kinks in *discrete* ϕ^4 models with the exceptional property that stationary kinks may be centred at arbitrary points between the lattice sites. We prove that, while this does lead to a drastic increase in mobility of the kinks, they still lose energy to radiation waves for most nonzero velocities; however, we discover *isolated* values of velocity for which radiationless kink propagation becomes possible. We provide a unification of the known exceptional models by showing that their equations of motion are composed from an underlying one-dimensional map. A simple algorithm based on this observation generates three new families of exceptional discretisations.

To discover whether the effective translational invariance in exceptional models is a prerequisite for radiationless soliton propagation, we search for vanishing radiation in nonexceptional equations. For the Frenkel–Kontorova model we are unsuccessful, so we turn to pulse solitons in the discrete nonlinear Schrödinger equation, which models an array of optical waveguides. When the nonlinearity is of the cubic type, the radiation amplitude is shown to be nonzero for all velocities, but for a *saturable* nonlinearity, we discover complete suppression of the radiation at isolated velocities. We demonstrate that a discrete soliton moving at a general speed will experience radiative deceleration until it either stops and remains pinned to the lattice or locks, metastably, onto one of the radiation-free velocities. When the soliton's amplitude is small, however, the discrete soliton may spend an exponentially long time travelling with virtually unchanged amplitude and speed.

Finally, we study a single waveguide (described by the nonlinear Schrödinger equation with a square-well potential) in greater detail. We derive explicit analytical expressions for spatial solitons in the system, and show that all nodeless solitons are stable. We demonstrate, however, that this does *not* imply the violation of the well-known Vakhitov–Kolokolov stability criterion as has been recently mooted.

Acknowledgements

I would like first and foremost to thank my supervisor, Prof. Igor Barashenkov for being such an inspiration to me. None of this would have been possible without him. I am indebted to Prof. Dmitry Pelinovsky for useful comments on my work and for updating me on the latest research in the field of nonlinear travelling waves. Also, most of the results described in this thesis came about through collaborations with Profs Barashenkov and Pelinovsky, from which I have benefitted enormously. In addition I would like to thank Dr Nora Alexeeva for assistance with references and Prof. Alexander Tovbis for helpful discussions.

I am grateful for the generous funding provided by the National Research Foundation and the University of Cape Town over the last four years to make this work possible. Opinions expressed and conclusions arrived at are my own and are not necessarily to be attributed to the NRF. Much appreciation goes to Igor and Nora for repeatedly writing reference letters for my funding applications, and to the staff of the Postgraduate Funding Office for their friendly and efficient help.

Last but not least I would like to thank my family and friends for keeping me sane and happy. Special thanks go to Amanda for the holiday of a lifetime, Peter for making sure my weekends were not squandered on work, Chris for long and entertaining discussions about sport, my dad for his guiding hand in my life, and my mum for all the lovely food that over the course of the last $3\frac{1}{2}$ years has gone into producing this stack of pages! I'd like to say an extra-special thank-you to my 'little' brother Sven for being my companion down the years and a willing victim for technical and mathematical discussions. Finally, a grudging mention must go to Harry the cat for pinning me to my chair during the latter phases of writing this thesis.

a localised, long-lived nonlinear energy packet. This is the definition we shall be adopting in this thesis.

Although integrable systems are rare, most of the equations mentioned in this section are rich in applications. In fact, the KdV equation (1.1) is a generic equation for describing, at the lowest order of nonlinearity, any long waves propagating unidirectionally in a dispersive and energy conserving medium. Similarly, the NLS equation (1.2) generically describes weakly nonlinear modulated waves in dispersive, conservative media. Its most famous application has been to pulses in optical fibres [24], but it also describes hydrodynamic waves on deep water [25], Langmuir waves in plasmas [26, 27], self-trapping of heat pulses in solids [28], self-focussing of plane-waves in two dimensions [29, 30] and spin waves in magnetic media [31]. The KdV equation describes, aside from the hydrodynamic waves for which it was derived [4], ion-acoustic waves in plasmas [6, 32], pressure waves in a liquid/gas-bubble mix [33], rotating fluid flow though a tube [34], blood-pressure pulse propagation [35, 36, 37] and surface-dynamics on a liquid drop [38]. The sine–Gordon equation (1.3) describes crystal dislocations [14, 39], domain walls in ferroelectric and ferromagnetic materials [40], long Josephson junctions [41], splay waves on biological membranes [42] and self-induced transparency of optical pulses [43]. It was also proposed as a model of elementary particles [15]. Finally, the Toda lattice (1.5) can be experimentally realised as an electrical circuit involving inductors and nonlinear capacitors [44].

1.3 Solitons in nonintegrable systems

In nonintegrable systems, solitons lose the ideal properties of their integrable counterparts. For instance (as mentioned before), colliding solitons usually do not emerge completely unscathed from the encounter, but lose some of their energy to radiation (small amplitude linear waves). Sometimes, however, the consequences of nonintegrability are more interesting, and lead to qualitatively new phenomena. For instance, a soliton may acquire an *internal mode* [45, 46], a degree of freedom corresponding to a shape deformation. By contrast, in integrable systems such as the sine–Gordon equation, the only degrees of freedom come from symmetries of the equation, for instance translational and phase-rotation invariances. Thus, a consequence of nonintegrability is that solitons may carry with them an internal store of energy.

In chapter 2, we construct a perturbative expression for the internal mode (known descrip-

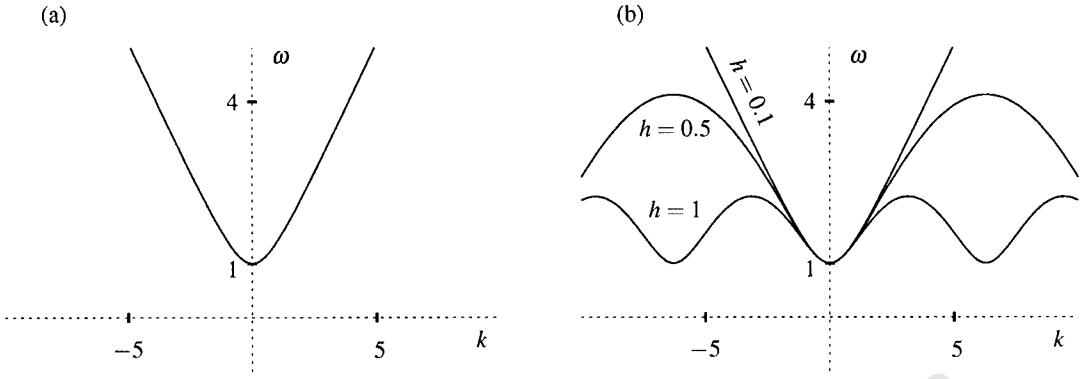

Figure 1.1: The dispersion relations for the ϕ^4 equation (1.7) (left) and its discrete counterpart, eq. (1.11) (right). The parameter h represents the lattice spacing, or inverse coupling strength between lattice sites.

tively as the 'wobbling mode') of the kink in ϕ^4 theory. The ϕ^4 equation,

$$\phi_{tt} - \phi_{xx} - \frac{1}{2}\phi + \frac{1}{2}\phi^3 = 0, \tag{1.7}$$

is perhaps the simplest example of a kink-bearing nonlinear PDE, and thus an ideal candidate for understanding their phenomenology. It does, also, have applications in its own right – to chemical bond rotation in a continuum model of polyacetylene [47, 48], and as a model equation in statistical mechanics [49] and quantum field theory [50]. Equation (1.7) is very similar to the sine–Gordon equation (1.3), in that its Hamiltonian has a double-well potential term. The sine–Gordon potential has an infinite number of minima, but only two of them are involved in single kink solutions. In fact, by Taylor-expanding the potential of the sine–Gordon equation, $-\cos\theta$, about a maximum: $\theta = \pi + \phi$, and retaining terms up to quartic, one obtains the ϕ^4 equation (1.7) after an elementary rescaling. Despite these similarities, the kink of the integrable sine–Gordon equation does not have the internal mode of its ϕ^4 cousin [46].

Another similarity between the sine–Gordon and ϕ^4 equations is that both admit oscillating solitons which decay to the *same* potential minimum at both infinities (a multiple of 2π for the sine–Gordon equation and ± 1 in the ϕ^4 model) [51, 52]. In the sine–Gordon case, this excitation is known explicitly, and can be viewed as a bound state of a kink and an antikink (mirror-image of the kink). Let us consider the dispersion relation for linear (small-amplitude) oscillations about the potential minima. In both equations this is

$$\omega = \pm\sqrt{1+k^2}.$$

This is sketched in figure 1.1(a) for positive ω. There is a forbidden band in the spectrum for $-1 < \omega < 1$ – i.e., a range of frequencies for which linear waves may not propagate. The soliton's fundamental frequency lies in this band (it bifurcates from the constant solution at $k = 0$). Since it oscillates at a (linearly) forbidden frequency, the soliton does not directly excite radiation waves. However, higher harmonics generated by the nonlinearity will inevitably be resonant with linear modes, and can therefore be expected to generate radiation tails which will gradually drain energy from the oscillating hump. Amazingly, these resonances cancel in the sine–Gordon model (as we know from the explicit, radiationless solution known as a *breather*). In its nonintegrable counterpart (1.7), on the other hand, this is not the case – although it took some time to establish this fact as the radiation turns out to be *exponentially small* in the soliton's amplitude, i.e. tends to zero faster than any power of the amplitude. The radiation appeared to be absent in numerical experiments, leading to some controversy which was eventually resolved by Segur and Kruskal's pioneering paper [52] in which the method of 'asymptotics beyond all orders' was developed. This is the origin of the method used in chapters 3–6 to measure exponentially small radiation in lattice equations. In this work it is applied for the first time to equations involving both finite differences and derivatives.

In contrast to the sine–Gordon and ϕ^4 equations, the NLS equation does not generate higher harmonics; $\psi(x,t) = \Psi(x)e^{i\omega t}$ solves (1.2) provided $\Psi(x)$ solves the appropriate stationary equation. Therefore the equation admits a 'trivial' breather solution even with nonlinearities of a form other than cubic, which render the equation nonintegrable.

In nonintegrable systems, many localised solutions can be found which have nondecaying oscillatory tails, owing to a resonance with linear radiation. For instance, if higher-order dispersion terms are included in the NLS equation, travelling pulses will often leave Cherenkov radiation in their wake [53], slowing down as a result. Despite this resonance, one can sometimes find particular parameter values for which the radiation vanishes. In this case the pulse is known as an *embedded soliton* [54]. Many examples have been found in integrable equations modified with the addition of small higher-derivative terms. These represent higher-order terms in the dispersion relation which were neglected in the derivation of the integrable equation. Embedded solitons are typically semistable – some perturbations will cause the soliton to shed energy and relax back to its starting shape, while others will cause it to radiate and decay. For a review of embedded solitons, see ref. [55]. In this thesis, where we search for travelling lattice solitons, we identify embedded solitons in discrete ϕ^4 and discrete NLS models (chapters 3 and

6, respectively).

Aside from perturbations of integrable equations, many fundamental equations in nonlinear science are nonintegrable in essence. A large class of these are known as *reaction-diffusion* equations. In these equations, nonlinearity acts to counter the spreading effect of *diffusion* rather than dispersion and thus create a stable propagating soliton at a fixed velocity. Of course, a source of energy is needed to overcome the diffusive losses; this is either supplied through the boundaries or as 'source terms' in the equation which represent internal supplies of energy which are unlocked as the wave propagates: hence *reaction*-diffusion. In one dimension, examples are the Burgers equation [56], proposed to model turbulent fluids, and the Hodgekin–Huxley [57] and Fitzhugh–Nagumo [58] models of nerve-impulse transmission. The book by Scott [9] contains a thorough overview of nerve-fibre models. In two dimensions, the same types of equation describe the formation of patterns such as spreading rings in the Belousov–Zhabotinsky autocatalytic reaction [59] as well as on the surface of mushrooms [60], and spiral waves in excitable chemical media [61]. The Belousov–Zhabotinsky reaction also displays three dimensional structures known as 'scroll rings' [62], which are related to fibrillation in the human heart [63]. Three-dimensional reaction-diffusion equations also describe Turing patterns, which arise in a model for biological morphogenesis [64].

We have mentioned the systems above for completeness. In this thesis we shall not be considering nonlinear diffusion, but will concentrate our efforts on energy-conserving models.

1.4 Optical solitons

The most intensively-studied equation in nonlinear optics, the nonlinear Schrödinger (NLS) equation (1.2) was originally derived by Zakharov (shortly before he and Shabat succeeded in integrating it) to describe the time evolution of the modulation envelope of a train of waves in deep water [65]. It was then shown to describe the evolution of a light-wave envelope in an optical fibre by Hasegawa and Tappert [24]. Previously, it had been proved that a continuous light wave propagating in a nonlinear dispersive medium exhibited *modulational instability*, or a tendency to break up into separate wavepackets with sech-shaped amplitude modulation [66]. These envelopes are the NLS solitons known in optics as *temporal solitons*. In an optical fibre, the nonlinearity is a result of the dependence of the index of refraction on intensity. For moderate powers the relation is linear, leading to the cubic nonlinearity in the NLS equation known as the

Kerr nonlinearity. For higher powers, the relation between index of refraction and intensity departs from a straight line; in all materials it will eventually saturate at some maximum value. Therefore when higher powers are involved, one must consider a different form of nonlinearity in the NLS equation.

In temporal solitons, nonlinearity counters the tendency of dispersion to spread the pulse in the direction of its travel. To confine the light in the directions transverse to its travel requires a waveguide such as an optical fibre. On the other hand, *spatial solitons* are stationary beams of light self-trapped in one or both transverse spatial dimensions. Here, nonlinearity acts to counter the spreading effect of *diffraction*. The idea of self-trapping, discovered in 1963 [67], is that when a light beam locally exceeds a certain critical power, it modifies the index of refraction enough to create a virtual waveguide in the optical medium; the change in refractive index at the boundaries of this virtual waveguide is enough to confine light inside the channel just as in a normal waveguide. In addition to temporal and spatial solitons, *spatiotemporal* solitons—or 'light bullets'—have recently been discovered [68]. As their name suggests, these are parcels of light which are self-localised in all directions. In this thesis we shall consider only spatial solitons. In chapter 7, we consider the interesting case of optical spatial solitons confined both by self-localisation *and* an additional waveguide.

For optical solitons, the variable t in the NLS equation (1.2) represents the *spatial* coordinate in the direction of light propagation. For spatial solitons, x is a transverse spatial coordinate, but for temporal solitons it stands for the retarded time. Throughout this thesis we shall stick to t and x in the style of the mathematical literature. In optics, more meaningful names are usually given. For instance, t is usually named z or ξ.

Much higher powers are needed to counter the effects of diffraction than dispersion, which means that for temporal solitons, a cubic term in the NLS equation represents a good approximation, whereas for spatial solitons, it is important to consider higher-order terms in the nonlinearity to represent its deviation from the pure-Kerr case. The saturable nonlinearity, in which the index of refraction n is written in terms of the intensity I as

$$n(I) = \frac{n_0}{1 + I/I_s},$$

where I_s is the saturation intensity, describes the photorefractive media which are increasingly popular among experimentalists [69]. For photovoltaic solitons the model has been derived from

first principles [70]. Another common nonlinearity, known as 'cubic-quintic', is described by

$$n(I) = n_0 + n_1 I + n_2 I^2,$$

where n_1 and n_2 are opposite in sign. One obtains a cubic-quintic nonlinearity as the first two terms in the Taylor expansion of the saturable expression. In chapter 6 we shall be considering a saturable nonlinearity, and in chapter 7, a cubic-quintic nonlinearity.

Temporal optical solitons, though not studied in this thesis, deserve a place in this introduction because of the important applications they have found in the field of optical-fibre communications. The immunity of solitons to spreading through dispersion eliminates one of the biggest bandwidth limitations encountered in linear fibre-optics. Of course, solitons are still subject to gradual energy loss as they pass through fibres, due to various real-world effects such as damping, and so amplification is still required to prevent them falling below the critical power for self-focusing to occur. To maximise bandwidth and minimise the need for repeaters, an important technique is *dispersion management* (see the review in [71]), in which fibres are made with decreasing dispersion along their length. This prevents dispersion from gaining the upper hand over nonlinearity as the pulse loses power. In an exciting recent development, it has been shown that optical pulses can be almost perfectly sustained over a length as long as 75km when the optical fibre is turned into a laser cavity [72], a very significant development in the quest for lossless transmission in fibre-optic communications.

The optical solitons considered so far have the form of pulses on a zero background and are known as *bright* solitons. Temporal bright solitons form in the 'anomalous' dispersion regime (where the index of refraction decreases with increasing frequency) whereas so-called *dark solitons* can appear in the 'normal' dispersion regime [73]. As the name suggests, dark solitons are intensity dips on a continuous-wave background. Spatial dark solitons can also exist [74]; whereas spatial bright solitons exist when the nonlinearity is self-focussing, dark spatial solitons exist for self-defocussing nonlinearities. In eq. (1.2), the self-focussing case corresponds to the '+' sign and the self-defocussing case to the '−' sign.

There are many other kinds of solitons which occur in optical systems [68]:

- Bragg solitons (also known as gap solitons) can form in nonlinear fibres whose index of refraction has a weak periodic variation along its length. They are described either by 'coupled-mode' equations or, under certain conditions, by an effective NLS equation.

- Two-dimensional spatial solitons can form due to self-focussing, described by the NLS

equation in (2+1) dimensions.

- The (3+1)-dimensional NLS describes 'light-bullets' in three dimensions under appropriate conditions.
- Vortex solitons are generalisations of dark solitons to two dimensions and exist only when the nonlinearity is self-defocussing. They are phase-singularities within a plane-wave background.
- Vector solitons and quadratic solitons arise when one considers multiple coupled fields in optical fibres.

The books by Kivshar and Agrawal [68], and Akhmediev and Ankiewicz [53], are comprehensive references on optical solitons.

1.5 Discrete systems

Perhaps the simplest kind of nonlinear lattice is the one studied by Fermi, Pasta, and Ulam [5]: a one-dimensional array of masses coupled with weakly-nonlinear springs,

$$\frac{d^2 r_n}{dt^2} = V'(r_{n+1}) - 2V'(r_n) + V'(r_{n-1}). \tag{1.8}$$

Here $V'(r) = r + \alpha r^m$, where $m = 2$ or 3, is the derivative of the spring potential, and r_n is the displacement of the nth spring from its equilibrium length. The integrable Toda lattice (1.5) differs only in the form of the spring potential. The fact that the Fermi–Pasta–Ulam (FPU) model reduces to the KdV equation in the continuum limit (as shown by Zabusky and Kruskal [6]) suggests that it does have solitary waves; recently this has been demonstrated numerically for the FPU model itself by Eilbeck and Flesch [75]. (A rigorous mathematical proof of the solitary wave's existence has been given by Friesecke and Wattis [76].) The Toda lattice, of course, has explicit soliton solutions. The solitary waves of both lattices are compression waves which propagate along the chain at a velocity related to their amplitude; stationary solutions do not exist. Interestingly, solitary waves are found to travel *faster* than low-amplitude linear waves in these models. This phenomenon had already been experimentally observed in air by John Scott Russell, who noted that the large-amplitude clap of a cannon firing reached him before the quieter command to fire it [77].

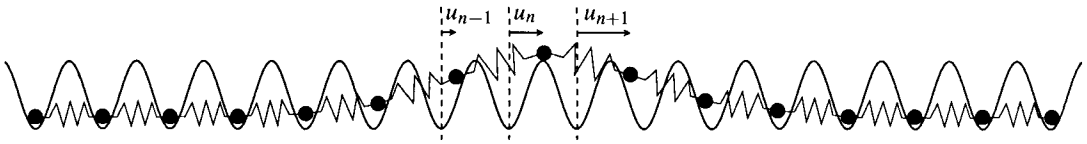

Figure 1.2: The kink of the Frenkel–Kontorova model. The smooth line shows the sinusoidal substrate potential. From left to right, the displacement of the atoms from their corresponding potential minima grows from 0 to 2π.

The earliest recorded study of a nonlinear lattice was by Frenkel and Kontorova in 1939 [78], who modelled plastic deformations in crystals using the equation

$$\frac{d^2u_n}{dt^2} - \frac{u_{n+1} - 2u_n + u_{n-1}}{h^2} + \sin u_n = 0. \tag{1.9}$$

Equation (1.9), now known as the Frenkel–Kontorova (FK) model, is a discrete version of the sine–Gordon equation (1.3) – that is, it reduces to (1.3) in the limit $h \to 0$, where h represents the lattice spacing. In this limit, known as the continuum limit, the chain of discrete variables u_n ($n \in \mathbb{Z}$), is replaced by the continuous function $\theta(x)$, where $u_n = \theta(hn)$.

In contrast to the FPU and Toda lattices, the FK model supports a stationary structure, known as the kink. The model comprises an array of linearly coupled masses sitting in a fixed sinusoidal potential induced by another, fixed chain of atoms; this is depicted in figure 1.2. The kink is the dislocation in the regular crystal structure that forms when one of the minima in the substrate potential is missing an atom. Clearly, the kink is a localised concentration of potential energy. This discrete kink, like its continuous counterpart [eq. (1.4)], is a topological soliton, since it would require a non-local intervention to remove it; an endless sequence of particles would have to shift to a neighbouring potential minimum. The book by Remoissenet [8] describes a great many simple experimental realisations of nonlinear lattices in which kinks, in particular, can be observed.

The lattice equation now known as the discrete nonlinear Schrödinger (DNLS) equation,

$$i\dot{\psi}_n + \psi_{n+1} + \psi_{n-1} + 2|\psi_n|^2\psi_n = 0, \tag{1.10}$$

was first derived by Holstein in 1959 [79], as a model for the nonlinear self-trapping of the wavefunction of an electron in a one-dimensional crystal lattice. This self-trapped electron, known as the *polaron*, had first been proposed by 1933 [80] when Landau showed that a distortion of the lattice could confine the electron's wavefunction. In (1.10), the $|\psi_n|^2$ factor acts like a potential

in a linear Schrödinger equation; thus we see that nonlinearities cause the electron to form its own potential trap. This is a result of the lattice becoming locally deformed – in rigid lattices, on the other hand, the electron wavefunction will always spread out to form a Bloch wave.

Despite this example of nonlinear localisation in a discrete system, the perception among researchers of solid state physics until recently was that nontopological localised modes could only exist in a lattice structure if there was some inhomogeneity (e.g. an impurity) in the lattice [81]. Only in 1988 was this view changed, by the remarkable discovery of discrete breathers, or 'intrinsic localised modes' [82, 83, 84] in defect-free, but nonlinear, lattices. Whereas in continuous systems, the only example of a true breather is in the sine–Gordon equation, discrete breathers are generic excitations in nonintegrable discrete systems. To illustrate, consider a discrete form of the ϕ^4 model (1.7) considered earlier:

$$\frac{d^2u_n}{dt^2} - \frac{u_{n+1} - 2u_n + u_{n-1}}{h^2} - \frac{1}{2}u_n + \frac{1}{2}u_n^3 = 0. \tag{1.11}$$

The dispersion relation for linear waves $u_n = \pm 1 + \varepsilon e^{ik(hn)-i\omega t}$, is

$$\omega = \pm\sqrt{1 - \frac{2}{h^2}(\cos kh - 1)}$$

(as for the Frenkel–Kontorova model). This is sketched in figure 1.1(b), alongside the continuous case [fig. 1.1(a)], for various values of h. For large h (large lattice spacing or weak coupling) the allowed band for linear waves is narrow; if it is narrow enough, the second harmonic of the breather (whose fundamental frequency lies below the band, as in the continuous case) lies *above* the radiation band, as (of course) do all the other harmonics. Thus, a discrete breather is inherently stabilised against radiation decay by discreteness. In addition, another kind of discrete breather exists in which neighbouring lattice points perform large-amplitude oscillations out of phase with each other. The fundamental frequency (and hence all the harmonics) of this large-amplitude breather lies *above* the transmission band and thus it, too, is immune from decay. Ref. [81] reviews the experimental observations of intrinsic localised modes, for instance in Josephson ladders, optical waveguide arrays and photonic crystals. They are also expected to contribute to the thermal properties of crystals [83]. On the theoretical side, the origins of discrete breathers have been probed by Flach and Willis [85, 86]. The same authors provide a full review of discrete breathers in [87].

Apart from their applications in solid state physics and optics, lattice equations describe many chemical and biological systems, where discreteness occurs on the molecular level. Examples are α-helix proteins, modelled by Davydov's equations [88, 89], globular proteins [90],

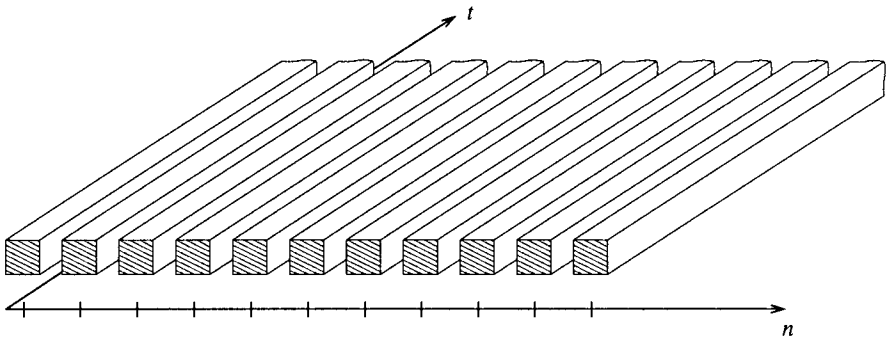

Figure 1.3: An optical waveguide array. The t coordinate represents *distance* along the waveguides. In recent experiments, arrays of around 50 waveguides, typically 4μm wide and a few millimetres long and with spacings between 2 and 7 μm, have been used [96, 97].

and buckling of biopolymer chains [91]. Many mathematical models also exist for various aspects of the behaviour of DNA [92], one of which is the Frenkel–Kontorova equation (1.9). In these biological systems it is usually impossible to observe solitons in isolation due to the relatively high temperature of the human body, making experimental verification a challenge. Whereas a continuous reaction-diffusion equation describes nerve-impulse propagation down a homogeneous fibre (as mentioned in section 1.3), motor nerves and brain axons in vertebrates are composed of nodes separated by long insulated sections, along which little diffusion occurs; the propagation of electrical pulses in these 'myelinated' nerves is described by a nonconservative lattice equation [93]. Finally, the replication of form by cellular automata is described by a two-dimensional discrete reaction-diffusion system [94].

1.5.1 Optical waveguide arrays

In optics, a one-dimensional lattice structure can be produced as a stack of waveguides, depicted in figure 1.3. Provided the coupling between waveguides is weak (and hence only nearest-neighbour interactions are taken into account), the array can be modelled by the DNLS equation (1.10) [95]. In solid-state physics this approximation is known as the tight-binding approach, in which the atomic wavefunctions in a crystal are assumed to decay on a scale much shorter than the lattice spacing, so that their overlap is minimal and interactions are weak. In the DNLS equation (1.10), the integer variable n enumerates the waveguides while t represents the longitudinal *spatial* coordinate (i.e. the distance along the waveguides). $|\psi_n(t)|^2$, then, is the light intensity at a distance t along the nth waveguide. For nonlinearities deviating from the pure Kerr case,

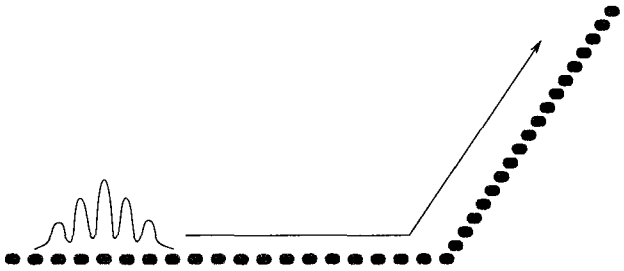

Figure 1.4: Intensity profile of a lattice solitary wave travelling in a waveguide array. The waveguides extend into the page; as we move down them the pulse shifts to the right. It can be guided around corners such as the one shown [103].

the final term in (1.10) would be modified accordingly. For instance, in chapter 6 we consider a DNLS equation with a saturable nonlinearity, as is found in many photorefractive materials. Recently, spatial solitons have been observed in optical waveguide arrays in several experiments [96, 97]. In the discrete case, nonlinearity balances *discrete diffraction*, which would cause light to spread from one waveguide to the other. Another way to think about this self-trapping is to realise that, due to nonlinearity, the frequency of the modulating wave is amplitude-dependent. Hence, if the power is sufficiently concentrated on one waveguide, the transfer of energy to neighbouring waveguides becomes difficult due to the absence of resonance between the frequencies of the neighbouring modulation waves.

The DNLS equation admits not only bright solitons, but dark ones as well [98]. For cases when the tight-binding approximation is not valid, Sukhorukov and Kivshar have developed a more realistic model [99]. Unlike the DNLS equation, this model has multiple forbidden bandgaps, which allows for the possibility of gap solitons to exist, aside from the basic soliton [100].

Traditionally, optical waveguide arrays would be fabricated as a lattice of separate waveguides. However, it has recently been shown [101, 102] that waveguide arrays can be optically induced in real time in *homogeneous* media with a photorefractive nonlinearity. By shining counterpropagating plane-waves in from the sides, the resulting interference pattern locally modifies the index of refraction in such a way as to create an effective waveguide array in the bulk.

An exciting future application for solitons in waveguide arrays is the fabrication of 'soliton wires' [103, 104]: waveguide arrays in which solitons move transverse to the axes of the waveguides. The waveguide array may be bent to guide the solitons around corners – hence the

analogy with a wire. This is depicted in figure 1.4. It has been shown [103] that at a *junction* of these wires, solitons can be routed along one of the paths by placing a 'blocking' soliton at the entrance to the other path. The travelling pulse or 'signal' soliton interacts elastically with the blocker and is routed along the other branch. These blocking solitons, in contrast to the signal solitons shown in fig. 1.4, are localised to a single lattice site and immobile. Thus, solitons can be routed along specific pathways in the two dimensions perpendicular to the waveguides. Furthermore, *control* solitons, which do interact coherently with the blockers, can be sent along the soliton wires to shift the blockers around by one waveguide at a time. This opens the door to all-optical logic functions and hence more general computational tasks. Obviously, the mobility of moving solitons in the waveguide array is key to the scheme, and this is the subject of chapter 6 of this thesis. For a review of the latest developments in optical waveguide arrays, see ref. [105].

Lastly, we mention that the DNLS equation can also be used to describe Bose–Einstein condensates under certain conditions [106]. If the condensate is strongly confined by a cigar-shaped magnetic trap, its dynamics become effectively one-dimensional along the long axis. In addition, there must be a periodic potential whose oscillations occur along the long axis. Provided the potential is of sufficient strength as to bring about weak interaction between the wavefunction (order-parameter) in neighbouring troughs of the potential, then the DNLS equation is an appropriate model. Hence, the same structures that occur in optical waveguide arrays—notably intrinsic localised modes—are also found in arrays of Bose–Einstein condensates [107]. In general, the DNLS equation is a simplified model of any medium described by the NLS equation which has a strong periodic potential [108].

1.5.2 Travelling discrete solitons

Whereas in continuous systems, Galilean or Lorentz invariance implies the existence of a moving soliton whenever a stationary one exists, there is no such luxury in discrete models. Indeed, even continuous translation invariance is lost. On lattices with a substrate potential, for which stationary solutions exist, there are typically only two unique possibilities: one solution centred on a lattice point and the other centred between two points [109]. The difference in potential energy between the two, termed the Peierls–Nabarro (PN) barrier, must be surmounted in order to move the soliton along the lattice [110].

To illustrate the difficulties faced in trying to find travelling waves on lattices, we consider

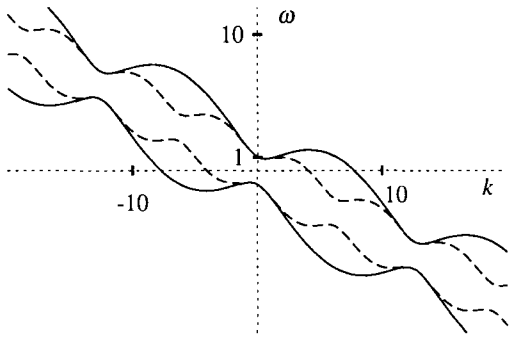

Figure 1.5: The dispersion relation (1.12) for eq. (1.11) in the frame of reference moving at velocity $v = 0.5$. Solid line: $h = 0.5$; dashed line: $h = 1$.

the discrete ϕ^4 chain (1.11); its dispersion relation is sketched in figure 1.1(b). Now, if we convert to a travelling-wave coordinate $z = n - vt$, then the dispersion relation is modified by changing ω to $\omega + vk$, i.e., it is

$$\omega = -vk \pm \sqrt{1 - \frac{2}{h^2}(\cos kh - 1)}. \tag{1.12}$$

We are searching for solitons which are not propagating relative to the travelling coordinate z, though they may be oscillating. As in the stationary case, we aim to find a gap in the linear-wave spectrum where the soliton can exist without exciting radiation. The dispersion relation above is sketched in figure 1.5. We see that, in contrast to the stationary case, there is no gap in the linear spectrum where we could hope to find a soliton, let alone its harmonics. This absence of gaps is a result of the periodic nature of the dispersion relation in the stationary frame, which is a feature of all discrete systems. So, the dispersion relation fails to provide an easy answer in the search for moving solitons, and one has to turn to other techniques.

Of course, for rare integrable lattice equations such as the Toda lattice (1.5) and Ablowitz–Ladik equation (1.6), travelling solitons are known. For general discrete equations, on the other hand, Eilbeck and Flesch have devised a numerical spectral method for calculating moving solitary waves [75]. They have applied the method to an FPU lattice and successfully calculated the amplitude-velocity relationship for travelling discrete solitons. Claude, Kivshar, Kluth and Spatschek then confirmed the existence of these FPU solitary waves with an analytical method based on perturbation from the Ablowitz–Ladik equation [111]. Further progress was made for equations of FPU type when Friesecke and Wattis rigorously proved existence of solitary waves under certain conditions [76].

In contrast, for lattice equations with an on-site potential the search for moving localised modes has been less successful, for instance in nonlinear Klein–Gordon chains [111] and discrete NLS equations [112], with most early investigations being of a numerical nature – see [113], where travelling solitons in many different equations are studied. However, Flach and Kladko have established the relationship between frequency, velocity and width of these travelling nonlinear waves [114]. As we shall show, lattice solitary waves are typically accompanied by exponentially small radiation, which makes it particularly difficult to extract conclusive results from numerical studies [114].

An interesting advance was made by Speight and Ward, who generated exceptional discrete versions of the sine–Gordon and ϕ^4 equations which are free of the PN barrier [115, 116, 117]. Previously, the PN barrier had been blamed for the nonexistence of travelling solitons [111, 118], and indeed Speight's numerical simulations suggest that the kink is never pinned to the lattice [116, 117]. In this thesis, we take up the search for moving lattice solitons at this point; chapter 3 is devoted to investigating the existence of travelling solutions in systems such as these.

An inverse approach to the problem of discrete travelling waves was taken by Flach, Zolotaryuk and Kladko [119], who start with an assumed form of travelling solution and generate the corresponding form of nonlinearity therefrom. In the resulting models, the nonlinearity depends, parametrically, on the velocity and width of the soliton. For fixed parameter values, corresponding to a given velocity and width, one has a nonlinear wave equation which admits the known radiationless soliton for those particular values of its velocity and width. However, since the generated nonlinearity depends on the shape of the assumed wave profile, there is no systematic way of controlling the nonlinearity that is produced. The method cannot, therefore, be used as a tool to study a known equation. On the other hand, it has been used to prove the important theoretical result that these models can posess a nonzero PN barrier [119], and therefore that the presence of a PN barrier does not necessarily preclude radiationless transport at isolated velocities.

A novel way to improve discrete soliton mobility in an optical waveguide array was recently discovered by Sukhorukov [120]. He showed that by modulating the lattice coupling constants or index of refraction so as to be a quasiperiodic function of the waveguide index, soliton mobility is dramatically enhanced and radiation reduced. Whereas the inverse method of Flach and co-authors and the method of Speight and Ward generate entirely new models, this procedure can be physically realised simply by rearranging the waveguide spacing.

Finally, in the context of travelling waves in discrete reaction-diffusion systems (such as the myelinated nerves mentioned in section 1.5), Keener has showed that *propagation failure* occurs when the discreteness becomes too great [121].

For reviews of lattice travelling waves, with particular reference to the DNLS model, see the papers [122, 123, 124].

1.6 Aims of this thesis

We begin in chapter 2 by considering kinks of the continuous ϕ^4, or quartic-coupling, model. As we mentioned in section 1.3, the ϕ^4 equation is a generic model for nonintegrable kink-bearing systems, and the ϕ^4 kink allows for an oscillating shape-deformation (a linear excitation of the stationary kink) known variously as the internal mode, shape mode, or wobbling mode [125]. In the first analytical construction of the wobbling kink, Segur performed a regular perturbation expansion from the kink [126]. He obtained the expression for radiation emitted by the wobbling mode at second order in the small wobbling amplitude. However, he observed that the perturbation expansion would break down at higher orders due to the appearance of spatially unbounded terms. Our first objective in chapter 2 is to repeat the perturbative construction of the internal mode using the method of multiple scales. Unlike regular perturbation theory, the multiple scales method is able to deal with situations in which parameters introduced in the perturbative construction have a slow dependence on the space and time variables, and allows one to determine this dependence. We shall show that this slow dependence is a result of the energy carried away from the internal mode by the radiation waves. We will also find that, even in the method of multiple scales, care needs to be taken to avoid arithmetic unboundedness in the radiation functions.

The second aim of chapter 2 also relates to radiation from the wobbling mode. In various recent papers, Quintero, Sánchez and Mertens have used collective-coordinate theory to study the wobbling kink under the influence of direct [127, 128] and parametric [129] driving. Their method assumes a specific functional dependence of the kink on just two parameters: velocity and width. Therefore, in this method the radiation is entirely ignored. We would like to overcome this limitation, by extending our multiple scales analysis to include driving and damping. We shall find that there are important differences in our conclusions compared to those of the collective coordinate method.

In the next chapter (chapter 3) we again consider kinks of ϕ^4 equations, but this time in spatially *discrete* varieties. Indeed, chapters 3–6, all deal with discrete models and aim to find radiationless solitary waves, which we call *sliding solitons*. Progress made so far in this search was outlined in the previous section (section 1.5.2). To begin our contribution to this topic, chapter 3 is an attempt to discover the extent to which the Peierls–Nabarro barrier hinders the propagation of travelling solitons.

There are several reasons for hoping that the PN barrier will be the only obstacle to the existence of radiationless travelling kinks at arbitrary velocities.

- Firstly, on an intuitive level, one might suppose that the radiation is a direct consequence of the periodic acceleration and deceleration of the pulse as it stutters across the (roughly) sinusoidal landscape of the PN potential [111, 118].
- Secondly, in the case of Fermi–Pasta–Ulam lattices (lattices with nonlinear interactions but no on-site potential), travelling solitons are known to exist [76]. In these lattices, there is no concept of a PN barrier [130], and indeed no on-site potential to hold a stationary solution in place (or, in fact, to allow it to exist at all).
- Thirdly, the numerical investigations of Speight [116, 117] have suggested that kinks are not pinned to the lattice in PN-free discretisations (and hence, after some transients, stop losing their energy to radiation).
- Fourthly, from a mathematical perspective, the elimination of the PN barrier restores an effective translational symmetry to the stationary solitons, since they are no longer restricted to the PN potential's maxima and minima, but can exist anywhere with respect to the lattice. Therefore we may hope that this restored symmetry will go hand-in-hand with a restored effective velocity-boost symmetry.
- Finally, and relatedly, the model proposed by Kevrekidis, whose kink has effective translational symmetry, is shown to conserve momentum [131]. Most discrete equations do *not* conserve momentum, in contrast to their continuous counterparts, and so this property is very suggestive of the existence of travelling waves with nondecaying velocities (and therefore no radiation tails).

Thus the primary aim of chapter 3 is to find out whether sliding kinks exist for arbitrary velocities in these *exceptional* models with effective translational invariance and vanishing PN barriers. We search for travelling solitons in the known exceptional discrete ϕ^4 models, which were all discovered recently [116, 131, 132].

Our approach follows logically from that used in chapter 2; we seek to construct the moving discrete kink as a perturbation expansion starting from the moving kink of the continuous model (1.7) (which is simply the Lorentz-boosted stationary kink $\tanh x$). Ideally, the hope is that the method of multiple scales will reveal that the radiation has an amplitude of zero. Unfortunately we shall see that the radiation turns out to be exponentially small, and so cannot be captured by any order of the perturbation expansion. Thus we shall unleash a more advanced technique—namely the method of asymptotics beyond all orders—on the problem. This method dates back to the self-same continuous ϕ^4 equation which is studied in chapter 2, but to its breather rather than its kink. It was devised by Segur and Kruskal in 1987 [52] in order to measure the exponentially small radiation from this breather, and received an important modification by Pomeau, Ramani and Grammaticos [133] shortly thereafter. This eliminated the need to numerically solve an initial-value problem, a particularly tricky issue for discrete equations, replacing it instead with the elementary algebraic problem of computing the limit of a recurrence relation. This method has been applied to measure radiation in continuous equations [134, 135, 136] and discrete equations [137, 138, 139], but never (to the author's knowledge) to an equation involving both finite differences and derivatives. This is the equation that arises in chapter 3 after a travelling wave ansatz is made, and on which we aim to use the method.

Since exceptional discretisations (discretisations which admit stationary solutions with effective translation invariance) are found to be favourable to travelling solitons, our aim in the next chapter, chapter 4, is to generate new exceptional discretisations in the hope of finding physically realisable examples. A second objective is to identify and understand the mechanism behind exceptionality by unifying the known models. These models were generated by their inventors in fundamentally different ways: the models of Speight and Ward [115, 116] through a Bogomolny energy minimisation method and the models of Kevrekidis [131] by starting from a conserved two-point quantity corresponding to momentum, and the model of Bender and Tovbis [132] by asserting a necessary condition for the elimination of resonant radiation (this technique will be described in section 4.3). Finally, whether physically applicable or not, exceptional discretisations are useful for simulating continuous equations numerically. Using the finite-difference method, it is necessary to discretise the continuous equation, and so an equation with effective translation invariance is a more accurate approximation than one without since it more closely matches the properties of the original continuous equation. Therefore it would be worthwhile to look for a particularly simple exceptional discretisation for this purpose.

Next, chapter 5 is an attempt to find moving kinks (of amplitude 2π) in the Frenkel–Kontorova model (which is *not* exceptional, i.e. has a PN barrier [109]). We aim to answer definitively the important question of the existence of sliding solitons in the FK model. A negative answer has already been given based on a numerical method [113] (albeit a reliable one), but earlier simulations were suggestive of the existence of sliding kinks [109], so the problem is worth investigating once more from a different angle. Since it has many applications (which we list in section 5.1), radiationless energy transport in the FK model is a sought-after phenomenon.

Our second main objective for chapter 5, which connects with our investigations of exceptional discretisations in chapters 3–4, is to show that the translation invariance of static kinks is *not* a necessary condition for the existence of sliding solitons. Although the discovery of sliding solitons in exceptional discretisations in chapter 3 hints at this correspondence, it was found in ref. [119] that sliding kinks can exist in a system with a nonzero PN barrier – and the presence of a PN potential immediately rules out the translation invariance of static solutions (this is because all members of a continuous family of time-independent solutions must have the same potential energy). We would like to provide independent verification of this result, however, to counter the strong intuitive expectation that the PN potential is always responsible for the emission of radiation. If we are able to find sliding kinks in the FK model, it will confirm that there is no rigid connection between the two. A similar question which stems from chapter 3 is whether it is necessary for the nonlinearity to be nonlocal—that is, to depend on multiple lattice sites—since all the sliding kinks found there occur in such models. However, the same counterexample in ref. [119] refutes this. Once again, we would like to provide confirmation of this result in chapter 5.

A further motivation for this study is to find out how to derive the inner equations and hence calculate Stokes constants in a model with nonpolynomial nonlinearity. As we shall show, this requires some modifications to the standard procedure. By presenting the method of beyond-all-orders asymptotics a second time, we are able to gloss over confusing details and, therefore, hope to provide a more intuitively appealing overview of the method.

Chapter 6 continues the search for sliding solitons, this time in the saturable DNLS equation. We will now be looking for pulse solitons rather than kinks. We are motivated by recent numerical studies which have indicated enhanced mobility of solitons in optical waveguide arrays with saturable nonlinearities [140, 141], and also by the fact that there is presently great interest in these systems among experimentalists [101, 102, 142]. Aside from the potential importance of

finding sliding solitons for their own sake, our aims for chapter 6 are substantially the same as for the previous chapter: We are again searching for a counter-example which will confirm the findings in ref. [119] that both exceptionality and the nonlocal discretisation of the nonlinearity are not prerequisites for the existence of sliding solitons. In this chapter we also aim to calculate rigorously the radiation amplitudes for the travelling lattice soliton. Whereas in chapters 3–5 we are content to demonstrate existence or nonexistence of sliding solitons, with only a heuristic argument that the radiation amplitudes are proportional to the Stokes constant, we propose to prove this in chapter 6. This will allow us to work out the time-evolution of the parameters of the radiating lattice solitons. The situation will be more complicated—and therefore interesting—than for kinks, because moving pulses have two 'internal' parameters (amplitude and velocity) which could vary as a result of radiation emission, whereas kinks do not have an amplitude; the lattice-spacing parameter which determines their width is external and cannot vary. For kinks, one would expect radiation emission simply to slow them down, but with two parameters, more interesting questions arise, such as whether the pulses will be pinned to the lattice before they have had a chance to decay, or vice-versa. We also aim to answer the question of how radiating solitons behave near to sliding velocities and, crucially, whether the radiationless sliding state is a stable one.

Another important objective of chapter 6 is to resolve the long-standing question of whether sliding kinks exist in the DNLS model with cubic nonlinearity. The cubic DNLS model arises as the limit of our saturable model when the saturation intensity of the medium tends to infinity, and therefore the search for sliding solitons in the cubic equation falls into the same analysis as for the saturable one.

Whereas in chapter 6 we were studying a lattice of waveguides coupled together (with particular reference to the photorefractive nonlinearity), in chapter 7 our aim is to study in more detail how light behaves in just a single waveguide, also with photorefractive nonlinearity. Our objective is to construct soliton solutions explicitly and to study their stability. Another motivation for studying the single-waveguide system comes from the numerical study of Gisin, Driben and Malomed [143]. In this paper, solitons are numerically constructed and their stability analysed. It is shown that two branches of stable solitons coexist, and that for one branch, the derivative of the integral power with respect to the wavenumber of the soliton's carrier wave is positive, and for the other, it is negative. In the standard cubic-quintic NLS, the well-known Vakhitov–Kolokolov stability criterion [144] would then imply that the two branches should

have opposite stability. However, it would seem that when the waveguide is added, this criterion no longer holds; either that, or the numerical analysis of ref. [143] contains a flaw. We aim to find out if this is true and, if not, to find the reasons for the failure of the Vakhitov–Kolokolov theorem by performing a stability analysis from scratch, and to see whether its correct prediction of the stability of one of the branches is an accident or simply an application of the theorem under correct conditions.

In chapter 8 we summarise the conclusions arrived at and discuss our work, as well as suggesting some directions for future investigations.

Chapter 2

Wobbling kinks in ϕ^4 theory

As mentioned in section 1.3, ϕ^4 kinks have an internal mode (also called a 'shape' or 'wobbling' mode) which allows the kink to carry energy with it. In this chapter, our aim is to construct the wobbling kink using the method of multiple scales, in order to complement the results found using a variational approach in refs [127, 128, 129].

2.1 Introduction

The ϕ^4 equation in 1+1 dimensions with the repulsive nonlinearity,

$$\frac{1}{2}\phi_{tt} - \frac{1}{2}\phi_{xx} - \phi + \phi^3 = 0, \tag{2.1}$$

admits the kink solution $\phi(x,t) = \tanh x$. Since the analytical expression for the kink is so simple, eq. (2.1) is often used as a paradigm for nonintegrable kink-bearing systems. Kinks have been used to describe crystal dislocations [78, 145], domain walls representing structural phase transitions in incommensurate [146], ferroelectric [147, 148], and ferromagnetic [149] systems, polymerisation mismatches in polyacetylene [47, 48], spin waves [150] and charge-density waves [151], and energy transfer along hydrogen-bonded molecular chains [152, 153].

In contrast to the kink of the (integrable) sine–Gordon equation, the ϕ^4 kink has an internal or shape mode [125], discovered by Rice and Mele [154] in 1980. This extra degree of freedom allows for oscillations in the width of the kink, which are accompanied by the emission of radiation – a manifestation of the nonintegrability of the ϕ^4 equation. Initially, an oscillation *was* observed in the kink of the sine–Gordon equation [155], but this is not a genuine wobbling mode [125] (i.e. not a linear mode of the kink, but a consequence of the excitation of radiation),

and has since been shown to be a consequence of the discretisation of the equation for numerical simulation rather than a property of the PDE itself [156]. Energy can be stored in the wobbling mode and released from it upon collision [155, 157], when the kink encounters an inhomogeneity [158], or when it moves near a resonant velocity over a periodically modulated potential [159]. Also, the internal mode can be excited by direct [128] or parametric [129] driving, which we also consider in this chapter.

Segur [126] constructed a regular perturbation expansion of the wobbling kink, obtaining the first three orders of the series. He noted the imminent appearance of 'secular' (unbounded) terms at the next order of the expansion, and the consequent breakdown of the expansion.

More recently, Quintero, Sánchez and Mertens have considered the dynamics of ϕ^4 kinks when subjected to direct (external, or ac) driving [127, 128] and parametric driving [129]. They have employed a variational method which neglects the radiation, assuming a specific functional dependence of the kink on the 'collective coordinates', which in this case are the width and position of the kink. By inserting this structure into the Hamiltonian one obtains new equations of motion for these two degrees of freedom, a simplification from the the infinite number of degrees of freedom present in the partial differential equation. The drawback of this method is that one has no assurance that the omission of these degrees of freedom has no qualitative impact on the kink's dynamics. Specifically, the ansatz chosen excludes the radiation emitted as the kink wobbles.

In this chapter, we construct a perturbation expansion for the moving, wobbling kink and, using the method of multiple scales, obtain equations for the slow-time evolution of the wobbling amplitude and kink velocity by eliminating secular terms from our expansion. We consider the same forms of driving at the same resonant frequencies as Quintero, Sánchez and Mertens in [127, 128, 129]. Unlike the variational approach, perturbation theory does not neglect the radiation. Whilst most of our results confirm theirs, we detect a resonance when the kink is directly driven at its natural frequency which was not predicted by the variational method. This suggests that radiation can play a role in the transfer of energy to the internal mode.

2.2 Freely oscillating wobbling kink

In this section, we shall construct a moving wobbling kink of the ϕ^4 equation (2.1). We begin by transforming (2.1) to the co-moving frame of reference using the change of variables

$$\xi = x - \int_0^t v(t')dt' \quad \text{and} \quad \tau = t,$$

which yields

$$\frac{1}{2}\phi_{\tau\tau} - v\phi_{\xi\tau} - \frac{1}{2}v_\tau\phi_\xi - \frac{1}{2}(1-v^2)\phi_{\xi\xi} - \phi + \phi^3 = 0. \tag{2.2}$$

We shall determine the unknown function $v(t)$, representing the kink's velocity, by imposing in our perturbation expansion the condition that the kink be always centred at $\xi = 0$ [i.e. at $x = x_0(t)$].

We now apply the method of multiple scales to the equation. We perform a perturbation expansion about the kink $\phi_0 \equiv \tanh X$:

$$\phi = \phi_0 + \varepsilon\phi_1 + \varepsilon^2\phi_2 + \ldots \tag{2.3}$$

where ε is a small parameter. We further introduce the slow time and space variables

$$X_n \equiv \varepsilon^n \xi \quad \text{and} \quad T_n \equiv \varepsilon^n \tau,$$

which describe long times and distances. In the method of multiple scales, we assume that $\varepsilon \to 0$ to obtain an asymptotic expression for the solution. In this limit the different scales become uncoupled and may be considered as independent variables. We shall use the notation

$$\partial_n \equiv \frac{\partial}{\partial X_n} \quad \text{and} \quad D_n \equiv \frac{\partial}{\partial T_n}.$$

We expand derivatives with respect to the original variables in terms of the scaled variables by using the chain rule, so that

$$\frac{\partial}{\partial \xi} = \partial_0 + \varepsilon\partial_1 + \varepsilon^2\partial_2 + \ldots \qquad \text{and}$$
$$\frac{\partial}{\partial \tau} = D_0 + \varepsilon D_1 + \varepsilon^2 D_2 + \ldots$$

Substituting these expansions into the ϕ^4 equation (2.2), along with the expansion of ϕ, (2.3), and equating like powers of ε, we obtain a hierarchy of equations. We assume that v is slowly varying and, for simplicity, that it is small, i.e. $v = \varepsilon V$ [$V \sim \mathcal{O}(1)$] where $V = V(T_1, T_2, \ldots)$.

At $\mathcal{O}(\varepsilon^1)$ we obtain the linearisation of (2.1) about $\tanh X_0$:

$$\frac{1}{2}D_0^2\phi_1 + \mathcal{L}\phi_1 = 0,$$

where

$$\mathcal{L} = -\frac{1}{2}\partial_0^2 - 1 + 3\phi_0^2 = -\frac{1}{2}\partial_0^2 + 2 - 3\operatorname{sech}^2 X_0. \tag{2.4}$$

We split the temporal and spatial dependence using separation of variables.

$$\phi_1(X_0, \ldots, T_0, \ldots) = Af(X_0)g(T_0),$$

which implies that

$$D_0^2 g + 2\lambda g = 0 \quad \text{and} \quad \mathcal{L}f = \lambda f,$$

where λ is the eigenvalue. A is a function of the slow time and space variables. $\mathcal{L}$ has the following discrete eigenvalues and associated eigenfunctions:

$$\begin{aligned}
&\lambda = 0: && f = \operatorname{sech}^2 X_0 && g = 1,\\
&\lambda = \frac{3}{2}: && f = \operatorname{sech} X_0 \tanh X_0 && g = e^{i\omega T_0} + c.c.,\\
&\lambda = 2: && f = 3\operatorname{sech}^2 X_0 - 2 && g = e^{2iT_0} + c.c.
\end{aligned}$$

where $\omega \equiv \sqrt{3}$. The $\lambda = 0$ eigenfunction is the translation mode, which we shall not include in our solution as the kink must be centred at $X_0 = 0$. The asymmetric $\lambda = 3/2$ eigenfunction is the wobbling mode; it oscillates with a frequency ω. The $\lambda = 2$ eigenfunction does not decay to zero at infinities, and so will not be included.

The continuous spectrum of $\mathcal{L}$ begins at $\lambda = 2$. Solutions in the continuous spectrum were found by Segur [126] using Gel'fand and Levitan's triangular representation: For every $\lambda > 2$, two linearly independent solutions of $\mathcal{L}f = \lambda f$ are

$$f = e^{ipX_0}\left[1 + \frac{3(1-ip)}{1+p^2}\tanh X_0(1+\tanh X_0) - \frac{3(2-ip)}{4+p^2}(1+\tanh X_0)^2\right] \tag{2.5}$$

and its complex conjugate. Here, $p^2 = 2(\lambda - 2)$. This formula in fact produces correct solutions for $\lambda < 2$ as well, i.e. $p^2 < 0$ (these solutions are, of course, not bounded). The only values for which it breaks down are $p^2 = -1$ and $p^2 = -4$, which correspond to the discrete eigenvalues.

We assume that there is no incoming radiation at infinity, and this implies that none of the solutions in the continuous spectrum should be added. Therefore the first-order perturbation comprises only the wobbling mode:

$$\phi_1 = A(X_1, \ldots, T_1, \ldots)\operatorname{sech} X_0 \tanh X_0 e^{i\omega T_0} + c.c. \tag{2.6}$$

A, the amplitude of the wobbling mode, is an arbitrary constant with respect to X_0 and T_0 (at this stage). '*c.c.*' stands for the complex conjugate of the immediately preceding term.

The equation at second order in the perturbation expansion is

$$\begin{aligned}\frac{1}{2}D_0^2\phi_2+\mathcal{L}\phi_2 =&(\partial_0\partial_1-D_0D_1)\phi_1-3\phi_0\phi_1^2+VD_0\partial_0\phi_1+\frac{1}{2}D_1V\partial_0\phi_0-\frac{1}{2}V^2\partial_0^2\phi_0\\ =&-6|A|^2\operatorname{sech}^2X_0\tanh^3X_0+\frac{1}{2}D_1V\operatorname{sech}^2X_0-V^2\operatorname{sech}^2X_0\tanh X_0\\ &+\left[\partial_1A(2\operatorname{sech}^3X_0-\operatorname{sech}X_0)-i\omega D_1A\operatorname{sech}X_0\tanh X_0\right.\\ &\left.+i\omega VA(2\operatorname{sech}^3X_0-\operatorname{sech}X_0)\right]e^{i\omega T_0}+c.c.-3A^2\operatorname{sech}^2X_0\tanh^3X_0e^{2i\omega T_0}+c.c.\end{aligned}\tag{2.7}$$

This is a linear wave equation with forcing (or source terms) at the frequencies 0, ω and 2ω. The first two are resonant with the two discrete eigenmodes, and the third lies in the continuous spectrum. This forcing is localised to the region near the origin, thanks to the sech^2X_0 factor which decays exponentially fast, and acts as a source of radiation which spreads outward from there. Hence, the frequency-doubling effects of the nonlinearity have caused the kink's wobbling mode to become a source of radiation.

Once transients have died down, the solution will consist of only the harmonics present in the forcing, i.e.

$$\phi_2=\varphi_2^{(0)}+\varphi_2^{(1)}e^{i\omega T_0}+c.c.+\varphi_2^{(2)}e^{2i\omega T_0}+c.c.,$$

This implies that $\varphi_2^{(0)}$, $\varphi_2^{(1)}$ and $\varphi_2^{(2)}$ should satisfy the three nonhomogeneous equations

$$\begin{aligned}\mathcal{L}\varphi_2^{(0)}=&-6|A|^2\operatorname{sech}^2X_0\tanh^3X_0+\frac{1}{2}D_1V\operatorname{sech}^2X_0-V^2\operatorname{sech}^2X_0\tanh X_0,\\ (\mathcal{L}-\tfrac{3}{2})\varphi_2^{(1)}=&\partial_1A(2\operatorname{sech}^3X_0-\operatorname{sech}X_0)-i\omega D_1A\operatorname{sech}X_0\tanh X_0\\ &+i\omega VA(2\operatorname{sech}^3X_0-\operatorname{sech}X_0)\quad\text{and}\\ (\mathcal{L}-6)\varphi_2^{(2)}=&-3A^2\operatorname{sech}^2X_0\tanh^3X_0.\end{aligned}\tag{2.8}$$

We wish to find bounded solutions of these equations. For the first two (whose homogeneous solutions are discrete eigenfunctions), the Fredholm alternative states that this is the case when the right-hand side is orthogonal to the zero eigenfunction of the left-hand side. For this to be the case, we must set $D_1V=0$ and $D_1A=0$. Using the method of variation of parameters to obtain the solutions, we have

$$\varphi_2^{(0)}=|A|^2\operatorname{sech}^2X_0(2\tanh X_0-3X_0)-\frac{1}{2}V^2X_0\operatorname{sech}^2X_0\quad\text{and}\tag{2.9}$$

$$\varphi_2^{(1)}=-(\partial_1A+i\omega VA)X_0\operatorname{sech}X_0\tanh X_0.\tag{2.10}$$

It turns out that we obtain no restrictions on $\partial_n A$ when we apply solvability conditions at higher orders. Therefore, we are free to make our own choice for $\partial_n A$. Looking at equation (2.10), the simplest choice is obviously to set

$$\partial_1 A + i\omega V A = 0.$$

The solution of (2.8) requires some care. Using the method of variation of parameters, the naïve solution we obtain is

$$\varphi_2^{(2)} = A^2 f_1(X_0), \tag{2.11}$$

where f_1 is a function that describes right-moving radiation for positive X_0 and left-moving radiation for negative X_0; specifically

$$f_1(X_0) = \frac{1}{8}\big[6\tanh X_0 \operatorname{sech}^2 X_0 + (3 - \tanh^2 X_0 + ik\tanh X_0)(J_2^*(X_0) - J_2^\infty)e^{ikX_0} + (3 - \tanh^2 X_0 - ik\tanh X_0)J_2(X_0)e^{-ikX_0}\big]$$

where

$$J_n(x) = \int_{-\infty}^{x} e^{ik\xi}\operatorname{sech}^n \xi \, d\xi, \tag{2.12}$$
$$J_n^\infty = \lim_{x\to\infty} J_n(x) \quad \text{and} \quad k = \sqrt{8}.$$

One can show that f_1 is an odd function.

However, there is a problem with the solution (2.11) which only becomes apparent at higher orders. The source of the problem lies here, however. The problem with (2.11) is that any variation of A on the slow time scales will result in an instantaneous change in the amplitude of the radiation tail for all values of X_0, which does not make sense. There would be no objection if the radiation tails were localised in extent, as the higher order terms could account for the discrepancy, at least in the limit $\varepsilon \to 0$ (when the slow time scales slow down and the long length scales lengthen). However, when the radiation tails extend all the way to infinity, they cover all the long length scales for any finite value of ε, and secular terms cannot be avoided at higher orders. The problem stems from the fact that in integrating equation (2.8), we have covered the long length scales, whereas the differential equation (2.8) describes variations on the short scale X_0 and so is only meant to hold locally for distances $\mathcal{O}(1)$ and not $\mathcal{O}(1/\varepsilon)$.

It is easy to propose a solution which satisfies (2.8) locally for all values of X_0: Take

$$\varphi_2^{(2)} = B(X_1, \ldots, T_1, \ldots) f_1(X_0). \tag{2.13}$$

where B is an unknown 'envelope' function of the long scales, subject to the boundary condition

$$B(0,0,\ldots,T_1,\ldots) = A^2.$$

For finite values of X_0, $X_1 \to 0$ in the $\varepsilon \to 0$ limit (since $X_1 = \varepsilon X_0$). Hence, $B = A^2$ and (2.13) solves (2.8). On the other hand, if $|X_0| = \mathcal{O}\left(\varepsilon^{-1}\right)$, i.e. $|X_0| \to \infty$ in the $\varepsilon \to 0$ limit, the right hand side of (2.8) disappears and (2.13) still solves it, but now B is unconstrained (since $X_1 = \mathcal{O}(1)$ when $X_0 = \mathcal{O}\left(\varepsilon^{-1}\right)$; hence X_1 remains nonzero in the $\varepsilon \to 0$ limit).

Amplitude equations which govern the outward propagation of variations of A along B on the T_2 timescale are derived at higher orders of the perturbation expansion.

In summary, at second order we have

$$\begin{aligned}
\varphi_2^{(0)} &= |A|^2 \operatorname{sech}^2 X_0 (2\tanh X_0 - 3X_0) + \frac{1}{2} V^2 X_0 \operatorname{sech}^2 X_0, \\
\varphi_2^{(1)} &= 0 \qquad \text{and} \\
\varphi_2^{(2)} &= B f_1(X_0).
\end{aligned}$$

where $B(0,\ldots,T_1,\ldots) = A^2$.

Equating the terms of order ε^3 gives the equation

$$\begin{aligned}
\frac{1}{2} D_0^2 \phi_3 + \mathcal{L}\phi_3 = (\partial_0\partial_1 - D_0 D_1)\phi_2 + (\partial_0\partial_2 - D_0 D_2)\phi_1 + \frac{1}{2}(\partial_1^2 - D_1^2)\phi_1 - \phi_1^3 - 6\phi_0\phi_1\phi_2 \\
+ V D_0 \partial_0 \phi_2 + V D_0 \partial_1 \phi_1 + V D_1 \partial_0 \phi_1 + \frac{1}{2} D_2 V \partial_0 \phi_0 - \frac{1}{2} V^2 \partial_0^2 \phi_1. \quad (2.14)
\end{aligned}$$

Having evaluated the right hand side using the known functions ϕ_0, ϕ_1 and ϕ_2, we again split the solution into components proportional to simple harmonics as we did at $\mathcal{O}\left(\varepsilon^2\right)$. The solvability conditions for the zeroth and first harmonics give, respectively, $D_2 V = 0$ and

$$-\frac{2}{3} i\omega D_2 A + k_1 |A|^2 A + V^2 A = 0 \quad (2.15)$$

where

$$\begin{aligned}
k_1 &= \int_{-\infty}^{\infty} 6 \operatorname{sech}^2 X_0 \tanh^3 X_0 \left[-\frac{5}{2} \operatorname{sech}^2 X_0 \tanh X_0 + 3X_0 \operatorname{sech}^2 X_0 - f_1(X_0) \right] dX_0 \\
&= 0.8509 - 0.04636i.
\end{aligned}$$

The real part of the integral was obtained numerically, while the imaginary part can be evaluated analytically:

$$\operatorname{Im} k_1 = -\frac{3\pi^2 k}{\sinh^2\left(\frac{\pi k}{2}\right)}.$$

We have now obtained the leading order behaviour of the wobbling amplitude. As this is our main objective, we shall postpone the continuation of the perturbation expansion to higher orders until we come to consider the case of direct driving.

Writing $a = \varepsilon A$, so that a is the 'natural' amplitude of the wobbling mode—i.e. the small amplitude one would actually measure—and recalling that $\varepsilon^2 \frac{\partial}{\partial T_2} = \frac{\partial}{\partial t}$, we express the amplitude equation (2.15) in terms of unscaled variables:

$$\frac{da}{dt} = -\tfrac{1}{2} i\omega k_1 |a|^2 a - \tfrac{1}{2} i\omega v^2 a + \mathcal{O}\left(\varepsilon^5\right). \tag{2.16}$$

(Recall that $v = \varepsilon V$.)

Multiplying (2.16) by a^* and adding the complex conjugate gives

$$\frac{\partial}{\partial t}|a|^2 = \omega \,\mathrm{Im}(k_1)|a|^4 + \mathcal{O}\left(\varepsilon^6\right).$$

k_1 has a negative imaginary part; this equation describes the gradual decrease in the amplitude of the wobbling as it emits energy in the form of radiation.

The amplitude equation also gives us the leading order contributions to the amplitude-frequency relationship for the wobbling mode – the nonzero time derivative of the phase of a shifts the wobbling frequency away from $\omega = \sqrt{3}$, and we obtain:

$$\omega_{\text{wobbling}} = \omega\left[1 - \tfrac{1}{2}\mathrm{Re}(k_1)|a|^2 - \tfrac{1}{2}v^2 + \mathcal{O}\left(\varepsilon^4\right)\right]. \tag{2.17}$$

The v^2 term is a relativistic time-dilation factor which acts to decrease the frequency in the laboratory frame when the kink is moving. The $|a|^2$ term, on the other hand, is a nonlinear frequency shift.

Finally, we write the perturbation expansion in terms of the small variables:

$$\phi(x,t) = \tanh x + a\,\mathrm{sech}\, x \tanh x e^{i\omega t} + c.c. + |a|^2 \mathrm{sech}^2 x(2\tanh x - 3x) + \frac{1}{2}v^2 x \mathrm{sech}^2 x + b^2 f_1(x) e^{2i\omega t} + c.c. + \mathcal{O}\left(\varepsilon^3\right),$$

where $b = \varepsilon B$.

2.3 Parametric driving

2.3.1 Driving frequency near ω

We add damping and parametric driving to the ϕ^4 equation as follows:

$$\frac{1}{2}\phi_{tt} - \frac{1}{2}\phi_{xx} + \gamma\phi_t - [1 + h\cos(\Omega t)]\,\phi + \phi^3 = 0,$$

where γ and h are small damping and driving parameters, which we scale as follows:

$$\gamma = \varepsilon^2 \Gamma \quad \text{and} \quad h = \varepsilon^3 H$$

so that Γ and H are of order one. The driving frequency Ω is close to the natural wobbling frequency of the kink, $\omega = \sqrt{3}$:

$$\Omega = \omega(1+\rho),$$

where ρ is a small detuning parameter. We take

$$\rho = \varepsilon^2 R$$

where R is of order one.

For the sake of notational compactness, we shall make the transformation $t \longrightarrow T$ where

$$\Omega t = \omega T.$$

The equation now becomes

$$\frac{1}{2}(1+\rho)^2 \phi_{TT} - \frac{1}{2}\phi_{xx} + \gamma(1+\rho)\phi_T - [1 + h\cos(\omega T)]\,\phi + \phi^3 = 0$$

As before, we transform the equation to the moving frame described by the variables ξ and τ, where

$$\xi = x - \int_0^T v(T')dT' \quad \text{and} \quad \tau = T,$$

and obtain

$$(1+\rho)^2\left[\frac{1}{2}\phi_{\tau\tau} - v\phi_{\xi\tau} - \frac{1}{2}v_\tau \phi_\xi\right] - \frac{1}{2}(1-v^2)\phi_{\xi\xi}$$
$$+ \gamma(1+\rho)\left(\phi_\tau - v\phi_\xi\right) - [1 + h\cos(\omega\tau)]\,\phi + \phi^3 = 0.$$

Note that in practice, the best resonance will be obtained not when $\Omega = \omega$, but when ρ is slightly negative, since the frequency of wobbling is slightly less than ω according to (2.17).

The perturbative solution to this equation is the same as for the freely oscillating case until we reach $\mathcal{O}(\varepsilon^3)$. At $\mathcal{O}(\varepsilon^3)$, instead of the amplitude equation (2.15) we now have

$$D_2 A + \Gamma A + i\omega R A + \frac{1}{2} i\omega k_1 |A|^2 A + \frac{1}{2} i\omega V^2 A + i\omega \frac{\pi}{8} H = 0. \tag{2.18}$$

and

$$D_2 V = -2\Gamma V.$$

Expressing these equations in terms of the unscaled parameters gives:

$$\frac{da}{dt} = -\gamma a - i\omega\rho a - \frac{1}{2}i\omega k_1|a|^2 a - \frac{1}{2}i\omega v^2 a - i\omega\frac{\pi}{8}h + \mathcal{O}\left(\varepsilon^5\right) \tag{2.19a}$$

$$\frac{dv}{dt} = -2\gamma v + \mathcal{O}\left(\varepsilon^5\right). \tag{2.19b}$$

Provided the damping is of order ε^2, then equation (2.19b) will be dominated by the damping term and the velocity will decay to zero.

One can easily ascertain that (2.19a) with $v = 0$ (which is a dynamical system on the plane, since a is complex) does not admit solutions escaping to infinity, and one can apply Dulac's criterion to rule out the existence of closed orbits. The only option left, then, is that the solution will settle to a stable (nonzero) fixed point as $t \to \infty$.

The perturbation expansion [up to $O(\varepsilon^2)$], written in terms of the small variables, is

$$\phi(x,t) = \tanh x + a\,\mathrm{sech}\,x\tanh x e^{i\Omega t} + c.c. + |a|^2\,\mathrm{sech}^2 x(2\tanh x - 3x) + \frac{1}{2}v^2 x\,\mathrm{sech}^2 x + b^2 f_1(x)e^{2i\Omega t} + c.c. + \mathcal{O}\left(\varepsilon^3\right)$$

(the driving term only appears at $\mathcal{O}\left(\varepsilon^3\right)$). The only difference from the undriven case is that the oscillations now have the same frequency as the driving (Ω) rather than the natural frequency ω.

2.3.2 Driving frequency near 2ω

We now keep the same equation but with the driving frequency close to twice the natural wobbling frequency:

$$\frac{1}{2}\phi_{tt} - \frac{1}{2}\phi_{xx} + \gamma\phi_t - [1 + h\cos(2\Omega t)]\,\phi + \phi^3 = 0.$$

As before,

$$\Omega = \omega(1+\rho),$$

but we use a different scaling for h:

$$h = \varepsilon^2 H.$$

We transform the equation in exactly the same way as in the above case; i.e. we consider

$$(1+\rho)^2\left[\frac{1}{2}\phi_{\tau\tau} - v\phi_{\xi\tau} - \frac{1}{2}v_\tau\phi_\xi\right] - \frac{1}{2}(1-v^2)\phi_{\xi\xi} + \gamma(1+\rho)\left(\phi_\tau - v\phi_\xi\right) - [1 + h\cos(2\omega\tau)]\,\phi + \phi^3 = 0.$$

The perturbation expansion is unchanged from the undamped, undriven case at $\mathcal{O}(\varepsilon^0)$ and $\mathcal{O}(\varepsilon^1)$.

With the addition of driving, the equation at $\mathcal{O}(\varepsilon^2)$ has acquired additional terms on the right hand side as compared to equation (2.7):

$$\frac{1}{2}D_0^2\phi_2 + \mathcal{L}\phi_2 = \ldots + \frac{H}{2}\phi_0 e^{2i\omega T_0} + c.c.$$

Assuming that the solution is in the form $Hf_2(X_0)e^{2i\omega T_0}$ (plus its complex conjugate), we have to solve

$$(\mathcal{L} - 6)f_2(X_0) = \frac{1}{2}\tanh X_0. \tag{2.20}$$

The particular solution which obeys the radiation boundary conditions is

$$f_2(X_0) = -\frac{1}{96}\left[2\tanh X_0(5+\tanh^2 X_0) + (3-\tanh^2 X_0 - ip\tanh X_0)J_2(X_0)e^{-ipX_0} \right.$$
$$\left. +(3-\tanh^2 X_0 + ip\tanh X_0)(J_2^*(X_0) - J_2^\infty)e^{ipX_0}\right].$$

The function $J_2(X_0)$ is defined by (2.12). As H is a constant, independent of the long scales, it is now not necessary to introduce a further unknown (similar to B introduced in section 2.2) to take account of the fact that (2.20) should only hold locally over the short length scale. In summary, for the second harmonic we have

$$\varphi_2^{(2)} = B^2 f_1(X_0) + Hf_2(X_0).$$

The amplitude equation for A, which arises at $\mathcal{O}(\varepsilon^3)$, is now

$$D_2 A + \Gamma A + i\omega RA + \frac{1}{2}i\omega k_1|A|^2 A + \frac{1}{2}i\omega V^2 A + \frac{1}{2}i\omega k_2 HA^* = 0. \tag{2.21}$$

where

$$k_2 = \int_{-\infty}^{\infty} \operatorname{sech} X_0 \tanh X_0 \left[6\operatorname{sech} X_0 \tanh^2 X_0 f_2(X_0) + \frac{1}{2}\operatorname{sech} X_0 \tanh X_0\right] dX_0$$
$$= 0.5958 + 0.003863i.$$

Only the imaginary part of the integral is amenable to analytical evaluation:

$$\operatorname{Im} k_2 = \frac{\pi^2 k}{4\sinh^2\left(\frac{\pi k}{2}\right)}.$$

The solvability condition for the zeroth harmonic gives

$$D_2 V = -2\gamma V.$$

We finally write the amplitude and velocity equations in terms of the unscaled parameters and original time variable (as in the previous case)

$$\frac{da}{dt} = -\gamma a - i\omega\rho a - \frac{1}{2}i\omega k_1 |a|^2 a - \frac{1}{2}i\omega v^2 a - \frac{1}{2}i\omega k_2 h a^* + \mathcal{O}\left(\varepsilon^5\right) \tag{2.22a}$$

$$\frac{dv}{dt} = -2\gamma v + \mathcal{O}\left(\varepsilon^5\right). \tag{2.22b}$$

Again, provided the damping is no smaller than $\mathcal{O}\left(\varepsilon^2\right)$ the velocity tends to zero and one can verify that the long-term dynamics of a must be to settle to a fixed point. If $h < \frac{2\sqrt{\gamma^2+3\rho^2}}{\omega|k_2|}$ then the fixed point at $|a| = 0$ is stable and so the wobbling could die out, but for stronger driving it loses its stability and so as $t \to \infty$ the amplitude must settle to a nonzero fixed point.

The first three orders of the perturbation perturbation expansion give

$$\phi(x,t) = \tanh x + a\,\mathrm{sech}\, x \tanh x e^{i\Omega t} + c.c. + |a|^2 \mathrm{sech}^2 x (2\tanh x - 3x) + \frac{1}{2}v^2 x \mathrm{sech}^2 x + \left[b^2 f_1(x) + h f_2(x)\right] e^{2i\Omega t} + c.c. + \mathcal{O}\left(\varepsilon^3\right).$$

2.3.3 Discussion

Comparing the amplitude equations (2.19a) and (2.22a) for parametric driving near ω and 2ω respectively, we see that the driving term is *stronger* in the former case, where it is $\mathcal{O}(h)$ compared with $\mathcal{O}(ha)$. This is precisely the opposite behaviour to what we might naïvely expect based on our intuition about parametric driving. This counterintuitive behaviour was first reported by Quintero, Sánchez and Mertens in [129], where it was predicted by the 'collective coordinate' method.

To explain this surprising behaviour qualitatively, we write the driving term $h\phi\cos\Omega t$ as $h\phi_0\cos\Omega t + \mathcal{O}\left(h^2\right)$, which shows that the 'parametric' driving term is effectively a direct driving term but with odd rather than even parity. In essence, it is because the wobbling mode (which is being driven) sits on top of a much larger *static* profile (the kink) that the parametric driving is transformed to direct driving. Since the odd parity of this direct driving profile corresponds to the parity of the wobbling mode, this explains intuitively the strong driving at the frequency ω. The driving at the frequency 2ω is weaker because it only couples to the wobbling mode once its frequency has been halved via the nonlinearity.

Contents

Chapter 1

Introduction

1.1 Early history of the solitary wave

The solitary wave was discovered in 1834 by the Scottish engineer John Scott Russell [1], who at the time was studying horse-drawn canal boats. When a rope snapped and his rapidly-moving barge came to rest, he observed a hump of water several feet high gather at the front of the boat before detaching and travelling intact for several kilometres along the canal at a speed of eight or nine miles per hour. This behaviour was totally unexpected at the time; linear wave theory predicts that, in a dispersive medium such as water, wavepackets should broaden on a much shorter timescale due to the differing phase velocities of their Fourier components. Although the linear approximation is only valid for small perturbations about equilibrium, it had usually been assumed by physicists to be only a quantitative approximation, to which nonlinearity would add no qualitative changes. In fact, in the case of shallow-water waves a nonlinear theory *had* also been developed (by Airy), but this predicted that waves would always steepen and break. Convinced that he had discovered a fundamentally new phenomenon, Russell carried out further experiments in a wave tank which confirmed his observation and, indeed, showed that waves could move through each other completely unaltered.

Almost forty years later, Boussinesq [2] and Rayleigh [3] were the first to explain the permanence of the solitary wave, as an equilibrium between the competing effects of dispersion, which tends to broaden the wave, and nonlinearity, which tends to steepen it. In 1895, Korteweg and de Vries derived a model equation for these shallow-water waves [4], now known as the

Korteweg–de Vries (or 'KdV') equation,

$$u_t - 6uu_x + u_{xxx} = 0, \tag{1.1}$$

and found an explicit solution (a moving sech^2 pulse) describing the solitary wave. Their model was the first to take account of both nonlinearity *and* dispersion. In eq. (1.1), $u(x,t)$ is the height of water in the channel as a function of distance along the channel (x) and time (t), and the subscripts 't' and 'x' denote differentiation with respect to time and distance, respectively.

It was not until half a century later that these Korteweg–de Vries solitary waves were fully appreciated. In 1955, in one of the first ever computer simulations of a nonlinear system, Fermi, Pasta and Ulam [5] were studying a chain of nonlinearly coupled masses. With the initial excitation of a single frequency, they expected energy to leak into other modes as a result of the amplitude-dependence of frequency which is characteristic of nonlinear systems. Thus the system would be expected to end up, eventually, in a state of energy equipartition (thermal equilibrium). However, this is not what happened; after a certain time, the chain returned to almost exactly the same configuration it had started in, with nearly all the energy concentrated in one normal mode.

Zabusky and Kruskal were able to account for this puzzling recurrence phenomenon [6] by taking the continuum limit of Fermi, Pasta and Ulam's lattice equation, to obtain the KdV equation. They found, numerically, that solitary waves in the equation can pass through each other without alteration of their shape or velocity (thus confirming Russell's experimental observation of this fact). This robustness prompted Zabusky and Kruskal to name them 'solitons' in an analogy with elementary, indestructible, particles. They showed that each period of the initial sinusoidal wave breaks up into solitons travelling at different velocities. These pass through each other and solitons from neighbouring sinusoids, reflect off the ends of the chain, and finally the whole configuration resumes its initial state once again (with a slight inaccuracy introduced by small phase shifts as the soiltons collide). This property of the KdV equation is truly remarkable; it is as though there is a superposition principle at play, despite the fact that it is a nonlinear equation.

The discovery of the soliton by Zabusky and Kruskal precipitated a flood of research and firmly established the study of nonlinear waves at the forefront of nonlinear science. The books [7, 8, 9] are excellent general texts on solitons.

1.2 The discovery of integrable systems

Spurred on by the extraordinary properties of the KdV equation, Gardner, Greene, Kruskal and Miura succeeded in constructing a general solution for the equation [10]; for the purpose they invented the famous *Inverse Scattering Method* (ISM). Soon, other nonlinear partial differential equations (PDEs) were found which could be integrated using the ISM, as generalised by Lax [11]. Zakharov and Shabat [12] solved the nonlinear Schrödinger (NLS) equation,

$$i\psi_t + \psi_{xx} \pm 2|\psi|^2\psi = 0, \tag{1.2}$$

and Ablowitz, Kaup, Newell and Segur integrated the sine–Gordon equation [13],

$$\theta_{tt} - \theta_{xx} + \sin\theta = 0. \tag{1.3}$$

In fact, even before Zabusky and Kruskal had coined the term 'soliton', it was known [14, 15] that kink solutions in the sine–Gordon equation could survive collisions without change of shape or velocity. Another revelation provided by the ISM is that these integrable equations have an infinite sequence of conserved quantities; these were derived for the KdV equation by Miura [16] and for the NLS equation in Zakharov and Shabat's paper [12].

A kink is a type of soliton distinct from the pulse-shaped solitons of the KdV and NLS equations in that it links two different zeros of the potential energy function at its left and right infinities. For instance, the sine–Gordon kink

$$\theta(x,t) = 4\arctan\left[\exp\left(\frac{x-vt}{\sqrt{1-v^2}}\right)\right] \tag{1.4}$$

(with velocity $0 \leq v < 1$) interpolates between 0 and 2π. Kinks are known as *topological solitons* as it requires a non-local change to destroy them: Infinite energy would have to be expended to shift one of the infinite tails from one potential minimum to the other. This property makes them extremely stable. In higher dimensions, topological solitons can be characterised by a conserved quantity which is restricted to integer values and hence cannot be altered by any local change.

In addition to the discovery of the exactly solvable nonlinear PDEs listed above, an integrable lattice equation (i.e. a difference equation in space) was discovered – the so-called Toda lattice. The Toda lattice consists of a one-dimensional chain of particles interacting with each other through the exponential potential

$$V(r) = ar + \frac{a}{b}e^{-br},$$

where $a, b > 0$ and r is the displacement between two particles (so $V(r)$ is the potential energy of 'springs' connecting the particles). The resulting equations of motion are

$$\frac{d^2 r_n}{dt^2} = a(2e^{-br_n} - e^{-br_{n+1}} - e^{br_{n-1}}). \tag{1.5}$$

Toda produced explicit solutions for two-soliton collisions [17, 18], before Flaschka applied Inverse Scattering theory to prove the integrability of the lattice [19]. A consequence of integrability is that one can find an explicit solution, known as the N-soliton solution, containing any number of solitons with arbitrary positions and velocities.

An alternative to the Inverse Scattering Method for finding N-soliton solutions was developed by Hirota [20] shortly after the discovery of the Toda lattice. Hirota's method is much faster than going the inverse-scattering route, although it is not as powerful; whereas the ISM can be used to solve initial value problems, Hirota's method only generates N-soliton solutions. However, it provides a useful starting point from which to generate *new* integrable systems (see e.g. [21] and references therein).

It should be mentioned that, almost a century before, Bäcklund [22] had devised a transformation which generates a 1-soliton solution out of the vacuum, a 2-soliton solution from a 1-soliton solution, and so on, hence making it possible to find the N-soliton solution. The method is, however, only applicable to certain equations, among them the sine–Gordon equation (1.3).

Another integrable lattice equation which is relevant to this work is known as the Ablowitz–Ladik equation [23]

$$i\dot{\psi}_n + (\psi_{n+1} + \psi_{n-1})(1 + |\psi_n|^2) = 0, \tag{1.6}$$

which is a discrete version of the NLS equation (1.2). This equation has the exact moving solitons

$$\psi_n(t) = \sinh\varepsilon \,\mathrm{sech}[\varepsilon(n - vt)]e^{ikn + i\Omega t}$$

where $\Omega = 2\cosh\varepsilon\cos k$ and $v = (2/\varepsilon)\sinh\varepsilon\sin k$. The parameter ε need not be small. As $\varepsilon \to 0$, this lattice soliton approaches the continuous soliton of the NLS equation.

In the context of these integrable systems, the word 'soliton' has a mathematically precise meaning; however, many realistic equations are not integrable and may support solitary waves which do not exactly conform to the stipulation that collisions should leave them unaltered. It is the custom of physicists to refer to these solitary waves as solitons nonetheless, since they share their essential characteristics. From a physicist's point of view a soliton is thought of merely as

2.4 Direct driving

2.4.1 Driving frequency near ω

We now introduce direct driving near the natural wobbling frequency of the kink:

$$\frac{1}{2}\phi_{tt} - \frac{1}{2}\phi_{xx} + \gamma\phi_t - \phi + \phi^3 = h\cos(\Omega t),$$

where $\Omega = \omega(1+\rho)$. We use the following scalings for the small parameters:

$$h = \varepsilon^2 H, \quad \gamma = \varepsilon^2\Gamma \quad \text{and} \quad \rho = \varepsilon^2 R.$$

With the time rescaled so that $\Omega t = \omega T$, and transformed into the moving frame, the equation reads

$$(1+\rho)^2\left[\frac{1}{2}\phi_{\tau\tau} - v\phi_{\xi\tau} - \frac{1}{2}v_\tau\phi_\xi\right] - \frac{1}{2}(1-v^2)\phi_{\xi\xi} + \gamma(1+\rho)\left(\phi_\tau - v\phi_\xi\right) - \phi + \phi^3 = h\cos(\omega\tau).$$

Prior to $\mathcal{O}(\varepsilon^2)$, the perturbation expansion is the same as in the undamped, undriven case, i.e.

$$\phi_0 = \tanh X_0$$
$$\phi_1 = A\,\mathrm{sech}\,X_0\tanh X_0 e^{i\omega T_0} + c.c.$$

At $\mathcal{O}(\varepsilon^2)$, the first harmonic component is altered compared to the undriven case; it is

$$\varphi_2^{(1)} = H(1 - 2\,\mathrm{sech}^2 X_0).$$

As before, we have

$$\varphi_2^{(0)} = |A|^2\,\mathrm{sech}^2 X_0(2\tanh X_0 - 3X_0) + \tfrac{1}{2}V^2\,\mathrm{sech}^2 X_0$$

and

$$\varphi_2^{(2)} = Bf_1(X_0).$$

At $\mathcal{O}(\varepsilon^3)$, the solvability conditions determine the amplitude equations; the zeroth harmonic gives

$$D_2 V = -2\Gamma V, \tag{2.23}$$

and the 1st harmonic gives

$$D_2A+\Gamma A+i\omega RA+\frac{1}{2}i\omega k_1|A|^2A+\frac{1}{2}i\omega V^2A-\frac{3\pi}{4}VH=0. \tag{2.24}$$

We therefore see that the leading order driving term enters the equation in proportion to the velocity, which means that the wobbling is only sustained while the kink is moving. Since $D_2V=-2\Gamma V$, the kink will stop moving for values of γ of order ε^2. However, to check for higher order terms which might sustain the motion of the kink for smaller damping, we shall continue our perturbation expansion.

The zeroth harmonic component of the solution at $\mathcal{O}\left(\varepsilon^3\right)$ is

$$\varphi_3^{(0)}=-4H(A+A^*)(\operatorname{sech}X_0+\operatorname{sech}^3X_0),$$

and the solution for the first harmonic component is

$$\varphi_3^{(1)}=-\partial_2AX_0\operatorname{sech}X_0\tanh X_0+u_1(X_0)|A|^2A+\tfrac{1}{2}V^2AX_0\operatorname{sech}X_0(2\operatorname{sech}^2X_0-1)+i\omega VHu_2(X_0),$$

where $u_1(X_0)$ is the bounded solution of

$$\begin{aligned}(\mathcal{L}-3/2)u_1(X_0)=&-\frac{3}{2}k_1\operatorname{sech}X_0\tanh X_0\\&+6\operatorname{sech}X_0\tanh^2X_0\left(3X_0\operatorname{sech}^2X_0-\frac{5}{2}\operatorname{sech}^2X_0\tanh X_0-f_1(X_0)\right)\end{aligned}$$

and $u_2(X_0)$ is the bounded solution of

$$(\mathcal{L}-3/2)u_2(X_0)=-4\operatorname{sech}^2X_0\tanh X_0+\frac{3}{4}\pi\operatorname{sech}X_0\tanh X_0.$$

u_1, u_2 and all subsequent functions denoted u_n are determined numerically, using the method of variation of parameters and numerical integration.

Since $\mathcal{L}$ is parity-preserving and the right hand side above is odd, it follows that $u_1(X_0)$ is odd. Knowing this allows us to conclude that definite integrals involving u_1 multiplied by an even function evaluate to zero. Such integrals occur in higher order solvability conditions.

We choose $\partial_2A=0$. In fact, the situation is the same at higher orders, and for the greatest simplicity we may set $\partial_nA=0$ for all $n\geq 2$.

For the second harmonic component we must solve

$$\begin{aligned}(\mathcal{L}-6)\varphi_3^{(2)}=&(\partial_1B+2i\omega VB)\partial_0f_1(X_0)-2i\omega D_1Bf_1(X_0)\\&-6HA\operatorname{sech}X_0\tanh^2X_0(1-2\operatorname{sech}^2X_0).\end{aligned} \tag{2.25}$$

The asymptotic behaviour of $f_1(X_0)$ is as follows:

$$f_1(X_0) \sim \begin{cases} e^{-ikX_0} & \text{for } X_0 \gg 0 \\ e^{ikX_0} & \text{for } X_0 \ll 0. \end{cases}$$

This is the same asymptotic behaviour as the second harmonic homogeneous solutions given by equation (2.5) with $p = k = \sqrt{8}$. Hence, the first two terms on the right-hand side of (2.25) are resonant with the homogeneous solutions for large $|X_0|$, and lead to unbounded solutions of (2.25). They must therefore be suppressed. Plugging the asymptotic expressions for f_1 into the right hand side of (2.25), we see that the right hand side will vanish for large $|X_0|$ (i.e. $X_1 \neq 0$) if

$$\begin{aligned} -ik(\partial_1 B + 2i\omega VB) - 2i\omega D_1 B = 0 \quad \text{for } X_1 > 0 \\ ik(\partial_1 B + 2i\omega VB) - 2i\omega D_1 B = 0 \quad \text{for } X_1 < 0, \end{aligned}$$

that is,

$$D_1 B = \begin{cases} -\frac{k}{\omega}(\partial_1 B + 2i\omega VB) & \text{for } X_1 > 0 \\ \frac{k}{\omega}(\partial_1 B + 2i\omega VB) & \text{for } X_1 < 0, \end{cases} \tag{2.26}$$

or, writing as a single equation,

$$D_1^2 B = \frac{k^2}{4\omega^2}\partial_1^2 B + \frac{ik^2 V}{\omega}\partial_1 B - k^2 V^2 B. \tag{2.27}$$

This describes the propagation of an unchanging profile to the right for positive X_1 and to the left for negative X_1, at the group velocity of the radiation, $\frac{k}{\omega}$. Recall that B is forced at the origin by the condition $B|_{X_1=0} = A^2$; this equation describes the spreading of the envelope outwards in both directions, in such a way that the 'phase velocity' of B is equal to the group velocity of the linear radiation waves. There will, of course, be further contributions to this equation from higher order terms, which will turn the equation into a nonlinear Schrödinger equation. At this stage, however, the equation is not affected by the nonlinearity and would be predicted by standard linear wave theory for the operator $\frac{1}{2}D_0^2 + \mathcal{L}$.

The fact that $D_1 A = 0$, and that we are not interested in initial transients, means that we can, without inconsistency, set

$$D_1 B = 0, \quad \text{and} \quad \partial_1 B + 2i\omega VB = 0 \tag{2.28}$$

individually.

With the conditions (2.28) in place, the second harmonic component of the solution is

$$\varphi_3^{(2)} = EHf_3(X_0),$$

where E is a further variable dependent on the slow scales, such that $E(0,0,\ldots,T_1,\ldots) = A$, and higher orders of the expansion give the equations for propagation of variations of A along E. f_3 has been calculated:

$$f_3(X_0) = \tfrac{1}{2}\operatorname{sech}X_0 - 4\operatorname{sech}^3 X_0 - \tfrac{15}{32}ip(3-\tanh^2 X_0 + ip\tanh X_0)(J_1^*(X_0) - J_1^\infty)e^{ipX_0} + \tfrac{15}{32}ip(3-\tanh^2 X_0 - ip\tanh X_0)J_1(X_0)e^{-ipX_0}.$$

The function $J_1(X_0)$ is as previously defined in (2.12). One can show that $f_3(X_0)$ is an even function.

It will not be necessary to calculate the third harmonic component, as this does not contribute to the zeroth harmonic at $\mathcal{O}(\varepsilon^5)$, which is our ultimate goal.

At fourth order in ε, we find that the solvability condition for the zeroth harmonic gives $D_3V = 0$, and the solvability condition for the first harmonic gives $D_3A = 0$. These hold exactly; despite the fact that numerically-determined functions u_1 and f_1 are integrated, parity considerations mean that the integrands are odd and hence when integrated over an infinite interval, they evaluate to zero.

The zeroth harmonic component of the solution is

$$\varphi_4^{(0)} = |A|^4 u_3(X_0) + |B|^2 u_4(X_0) + \frac{1}{2}V^2|A|^2\left(6X_0^2\operatorname{sech}^2 X_0\tanh X_0 - 7X_0\operatorname{sech}^2 X_0 + 6X_0\operatorname{sech}^4 X_0\right) + \frac{1}{8}V^4\left(3X_0\operatorname{sech}^2 X_0 - 2X_0^2\operatorname{sech}^2 X_0\tanh X_0\right) - i\omega VH(A-A^*)u_5(X_0) + H^2(9X_0\operatorname{sech}^2 X_0 - 3\tanh X_0 - 8\operatorname{sech}^2 X_0\tanh X_0)$$

where $u_3(X_0)$, $u_4(X_0)$ and $u_5(X_0)$ are the bounded solutions of the following equations:

$$\begin{aligned}
\mathcal{L}u_3 &= -3\operatorname{sech}^2 X_0\tanh^2 X_0\left[f_1(X_0) + f_1^*(X_0)\right] - 6\operatorname{sech}^4 X_0\tanh^2 X_0(2\tanh X_0 - 3X_0) \\
&\quad - 6\operatorname{sech}X_0\tanh^2 X_0\left[u_1(X_0) + u_1^*(X_0)\right] - 3\operatorname{sech}^4 X_0\tanh X_0(2\tanh X_0 - 3X_0)^2, \\
\mathcal{L}u_4 &= -6\tanh X_0|f_1(X_0)|^2, \\
\mathcal{L}u_5 &= 4\operatorname{sech}X_0\tanh X_0(\operatorname{sech}^2 X_0 + 1) + 6\operatorname{sech}X_0\tanh^2 X_0 u_2(X_0).
\end{aligned}$$

Again, it follows from parity considerations that these three functions are odd.

For the first harmonic component the solution is

$$\varphi_4^{(1)} = -\frac{1}{2}i\omega VA\left(k_1|A|^2+V^2\right)X_0\operatorname{sech}X_0\tanh X_0 + HA^2u_6(X_0) + HB^2u_7(X_0) + H|A|^2u_8(X_0)$$
$$+ HV^2\left(u_9(X_0) + 2X_0\operatorname{sech}^2X_0\tanh X_0 - \frac{3}{4}\pi X_0\operatorname{sech}X_0\tanh X_0\right)$$
$$+ (\Gamma - i\omega R)VAX_0\operatorname{sech}X_0\tanh X_0 - \frac{2}{3}i\omega H(\Gamma+i\omega R)(3-4\operatorname{sech}^2X_0)$$

where u_6 to u_9 are the bounded functions which satisfy the following differential equations:

$$(\mathcal{L}-3/2)u_6 = 3\operatorname{sech}^2X_0\tanh^2X_0(7+10\operatorname{sech}^2X_0) + 12\operatorname{sech}^2X_0\tanh X_0 f_1(X_0),$$
$$(\mathcal{L}-3/2)u_7 = -6\tanh X_0 f_1(X_0),$$
$$(\mathcal{L}-3/2)u_8 = -6\operatorname{sech}^2X_0\tanh^2X_0(1-2\operatorname{sech}^2X_0) + 24\operatorname{sech}^2X_0\tanh^2X_0(1+\operatorname{sech}^2X_0)$$
$$-6\operatorname{sech}^2X_0\tanh X_0(2\tanh X_0 - 3X_0)(1-2\operatorname{sech}^2X_0),$$
$$(\mathcal{L}-3/2)u_9 = 3\partial_0u_2(X_0).$$

In order to avoid secular terms for the second harmonic component, the following conditions must hold:

$$i\omega D_2B = \begin{cases} -\frac{1}{2}ik\partial_2B + 5V^2B - i\omega B(\Gamma+2i\omega R) & \text{for } X_2>0 \\ \frac{1}{2}ik\partial_2B + 5V^2B - i\omega B(\Gamma+2i\omega R) & \text{for } X_2<0, \end{cases} \tag{2.29}$$

as well as

$$D_1E = 0 \quad \text{and} \quad \partial_1E + 2i\omega VE = 0.$$

These were obtained in the same way as (2.26) for the second harmonic component of ϕ_3. This time, however, we cannot choose $D_2B=0$, because $D_2A\neq 0$ and hence we must keep (2.29) as they stand in order to avoid secular terms.

Note that whenever B, C or E is multiplied by a localised function (i.e. one which tends exponentially to zero as $|X_0|\to\infty$), the result is equal to zero unless $X_1=X_2=\ldots=0$, since if this is not the case, $X_0\to\infty$ as $\varepsilon\to 0$. Therefore, in such a case we can replace B, C and E by their values at $X_1=X_2=\ldots=0$, i.e.

$$B(0,0,\ldots,T_1,\ldots) = A^2,$$
$$C(0,0,\ldots,T_1,\ldots) = A^3 \text{ and}$$
$$E(0,0,\ldots,T_1,\ldots) = A.$$

The second, third and fourth harmonics of ϕ_4 will not be calculated as they cannot influence the zeroth harmonic at $\mathcal{O}\left(\varepsilon^5\right)$, whose solvability condition is

$$D_4V = -\tfrac{3}{2}Hk_3|A|^2A + c.c. + 2\Gamma V^3 + \tfrac{3\pi}{4}i\omega H\Gamma(A-A^*) + \tfrac{9\pi}{4}RH(A+A^*) + 2\Gamma RV, \quad (2.30)$$

where

$$k_3 = -2.005 - 0.3823i.$$

Writing $a = \varepsilon A$ as before, we have the amplitude equations in terms of the unscaled parameters:

$$\frac{da}{dt} = -\gamma a - i\omega\rho a - \tfrac{1}{2}i\omega k_1|a|^2a - \tfrac{1}{2}i\omega v^2a + \tfrac{3\pi}{4}vh + \mathcal{O}\left(\varepsilon^5\right) \quad (2.31a)$$

For the velocity, we have two equations, (2.23) and (2.30), for the behaviour of V over different timescales. To combine these, recall the chain-rule expansion of the derivative:

$$\frac{\partial}{\partial\tau} = D_0 + \varepsilon D_1 + \varepsilon^2 D_2 + \varepsilon^3 D_3 + \varepsilon^4 D_4 + \ldots$$

(converting back to a derivative with respect to t involves multiplying by $\frac{d\tau}{dt} = \frac{dT}{dt} = 1+\rho$.) This yields

$$\frac{dv}{dt} = -2\gamma v - \tfrac{3}{2}k_3h|a|^2a + c.c. + 2\gamma v^3 + \tfrac{3\pi}{4}i\omega h\gamma(a-a^*) + \tfrac{9\pi}{4}\rho h(a+a^*) + \mathcal{O}\left(\varepsilon^7\right). \quad (2.31b)$$

It is essential to combine the slow-scale equations in this way before solving them, rather than solving the individual equations with the assumption that the different scales are independent. This does not work because in integrating the equations one is covering more than one timescale.

The presence of the driving term in the velocity equation (2.31b) shows that the driving does, in fact, sustain the translational motion of the kink and hence that, contrary to the predictions in refs [127] and [128], the resonance at the driving frequency ω does exist. This would seem to suggest that the ability of the driving to move the kink has something to do with the radiation modes, which are neglected in the variational analysis in [127] and [128]. Further evidence for this notion comes from the fact that $\mathcal{O}\left(\varepsilon^5\right)$, which is the first order at which driving enters the velocity equation, is also the lowest order at which the effects of the second harmonic radiation have an influence on the zeroth harmonic (although their first contribution to the zeroth harmonic is at $\mathcal{O}\left(\varepsilon^4\right)$, they have the wrong parity to enter the solvability condition).

The system of equations (2.31a) and (2.31b) is too complicated to analyse in detail here. We have simply performed a rudimentary numerical investigation which suggests that this three-dimensional system (remember that a is complex) always settles to a fixed point – either the

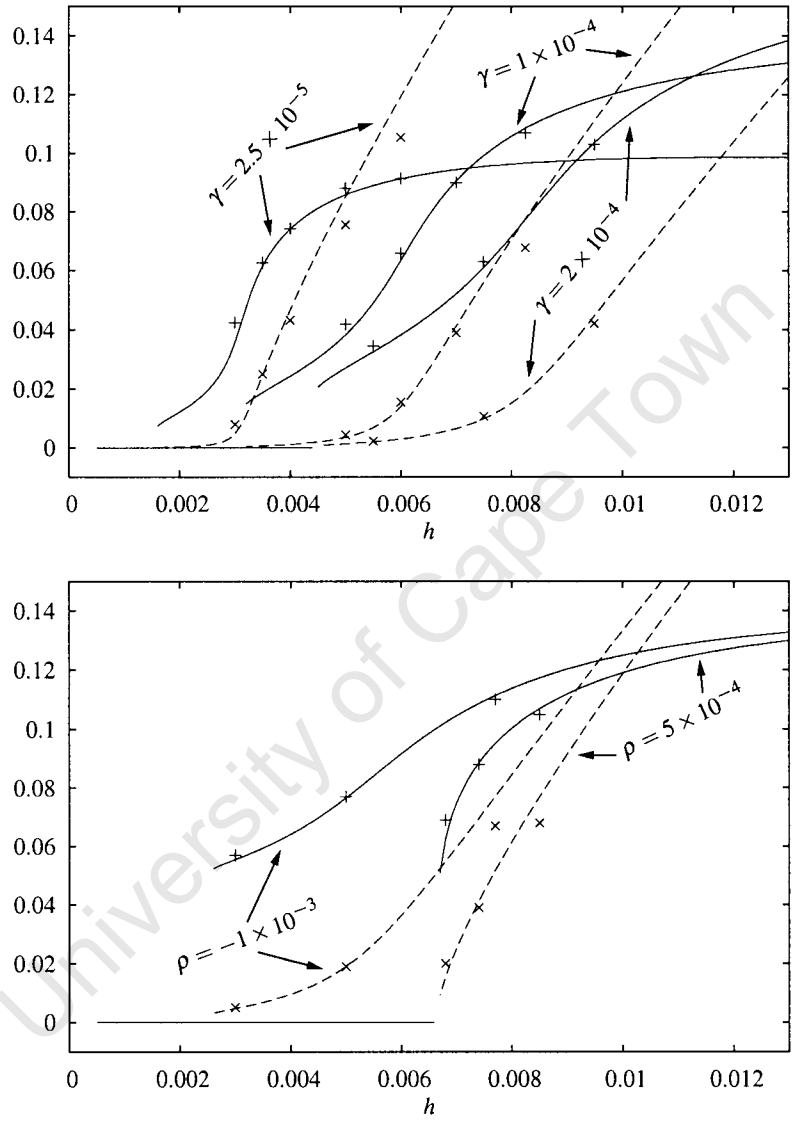

Figure 2.1: Long-term behaviour of the amplitude equations (2.31) for direct driving near the natural wobbling frequency. As a function of h, the solid lines show values of $|a|$ and the dashed lines values of v. The crosses are measured values of $|a|$ (+) and v (×) from numerical simulations of the original PDE, to be described in section 2.5. In the top panel, ρ is fixed at zero and three values of γ are considered, while in the bottom panel, $\gamma = 1 \times 10^{-4}$ and two values of ρ are selected.

origin or a nonzero fixed point if the driving strength h exceeds some critical value dependent on the damping γ and detuning ρ. Figure 2.1 summarises this $t \to \infty$ asymptotic behaviour as the parameters are varied.

Up to $\mathcal{O}(\varepsilon^2)$, the perturbation expansion gives

$$\phi(x,t) = \tanh x + a\,\mathrm{sech}\,x\tanh x e^{i\Omega t} + c.c. + |a|^2\,\mathrm{sech}^2 x(2\tanh x - 3x) + \frac{1}{2}v^2 x\,\mathrm{sech}^2 x + h(1-2\,\mathrm{sech}^2 x)e^{i\Omega t} + c.c. + \left[b^2 f_1(x) + h f_2(x)\right] e^{2i\Omega t} + c.c. + \mathcal{O}(\varepsilon^3).$$

2.4.2 Driving frequency near $\omega/2$

We again consider the case of direct driving, but at *half* the natural wobbling frequency:

$$\frac{1}{2}\phi_{tt} - \frac{1}{2}\phi_{xx} + \gamma\phi_t - \phi + \phi^3 = h\cos(\tfrac{\Omega}{2}t).$$

As before, $\Omega = \omega(1+\rho)$ and we keep the same scalings for the small parameters h, γ and ρ:

$$h = \varepsilon^2 H, \quad \gamma = \varepsilon^2\Gamma \quad \text{and} \quad \rho = \varepsilon^2 R.$$

Again we transform the time variable so that $\Omega t = \omega T$ and transform the equation into the moving frame. This gives

$$(1+\rho)^2\left[\frac{1}{2}\phi_{\tau\tau} - v\phi_{\xi\tau} - \frac{1}{2}v_\tau\phi_\xi\right] - \frac{1}{2}(1-v^2)\phi_{\xi\xi} + \gamma(1+\rho)\left(\phi_\tau - v\phi_\xi\right) - \phi + \phi^3 = h\cos\left(\tfrac{\omega}{2}\tau\right).$$

As before we have

$$\phi_0 = \tanh X_0$$
$$\phi_1 = A\,\mathrm{sech}\,X_0\tanh X_0 e^{i\omega T_0} + c.c.$$

At $\mathcal{O}(\varepsilon^2)$ the equation is

$$\frac{1}{2}D_0^2\phi_2 + \mathcal{L}\phi_2 = (\partial_0\partial_1 - D_0D_1)\phi_1 - 3\phi_0\phi_1^2 + \frac{1}{2}D_1V\partial_0\phi_0 + \frac{H}{2}e^{i\frac{\omega}{2}T_0} + c.c.$$

The only term on the right hand side which differs from the undamped, undriven case is the driving term. Therefore, splitting into simple harmonics in the usual way, we have to solve

$$(\mathcal{L} - 3/8)\varphi_2^{(1/2)} = \frac{H}{2}.$$

Now, $3/8$ is not an eigenvalue of $\mathcal{L}$, so by the Fredholm alternative there is always one bounded solution to this equation. To find it, we need the homogeneous solutions of this equation, i.e. solutions of

$$\mathcal{L}f = \frac{3}{8}f.$$

As mentioned previously, Segur's solution (2.5) for eigenvalues in the continuous spectrum also works for $\lambda < 2$. In our case, $\lambda = 3/8$ and so p^2 in (2.5) equals $2(3/8-2) = -13/4$. Substituting $p = \pm i\sqrt{\frac{13}{4}}$ into (2.5) gives the two real homogeneous solutions. We then use the method of variation of parameters to determine a particular solution. The unique bounded solution is

$$\varphi_2^{(1/2)} = \frac{4}{13}H(1-8\operatorname{sech}^2 X_0).$$

The other harmonics of ϕ_2 are the same as in the undamped, undriven case:

$$\varphi_2^{(0)} = |A|^2\operatorname{sech}^2 X_0(2\tanh X_0 - 3X_0) + \frac{1}{2}V^2 X_0\operatorname{sech}^2 X_0,$$
$$\varphi_2^{(1)} = 0 \text{ and } \varphi_2^{(2)} = Bf_1(X_0).$$

We also obtain $D_1V = 0$ and $D_1A = 0$ from the solvability conditions, as before.

The equation at $\mathcal{O}(\varepsilon^3)$ is

$$\frac{1}{2}D_0^2\phi_3 + L\phi_3 = (\partial_0\partial_1 - D_0D_1)\phi_2 + (\partial_0\partial_2 - D_0D_2)\phi_1 + \frac{1}{2}(\partial_1^2 - D_1^2)\phi_1 - \phi_1^3 - 6\phi_0\phi_1\phi_2$$
$$+VD_0\partial_0\phi_2 + VD_0\partial_1\phi_1 + VD_1\partial_0\phi_1 + \frac{1}{2}D_2V\partial_0\phi_0 - \frac{1}{2}V^2\partial_0^2\phi_1 - \Gamma D_0\phi_1 + \Gamma V\partial_0\phi_0 - RD_0^2\phi_1.$$

The right hand side now contains terms at frequencies $\frac{1}{2}\omega$ and $\frac{3}{2}\omega$. We shall not calculate the fractional harmonic components of the solution for ϕ_3, however, since there are no solvability conditions associated with them, and nor will they contribute to the solvability conditions at $\mathcal{O}(\varepsilon^4)$.

The solvability conditions at $\mathcal{O}(\varepsilon^3)$ are

$$D_2V = -2\Gamma V$$

for the zeroth harmonic, and

$$D_2A = -\Gamma A - i\omega RA - \tfrac{1}{2}i\omega k_1|A|^2A - \tfrac{1}{2}i\omega V^2A \tag{2.32}$$

for the first harmonic. The driving does not enter this equation, so we shall continue to higher orders.

At $\mathcal{O}(\varepsilon^4)$ the solvability conditions are

$$D_3 V = 0$$

and

$$D_3 A = i\omega \tfrac{60}{169}\pi H^2. \tag{2.33}$$

We now have two amplitude equations, (2.32) and (2.33), for the behaviour of A over different timescales. We combine these as before by using the chain-rule expansion of the time derivative to obtain

$$\frac{da}{dt} = -\gamma a - i\omega\rho a - \tfrac{1}{2}i\omega k_1 |a|^2 a - \tfrac{1}{2}i\omega v^2 a + \tfrac{60}{169}i\omega\pi h^2 + \mathcal{O}(\varepsilon^5) \tag{2.34a}$$

$$\frac{dv}{dt} = -2\gamma v + \mathcal{O}(\varepsilon^5). \tag{2.34b}$$

The first three orders of the perturbation expansion give

$$\phi(x,t) = \tanh x + a\,\mathrm{sech}\, x \tanh x e^{i\Omega t} + c.c. + |a|^2 \mathrm{sech}^2 x(2\tanh x - 3x) + \frac{1}{2}v^2 x \mathrm{sech}^2 x + \frac{4}{13}h(1 - 8\,\mathrm{sech}^2 X_0)e^{i\frac{\Omega}{2}T_0} + b^2 f_1(x)e^{2i\Omega t} + c.c. + \mathcal{O}(\varepsilon^4).$$

Yet again, as in both cases of parametric driving considered, the velocity equation is dominated by the damping if it is sufficiently large, and the amplitude equation (2.34a) provides a valid long-term description of the kink dynamics. If $v = 0$, a always approaches a (nonzero) fixed point, as in the case of parametric driving at frequency ω. In fact, our amplitude equation has exactly the same form as that one, but with a driving term proportional to h^2 rather than h.

2.4.3 Discussion

Intuitively, the reason that the driving does not couple directly to the wobbling mode in the case of direct driving (as it did in the case of parametric driving at the frequency ω) is the discrepancy in the parity of the driving profile and the wobbling mode.

The driving term enters the amplitude equation (2.31a) for direct driving near ω in proportion to vh, whereas in the case of the superharmonic resonance [see equation (2.34a)], it enters in proportion to h^2. Comparison of the relative strengths of the two resonances is difficult; if $v \sim O(\varepsilon)$ and $h \sim O(\varepsilon^2)$, the resonance at ω appears to be stronger. However, when driving at ω we have to keep the damping small so as not to overshadow the driving term in the velocity

equation, whereas in the $\omega/2$ case, it is not necessary for the velocity to be nonzero for the driving and hence wobbling to be sustained.

Parametric driving at the frequency 2ω couples to the wobbling mode through frequency halving manifest in our perturbation expansion in the term $\phi_0\phi_1\phi_2$. This term has the same parity as ϕ_2, which contains the driving profile. Hence we would expect in the direct driving case, where the driving has even parity, to have no resonance (or a weaker one due to a higher order term) at 2ω, since the driving is even here. In contrast, we would expect the superharmonic resonance at frequency $\omega/2$ to occur in the parametric driving case, since the driving of the wobbling mode comes from the term $\phi_0\phi_2^2$ where ϕ_2 contains the driving profile. This term is odd whether the driving is odd or even, so we would expect to have a driving term in the amplitude equation proportional to h^2. This would, however, be weaker than either of the two parametric resonances we have dealt with, where the driving terms are proportional to h and ha.

2.5 Numerical simulations

The partial differential equation

$$\frac{1}{2}\phi_{tt} - \frac{1}{2}\phi_{xx} + [\gamma + \lambda(x)]\phi_t - [1 + h_p\cos(\Omega t)]\phi + \phi^3 = h_d\cos(\Omega t) \tag{2.35}$$

was simulated by approximating the derivatives with finite differences on a grid of step size 0.1 in x and 0.05 in t. To simulate parametric or direct driving, h_d or h_p, respectively, can be set to zero. In order to prevent the radiation reflecting back from the boundaries of the system (we used free-end boundary conditions), damping was introduced near the edges to absorb the radiation. That is, the damping coefficient consists of the usual constant term γ plus an absorbing gasket $\lambda(x)$, defined as follows:

$$\lambda(x) = \begin{cases} \left[\frac{x-(L-100)}{100}\right]^4 & \text{for } x \geq L-100 \\ \left[\frac{x+(L-100)}{100}\right]^4 & \text{for } x \leq -L+100 \\ 0 & \text{otherwise} \end{cases}$$

The simulation was performed on the interval $x \in [-L, L]$, where L was chosen large enough to prevent the kink exiting the domain of integration. Typical values of L were of the order of 1000.

The position of the kink was measured from the zero crossing, and the amplitude of the wobbling mode was measured by taking the profile $\phi(x,t)$, subtracting the kink $\tanh[x - x_0(t)]$,

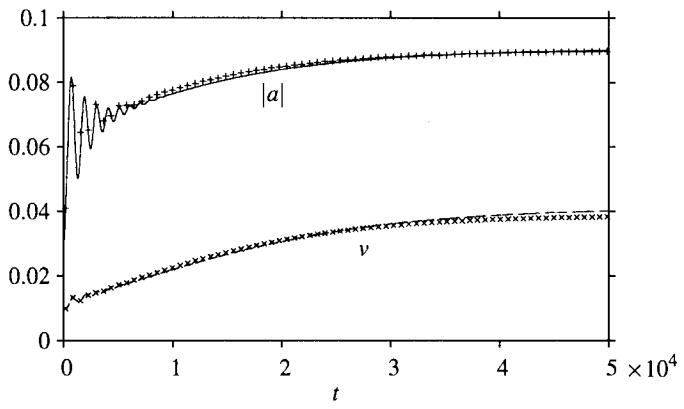

Figure 2.2: An example of the kink being accelerated by the direct driving at frequency ω. Here $h = 0.007$, $\gamma = 10^{-4}$ and $\rho = 0$. The crosses are measured values from numerical simulations of the original PDE, while the lines are the predictions of the amplitude equations. The slight discrepancy is attributable to higher-order terms. Note the separate timescales, with $|a|$ settling fast to equilibrium on the T_2 scale while v creeps gradually upwards on the T_4 scale.

and assuming the odd component of what remains to be the first harmonic wobbling mode, $a\,\mathrm{sech}\,X_0 \tanh X_0 e^{i\omega\tau}$. This technique is, of course, only a first order approximation because of the higher order terms in the perturbation expansion. Interpolation and smoothing were applied to counter the effects of the discreteness of the x values and the various oscillations occurring on the fast time scale.

The results of our numerical simulations of the undamped, undriven kink and the four cases of damped, driven kinks match the predictions of our amplitude equations. In particular, see figure 2.2 for numerical verification of our assertion that the resonance of the equation directly driven at the natural frequency exists. Refer also to figure 2.1 where numerical measurements verify the predictions of the asymptotic behaviour of the amplitude equations.

2.6 Chaos?

Chaotic kink dynamics have been reported in [127, 128] for the superharmonic resonance of the directly driven kink. Our results, however, do not corroborate this claim. We have not observed any chaos in numerical simulations and, as we discuss below, our amplitude equations do not predict the emergence of chaos.

Consider the amplitude equations (2.19), (2.22), (2.34) and (2.31). The first three become

two-dimensional dynamical systems when the velocity decays to zero, and so do not admit chaotic solutions. In the fourth, we do have a genuine three-dimensional system. However, the leading-order dynamics occur on the T_2 timescale in the equation for a but only on the T_4 timescale in the equation for v. This means that (for small ε) v is effectively a constant on the T_2 timescale and hence that no chaotic behaviour can occur on this timescale. Indeed, equation (2.31a) will quickly settle to a fixed point whose position is a function of the slowly-varying v. On the T_4 timescale, then, a is enslaved to v (i.e. is a function of v only) because, as v varies on the slow timescale, a will always settle immediately to a fixed point on the faster timescale. Equation (2.31b) is therefore effectively decoupled from (2.31a) and so the dynamics of v follow a 1-dimensional, albeit highly nonlinear, differential equation. Chaos is therefore not possible in the case of direct driving near ω either, at least for small ε.

It is on the basis of numerical simulations of the partial differential equation that the authors of [127, 128] claim to have observed chaotic behaviour, backed up by intuitive explanations based on the variational approach. In their numerical simulations, the energy of the full system is shown to increase for a time, while the position of the kink remains fixed, and then starts to exhibit 'chaotic' features, while the kink begins to wander erratically. We suggest that this irregular behaviour is merely the result of second-harmonic radiation returning to the kink and interfering with it after having travelled to the ends of the domain and reflecting back.

The variational approach breaks down at resonance with zero damping, where it predicts unbounded growth of the wobbling amplitude a (see ref. [127, 128]). The true behaviour of the PDE, the authors claim, is to exhibit chaotic behaviour. Our amplitude equations, however, do not predict this unbounded growth, which is arrested by the term $-\frac{1}{2}i\omega k_1|a|^2a$. This shows that the emission of radiation has the effect of damping the wobbling. In summary, when the damping is zero our amplitude equations do not break down and so do not allow the possibility that the real behaviour of the PDE is different to that predicted.

Figure 2.3 shows the numerical simulation of the directly driven, undamped kink using parameter values equivalent to those used to produce figure 1 of [127], in which chaotic behaviour is purportedly illustrated. In our scheme, the radiation emitted from the kink is absorbed at the ends of the domain as described in section 2.5, and no chaotic behaviour is evident.

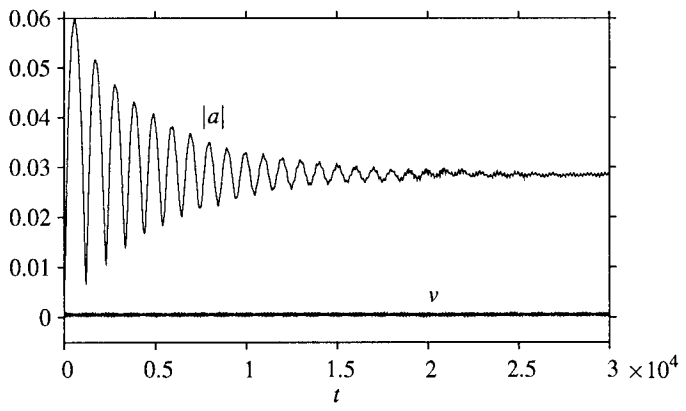

Figure 2.3: Measured wobbling amplitude and velocity from the numerical simulation of equation (2.35) with $h_d = 0.01$, $h_p = 0$, $\gamma = 0$ and $\Omega = \sqrt{2} \cdot 0.6100$ (this value is close to $\omega/2$). These parameters are equivalent to those used in figure 1 of [127] (our equations differ by a rescaling of x and t). No chaotic behaviour is in evidence.

2.7 Conclusion

We have shown that, in the case of direct driving near the natural wobbling frequency ω, the wobbling can only be sustained if the kink performs translational motion and that this translational motion can be sustained if the damping is not too great. We have suggested that the radiation plays a vital role in this resonance, and indeed the fact that translational motion is essential lends further support to this suggestion, as a stationary kink would have radiation escaping symmetrically from the core.

We predict regular, non-chaotic behaviour of the kink near all resonances. In [127], where chaotic dynamics were reported, the authors go on to conclude that, during the transient time of regular motion (when the kink velocity is zero) the internal mode of the kink is storing up energy, to be released when it reaches a state of saturation, via the translational mode – and attribute the onset of the kink's irregular motion to this mechanism. They furthermore propose that the mechanism which brings about the surprising superharmonic resonance is the coupling of the translation mode and the wobbling mode.

Our intuitive explanation for this is rather different: The superharmonic resonance arises simply from the frequency doubling effect of the nonlinearity, and the simultaneous altering of the parity of the driving profile by the nonlinearity, so as to produce a smaller, odd driving profile at the resonant frequency of the wobbling mode. This mechanism would seem, therefore,

to be unrelated to the translation mode.

Finally, we have provided an intuitive explanation for the parametric resonance at the wobbling frequency, namely that since the wobbling mode is a perturbation of the static kink, the parametric driving term becomes, to leading order, a direct driving term with odd parity. Since the parity of the wobbling mode is also odd, this explains why this resonance is the strongest of all, with the driving term appearing at $\mathcal{O}(h)$ in the amplitude equation.

Chapter 3

Travelling kinks in discrete ϕ^4 models

In this chapter we study *discrete* versions of the ϕ^4 model considered in chapter 2. There, we were successful in characterising radiation generated by the oscillations of the wobbling mode, and (as we have discussed), discrete solitary waves generically emit very small radiation as they pass over the lattice; our aim in this chapter is to detect this radiation in order to find out whether radiationless or 'sliding' solitons can exist for various different discretisations.

3.1 Introduction

Spatially discretised partial differential equations (or, equivalently, chains of coupled ordinary differential equations) have attracted considerable attention recently. One of the issues that has been vigorously debated and that will concern us in this chapter, is whether discrete systems can support solitary waves travelling without losing energy to resonant radiation and decelerating as a result. We address this issue for one of the prototype models of nonlinear physics, the ϕ^4-theory:

$$u_{tt} = u_{xx} + \frac{1}{2}u(1-u^2). \tag{3.1}$$

Since the early 1960s, this equation has been one of the workhorses of statistical mechanics [49] and quantum field theory [50]. Its kink solution, together with the sine–Gordon kink, are the simplest examples of topological solitons.

The ϕ^4-equation (3.1) is Lorentz-invariant, and so the existence of the travelling kink

$$u(x,t) = \tanh\frac{x-vt-s}{2\sqrt{1-v^2}}, \tag{3.2}$$

where $|v| < 1$ and $s \in \mathbb{R}$, is an immediate consequence of the existence of the stationary kink for $v = 0$. On the other hand, if we discretise equation (3.1) in x,

$$\ddot{u}_n = \frac{u_{n+1} - 2u_n + u_{n-1}}{h^2} + f(u_{n-1}, u_n, u_{n+1}), \tag{3.3}$$

the translation and Lorentz invariances are lost, and the existence of the travelling kink (and even of an arbitrarily centred stationary one) becomes a nontrivial matter. In equation (3.3), h is the lattice spacing, and the nonlinearity $f(u_{n-1}, u_n, u_{n+1})$ satisfies the continuity condition

$$f(u, u, u) = \frac{1}{2}u(1 - u^2). \tag{3.4}$$

We restrict ourselves to symmetric discretisations, i.e.

$$f(u_{n-1}, u_n, u_{n+1}) = f(u_{n+1}, u_n, u_{n-1}). \tag{3.5}$$

Equation (3.1) results from (3.3) in the continuum limit, where $u_n(t) = u(x_n, t)$, $x_n = nh$ and $h \to 0$. In this limit, the truncation error of the Taylor series is $\mathcal{O}(h^2)$. We shall be concerned with the discrete kink solutions of (3.3), which approach the continuous kink (3.2) as $h \to 0$.

For a variety of discrete nonlinearities f, eq. (3.3) admits stationary kink solutions [160, 161]. The discrete ϕ^4 kinks have been used to describe incommensurate systems and narrow domain walls in ferroelectrics and ferromagnets, structural phase transitions, topological excitations in biological macromolecules and hydrogen-bonded chains, and polymerisation mismatches in polymers [148, 162, 163, 164, 165]. Physically, one of the most significant properties of domain walls and topological defects is their mobility [161]; however whether the discrete equations (3.3) can admit travelling kinks remains an open question [119, 115, 116, 117, 131, 166, 167, 168, 169, 170].

The most common, one-site discretisation of the nonlinearity function in (3.3) is given by

$$f(u_{n-1}, u_n, u_{n+1}) = \frac{1}{2}u_n(1 - u_n^2). \tag{3.6}$$

It is a well established fact [171], however, that the discrete Klein–Gordon equation (3.3) with (3.6) admits only a countable set of stationary monotonic kinks with the boundary conditions

$$\lim_{n \to -\infty} u_n(t) = -1, \qquad \lim_{n \to +\infty} u_n(t) = +1. \tag{3.7}$$

Physically, this fact is related to the presence of the Peierls–Nabarro barrier, an effective potential periodic with the spacing of the lattice. Half of the stationary kinks are centred at the

minima (the on-site kinks) and the other half (the off-site kinks) at the maxima of the Peierls–Nabarro potential. There are no continuous families of stationary discrete kinks of the form $u_n = u(n-s)$, with s a free parameter, which would interpolate between the two solutions. We will be calling such families 'translationally invariant kinks' – an abuse of terminology because translation invariance is a property of an equation rather than a solution, and all lattice equations are of course *not* translationally invariant. As for propagating waves, of special importance are kinks moving at constant speed and without the emission of radiation. We will be referring to such kinks, i.e. solutions of the form $u_n = u(n-vt-s)$ where $u(\xi)$ is a monotonically growing function satisfying the boundary conditions (3.7), as *sliding kinks*, to emphasise the fact that they do not experience any radiative friction. Being an obstacle to the 'translational invariance' of static kinks, the Peierls–Nabarro barrier is also detrimental to the existence of sliding kinks – at least for small v (see reviews in [172] and [173]).

In an attempt to find a discrete model with 'translationally invariant' and sliding kinks, Speight and Ward [115, 116] considered a hamiltonian discretisation of the form

$$f(u_{n-1},u_n,u_{n+1}) = \frac{1}{12}(2u_n+u_{n+1})\left(1-\frac{u_n^2+u_nu_{n+1}+u_{n+1}^2}{3}\right) + \frac{1}{12}(2u_n+u_{n-1})\left(1-\frac{u_n^2+u_nu_{n-1}+u_{n-1}^2}{3}\right). \tag{3.8}$$

In the static limit, the corresponding energy admits a topological lower bound which is saturated by a first- (rather than second-) order difference equation. This equation is readily shown to have a one-parameter continuous family of stationary kink solutions $u_n = u(n-s)$ for $0 \le h \le 2$ (see Proposition 1 in [116]). The parameter s of the family defines the position of the kink relative to the lattice. Since all members of the family have the same (lowest attainable) energy, the stationary kink experiences no Peierls–Nabarro barrier. As for travelling kinks, Speight and Ward's numerical simulations tentatively suggest that moving kinks never become pinned to the lattice (and hence that they stop shedding energy as radiation), although they do initially emit Cherenkov radiation, and decelerate as a result (see figures 4 and 5 in [116]).

Another line of attack was chosen by Bender and Tovbis [132] who proposed a different discretisation supporting a continuous family of arbitrarily centred stationary kinks:

$$f(u_{n-1},u_n,u_{n+1}) = \frac{1}{4}(u_{n+1}+u_{n-1})(1-u_n^2). \tag{3.9}$$

In this case, the family arises due to the suppression of the stationary kink's resonant radiation.

In fact, the family of stationary kinks can be found explicitly as

$$u_n(t) = \tanh\left[a(n-s)\right], \tag{3.10}$$

where $a = \operatorname{arcsinh}(h/2)$ for all $h \in \mathbb{R}$. (The solution (3.10) coincides with the stationary dark soliton of the repulsive Ablowitz-Ladik equation [174].)

Another nonlinearity,

$$f(u_{n-1}, u_n, u_{n+1}) = \frac{1}{8}\left(u_{n+1} + u_{n-1}\right)\left(2 - u_{n+1}^2 - u_{n-1}^2\right), \tag{3.11}$$

was introduced by Kevrekidis [131], who demonstrated the existence of a two-point invariant and hence a first-order difference equation associated with the stationary equation. Consequently, the discretisation (3.11) also supports a continuous family of stationary kinks for all $h \in [0, h_0]$ with some $h_0 > 0$. The two-point invariant of the model (3.11) corresponds to a conserved discrete *momentum* [131], which is not normally available in a lattice equation. (For further investigations in this direction, see [175].)

Finally, we mention that one other way to generate nonlinear Klein–Gordon models with translationally-invariant kinks is through the method of Flach, Zolotaryuk and Kladko [119] (discussed in section 1.5.2); however, due to the inverse nature of the method there is no systematic way to generate discretisations which reduce to the ϕ^4 equation in the continuum limit, so we shall not be considering such nonlinearities in this chapter. Exceptional (i.e. 'translation-invariant') discretisations will be investigated further in chapter 4. See also refs [117] and [176].

Since the reasons for the nonexistence of 'translation-invariant' kinks and of sliding kinks are apparently related (the breaking of symmetries of the underlying continuum theory or, speaking physically, the presence of the Peierls–Nabarro barrier), the availability of 'translation-invariant' stationary kinks in the models (3.8), (3.9) and (3.11) suggests that they might have sliding kinks as well. Here it is our purpose to find out whether this is indeed the case. We shall analyse the persistence of continuous families of stationary kinks $u_n = u(n-s)$ for nonzero velocities; in other words, examine the existence of solutions of the form $u(n - vt - s)$ where $u(z)$ is a monotonically growing function satisfying (3.7) (i.e., has no oscillating tails), and $v \neq 0$. We develop an accurate numerical test in the limit $h \to 0$ which shows whether or not standing and sliding kinks of the discrete ϕ^4 model (3.3) bifurcate from the exact kink solutions (3.2) of its continuous counterpart (3.1). The analysis of this bifurcation poses a singular problem in perturbation theory which can be analysed using two (inner and outer) matched asymptotic scales on the complex plane [137, 138]. In particular, the nonvanishing of the Stokes constant in the

inner asymptotic equation serves as a sufficient condition for the non-existence of continuous solutions of the difference equations [138].

Our test will be based on computing the Stokes constant for the differential-difference equation underlying the lattice system. We will examine the four discretisations of the ϕ^4 theory reproduced above, i.e. equations (3.6), (3.8), (3.9) and (3.11). Since translationally invariant stationary kinks $u_n = u(n-s)$ do exist for the three exceptional nonlinearities (3.8), (3.9) and (3.11), the Stokes constant is *a priori* vanishing for $v = 0$ in these three cases. However, we will show that in all three cases the Stokes constant acquires a nonzero value as soon as v deviates from zero. It remains nonzero for all v except a few isolated values which define the particular velocities of the sliding kinks in the corresponding model. There is one such isolated zero of the Stokes constant for the nonlinearity (3.8) and three *sliding velocities* for the discretisation (3.11). Consequently, the main conclusion of this work is that the sliding kinks, i.e. kinks travelling at a constant speed without the emission of radiation, can occur only at particular values of the velocity. The sliding velocities are, of course, functions of the discretisation spacing h, so that sliding kinks arise along continuous curves on the (v,h)-plane.

We conclude this introduction with a remark on a convention adopted for the remainder of this chapter: namely, that the linear part of the function $f(u_{n-1},u_n,u_{n+1})$ in (3.3) can always be fixed to $\frac{1}{2}u_n$ without loss of generality. Indeed, the most general function satisfying (3.4) and (3.5) is $f = \left(\frac{1}{2}-2a\right)u_n + a(u_{n+1}+u_{n-1}) + \text{cubic terms}$, where a is arbitrary. Since h^2 in (3.3) is also a free parameter, we can always make a replacement $h \to \tilde{h}$ such that $1/h^2 + a = 1/\tilde{h}^2$. This gives

$$f(u_{n-1},u_n,u_{n+1}) = \frac{1}{2}u_n - Q(u_{n-1},u_n,u_{n+1}), \tag{3.12}$$

where Q is a homogeneous polynomial of degree 3 which is independent of the parameter h.

The outline of this chapter is as follows. In the next section (section 3.2) we describe the construction of the outer and inner asymptotic solutions in the limit $h \to 0$. Section 3.3 contains details of the numerical computation of the Stokes constants while the last section (section 3.4) summarises the results of our work.

3.2 Inner and outer asymptotic expansions in the limit $h \to 0$

We are looking for a sliding-kink solution of the discrete ϕ^4 models (3.3) in the form

$$u_n(t) = \phi(z), \qquad z = h(n-s) - vt, \tag{3.13}$$

where $\phi(z)$ is assumed to be a twice differentiable function of $z \in \mathbb{R}$ that satisfies the differential advance-delay equation

$$v^2\phi''(z) = \frac{\phi(z+h) - 2\phi(z) + \phi(z-h)}{h^2} + \frac{1}{2}\phi(z) - Q(\phi(z-h), \phi(z), \phi(z+h)), \tag{3.14}$$

with the boundary conditions $\phi(z) \to \pm 1$ as $z \to \pm\infty$. The velocity v is assumed to be smaller than 1 in modulus. If a solution to this boundary-value problem (i.e. a heteroclinic orbit) exists, then the parameter s is arbitrary due to the translation invariance of the advance-delay equation (3.14).

3.2.1 Outer asymptotic series

We begin by considering the Taylor series for the second difference,

$$\phi(z+h) - 2\phi(z) + \phi(z-h) = h^2\phi''(z) + \sum_{n=2}^{\infty} h^{2n} \frac{2}{(2n)!} \phi^{(2n)}(z). \tag{3.15}$$

Since the cubic polynomial $Q(u_{n-1}, u_n, u_{n+1})$ satisfies the continuity and symmetry relations (3.4) and (3.5), the nonlinearity of (3.14) can be expanded in the following Taylor series:

$$Q(\phi(z-h), \phi(z), \phi(z+h)) = \frac{1}{2}\phi^3(z) + \sum_{n=1}^{\infty} h^{2n} Q_{2n}\left(\phi, (\phi')^2, \ldots, \phi^{(2n)}\right), \tag{3.16}$$

where the coefficients Q_{2n} depend on even derivatives and even powers of odd derivatives of $\phi(z)$, and also $Q_{2n}(\phi, 0, \ldots, 0) = 0$. The differential advance-delay equation (3.14) can thus be written as

$$(1-v^2)\phi'' + \frac{1}{2}\phi(1-\phi^2) + \sum_{n=1}^{\infty} h^{2n}\left(\frac{2}{(2n+2)!}\phi^{(2n+2)} - Q_{2n}\left(\phi, (\phi')^2, \ldots, \phi^{(2n)}\right)\right) = 0. \tag{3.17}$$

For $h = 0$, equation (3.17) becomes the travelling wave reduction of the continuous model (3.1), with the explicit solution

$$\phi_0(z) = \tanh\xi; \quad \xi = \frac{z}{2\sqrt{1-v^2}}, \quad |v| < 1. \tag{3.18}$$

We will search for solutions of equation (3.17) of the form

$$\phi(z) = \phi_0(z) + \sum_{n=1}^{\infty} h^{2n}\phi_{2n}(z). \tag{3.19}$$

Substituting the expansion (3.19) into (3.17) we get, at order h^{2n},

$$\mathcal{L}\phi_{2n} = H_{2n},$$

where the linearised operator $\mathcal{L}$ is given by

$$\mathcal{L} = -\frac{d^2}{d\xi^2} + 4 - 6\,\mathrm{sech}^2\,\xi,$$

and H_{2n} are polynomials in $\phi_0, \phi_2, \ldots, \phi_{2n-2}$ and their derivatives. The kernel of $\mathcal{L}$ is one-dimensional, and spanned by an even eigenfunction $y_0 = \mathrm{sech}^2\,\xi$. The rest of the spectrum of $\mathcal{L}$ is positive. It is not difficult to prove by induction that if $\phi_{2k}(z)$ are all odd in z for $k = 0, 1, \ldots, n-1$, the nonhomogeneous term H_{2n} is also odd in z and hence, by the Fredholm alternative, there exists a unique odd bounded solution $\phi_{2n}(z)$ for $z \in \mathbb{R}$. Moreover, since H_{2n} decays to zero exponentially fast as $|z| \to \infty$, the function $\phi_{2n}(z)$ is also exponentially decaying for any $n \geq 1$. The perturbation $\phi_2(z)$ in particular satisfies the nonhomogeneous equation

$$\mathcal{L}\phi_2 = -\frac{1}{3}\left(\phi_0^{(\mathrm{iv})} + \alpha\phi_0'' + \beta\phi_0^2\phi_0'' + \gamma\phi_0(\phi_0')^2\right), \tag{3.20}$$

where the numerical coefficients depend on whether the nonlinearity function f is given by (3.6), (3.8), (3.9) or (3.11):

One-site (3.6):	$\alpha = \beta = \gamma = 0;$
Speight–Ward (3.8):	$\alpha = 1,\ \beta = \gamma = -4;$
Bender–Tovbis (3.9):	$\alpha = 3,\ \beta = -3,\ \gamma = 0;$
Kevrekidis (3.11):	$\alpha = 3,\ \beta = -9,\ \gamma = -6.$

The odd bounded solution $\phi_2(z)$ of the nonhomogeneous equation (3.20) is:

$$\phi_2(z) = \mathcal{A}\tanh\xi\,\mathrm{sech}^2\,\xi + \mathcal{B}\xi\,\mathrm{sech}^2\,\xi, \tag{3.21}$$

where

$$\mathcal{A} = \frac{(1-v^2)(\gamma+2\beta)+6}{72(1-v^2)^2}, \qquad \mathcal{B} = -\frac{(1-v^2)(\alpha+\beta)+1}{24(1-v^2)^2}.$$

We point out that the series (3.19) is asymptotic; it may or may not converge [137, 138], depending on the choice of v and Q in equation (3.14). We shall be referring to (3.19) as the outer asymptotic expansion.

Since, as mentioned above, all terms in the outer expansion at $\mathcal{O}\left(h^2\right)$ and higher decay to zero, any oscillatory terms which conflict with the boundary condition $\phi(z) \to \pm 1$ are smaller than all powers of h^2. Asymptotic analysis *beyond* all orders of perturbation theory was pioneered by Kruskal and Segur [52, 177] and has been utilised by many authors. It was extended by Pomeau, Ramani and Grammaticos [133] to allow the computation of radiation coefficients from Borel summation of series rather than from the numerical solution of differential equations. Essentially the same method has been applied to different problems by Grimshaw and Joshi [134, 135] and Tovbis and collaborators [136, 137, 138, 139]. In this work, we shall work with formal inner and outer asymptotic series for the problem (3.14) without attempting rigorous analysis of their asymptoticity.

3.2.2 Inner asymptotic series

The leading-order term (3.18) of the outer expansion (3.17) has poles at $\xi = \frac{\pi i}{2}(1+2n)$, where $n \in \mathbb{Z}$. We apply the scaling transformation

$$z = h\zeta + i\pi\sqrt{1-v^2}, \qquad \phi(z) = \frac{1}{h}\psi(\zeta) \tag{3.22}$$

to equation (3.14) in order to study the convergence of the formal asymptotic solution (3.19) near the pole $\xi = \frac{i\pi}{2}$ (see [137, 138]). This yields the following differential advance-delay equation for $\psi(\zeta)$:

$$v^2\psi''(\zeta) = \psi(\zeta+1) - 2\psi(\zeta) + \psi(\zeta-1) - Q(\psi(\zeta-1), \psi(\zeta), \psi(\zeta+1)) + \frac{h^2}{2}\psi(\zeta). \tag{3.23}$$

The following are the cubic functions Q for each of the four discretisations that we deal with in this chapter:

$$\begin{aligned}
\text{One-site (3.6):} \quad & Q = \frac{1}{2}\psi^3(\zeta); \\
\text{Speight–Ward (3.8):} \quad & Q = \frac{1}{36}\left[\psi^3(\zeta+1) + 3\psi^2(\zeta+1)\psi(\zeta) + 3\psi(\zeta+1)\psi^2(\zeta)\right. \\
& \left. +4\psi^3(\zeta) + 3\psi(\zeta-1)\psi^2(\zeta) + 3\psi^2(\zeta-1)\psi(\zeta) + \psi^3(\zeta-1)\right]; \\
\text{Bender–Tovbis (3.9):} \quad & Q = \frac{1}{4}\psi^2(\zeta)\left[\psi(\zeta+1) + \psi(\zeta-1)\right]; \\
\text{Kevrekidis (3.11):} \quad & Q = \frac{1}{8}\left[\psi^3(\zeta+1) + \psi^2(\zeta+1)\psi(\zeta-1) + \psi(\zeta+1)\psi^2(\zeta-1)\right. \\
& \left. +\psi^3(\zeta-1)\right].
\end{aligned}$$

We note that the heteroclinic orbit becomes small as $h \to 0$ under the normalisation (3.22): If $\phi(z) \to \pm 1$ as $z \to \pm\infty$, then $\psi(\zeta) \to \pm h$ as $\mathrm{Re}\,\zeta \to \pm\infty$. The asymptotic series (3.19) in the new variables (3.22) becomes

$$\psi(\zeta) = \psi_0(\zeta) + \sum_{n=1}^{\infty} h^n \psi_n(\zeta), \tag{3.24}$$

where each term $\psi_n(\zeta)$ can be expanded in a formal series in descending powers of ζ. In particular, the leading-order function $\psi_0(\zeta)$ has the general form

$$\hat{\psi}_0(\zeta) = \sum_{n=0}^{\infty} \frac{a_{2n}}{\zeta^{2n+1}}. \tag{3.25}$$

We use the hat in (3.25) to differentiate this asymptotic series (which may only converge in the limit $\zeta \to \infty$) from a convergent solution of eq. (3.23) in the limit $h \to 0$. By comparing the series (3.24) and (3.25) with the solutions (3.18) and (3.21) in variables (3.22), we note the correspondence:

$$a_0 = 2\sqrt{1-v^2}, \qquad a_2 = -\frac{(1-v^2)(\gamma+2\beta)+6}{9\sqrt{1-v^2}}.$$

We shall be referring to (3.24) as the inner asymptotic expansion. The odd powers of h in the inner asymptotic expansion (3.24) appear due to the matching conditions with the outer asymptotic expansion (3.19) under the scaling (3.22), as well as due to the non-zero boundary conditions for the heteroclinic orbits: $\psi(\zeta) \to \pm h$ as $\mathrm{Re}\,\zeta \to \pm\infty$.

3.2.3 Leading-order problem for an inner solution

Convergence of the formal inverse-power series (3.25) for the leading-order solution $\psi_0(\zeta)$ depends on the values of the Stokes constants [138]. Computation of the Stokes constants is based on Borel–Laplace transforms of the inner equation (3.23) [137]. Assuming continuity in h, we study the leading-order solution $\psi_0(\zeta) = \lim_{h\to 0} \psi(\zeta)$ of the truncated inner equation

$$v^2 \psi_0''(\zeta) = \psi_0(\zeta+1) - 2\psi_0(\zeta) + \psi_0(\zeta-1) - Q(\psi_0(\zeta-1), \psi_0(\zeta), \psi_0(\zeta+1)). \tag{3.26}$$

By substituting the series (3.25) into equation (3.26), one can derive a recurrence relation between the coefficients in the set $\{a_n\}_{n=0}^{\infty}$. The Stokes constants can be computed from the asymptotic behaviour of the coefficients a_n for large n. Alternatively, the leading-order solution $\psi_0(\zeta)$ and the Stokes constants can be defined by using the Laplace transform

$$\psi_0(\zeta) = \int_{\gamma} V_0(p) e^{-p\zeta} dp. \tag{3.27}$$

The choice of the contour of integration γ determines the domain of $\psi_0(\zeta)$ in the complex ζ-plane: If (3.27) were a traditional Laplace transform (i.e., with the path γ being the positive real axis) then, in general, it would not converge for $\mathrm{Re}\,\zeta < 0$. However, we require the integral in (3.27) to converge for all ζ along the line $-\infty < \mathrm{Re}\,\zeta < \infty$, $\mathrm{Im}\,\zeta < 0$ so that it corresponds to the continuation of a function defined on the whole real z axis. This can be achieved by choosing the contour γ so that $\arg p \to \pi/2$ as $|p| \to \infty$ along γ: Then, for all ζ along the infinite line of fixed negative $\mathrm{Im}\,\zeta$, we have $e^{-p\zeta} \to 0$ as $|p| \to \infty$ and so the integral converges provided that $V_0(p)$ is bounded.

We now define two solutions $\psi_0^{(s)}(\zeta)$ and $\psi_0^{(u)}(\zeta)$, which lie on the stable and unstable manifolds respectively, such that

$$\lim_{\mathrm{Re}\,\zeta \to +\infty} \psi_0^{(s)}(\zeta) = 0, \qquad \lim_{\mathrm{Re}\,\zeta \to -\infty} \psi_0^{(u)}(\zeta) = 0. \tag{3.28}$$

We note that the stable and unstable solutions tend to the stationary point at the origin, since the heteroclinic orbits connect the stationary points at $\psi = \pm h$ which move to the origin as $h \to 0$. The three stationary points coalesce to become a degenerate stationary point at the origin within the truncated inner equation (3.26).

The Laplace transform (3.27) produces the stable solution $\psi_0^{(s)}(\zeta)$ when the contour of integration γ_s lies in the first quadrant of the complex p-plane and extends from $p = 0$ to $p = \infty$. Similarly, it produces the unstable solution $\psi_0^{(u)}(\zeta)$ when the contour of integration γ_u lies in the second quadrant. Since, as discussed, we must choose the integration contours in such a way that $\arg p \to \pi/2$ as $p \to \infty$, it follows that γ_s and γ_u must be as shown in figure 3.1.

The Borel transform $V_0(p)$ satisfies the following integral equation, which follows from (3.26) and (3.27):

$$\left(4\sinh^2\frac{p}{2} - \nu^2 p^2\right) V_0(p) = \hat{Q}\left[V_0(p)\right]. \tag{3.29}$$

Here, $\hat{Q}[V(p)]$ denotes a double convolution of $V(p)$ with itself (in this case, the hat is used to denote an operator). We list below the convolutions $\hat{Q}[V(p)]$ for each of the four models under

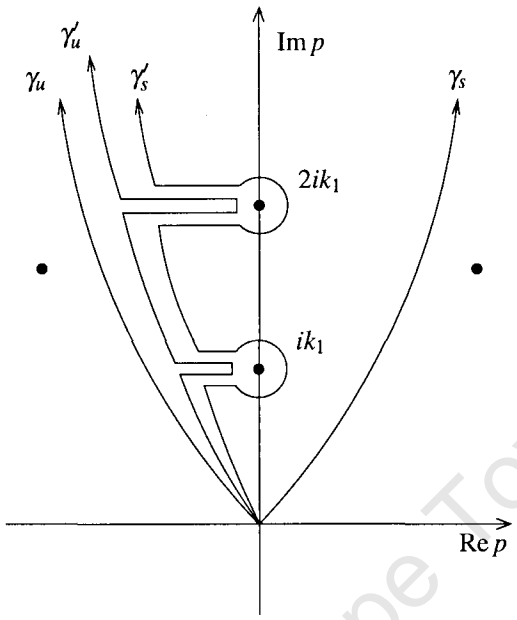

Figure 3.1: Contours of integration for the stable and unstable solutions $\psi_0^{(s)}$ and $\psi_0^{(u)}$. The curves γ_s' and γ_u' are deformations of the contours γ_s and γ_u respectively.

consideration:

$$\begin{aligned}
\text{One-site (3.6):} \quad & 2\hat{Q} = V(p) * V(p) * V(p); \\
\text{Speight–Ward (3.8):} \quad & 18\hat{Q} = \cosh p\ [V(p) * V(p) * V(p)] + 3\{\cosh p\ [V(p) * V(p)]\} * V(p) \\
& \quad + 3[\cosh p\, V(p)] * V(p) * V(p) + 2V(p) * V(p) * V(p); \\
\text{Bender–Tovbis (3.9):} \quad & 2\hat{Q} = [\cosh p\, V(p)] * V(p) * V(p); \\
\text{Kevrekidis (3.11):} \quad & 4\hat{Q} = \cosh p\ [V(p) * V(p) * V(p)] \\
& \quad + [\cosh p\, V(p)] * [e^{p} V(p)] * \left[e^{-p} V(p)\right],
\end{aligned}$$

where the asterisk $*$ denotes the convolution integral for the Laplace transform,

$$V(p) * W(p) = \int_0^p V(p - p_1) W(p_1) dp_1,$$

and the integration is performed from the origin to the point p on the complex plane, along the contour γ. In deriving (3.29), we have made use of the convolution theorem for the Laplace transform of the form (3.27), where the integration is over a contour in the complex plane rather than a positive real axis. The theorem states that

$$f(\zeta) g(\zeta) = \int_\gamma [F(p) * G(p)] e^{-p\zeta} dp. \tag{3.30}$$

The proof is provided in appendix 3.A at the end of this chapter. It depends on the integration contour being concave-up (as it clearly is – see fig. 3.1) and on the function $G(p)$ having no singularities between the contour and the imaginary axis, which is ensured by our requirement that the path lie above all the singularities with nonzero real part.

The inverse power series (3.25) for the limiting solution $\psi_0(\zeta)$ becomes the following power series for the Borel transform $V_0(p)$:

$$\hat{V}_0(p) = \sum_{n=0}^{\infty} c_{2n} p^{2n}, \qquad c_{2n} = \frac{a_{2n}}{(2n)!}, \tag{3.31}$$

where $c_0 = a_0 = 2\sqrt{1-v^2}$. The hat differentiates the power series, which might only converge for some values of p, from a general solution of (3.29). The virtue of the integral form (3.29) is that the limiting behaviour of c_n for large n can be related to singularities of $V_0(p)$, which in turn correspond to the oscillatory tails of $\psi_0(\zeta)$.

If the sliding kink exists, its perturbation expansion will converge due to the absence of radiation, and so its continuation, the inverse-power series for $\psi_0(\zeta)$, will converge for all $\zeta \in \mathbb{C}$ such that $\operatorname{Im}\zeta < 0$. This implies that the stable and unstable solutions $\psi_0^{(s)}(\zeta)$ and $\psi_0^{(u)}(\zeta)$ coincide, i.e. that the contour γ_s in the right half of the complex p-plane can be continuously deformed to the contour γ_u in the left half-plane (see figure 3.1). If, however, there are any singularities between the two contours, then a continuous deformation is possible only if the residues are zero. The residues are proportional to the values of the Stokes constants. When the Stokes constants are nonzero, the formal power series (3.31) for the solution $V_0(p)$ of the integral equation (3.29) diverges for some values of p in the sector between the contours γ_s and γ_u.

3.2.4 Stokes constants

The Borel transform $V_0(p)$ is singular near the points in the p-plane where the coefficient in front of $V_0(p)$ on the left-hand side of the integral equation (3.29) vanishes [138], except for the point $p = 0$ where the right hand side is also zero. That is, singularities occur when $(2/p)\sinh(p/2) = \pm v$. The location of these singularities is important because the stable and unstable solutions are not, in fact, uniquely defined by (3.28); different solutions are generated depending on where the contours lie relative to the singularities of $V_0(p)$ with $\operatorname{Re} p \neq 0$. Exploiting this nonuniqueness, we wish to choose the contours γ_s and γ_u to lie above all the singularities with nonzero real part; this will minimise the number of singularities between the stable and unstable solutions.

It is not difficult to show that the contour γ_s extending from 0 to ∞ can be chosen in such a way, i.e. so that that there are no singularities between it and the imaginary axis. Indeed, assume, for definiteness, that $v > 0$. Let $(2n_v - 1)$ be the number of positive roots of the equation $\sin q = vq$ and denote the real and imaginary parts of $p/2$ by κ and q: $p/2 = \kappa + iq$. In the (κ, q)-plane, consider a rectangular region $\mathcal{D}$ bounded by the horizontal segments $q = 2\pi n$ and $q = \varepsilon$ at the top and bottom, and vertical segments $\kappa = -\varepsilon$ and $\kappa = \varepsilon$ on the left and right. Here n is any positive integer greater than n_v and $\varepsilon > 0$ is taken to be small. Using the argument principle, we can count the number of (complex) roots of the equation $\sinh(p/2) = v(p/2)$ in the region $\mathcal{D}$. We have

$$\tan \arg \frac{p}{2} = \frac{\cosh \kappa \sin q - vq}{\sinh \kappa \cos q - v\kappa}.$$

On the right lateral side, where $\kappa = \varepsilon$, this becomes

$$\tan \arg \frac{p}{2} \approx \frac{1}{\varepsilon} \frac{\sin q - vq}{\cos q - v}. \tag{3.32}$$

As we move from $q = \varepsilon$ to $q = 2\pi n$, the numerator in (3.32) will change sign $(2n_v - 1)$ times. In a similar way, moving down along the left side there will be $(2n_v - 1)$ more zero crossings, while no zero crossings will occur along the horizontal segments. This means that the argument can change by no more than $(4n_v - 2)\pi$ and hence there are at most $(2n_v - 1)$ roots in the region $\mathcal{D}$, no matter how large n is. Similarly, we can show that the equation $\sinh(p/2) = -v(p/2)$ has no more than $2n_v$ roots in the region $\mathcal{D}$, if $2n_v$ is the number of positive roots of $\sin q = -vq$. The upshot is that for any finite v, there are only a finite number of singularities with small real parts: the singularities cannot accumulate to the imaginary axis. For $v \neq 0$, the singularities with nonzero real parts lie on the curves

$$q = \pm \sqrt{\frac{1}{v^2} \cosh^2 \kappa - \kappa^2 \coth^2 \kappa} \to \pm \frac{1}{v} \cosh \kappa \quad \text{as } |\kappa| \to \infty.$$

Accordingly, in order for the integration contours γ_s and γ_u to lie above these singularities, they must be curvilinear (and not just rays) as shown in figure 3.1.

Having chosen the contours γ_s and γ_u to lie above the singularities in the first and second quadrants respectively, the only singularities of $V_0(p)$ that determine whether the stable solution $\psi_0^{(s)}(\zeta)$ can be continuously transformed into the unstable solution $\psi_0^{(u)}(\zeta)$ are those at non-zero pure imaginary values of p. We will be referring to these values as resonances. The set of resonances $\mathcal{R}_v$ is defined by the transcendental equation

$$\mathcal{R}_v = \left\{ p = ik, k \in \mathbb{R}_+ : \quad \frac{2}{k} \sin \frac{k}{2} = \pm v \right\}. \tag{3.33}$$

When $v = 0$, the set $\mathcal{R}_0$ is infinite-dimensional and can be described explicitly:

$$\mathcal{R}_0 = \{p = 2\pi ni, \quad n \in \mathbb{N}\}.$$

Let $p_1 = ik_1$ be the smallest imaginary root in the set $\mathcal{R}_v$. It is clear from (3.33) that $0 < k_1 < 2\pi$ for $v \in (0,1)$, so that $k_1 \to 2\pi$ as $v \to 0^+$ and $k_1 \to 0$ as $v \to 1^-$. The set of resonances $\mathcal{R}_v$ is finite-dimensional for $v \in (0,1)$ and it consists of only one root $p_1 = ik_1$ for $v \in (v_1, 1)$, where $v_1 \approx 0.22$.

Due to the resonances, a function $\psi_0(\zeta)$ that satisfies the truncated inner equation (3.26) may have oscillatory tails as $|\mathrm{Re}\,\zeta| \to \infty$. Adding the solutions of equation (3.26) linearised about $\hat{\psi}_0(\zeta)$, the general bounded solution of (3.26) in the limit $|\zeta| \to \infty$ can be represented as [137]:

$$\psi_0(\zeta) = \hat{\psi}_0(\zeta) + \sum_{ik_n \in \mathcal{R}_v} \alpha_n \hat{\varphi}_n(\zeta) e^{-ik_n\zeta} + \text{multiple harmonics}. \tag{3.34}$$

Here, $\hat{\psi}_0(\zeta)$ is given by the power series (3.25); α_n are coefficients which we will be referring to as amplitudes in what follows; $k_n > 0$ are roots of (3.33) for $p = ik_n$, and the functions $\hat{\varphi}_n(\zeta)e^{-ik_n\zeta}$, $n \geq 1$, satisfy the linearised truncated inner equation (3.26). In particular, the equation for the leading-order term $\hat{\varphi}_1(\zeta)$ is

$$\begin{aligned} e^{-ik_1}\hat{\varphi}_1(\zeta+1) + (v^2k_1^2 - 2)\hat{\varphi}_1(\zeta) + e^{ik_1}\hat{\varphi}_1(\zeta-1) + 2iv^2k_1\hat{\varphi}_1'(\zeta) - v^2\hat{\varphi}_1''(\zeta) \\ = D_1Q\,\hat{\varphi}_1(\zeta-1) + D_2Q\,\hat{\varphi}_1(\zeta) + D_3Q\,\hat{\varphi}_1(\zeta+1), \end{aligned} \tag{3.35}$$

where $D_{1,2,3}Q$ are the partial derivatives of $Q(\psi_0(\zeta-1), \psi_0(\zeta), \psi_0(\zeta+1))$ with respect to its first, second and third argument respectively, evaluated at $\psi_0 = \hat{\psi}_0(\zeta)$.

If the amplitude α_n is nonzero for some n, the inverse-power series (3.25) does not converge because the solution (3.34) does not decay as $|\mathrm{Re}\,\zeta| \to \infty$. The amplitudes α_n will be shown to be proportional to the 'Stokes constants' computed for the inverse-power series (3.25) or, equivalently, its Laplace transform (3.31). Each oscillatory term in the sum (3.34) becomes exponentially small in h when we transform from ζ to z using the transformation (3.22). Since $p_1 = ik_1$ is the element of $\mathcal{R}_v$ with the smallest imaginary part, it follows that the $n = 1$ term dominates the sum in (3.34) when the transformation (3.22) is made (unless $\alpha_1 = 0$). Furthermore, when $v \in (v_1, 1)$, where $v_1 \approx 0.22$, it is the *only* term in the sum since the resonant set $\mathcal{R}_v$ consists of just the one root $p_1 = ik_1$. We shall, therefore, only be concerned with the leading-order Stokes constant, which multiplies the function $\hat{\varphi}_1(\zeta)$.

If $\hat{\psi}_0(\zeta)$ is given by the inverse-power series (3.25), the solution of the linearised equation (3.35) can be represented by a similar series:

$$\hat{\varphi}_1(\zeta) = \zeta^r \sum_{\ell=0}^{\infty} b_\ell \zeta^{-\ell}, \tag{3.36}$$

where we can set $b_0 = 1$ due to the linearity of (3.35). Substituting (3.25) and (3.36) into (3.35) and using (3.33), the coefficient b_1 can be determined from

$$\begin{aligned} &2ir\zeta^{r-1}\left(\nu^2 k_1 - \sin k_1\right) \\ &\quad + \zeta^{r-2}\left[r(r-1)(\cos k_1 - \nu^2) + 2ib_1(r-1)(\nu^2 k_1 - \sin k_1) - 6(1-\nu^2)\right] + \mathcal{O}\left(\zeta^{r-3}\right) = 0. \end{aligned}$$

In this equation, the coefficient of each power of ζ should be set to zero. In order to set the coefficient in front of the first term to zero in the situation where $\nu \neq 0$, we must choose $r = 0$. The second term then gives

$$b_1 = \frac{3i(1-\nu^2)}{\nu^2 k_1 - \sin k_1},$$

after which all the other coefficients $b_2, b_3, \ldots$, can be computed recursively. On the other hand, in the situation with $\nu = 0$, we have $k_1 = 2\pi$ and the coefficient in front of ζ^{r-1} is zero regardless of the value of r. Setting the coefficient in front of ζ^{r-2} to zero requires that we choose either $r = 3$ or $r = -2$, and hence we have two different descending-power series, one starting with ζ^3 and the other one with ζ^{-2}. We shall focus on the former as it dominates the latter in the limit $\zeta \to \infty$. Again, the succeeding terms in (3.36) are determined recursively.

Thus, we have established that the leading-order oscillatory term in the expansion (3.34) behaves as

$$\begin{cases} \alpha_1 \left[1 + \dfrac{b_1}{\zeta} + \mathcal{O}\left(\dfrac{1}{\zeta^2}\right)\right] e^{-ik_1\zeta} & \text{for } \nu \neq 0 \text{ and} \\ \alpha_1 \left[\zeta^3 + b_1\zeta^2 + \mathcal{O}\left(\zeta^1\right)\right] e^{-2\pi i\zeta} & \text{for } \nu = 0. \end{cases} \tag{3.37}$$

For $\nu \neq 0$, the two leading order terms in the expression above are generated by, respectively, a simple pole and a logarithmic singularity of the Borel transform $V_0(p)$ at $p = ik_1$. For $\nu = 0$ they are generated by a quadruple pole of $V_0(p)$ at $p = 2\pi i$. From the fact that V_0 is an even function of p, we deduce the structure of this function near the poles:

$$V_0(p) \to \begin{cases} \dfrac{k_1^2 K_1(\nu)}{p^2 + k_1^2} - \sigma(\nu)\ln(p^2 + k_1^2) + \ldots & (\text{for } \nu \neq 0) \\ \dfrac{6(2\pi)^8 S_1}{\left(p^2 + 4\pi^2\right)^4} + \dfrac{2(2\pi)^6 \rho}{\left(p^2 + 4\pi^2\right)^3} + \ldots & (\text{for } \nu = 0) \end{cases} \tag{3.38}$$

as $p \to \pm ik_1$. Here $K_1(\nu)$ and S_1 are the leading-order Stokes constants for $\nu \neq 0$ and $\nu = 0$, respectively; $\sigma(\nu)$ and ρ are independent of p, and ... stands for terms with even slower growth as $p \to ik_1$.

To show that these singularities do indeed give rise to the oscillatory tails in (3.37), we compare the two integrals $\psi_0^{(s)}$ and $\psi_0^{(u)}$ for a given value of ζ. To this end, we deform the paths of integration γ_s and γ_u to γ_s' and γ_u' respectively, without crossing any singularities. This is illustrated in figure 3.1. There are two contributions to the difference $\psi_0^{(s)}(\zeta) - \psi_0^{(u)}(\zeta)$. The first comes from integrating around the pole at $p = ik_1$, and is equal to $2\pi i$ times the residue of the function $V_0(p)e^{-p\zeta}$ at $p = ik_1$, determined from (3.38). The second contribution arises because the *integrand* increases as the singularity is encircled, since it is a branch point of the logarithm. Since $\ln z$ can be written as $\ln|z| + i\arg z$, where $z = p - ik_1$, we see that $V_0(p)$ increases by $-2\pi i\sigma(\nu)$ as the branch point $p = ik_1$ is encircled in the $\nu \neq 0$ case. Therefore, the difference in the integrand of (3.27) along the paths γ_s' and γ_u' is $-2\pi i\sigma(\nu)e^{-p\zeta}$, which must be integrated along the path of integration from $p = ik_1$ to infinity, to give $-2\pi i\sigma(\nu)e^{-ik_1\zeta}/\zeta$. (We have considered the integration on a Riemann surface in order to account for branch points.) Adding together the two contributions discussed above, we have

$$\psi_0^{(s)}(\zeta) - \psi_0^{(u)}(\zeta) = \begin{cases} \left[\pi k_1 K_1(\nu) - \dfrac{2\pi i\sigma(\nu)}{\zeta} + \mathcal{O}\left(\dfrac{1}{\zeta^2}\right)\right] e^{-ik_1\zeta} & \text{for } \nu \neq 0 \\ -\frac{1}{128}\left[16\pi^3 iS_1\zeta^3 + (192\pi^4 S_1 + \rho)\zeta^2 + \mathcal{O}\left(\zeta^1\right)\right] e^{-2\pi i\zeta} & \text{for } \nu = 0. \end{cases} \tag{3.39}$$

If we take the limit $\mathrm{Re}\,\zeta \to -\infty$, then the unstable solution $\psi_0^{(u)}(\zeta)$ decays to zero as a power law, according to the expansion (3.25). Thus, the stable solution $\psi_0^{(s)}(\zeta)$ has the oscillatory tail given by the representation (3.34) with the amplitude factor

$$\alpha_1 = \begin{cases} \pi k_1 K_1(\nu) & \text{for } \nu \neq 0 \\ -\dfrac{i\pi^3}{8} S_1 & \text{for } \nu = 0. \end{cases} \tag{3.40}$$

Similarly, if we take the limit $\mathrm{Re}\,\zeta \to +\infty$, then the stable solution $\psi_0^{(s)}(\zeta)$ decays to zero, while the unstable solution $\psi_0^{(u)}(\zeta)$ has the representation (3.34) with the amplitude factor given by the negative of expression (3.40). By comparing the other terms on the right-hand side of (3.39) to the corresponding terms in (3.37), $\sigma(\nu)$ and ρ can be uniquely determined.

We now match the leading-order singular behaviour of $V_0(p)$ near $p = \pm ik_1$, given by (3.38),

to the formal power series (3.31). Expanding the expressions in (3.38) as power series gives us

$$V_0(p) \to \begin{cases} K_1(\nu) - \sigma(\nu)\ln(k_1^2) + \ldots \\ \qquad + \sum_{n=1}^{\infty} (-1)^n k_1^{-2n} \left(K_1(\nu) + \dfrac{\sigma(\nu)}{n} + \ldots \right) p^{2n} & \text{for } \nu \neq 0 \\ \sum_{n=0}^{\infty} \dfrac{(-1)^n (n+2)(n+1)}{(2\pi)^{2n}} \Big[(n+3) S_1 + \rho + \ldots \Big] p^{2n} & \text{for } \nu = 0, \end{cases} \tag{3.41}$$

as $p \to \pm i k_1$. These series converge for all $|p| < k_1$; in particular, they are valid for $p \to \pm i k_1$, provided $|p| < k_1$. Hence we can replace (3.38) with (3.41) in this neighbourhood. In (3.41), the ellipses '...' stand for coefficients of the expansion of terms with a slower growth as $p \to \pm i k_1$ which were dropped in (3.38). The discarded terms would modify the coefficients of the power series (3.41); however, there are terms which would not be affected by these modifications, namely terms with large n. For example, the coefficients proportional to $\sigma(\nu)$ and ρ in (3.41) are a factor of n smaller than those proportional to $K_1(\nu)$ and S_1; the discarded coefficients would be even smaller. Therefore the leading singular behaviour of $V_0(p)$ as $p \to \pm i k_1$ is determined just by the large-n coefficients of the power series (3.41), and hence only the large-n coefficients should be matched to the coefficients of the expansion (3.31). This gives the Stokes constant as a limit of the coefficients v_{2n} of the series (3.31):

$$\begin{cases} K_1(\nu) = \lim\limits_{n\to\infty} (-1)^n k_1^{2n} v_{2n} & \text{for } \nu \neq 0 \\ S_1 = \lim\limits_{n\to\infty} \dfrac{(-1)^n (2\pi)^{2n} v_{2n}}{(n+3)(n+2)(n+1)} & \text{for } \nu = 0. \end{cases} \tag{3.42}$$

This formula is used in the next section for numerical computations of the leading-order Stokes constant $K_1(\nu)$ for $\nu \neq 0$.

Note that, since (3.31) matches (3.41) in the limit $n \to \infty$, the power series $\hat{V}_0(p)$ also has radius of convergence k_1. However, the formal inverse-power series $\hat{\psi}_0(\zeta)$ diverges for all ζ unless $\hat{V}_0(p)$ converges everywhere (which requires that all the Stokes constants be zero).

We note from (3.42) that as $\nu \to 0$, the Stokes constant $K_1(\nu)$ does not tend to S_1. This discontinuity is due to the fact that, as $\nu \to 0$, pairs of simple roots in the resonant set $\mathcal{R}_\nu$ coalesce (ik_1 coalesces with ik_2 at $2\pi i$, and so on). As a result, all roots are double and the representation of $\hat{\varphi}_1(\zeta)$ is discontinuous at $\nu = 0$, with the power degree r of the prefactor in (3.36) jumping from $r = 0$ for $\nu \neq 0$ to $r = 3$ for $\nu = 0$. In particular, in exceptional models, i.e., discrete models with continuous families of stationary kinks [like (3.8), (3.9) and (3.11)]

the constant S_1 is *a priori* zero while the limit of $K_1(v)$ as $v \to 0$ may be nonvanishing. In fact, numerical computations of the top limit in (3.42) indicate that the Stokes constant blows up as $v \to 0$. Renormalisation of $K_1(v)$ for small v is, however, a nontrivial asymptotic problem which is beyond the scope of our current investigation.

For $v \in (v_1, 1)$, where $v_1 \approx 0.22$, the resonant set $\mathcal{R}_v$ contains only one root ik_1 and, therefore, there is just one Stokes constant $K_1(v)$, which completely determines the convergence of the formal inverse-power series for $\hat{\psi}_0(\zeta)$. If $K_1(v_0) = 0$ at some point $v_0 \in (v_1, 1)$, the stable and unstable solutions $\psi_0^{(s)}(\zeta)$ and $\psi_0^{(u)}(\zeta)$ coincide to leading order. Arguments based on the implicit function theorem (see [136]) reveal that a heteroclinic bifurcation occurs on crossing a smooth curve $v = v_*(h)$ on the (v,h)-plane, with $v_*(0) = v_0$.

On the other hand, for $v \in (0, v_1)$ the resonant set $\mathcal{R}_v$ contains more than one root. If $K_1(v_0) = 0$ for some $v_0 \in (0, v_1)$, this alone is not sufficient for the convergence of the series $\hat{\psi}_0(\zeta)$. The higher-order Stokes constants $K_2(v)$, $K_3(v)$, ..., must be introduced and computed from the asymptotic behaviour of the power series $\hat{V}_0(p)$.

As we shall show in the next section, the function $K_1(v)$ does have zeros in the case of the discretisations (3.8) and (3.11). All these zeroes are 'safe'; that is, all v_0 values lie in the interval $(v_1, 1)$, so that the higher-order Stokes constants do not have to be computed.

3.3 Numerical computations of the Stokes constant

In this section, we describe the numerical computation of the Stokes constants $K_1(v)$ for the four different discretisations of the ϕ^4 model (3.3) under consideration. Our numerical method uses the expression (3.42) of the Stokes constant in terms of the coefficients of the formal power series solution (3.31). First, we obtain the recurrence relation for the coefficients in the set $\{v_n\}_{n=0}^{\infty}$ by substituting the power series expansion (3.31) into the limiting integral equation (3.29), and using the convolution formula

$$p^n * p^m = \frac{n!\, m!}{(n+m+1)!} p^{n+m+1}. \tag{3.43}$$

After that, we compute the asymptotic behaviour of these coefficients as $n \to \infty$ and evaluate the limit (3.42) numerically for a fixed value of $v \neq 0$.

In order to calculate the Stokes constants for the four models in a uniform way, we write a

general symmetric homogeneous cubic polynomial $Q(u_{n-1},u_n,u_{n+1})$ as

$$Q=\sum_{\alpha=-1}^{1}\sum_{\beta=\alpha}^{1}\sum_{\gamma=\beta}^{1}a_{\alpha,\beta,\gamma}\,u_{n+\alpha}u_{n+\beta}u_{n+\gamma}, \tag{3.44}$$

where $a_{\alpha,\beta,\gamma}$ are numerical coefficients, with $\alpha,\beta,\gamma\in\{-1,0,1\}$ and $\alpha\le\beta\le\gamma$. The symmetry implies that $a_{\alpha,\beta,\gamma}=a_{-\gamma,-\beta,-\alpha}$ and therefore it is sufficient to specify just six coefficients. The values of these coefficients for the four nonlinearities in question are given in table 3.1.

Model	$a_{1,1,1}$	$a_{0,0,0}$	$a_{0,1,1}$	$a_{0,0,1}$	$a_{-1,1,1}$	$a_{-1,0,1}$
One-site (3.6)	0	1/2	0	0	0	0
Speight–Ward (3.8)	1/36	1/9	1/12	1/12	0	0
Bender–Tovbis (3.9)	0	0	0	1/4	0	0
Kevrekidis (3.11)	1/8	0	0	0	1/8	0

Table 3.1: The coefficients $a_{\alpha,\beta,\gamma}=a_{-\gamma,-\beta,-\alpha}$ of the cubic polynomial (3.44) for the four models under consideration.

By applying the Laplace transform (3.27) to equation (3.26) with Q as in (3.44), we obtain the corresponding cubic convolution function $\hat{Q}[V(p)]$ on the right hand side of the integral equation (3.29):

$$\hat{Q}[V(p)]=\sum_{\alpha=-1}^{1}\sum_{\beta=\alpha}^{1}\sum_{\gamma=\beta}^{1}a_{\alpha,\beta,\gamma}\,e^{\alpha p}V(p)*e^{\beta p}V(p)*e^{\gamma p}V(p). \tag{3.45}$$

To derive the recurrence formula for the coefficients c_{2n} in (3.31), it will be more convenient to consider the power series expansion which consists of both even and odd powers of p:

$$\hat{V}_0(p)=\sum_{n=0}^{\infty}c_n p^n. \tag{3.46}$$

We now substitute the series (3.46) into (3.29) with $\hat{Q}[V(p)]$ given by (3.45) and use the convolution formula (3.43). Equating the coefficients of p^{n+2} where $n=0,1,2,\ldots$, in the resulting equation, we find that

$$\sum_{i=0}^{[n/2]}\frac{2}{(2i+2)!}c_{n-2i}-\nu^2c_n=\sum_{\alpha=-1}^{1}\sum_{\beta=\alpha}^{1}\sum_{\gamma=\beta}^{1}\frac{a_{\alpha,\beta,\gamma}}{(n+2)(n+1)}\left\{\sum_{i=0}^{n}\left(\sum_{k=0}^{n-i}\frac{\alpha^k}{k!}c_{n-i-k}\right)\right.$$
$$\left.\times\left[\sum_{j=0}^{i}\left(\sum_{l=0}^{j}\frac{\beta^l}{l!}c_{j-l}\right)\left(\sum_{m=0}^{i-j}\frac{\gamma^m}{m!}c_{i-j-m}\right)\frac{j!(i-j)!}{i!}\right]\frac{i!(n-i)!}{n!}\right\}, \tag{3.47}$$

where $[n/2]$ is the integer part of $n/2$ and $0^0 = 1$. Equation (3.47) is a recurrence relation between the coefficients $\{v_n\}_{n=0}^{\infty}$. Solving equation (3.47) with $n = 0$, we get $c_0 = 2\sqrt{1-v^2}$ (note that this first coefficient is independent of the choice of $a_{\alpha,\beta,\gamma}$, i.e. independent of the model). Letting $c_1 = 0$ and making use of the symmetry of Q, one can show by induction that the coefficients of all odd powers in (3.46) are zero (as we concluded previously on the basis that the outer expansion is odd in z).

To prevent overflow or underflow when evaluating the recurrence relation numerically, we shall work with the normalised coefficients

$$w_n = (-1)^n k_1^{2n} c_{2n}$$

so that the Stokes constant (3.42) for $v \neq 0$ is given by

$$K_1(v) = \lim_{n\to\infty} w_n. \tag{3.48}$$

Reformulating (3.47) in terms of w_n, we use the relation (3.48) to compute K_1 numerically. We truncate the sums involving $1/(2i+2)!$, $1/l!$ and $1/m!$ when these factors become smaller than 10^{-50}, and evaluate the sums involving the combinatorial factors in two halves. In the first, the summation index increases from zero to the halfway point, and in the second it decreases from its maximum. This ensures that the combinatorial factors are always decreasing from one step to the next so that they can be accurately determined recursively. We also truncate these sums when the combinatorial factors fall below 10^{-50}.

These expedients result in a numerical routine fast enough to allow for evaluation of the recurrence relation up to very large n; this is essential given the slow convergence of w_n to a constant. Matching (3.31) to (3.41) yields

$$c_{2n} \to (-1)^n k_1^{-2n}[K_1(v) + \sigma(v)/n] \quad \text{as } n \to \infty;$$

therefore, the rate at which w_n converges to $K_1(v)$ is of order $1/n$:

$$w_n = K_1(v) + \frac{\sigma(v)}{n} + \frac{\tilde{\sigma}(v)}{n^2} + \mathcal{O}\left(\frac{1}{n^3}\right). \tag{3.49}$$

Although the convergence of w_n to $K_1(v)$ is extremely slow, we can accelerate the process by using (3.49). Defining

$$\tilde{w}_n \equiv w_n + n(w_n - w_{n-1}),$$

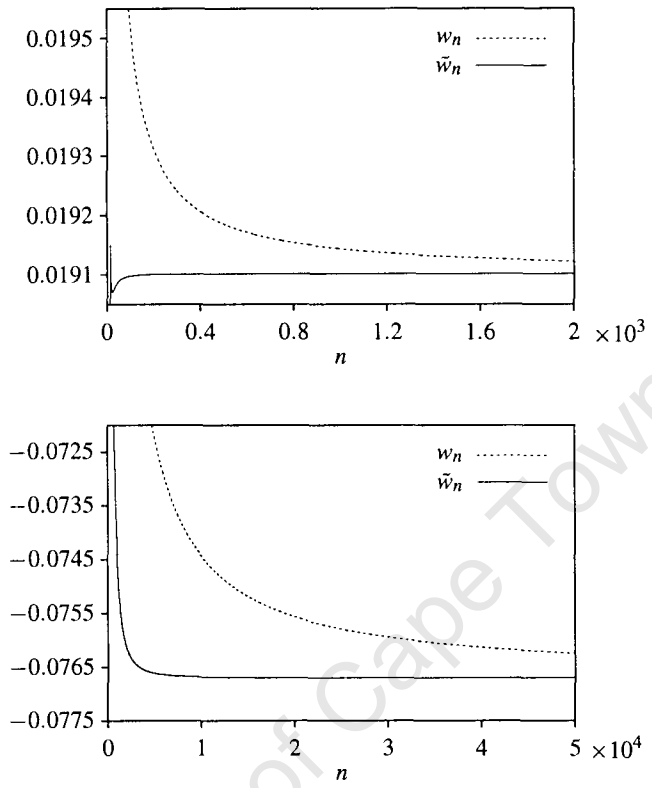

Figure 3.2: Convergence of the sequence w_n and its accelerated counterpart $\tilde{w}_n$ to the Stokes constant $K_1(\nu)$. The dashed line depicts the values of w_n and the solid line marks the accelerated sequence $\tilde{w}_n$. Top: the Kevrekidis discretisation (3.11) with $\nu = 0.5$. Bottom: Speight–Ward discretisation (3.8) with $\nu = 0.005$.

we get

$$\tilde{w}_n = K_1(\nu) - \frac{\sigma(\nu) + \tilde{\sigma}(\nu)}{n^2} + \mathcal{O}\left(\frac{1}{n^3}\right).$$

The convergence of the sequence $\tilde{w}_n$ is much faster than that of w_n; see figure 3.2. The relative error

$$E(n) = \frac{\sigma(\nu) + \tilde{\sigma}(\nu)}{n^2} \frac{1}{K_1(\nu)}$$

can be written as

$$E(n) = \frac{n}{2} \frac{\tilde{w}_n - \tilde{w}_{n-1}}{\tilde{w}_n}$$

plus terms of order $1/n^4$. This gives an empirical criterion for the termination of the process. We continued our computations until $E(n)$ reached a value smaller than 10^{-3}, i.e. until the percentage error dropped below 0.1%. For $\nu > 0.5$, the value of n to which we have to compute in order

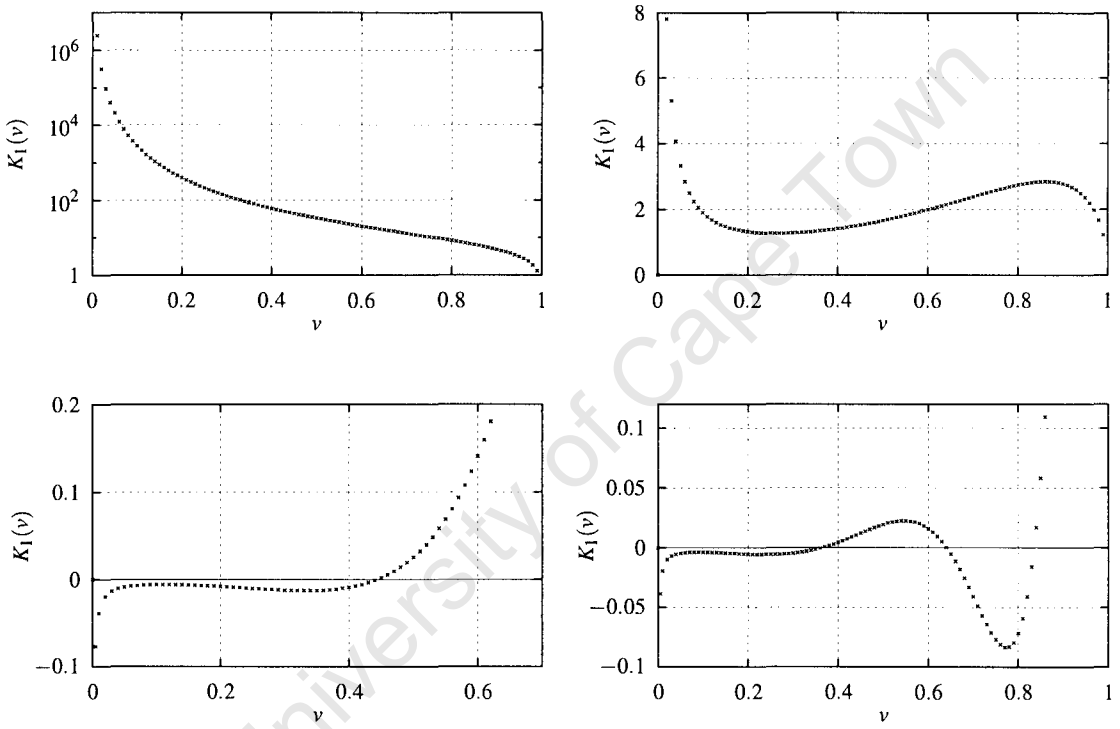

Figure 3.3: The Stokes constant K_1 as a function of the kink's speed v for the four discretisations of the ϕ^4 model. Clockwise from top left: one-site (3.6); Bender–Tovbis (3.9); Kevrekidis (3.11); Speight–Ward (3.8)

to achieve this accuracy is less than 100, increasing for smaller values of v to approximately 5000 for $v = 0.005$.

Figure 3.3 displays the Stokes constant computed using the above numerical procedure, for the four models of table 3.1. We see that, in all four models, the Stokes constant $K_1(v)$ vanishes almost nowhere in the region $v \neq 0$. There are, however, several isolated zeros: $K_1(v) = 0$ for $v_0 \approx 0.45$ in the case of the Speight–Ward nonlinearity (3.8) and for $v_0 \approx 0.37$, 0.63 and 0.83 in the case of the Kevrekidis discretisation (3.11). Importantly, all of these lie in the region $(v_1, 1)$ where the resonance set (3.33) consists of only one value, $p_1 = ik_1$. (Here $v_1 \approx 0.22$.) Therefore, there is a sliding kink in the $h \to 0$ limit for each of these isolated values of velocity. Furthermore, strong parallels between our current setting and that of solitons of the fifth-order KdV equation [136] suggest that sliding kinks should exist along a curve on the (v,h) plane emanating from each of the points $(v_0, 0)$. In other words, we conjecture that there is a radiationless kink travelling with a certain particular speed $v_*(h)$ for each h in the case of the Speight–Ward nonlinearity, and that there are three such velocities (for each h) in the case of the Kevrekidis model. For small h, $v_*(h)$ should be close to the above values v_0.

In order to verify the existence of kinks sliding at these isolated velocities by an independent method, we solved the differential advance-delay equation (3.14) numerically. The infinite line was approximated by an interval of length $2L = 200$, with the antiperiodic boundary conditions $\phi(-L) = -\phi(L)$. We made use of Newton's iteration with an eighth-order finite-difference approximation of the second derivative; the step size was chosen to be $h/10$. The continuum solution (3.2) was used as an initial guess.

If we find a solution to the advance-delay equation with $\phi(z)$ decaying to a constant for large positive and negative z, then we regard this solution as (a numerical approximation to) a radiationless travelling kink. We find that we are able to tune v for a fixed value of h so that the radiation is reduced to the order of 10^{-12}, whereupon the finite accuracy of the numerical scheme prevents any further reduction. To make sure that the radiation does vanish rather than reaching a local minimum but remaining nonzero, we plot the average magnitude of the radiation near the ends of the interval as a function of v, for fixed h. This is defined as the average of $\left[\phi(z) - \overline{\phi}\right]^2$ over the last 20 units of the interval, where $\overline{\phi}$ is the average value of $\phi(z)$ over these last 20 units. The results are shown in figure 3.4. Note the straight-line behaviour of the graphs near the isolated values of v; this indicates that the coefficient of the sinusoid superimposed over the kink's flat asymptote crosses through zero (rather than attaining a small but nonzero

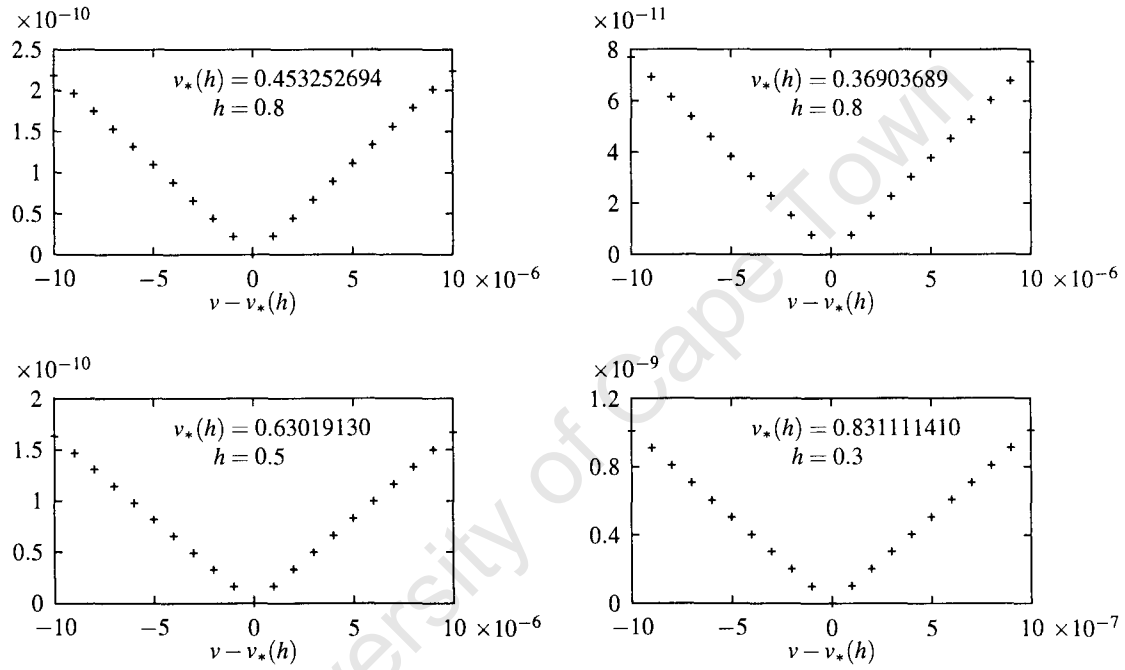

Figure 3.4: The numerical evidence for the disappearance of radiation at isolated values of $v = v_*$ in Speight and Ward's model (top left panel) and Kevrekidis' model (three other panels). The magnitude of the oscillatory tails, as defined in the text, is plotted as a function of v for a fixed value of h. The minimum radiation is attained at the value $v_*(h)$ which is found numerically. (This $v_*(h)$ is of course slightly different from the value $v_*(0)$ for which the Stokes constant vanishes.)

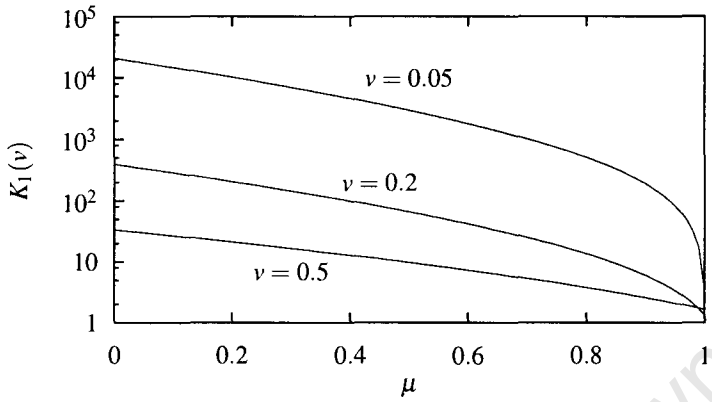

Figure 3.5: The Stokes constant as a function of μ in the model (3.50). Note the logarithmic scale of the vertical axis.

minimum). The suppression of radiation at the isolated points is thereby verified. This same behaviour is depicted in figure 5 of ref. [119], which shows the amplitude of the oscillatory background for velocities close to the sliding velocity, in a Klein–Gordon model constructed so as to have a sliding kink.

The final question we would like to address is whether the intensity of the radiation from the moving discrete kink depends on the type of discretisation. More specifically, we would like to know whether the choice of one of the exceptional discretisations (which, by definition, support translationally invariant *stationary* kinks) serves to reduce the radiation from the *moving* kinks. Speight and Ward have already given an affirmative answer for their exceptional discretisation; here we consider the one-parameter nonlinearity

$$Q = \frac{(1-\mu)}{2}u_n^3 + \frac{\mu}{4}u_n^2(u_{n+1} + u_{n-1}), \tag{3.50}$$

which interpolates between the one-site nonlinearity (3.6) (for which $\mu = 0$) and the exceptional discretisation (3.9) of Bender and Tovbis (for which $\mu = 1$). Figure 3.5 shows the Stokes constant for the model (3.50), as μ changes from 0 to 1 for fixed values of v. The Stokes constant is indeed seen to be drastically reduced as μ approaches 1 – that is, in the limit of the exceptional discretisation. (It nonetheless remains nonzero, of course, unless $v = 0$.)

3.4 Concluding remarks

In this chapter we have investigated the existence of sliding kinks—i.e., discrete kinks travelling at a constant velocity over a flat background, without emitting any radiation—in four discrete versions of the quartic-coupling theory. One of these models is the most common, one-site, discretisation. Like the overwhelming majority of discrete ϕ^4-equations, it supports travelling kinks, but these kinks do radiate and decelerate as a result. The other three discretisations we have considered are all exceptional in the sense that they all support one-parameter continuous families of stationary kinks where the free parameter defines the position of the kink relative to the lattice. This property is clearly nongeneric; the translation invariance of the continuous ϕ^4-theory is broken by the discretisation and hence in generic disretisations kinks may only be centred at a site or midway between two sites. Since the nonexistence of 'translation-invariant' and of sliding kinks in the generic models can be ascribed to similar factors, *viz.*, the breaking of the translation and Lorentz invariances, it was hoped that the exceptional discretisations might turn out to be equally exceptional from the point of view of sliding kinks. Our approach was based on the computation of the Stokes constants associated with the putative sliding kink in a given equation.

The main conclusion of our work is that sliding kinks do exist in the discrete ϕ^4 theories, but only with special, isolated, velocities (which of course depend on h). There is one such velocity in the exceptional model of Speight and Ward, and three different sliding velocities in the discretisation of Kevrekidis. Although embedded solitons are usually only semistable, one may hope that the sliding kinks play the role of attractors similarly to the fronts moving with 'stable velocities' in dissipative systems; that is, that radiating travelling kinks evolve into kinks travelling with the sliding velocities – if there are such velocities in the system. This has not been investigated for discrete ϕ^4 models, but our results for the discrete nonlinear Schrödinger equation in chapter 6 show that, in fact, the sliding solitons are metastable states. Not every discretisation supports sliding kinks, of course; in particular, no sliding velocities arise for the generic, one-site, nonlinearity and even for the exceptional discretisation of Bender and Tovbis.

One natural way of trying to construct the sliding kinks is via power series expansions in powers of v^2; for the exceptional discretisations, this construction can be carried out to any order. This approach was pursued in the recent work of Ablowitz and Musslimani [178]. Our results indicate, however, that these power series will not converge and exponentially small terms (terms lying beyond all orders of the power expansion) emerge because of the singular

behaviour of the Stokes constant $K_1(v)$ as $v \to 0$.

The exceptional discretisations have richer underlying symmetries than generic nonlinearities but the 'translational invariance' of the stationary kink alone does not automatically guarantee the existence of sliding velocities. The exact relation between the 'translation invariance' and radiation damping of moving kinks is still to be clarified; one definite conclusion which can be made at this stage is that the Stokes constant associated with a moving kink (and hence its radiation amplitude) is several orders of magnitude smaller in exceptional models than in generic discretisations. This work also raises the question of whether sliding kinks can *only* exist in exceptional models. A counterexample has already been provided in ref. [119], where a system constructed to have a sliding kink is shown to have a nonzero Peierls–Nabarro barrier. Given that sliding kinks are not restricted to rare exceptional discretisations, then, an important remaining goal is to find sliding solitons in physically motivated equations. In particular, one may wonder whether it is necessary for the discretisation of the nonlinearity to include u_{n+1} and u_{n-1} or whether a local discretisation will do. The Speight–Ward and Kevrekidis nonlinearities, for which sliding kinks were found in this chapter, both have nonlocal discretisations of their nonlinearities, as do the 'FPU' lattices for which travelling pulses have been found by Eilbeck and Flesch [75]. The same counterexample [119], however, shows that a one-site nonlinearity can also produce sliding kinks.

It is instructive to point out some parallels with the earlier work of Flach, Zolotaryuk and Kladko [119], who also studied the phenomenon of kink sliding in Klein–Gordon lattices. In the scheme of [119], one postulates an analytical expression for the sliding kink, $u_n(t) = \phi(n - vt - s)$, with some explicit function $\phi(z)$, and then reconstructs the Klein–Gordon nonlinearity for which this is an exact solution. Our present conclusions are in agreement with the results of these authors who observed that for a given h, the kink may only slide at a particular, isolated, velocity. The two approaches, ours and that of [119], are reciprocal; while we examine the existence of sliding kinks for particular discretisations of the ϕ^4-theory in the 'inverse method' of [119] one assumes an explicit solution of a particular form but has no control over the resulting nonlinearities. Consequently, the discrete Klein–Gordon models generated by the 'inverse method' are not discretisations of the ϕ^4-theory.

Our final remarks relate to the wobbling kinks studied in the continuum limit in chapter 2. Although we have not analysed the wobbling mode in the present chapter, the results of chapter 2 could still be applied to the discrete ϕ^4 equation near to the continuum limit. Since

the radiation coming from the wobbling mode has amplitude $\mathcal{O}\left(a^2\right)$ (where a is the wobbling amplitude), this will dwarf the exponentially small terms unless the wobbling amplitude $|a|$ is extremely small; hence we would expect to see no fundamental changes to the conclusions of the last chapter in the case of the discrete equation. An interesting new phenomenon in the discrete case is suggested by the work of Fei, Konotop, Peyrard and Vázquez [159], who analysed a ϕ^4 model with periodic modulation of the nonlinearity. They found that, if the kink is moving at the right velocity, its motion with respect to the periodic modulation is in resonance with the internal mode, which thereby gains energy from the translational motion of the kink. One would expect the system with periodic modulation to have similarities to the discrete ϕ^4 model, where the Peierls–Nabarro barrier plays the role of the periodic substrate. Thus a similar resonance phenomenon might well be observed in the discrete case.

Lastly, it is interesting to make a comparison between the radiation from the wobbling kink in chapter 2, which appears at $\mathcal{O}(\varepsilon)$ in the perturbation expansion, and the radiation studied in this chapter. As we found in section 3.2.1, the radiation does not appear at any order of the perturbation expansion, which was explained later on by the fact that it is exponentially small (see section 3.2.4). The intuitive reason for this difference is the comparative length scales of the profile causing the radiation and the radiation itself. In chapter 2, the localisation length of the wobbling mode is of order ε^0, where ε was the perturbation parameter (see eq. (2.6)). The wavelength of radiation has the same scale – the wavenumber was found to be $k = \sqrt{8}$. Here, the obstacle to the excitation of radiation is that the frequency of the wobbling does not lie in the spectrum of linear radiation. However, the frequency-doubling effect of nonlinearity results in radiation appearing at the very next order of the perturbation expansion [see eq. (2.13)]. On the other hand, in this chapter the travelling kink has characteristic length $\mathcal{O}\left(h^{-1}\right)$ in units of n [i.e., its width is $\mathcal{O}\left(h^0\right)$ on the long z scale – see eqs (3.18) and (3.13)], whereas the radiation has shorter wavelength, of order h^0 in units of n or order h in units of z [since, linearising (3.14), one obtains linear waves with wavenumber k/h where k is a member of the set (3.33) in the limit $h \to 0$]. Since they exist on the two separate length scales, the kink and the radiation do not couple at any order of the perturbation expansion, even though the frequency of the kink (zero) does lie in the infinite allowed band of linear excitations (for which the dispersion relation was plotted in fig. 1.12). Thus, this difference in length scales provides us with an intuitive explanation for the exponential smallness of radiation from travelling discrete solitary waves

Appendix 3.A Convolution theorem for the Laplace transform in the complex plane

This appendix deals with the convolution property of the modified Laplace transform of the form

$$\psi(\zeta) = \int_\gamma F(p)e^{-p\zeta}dp$$

[eq. (3.27); also eqs (5.14) and (6.37) in future chapters], where the integration is along an infinite contour in the complex plane rather than the positive real axis. In the context of asymptotics beyond all orders, this transform was pioneered by Grimshaw and Joshi [134]. Since no proof of the convolution result (3.30) is available in literature, and since it requires a nontrivial property (concavity) of the integration contour, we produce such a proof here.

We wish to show that

$$\int_\gamma e^{-p\zeta}F(p)dp \int_\gamma e^{-p'\zeta}G(p')dp' = \int_\gamma e^{-p\zeta}\left[\int_0^p F(p_1)G(p-p_1)dp_1\right]dp, \tag{3.51}$$

where $\int_0^p$ stands for an integral along the curve γ from the origin to the point p on that curve. We assume that the curve γ extends from the origin to infinity on the complex plane; lies in its first quadrant ($\mathrm{Re}\,p > 0$, $\mathrm{Im}\,p > 0$); is described as a graph of a single-valued function $\mathrm{Im}\,p = f(\mathrm{Re}\,p)$ (i.e. never turns back on itself), and is concave-up everywhere:

$$\frac{d^2 f}{d(\mathrm{Re}\,p)^2} > 0 \quad \text{for } p \text{ on } \gamma.$$

We also assume that the function $G(p)$ is analytic in the region between the contour γ and the imaginary axis.

We begin by writing the left-hand side of (3.51) as

$$\begin{aligned}&\int_\gamma\int_\gamma e^{-(p+p')\zeta}F(p)G(p')dp'dp\\ &= \int_\gamma F(p)\left[\int_{\Gamma_p} e^{-r\zeta}G(r-p)dr\right]dp,\end{aligned} \tag{3.52}$$

where $r = p' + p$. The curve Γ_p is the path traced out by r as p' traces out the curve γ, for a given p (which also lies on γ) – this is depicted in figure 3.6. The path Γ_p is the same as the path γ but translated from the origin to the point p.

For each given p we deform the path Γ_p so that it now lies on γ, still starting at the point p. We call this deformed path Γ_p'. The point $r - p = p'$, which lay on the path γ before the

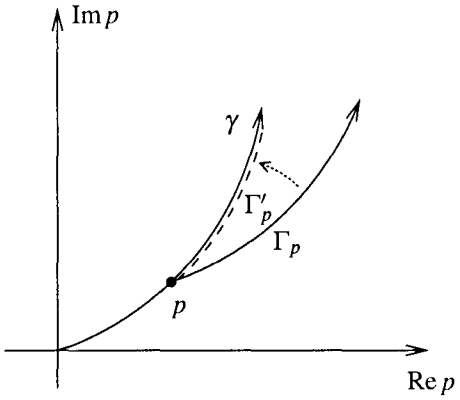

Figure 3.6: Deformation of the integration contour Γ_p to Γ'_p.

deformation, will now move inside the region bounded by γ (i.e. the region to the left of γ), since all points on Γ'_p lie inside the region bounded by Γ_p. This follows from the fact that the path Γ_p is concave-up. The point $r-p$ will, however, stay to the right of the imaginary axis, since after the deformation all points r on Γ'_p lie to the right of the point p. This follows from the fact that the curve γ never turns back on itself. Since $G(p')$ is analytic for all p' between the imaginary axis and γ, the value of the integral (3.52) will not be affected by the deformation.

After the deformation, both integrals in (3.52) follow the path γ, with the inner one starting at the point p. By parameterising the path γ it is now straightforward to change the order of integration, and end up with the desired result (3.51).

The argument holds, with the obvious modifications, for paths in the second quadrant.

Chapter 4

Translationally invariant discrete kinks from one-dimensional maps

Although we found in chapter 3 that exceptional discretisations do not admit sliding solitons at all velocities, we have shown that radiation is dramatically reduced and that sliding solitons may often exist at isolated velocities when the discretisation is exceptional. Therefore exceptional models clearly warrant further attention. In this chapter we shall attempt to unify the known models in order to gain a better understanding of the phenomenon of exceptionality, and also search for further exceptional discretisations in the hope of finding physically realisable models.

4.1 Introduction

When the continuous ϕ^4 equation

$$\phi_{tt} = \phi_{xx} + \frac{1}{2}\phi(1-\phi^2) \tag{4.1}$$

is spatially discretised, we obtain discrete ϕ^4 equations

$$\ddot{\phi}_n = \frac{\phi_{n+1} - 2\phi_n + \phi_{n-1}}{h^2} + f(\phi_{n-1}, \phi_n, \phi_{n+1}), \tag{4.2}$$

where h is the lattice spacing: $\phi_n(t) = \phi(x_n, t)$, with $x_n = hn$, and the function f is chosen to reproduce the nonlinearity of (4.1) in the continuum limit:

$$f(\phi,\phi,\phi) = \frac{1}{2}\phi(1-\phi^2). \tag{4.3}$$

The continuous ϕ^4-equation (4.1) is Lorentz-invariant, and so the existence of a travelling kink is an immediate consequence of the existence of the stationary soliton,

$$\phi(x,t) = \tanh(x/2). \tag{4.4}$$

The discretisation breaks the Lorentz invariance and the existence of travelling discrete kinks becomes a nontrivial matter. In fact, the discretisation even breaks the translation invariance of eq. (4.1). As a result, the stationary kink can be centred only at a countable number of points – usually on a site, and midway between two adjacent sites [160, 161]. This breaking of the translation invariance is connected with the presence of the Peierls–Nabarro barrier, an additional periodic potential induced by discreteness.

Miraculously, the *exceptional* discretisations studied in chapter 3, while breaking the translation invariance of the equation, allow the existence of translationally invariant kinks; that is, kinks centred at an arbitrary point between the sites. One such discretisation was discovered by Speight and Ward using a Bogomolny-type energy-minimality argument [115, 116]:

$$f = \frac{2\phi_n + \phi_{n+1}}{12}\left(1 - \frac{\phi_n^2 + \phi_n\phi_{n+1} + \phi_{n+1}^2}{3}\right) + \frac{2\phi_n + \phi_{n-1}}{12}\left(1 - \frac{\phi_n^2 + \phi_n\phi_{n-1} + \phi_{n-1}^2}{3}\right). \tag{4.5}$$

Another one derives from the Ablowitz–Ladik integrable discretisation of the nonlinear Schrödinger equation; it was reobtained by Bender and Tovbis [132] from the requirement of suppression of the kinks' resonant radiation:

$$f = \frac{1}{4}(\phi_{n+1} + \phi_{n-1})\left(1 - \phi_n^2\right). \tag{4.6}$$

Finally, the nonlinearity

$$f = \frac{\phi_{n+1} + \phi_{n-1}}{4} - \frac{(\phi_{n+1}^2 + \phi_{n-1}^2)(\phi_{n+1} + \phi_{n-1})}{8} \tag{4.7}$$

was identified by Kevrekidis [131], who demonstrated the existence of a two-point invariant associated with the stationary equation

$$\frac{\phi_{n+1} - 2\phi_n + \phi_{n-1}}{h^2} + f(\phi_{n-1}, \phi_n, \phi_{n+1}) = 0, \tag{4.8}$$

with f as in (4.6) and (4.7).

Although the translation invariance of a stationary kink does not automatically guarantee the existence of a travelling soliton, it is natural to expect it to be a prerequisite for kink mobility.

For example, in the variational description of the slowly moving kink, the solution is sought as a stationary kink with a free continuous parameter defining its position on the line [115]. Also, in chapter 3 of this thesis the Stokes constants measuring the intensity of resonant radiation from the translationally invariant kinks were found to be at least an order of magnitude smaller than the corresponding constants in models with noninvariant kinks. With an eye to a further attack on travelling kinks, it would be useful to identify all discretisations of the ϕ^4 theory supporting translationally invariant stationary kinks. The purpose of this chapter is to provide a general recipe for the generation of such exceptional discretisations $f(\phi_{n-1}, \phi_n, \phi_{n+1})$.

4.2 Two-point maps

We start with a simple observation which, however, holds the key to our construction. Assume we have a nonlinearity f which supports a stationary discrete kink, i.e. a monotonically growing sequence ϕ_n: $-1 < \phi_n < \phi_{n+1} < 1$ for $-\infty < n < \infty$. Furthermore, assume there exists a continuous monotonically growing function $g(x)$, defined for all real x, such that $\phi_n = g(n)$. (The function g can also depend on h parametrically but we omit this dependence for simplicity of notation.) This function generates a family of kinks centred at an arbitrary point $x^{(0)}$ on the line: $\phi_n = g(n - x^{(0)})$. It is important to emphasise that such a continuous function can exist only for exceptional discretisations. For generic discretisations, the function $g(x)$ can be defined only on integers.

The existence of the function $g(x)$ defined on the entire real line—or, equivalently, the translation invariance of the kink—implies that the stationary equation (4.8) derives from a two-point map. Indeed, since $g(x)$ is monotonic, we can write $n = g^{-1}(\phi_n)$. Now since $\phi_{n+1} = g(n+1)$, we have $\phi_{n+1} = g(g^{-1}(\phi_n) + 1) \equiv F(\phi_n)$, which is a well-defined one-dimensional map.

This observation suggests the following strategy for the construction of exceptional discretisations. Assume we have a 1D map which we will write in the form

$$\phi_{n+1} - \phi_n = hH(\phi_{n+1}, \phi_n). \tag{4.9}$$

Let H satisfy the following continuity condition:

$$H(\phi, \phi) = \frac{1}{2}(1 - \phi^2). \tag{4.10}$$

This condition is necessary to make sure that the map (4.9) becomes

$$\phi_x = \frac{1}{2}(1 - \phi^2) \tag{4.11}$$

in the continuum limit. The stationary kink solution (4.4) of eq. (4.1) is, simultaneously, a solution of the first-order equation (4.11). Imposing (4.10) we ensure that the discrete kink of (4.9) will have the correct continuum limit. Next, equation (4.10) implies that the map (4.9) has just one pair of fixed points, $\phi_* = \mp 1$. For small h, ϕ_{n+1} remains close to ϕ_n and hence, $H(\phi_{n+1}, \phi_n)$ remains close to (4.10) which is positive for $|\phi| < 1$. Consequently, no matter what $|\phi_0| < 1$ we start with, the sequence ϕ_n is monotonically growing – at least until $|\phi_n|$ is not very close to 1. To ensure that it remains such near the fixed points, we assume that $\phi_* = -1$ is a source and $\phi_* = 1$ a sink. (That is, small perturbations $\delta\phi_n = \phi_n - \phi_*$ satisfy $\delta\phi_{n+1} = \lambda\delta\phi_n$ with $\lambda > 1$ near $\phi_* = -1$ and $0 < \lambda < 1$ near $\phi_* = 1$.) Then, for any h smaller than some $\bar{h}$ and any ϕ_0 between -1 and 1, there is a number N such that $|\phi_N - \phi_*|$ is so small that all ϕ_n with $n > N$ are entrapped by the 'linear neighbourhood' of $\phi_* = 1$ and those with $n < -N$ are all in a neighbourhood of $\phi_* = -1$. This means that each ϕ_0 with $|\phi_0| < 1$ defines a monotonic kink solution and so for any sufficiently small h we have a one-parameter family of stationary kinks. Speight [117] gives a less intuitively appealing but more rigorous proof of this fact; he also shows that our assumption on the character of the fixed points can be relaxed.

Next, squaring both sides of (4.9) and subtracting the square of its back-iterated copy,

$$\phi_n - \phi_{n-1} = hH(\phi_n, \phi_{n-1}), \tag{4.12}$$

produces an exceptional stationary Klein–Gordon equation

$$\frac{\phi_{n+1} - 2\phi_n + \phi_{n-1}}{h^2} = \frac{H^2(\phi_{n+1}, \phi_n) - H^2(\phi_n, \phi_{n-1})}{\phi_{n+1} - \phi_{n-1}}. \tag{4.13}$$

If H is symmetric: $H(\phi_n, \phi_{n-1}) = H(\phi_{n-1}, \phi_n)$, the numerator vanishes exactly where the denominator equals zero, so the discretisation (4.13) is nonsingular.

If we want to have polynomial discretisations of the ϕ^4 theory, the function H^2 has to be a quartic polynomial. This leads to two possibilities, one where H is the square root of a polynomial, and the other where H is a polynomial itself. These can be written jointly as

$$(\phi_{n+1} - \phi_n)^m = h^m P_{2m}(\phi_{n+1}, \phi_n), \tag{4.14}$$

where $m = 1$ or 2, and $P_{2m}(u, v)$ is a polynomial of degree $2m$ that satisfies the symmetry and continuity conditions

$$P_{2m}(u, v) = P_{2m}(v, u), \tag{4.15}$$

$$P_{2m}(\phi, \phi) = 2^{-m}(1 - \phi^2)^m. \tag{4.16}$$

The condition (4.16) is a consequence of eq. (4.10).

Before we proceed to the classification of the resulting models, we note as we did in the previous chapter that the linear part of the function f in (4.2) can always be fixed to $\frac{1}{2}\phi_n$ without loss of generality. The most general function satisfying (4.3) is $f = a\phi_n + \frac{1}{2}\left(\frac{1}{2} - a\right)(\phi_{n+1} + \phi_{n-1}) +$ cubic terms, and since h^2 in (4.8) is a free parameter, we can always make a replacement $h \to \tilde{h}$ such that $a - 2/h^2 = \tilde{a} - 2/\tilde{h}^2$. In particular, we can set $\tilde{a} = \frac{1}{2}$ which gives

$$f(\phi_{n-1}, \phi_n, \phi_{n+1}) = \frac{1}{2}\phi_n - Q(\phi_{n-1}, \phi_n, \phi_{n+1}), \tag{4.17}$$

where Q is a homogeneous polynomial of degree 3.

4.2.1 The case $m = 2$

Let, now, $m = 2$ in equation (4.14). Provided P_4 satisfies conditions (4.15) and (4.16), the numerator $P_4(\phi_{n+1}, \phi_n) - P_4(\phi_n, \phi_{n-1})$ of the fraction in the right-hand side of eq. (4.13) divides $(\phi_{n+1} - \phi_{n-1})$ and so eq. (4.13) will be of the form (4.8) with some cubic function f. The most general choice for such a polynomial is

$$P_4(u, v) = \frac{1}{4} - \mu(u - v)^2 - \frac{1}{2}uv + \frac{1}{20}\left[\alpha(u^4 + v^4) + \beta uv(u^2 + v^2) + \gamma u^2 v^2\right], \tag{4.18}$$

where α, β, γ satisfy $2\alpha + 2\beta + \gamma = 5$ and μ is arbitrary. Picking the positive value of $\sqrt{P_4}$ and assuming that h is sufficiently small, one can check that the fixed points $\phi_* = \mp 1$ of the map (4.14) are a source and a sink, for any μ, α and β. Consequently, the resulting cubic polynomial,

$$\begin{aligned} Q = \frac{1}{20}\big[&\alpha(\phi_{n+1} + \phi_{n-1})(\phi_{n+1}^2 + \phi_{n-1}^2) + \gamma\phi_n^2(\phi_{n+1} + \phi_{n-1}) \\ &+ \beta\phi_n(\phi_{n+1}^2 + \phi_n^2 + \phi_{n-1}^2 + \phi_{n+1}\phi_{n-1})\big] \end{aligned} \tag{4.19}$$

with $\gamma = 5 - 2(\alpha + \beta)$ defines a two-parameter family of models with translationally invariant kink solutions.

The discretisation (4.19) includes, as particular cases, the Bender-Tovbis function (4.6) (which results from setting $\alpha = \beta = 0$) and the Kevrekidis nonlinearity (4.7) (for which $\alpha = \frac{5}{2}$, $\beta = 0$). Another simple function arises by letting $\alpha = \gamma = 0$; this is a new model:

$$Q = \frac{1}{8}\phi_n(\phi_{n+1}^2 + \phi_n^2 + \phi_{n-1}^2 + \phi_{n+1}\phi_{n-1}).$$

4.2.2 The case $m = 1$

Now let $m = 1$. The most general quadratic P_2 satisfying (4.15)–(4.16) is

$$P_2(u,v) = \frac{1}{2} - \alpha(u-v)^2 - \frac{1}{2}uv, \tag{4.20}$$

with an arbitrary α. Note that for $h < 2$ and any α, $\phi_* = \mp 1$ are a source and a sink. Hence all resulting models will exhibit continuous families of kinks. Substituting eq. (4.20) for H in (4.13), we obtain just a particular case of the nonlinearity (4.19), corresponding to the choice of the quartic (4.18) in the form of a complete square: $P_4 = P_2^2$. To obtain *new* models, we need to note a symmetry $I_3(\phi_{n-1}, \phi_n, \phi_{n+1}) = 0$ which follows from eq. (4.14) with $m = 1$.[†] Here

$$I_3 \equiv P_2(\phi_{n+1}, \phi_n)(\phi_n - \phi_{n-1}) + P_2(\phi_n, \phi_{n-1})(\phi_n - \phi_{n+1}).$$

Equation (4.13) remains valid if βI_3 is added to its right-hand side, with an arbitrary coefficient β. The resulting function Q has the form

$$\begin{aligned} Q = {} & \alpha^2(\phi_{n+1}^3 + \phi_{n-1}^3) + 2\gamma(\alpha-\beta)\,\phi_{n+1}\phi_n\phi_{n-1} + \alpha(\alpha-\beta)\,\phi_{n+1}\phi_{n-1}(\phi_{n+1}+\phi_{n-1}) \\ & + \left[2\alpha^2 + \gamma^2 + \beta(\gamma-\alpha)\right]\phi_n^2(\phi_{n+1}+\phi_{n-1}) + \alpha(2\gamma+\beta)\,\phi_n(\phi_{n+1}^2+\phi_{n-1}^2) + 2\alpha(\gamma+\beta)\,\phi_n^3, \end{aligned} \tag{4.21}$$

where $\gamma = \frac{1}{2} - 2\alpha$. Equation (4.21) defines a two-parameter family of discretisations supporting translationally-invariant kinks. These models cannot be obtained within the $m = 2$ analysis above – unless $\beta = 0$, of course.

Letting $\alpha = \beta = \frac{1}{6}$, we recover the model of Speight and Ward, eq. (4.5). Another particularly simple, new, model is obtained by taking $\alpha = 0$ and $\beta = -\frac{1}{2}$:

$$Q = \frac{1}{2}\phi_{n-1}\phi_n\phi_{n+1}. \tag{4.22}$$

4.3 Vanishing Stokes constants

It is instructive to compare discretisations furnished by our method with those arising from the requirement of the absence of resonant radiation from the kink [132]. The advance-delay equation associated with eq. (4.8),

$$\phi(x+h) - 2\phi(x) + \phi(x-h) + h^2 f(\phi(x-h), \phi(x), \phi(x+h)) = 0, \tag{4.23}$$

[†]This crucial symmetry was found by Igor Barashenkov.

can be solved to all orders as a perturbation expansion in h (see chapter 3); the resultant solution depends continuously on the position parameter $x^{(0)}$. It is, therefore, only the terms which lie beyond all orders in h which present an obstacle to the existence of a translationally invariant kink. These terms vanish if Stokes constants at all orders vanish. The leading Stokes constant vanishes if there exists a convergent solution in powers of z^{-1} to the 'inner' equation

$$\varphi(z+1)-2\varphi(z)+\varphi(z-1)-Q(\varphi(z-1),\varphi(z),\varphi(z+1))\big|_{h=0}=0 \tag{4.24}$$

(see chapter 3). This equation comes from a rescaling of eq. (4.23) near the singularities of its leading-order solution (4.4) at $x_n=\pi i(1+2n)$, $n\in\mathbb{Z}$, in the limit $h\to 0$. The convergence of a power-series solution to eq. (4.24) is necessary for the absence of oscillatory radiation tails in its 'parent' equation (4.23).

In general, a numerical procedure is required to determine whether the series converges for a given Q, but we can easily generate a class of models for which it truncates after the first term. This was the method employed in ref. [132] in deriving equation (4.6). It is a matter of direct substitution to check that the most general cubic polynomial for which $\varphi=2/z$ is a solution of eq. (4.24), is

$$\begin{aligned} Q=\sigma\phi_n(\phi_{n+1}+\phi_{n-1})^2-2\sigma\phi_{n+1}\phi_{n-1}(\phi_{n+1}+\phi_{n-1}) \\ +\left(\frac{1}{4}-\frac{\beta}{2}\right)\phi_n^2(\phi_{n+1}+\phi_{n-1})+\beta\phi_{n-1}\phi_n\phi_{n+1}, \end{aligned} \tag{4.25}$$

with σ,β arbitrary constants.

The fact that the leading-order Stokes constant is zero is necessary but not sufficient for equation (4.23) to have continuous families of kinks for finite h. We have tested, numerically, a particular representative from the class (4.25):

$$Q=\phi_{n+1}\phi_{n-1}\frac{\phi_{n+1}+\phi_{n-1}}{2}-\phi_n\frac{\phi_{n+1}^2+\phi_{n-1}^2}{4}. \tag{4.26}$$

This model is obtained by letting $\sigma=-\frac{1}{4}$ and $\beta=\frac{1}{2}$. To check whether translationally-invariant kinks exist or not, we have computed a stationary on-site kink for the model (4.26) and calculated eigenvalues of the associated linearised operator for an equidistant sequence of h-values, ranging from $h=0$ to $h=1.179$ with increment 0.001. For h smaller than 0.556, the smallest-modulus eigenvalue was found to be smaller than 10^{-12} which is our numerical error of computation. However as h increases from 0.556, the smallest eigenvalue grows to $\lambda=9\times10^{-7}$ at $h=0.955$, then decreases, crosses through zero at $h=0.993$, after which grows in modulus to

$\lambda = -6 \times 10^{-4}$ at $h = 1.179$ – see figure 4.1. Thus, the zero eigenvalue, indicating the existence of a continuous family of solutions, is not present in the spectrum for $h > 0.556$. For $h < 0.556$, the smallest λ is apparently also nonzero (though very small). The only exception is the value $h = 0.993$ for which the zero mode does exist. This means that the model (4.26) supports a continuous family of kinks for just one, isolated, value of h.

4.4 A further exceptional family

Although the suppression of the Stokes constants did not yield a family of exceptional discretisations, we now show that there is a family which reduces to (4.25) in the limit $h \to 0$. When $\alpha = 0$ in eq. (4.20), the map (4.14) has one more symmetry: $I_2(\phi_{n-1}, \phi_n, \phi_{n+1}) = 0$, where

$$I_2 \equiv \left(1 + \frac{h^2}{4}\right) \phi_n(\phi_{n+1} + \phi_{n-1}) - 2\phi_{n-1}\phi_{n+1} - \frac{h^2}{2}.$$

We can add $\sigma(\phi_{n+1} + \phi_{n-1})I_2$ to the right-hand side of (4.13), along with βI_3 (with σ, β arbitrary constants.) This gives rise to the following family of exceptional discretisations:

$$\begin{aligned} Q = {} & \sigma\phi_n(\phi_{n+1} + \phi_{n-1})^2 - 2\sigma\phi_{n-1}\phi_{n+1}(\phi_{n+1} + \phi_{n-1}) \\ & + \left(\frac{1}{4} - \frac{\beta}{2}\right)\phi_n^2(\phi_{n+1} + \phi_{n-1}) + \beta\phi_{n-1}\phi_n\phi_{n+1} + \frac{1}{4}\sigma h^2\phi_n(\phi_{n+1} + \phi_{n-1})^2. \end{aligned} \quad (4.27)$$

Except for the last, $\mathcal{O}(h^2)$, term, this coincides with eq. (4.25).

For the map given by (4.14) and (4.20) with $\alpha = 0$, the kink can be found explicitly. This implies that the discretisations (4.27) also share an explicit kink solution (for all β and σ): $\phi_n = \tanh(an - x^{(0)})$, with $\tanh a = h/2$.

4.5 Concluding remarks

Our first remark is on the conserved quantities of equation (4.2). The translation invariance of the stationary kink does not imply that eq. (4.2) has translation symmetry and hence the conserves momentum. The discretisation (4.13) [and hence (4.19)] conserves momentum [131], whereas the nonlinearities (4.21) and (4.27) (with $\beta, \sigma \neq 0$), do not. Moreover, that the discretisation f is exceptional does not guarantee that eq. (4.2) has any integral of motion whatsoever. In particular, out of the three families (4.19), (4.21), and (4.27), only one model conserves energy, namely Speight and Ward's, eq. (4.5).

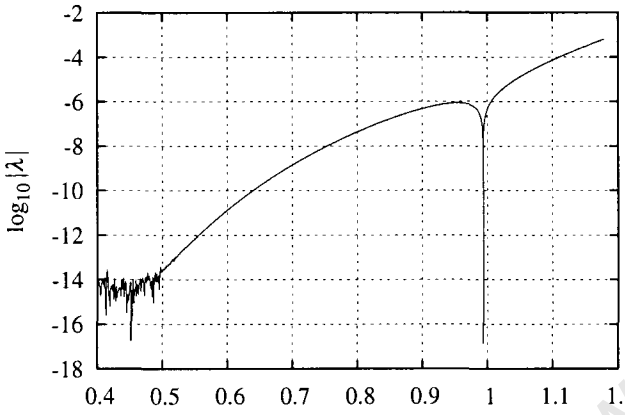

Figure 4.1: The smallest-modulus eigenvalue as a function of h. The cusp occurs at the point $h = 0.993$ where λ changes sign.

Secondly, we point out that exceptional discretisations have useful numerical applications. In simulating a continuous equation using a finite-difference method (as we did in chapter 2 for the ϕ^4 model), the equation must be discretised. An exceptional discretisation is more faithful than a nonexceptional one to the properties of the continuous equation, since it exhibits translational invariance as well as reduced radiation. Because of its simplicity, the discretisation (4.22) would be particularly well suited to this purpose. The availability of a two-point map in exceptional models also makes it very easy to generate stationary kinks numerically, without the need for shooting methods.

In conclusion, we have identified three families of discretisations of the ϕ^4 equation which support translationally invariant stationary kinks: equations (4.19), (4.21) and (4.27). In each case we have exhibited, explicitly, the underlying 1D map. Our method demonstrates the underlying mathematical property unifying all exceptional discretisations: their equations of motion are all composed, in the stationary case, from a two-point map.

Thus we see that the three exceptional equations studied in chapter 3 were just isolated members of a much larger class of discretisations. Unfortunately, though, we have failed to produce any further energy-preserving exceptional discretisations. Although conservation of energy is, of course, not a prerequisite for a system to be physically realisable, its absence excludes an enormous class of physical systems. Further studies could consider nonlinearities other than polynomials: rational functions, for instance. However, it is clear that exceptional discretisations are very rare and so are of mostly theoretical interest. It should be pointed out,

though, that Speight and Zolotaryuk *have* found a physical system—a chain of electric dipoles constrained to lie in a plane parallel to the chain [179]—described by the exceptional sine–Gordon model [115].

The most promising aspect of our studies of exceptional discretisations so far has been the discovery of sliding kinks. We know that exceptionality does not *guarantee* that sliding kinks will exist in a given model, and indeed that it is not even *necessary* for the model to be exceptional [119]. We therefore turn our attention to trying to find sliding solitons in nonexceptional models and, in particular, in models with important physical applications.

Chapter 5

Travelling kinks in the Frenkel–Kontorova model

In this chapter we describe the computation of the Stokes constant for the Frenkel–Kontorova model. Apart from the fact that it has many physical applications, our motivation is to confirm that nonexceptional models, of which this is one [109], can support sliding kinks.

The procedure is essentially the same as in chapter 3 – indeed, the FK model is merely another discrete nonlinear Klein–Gordon equation. We shall therefore gloss over the details which are essentially unchanged from that case. However, the derivation of the inner equations does present a somewhat greater challenge in this case. We also take the opportunity to use this example as an overview of the method presented earlier, without being weighed down by too much detail.

5.1 Introduction

The Frenkel–Kontorova model

$$\frac{d^2u_n}{dt^2} - \frac{u_{n+1} - 2u_n + u_{n-1}}{h^2} + \sin u_n = 0 \tag{5.1}$$

is a discrete version of the integrable sine–Gordon equation. Here, the parameter h represents the lattice spacing. This equation has many applications [180]; as mentioned in section 1.5, it was originally derived to describe crystal dislocations [78]. It also describes systems with incommensurate phases in solid-state physics [180], ladder networks of shunt Josephson junctions

[181], bond-rotation in certain molecular crystals [182, 183] and opening of base pairs in DNA [92, 184].

The sine–Gordon equation (1.3) admits the travelling kink solutions (1.4). Equation (5.1) also admits stationary kinks, as discussed in section 1.5. However, whether or not sliding kinks exist in the model is not totally clear. Peyrard and Kruskal [109] have found what appear to be sliding kinks in numerical simulations of equation (5.1) for relatively large values of h, where the kink extends over only a few lattice sites; that is, in the highly discrete regime. Their simulations revealed preferred velocities at which kinks propagate semi-stably, apparently without the emission of radiation. For other velocities, the kinks were found to radiate strongly. This seems like the signature of sliding kinks. However, Duncan, Eilbeck, Feddersen and Wattis [113] were unable to generate a kink with vanishing radiation tails using their pseudospectral method [75], in the light of which it is most probable that there exist only minima, rather than zeros, of the radiation amplitudes at the preferred velocities observed by Peyrard and Kruskal. Nonetheless, given how suggestive their results are, in this chapter we would like to make quite sure of the nonexistence of sliding kinks, at least in the continuum limit, by calculating the Stokes constant as a function of kink velocity.

If we make the travelling-wave ansatz in (5.1), $u_n(t) = \phi(z)$ where $z = n - vt$, then we obtain the differential-difference advance-delay equation

$$v^2\phi'' - \frac{\phi_+ - 2\phi + \phi_-}{h^2} + \sin\phi = 0. \tag{5.2}$$

Here, $\phi_\pm = \phi(z \pm h)$.

5.2 Regular perturbation expansion

We expand ϕ in a perturbation expansion as follows:

$$\phi = \phi_0 + h^2\phi_2 + \ldots \tag{5.3}$$

At $\mathcal{O}\left(h^0\right)$ this yields

$$(1 - v^2)\phi_0'' = \sin\phi_0$$

which supports the sine–Gordon kink

$$\phi_0(z) = 4\arctan\left[\exp\left(\frac{z - z_0}{\sqrt{1 - v^2}}\right)\right]. \tag{5.4}$$

We have chosen to restrict ourselves to the kink which connects zero at the left infinity to 2π at the right infinity.

At $\mathcal{O}\left(h^2\right)$ we have the linear nonhomogeneous equation

$$(1-v^2)\phi_2'' - (\cos\phi_0)\phi_2 = -\frac{1}{12}\phi_0''''.$$

The bounded solution is

$$\phi_2(Z) = \frac{1}{2(1-v^2)}\operatorname{sech} Z(3\tanh Z - Z + \alpha) \tag{5.5}$$

where $Z = \frac{z-z_0}{\sqrt{1-v^2}}$. The homogeneous solution, $\operatorname{sech} Z$, is the translation mode of the kink. Since it corresponds to a trivial symmetry of the advance-delay equation (5.2), we exclude it by setting $\alpha = 0$.

We have now established the first two terms, (5.4) and (5.5), of the perturbation series (5.3), known as the outer expansion. As in section 3.2.1, the expansion can be continued to any order, and solutions at all orders decay exponentially to zero as $|Z| \to \infty$. To detect the exponentially small radiation, we must invoke the method of asymptotics beyond all orders [52].

5.3 Inner equation

The leading-order solution ϕ_0 given by eq. (5.4) has singularities at $Z = \frac{i\pi}{2} + i\pi n$, $n \in \mathbb{Z}$. If we introduce the inner variable ζ such that

$$Z = \frac{i\pi}{2} + \frac{h\zeta}{\sqrt{1-v^2}} \tag{5.6}$$

and expand $\phi = \phi_0 + h^2\phi_2 + \mathcal{O}\left(h^4\right)$ in inverse-powers of ζ and powers of h, we obtain

$$\hat{\phi}(\zeta) = -i\ln h^2 - i\left[\ln\zeta^2 + 2\pi i - \ln 4(1-v^2) + \frac{3}{2(1-v^2)}\frac{1}{\zeta^2} + \mathcal{O}\left(\zeta^{-4}\right)\right] + h^2\left(\frac{i\zeta^2}{6(1-v^2)} + \mathcal{O}\left(\zeta^0\right)\right) + \mathcal{O}\left(h^4\right). \tag{5.7}$$

The hat, as before, denotes a series which may not converge for finite ζ.

The inner equation is usually found by making the change of variables (5.6) in (5.2). A solution is then sought which is asymptotic to the perturbative solution of (5.2) (the outer solution) on the real axis, i.e. asymptotic to the expression (5.7) in the limit $\operatorname{Im}\zeta \to -\infty$. In this limit the terms at $\mathcal{O}\left(h^2\right)$ and higher in (5.7) grow to infinity and dwarf the $\mathcal{O}\left(h^0\right)$ terms, and therefore it

is necessary to 'truncate' the inner equation by taking the limit $h \to 0$. However, we see that the expression above is divergent as $h \to 0$, and hence it will not be possible to truncate the inner equation and still hope to find a solution asymptotic to (5.7). Another difficulty is that, even when the $\mathcal{O}(h^2)$ terms are eliminated, (5.7) does not tend to zero as $|\zeta| \to \infty$, and so will not be representable as a Laplace transform, as we require when we convert the inner equation to an integral equation.

To solve both of these problems we make the transformation

$$\psi = \phi + i\left[\ln h^2 + \ln \zeta^2 + 2\pi i - \ln 4(1-v^2)\right] \tag{5.8}$$

in addition to (5.6) in (5.2) to get the (nonautonomous) inner equation

$$v^2\psi_{\zeta\zeta} + 2iv^2\frac{1}{\zeta^2} - [\psi(\zeta+1) - 2\psi(\zeta) + \psi(\zeta-1)] + 2i\ln\left(1-\frac{1}{\zeta}\right) + 2i(1-v^2)\frac{1}{\zeta^2}e^{-i\psi} - \frac{ih^4\zeta^2}{8(1-c^2)}e^{i\psi} = 0. \tag{5.9}$$

To neaten this up we can take $\varphi = -i\psi$. Taking the limit $h \to 0$, as discussed, and expanding the logarithm in a power series and rearranging terms, the inner equation becomes

$$\varphi(\zeta+1) - 2\varphi(\zeta) + \varphi(\zeta-1) - v^2\varphi_{\zeta\zeta} + 2\sum_{n=2}^{\infty}\frac{1}{n}\frac{1}{\zeta^{2n}} - 2(1-v^2)\frac{1}{\zeta^2}(e^{\varphi}-1) = 0. \tag{5.10}$$

The expansion for φ corresponding to (5.7) is

$$\hat{\varphi}(\zeta) = \frac{3}{2(1-v^2)}\frac{1}{\zeta^2} + \mathcal{O}\left(\zeta^{-4}\right). \tag{5.11}$$

By linearising (5.10) about the perturbation series (5.11) we obtain the 'exponential expansion'

$$\varphi(\zeta) = \hat{\varphi}(\zeta) + \alpha_1^{(\pm)}\left[1 - \frac{i(1-v^2)}{\sin k_1 - v^2k_1^2}\frac{1}{\zeta} + \mathcal{O}\left(\zeta^{-2}\right)\right]e^{-ik_1\zeta} + \text{higher-wavenumber terms}, \tag{5.12}$$

valid for $v \neq 0$. (We will not consider the $v = 0$ case here.) This expression, being a linearisation, is accurate when α_1 is small or ζ has a large negative imaginary part. In order to continue this expression back to the real axis, the limit $\operatorname{Im}\zeta \to -\infty$ must be taken, in which case the terms with higher wavenumber become exponentially small by comparison with the $e^{-ik_1\zeta}$ term, and so can safely be ignored. The wavenumber k_1 is the smallest positive root of

$$\frac{2}{k}\sin\frac{k}{2} = \pm v. \tag{5.13}$$

For any fixed and finite $\mathrm{Im}\,\zeta$, (5.12) only holds in the limit $|\mathrm{Re}\,\zeta| \to \infty$ since it is based on a linearisation not about a solution, but about a series *asymptotic to* a solution in the limit $|\zeta| \to \infty$. Therefore the amplitudes of the radiation tails as $\mathrm{Re}\,\zeta \to +\infty$ ($\alpha_1^{(+)}$) and $\mathrm{Re}\,\zeta \to -\infty$ ($\alpha_1^{(-)}$) will be unrelated. Of course, since the expansion (5.12) is also valid in the limit $\mathrm{Im}\,\zeta \to -\infty$, these two tails should match up in this limit, and indeed they do, since both tend exponentially to zero.

5.4 Inner integral equation

In order to convert (5.10) to an integral equation, we write φ as a Laplace transform:

$$\varphi(\zeta) = \int_\gamma V(p) e^{-\zeta p} dp, \tag{5.14}$$

as before. Once again, γ must be a concave-up path which lies between the imaginary axis and all complex singularities of $V(p)$ and for which $\arg p \to \pi/2$ as $|p| \to \infty$ along the path. We substitute (5.14) into (5.10), dealing with the nonlinear term e^{φ} by series expansion, to obtain the integral equation

$$(4\sinh^2\frac{p}{2} - v^2p^2)V(p) + 2\sum_{n=2}^{\infty}\frac{1}{n}\frac{1}{(2n-1)!}p^{2n-1} = 2(1-v^2)\sum_{n=1}^{\infty}\frac{1}{n!}p*^nV(p). \tag{5.15}$$

Here, $*$ has the usual meaning of the convolution operator,

$$V(p)*W(p) = \int_0^p V(p')W(p-p')dp', \tag{5.16}$$

where the integration is along the contour γ, and the notation '$^nV(p)$' has the meaning

$${}^nV(p) = \underbrace{V(p)*V(p)*\ldots*V(p)}_{n\text{ times}}. \tag{5.17}$$

As we did in section 3.2.3, we have used the result proved in appendix 3.A of chapter 3 that the convolution theorem for Laplace transforms along paths on the complex plane can be applied in the same way as for traditional Laplace transforms. The conditions of the theorem are fulfilled as our paths of integration are concave-up and lie above all singularities of $V(p)$ with a nonzero real part.

5.5 Recurrence relation

To produce the even inverse-power series (5.11) when Laplace-transformed, $V(p)$ should have an odd power-series expansion

$$V(p) = \sum_{n=0}^{\infty} w_n p^{2n+1}. \tag{5.18}$$

Of course, we only know that the first few terms of (5.11) are even; however, this is sufficient to ensure that the whole series is even. To verify this, we assume a general power series for $V(p)$ and find the coefficients to be nonunique: The coefficient of the p^2 term can be chosen arbitrarily. This term, though, corresponds to the ζ^{-3} term in (5.11), which is absent. When we set the coefficient of the p^2 term to zero we obtain a unique, odd, power series for $V(p)$. To calculate the coefficients of this power series (and show that it is indeed unique) we substitute (5.18) into (5.15), and obtain the following recurrence relation for the coefficients w_n:

$$\sum_{m=0}^{n} \frac{2}{(2m+2)!} w_{n-m} - v^2 w_n + \frac{4}{(2n+4)!} - 2(1-v^2) \sum_{\alpha=1}^{n+1} \frac{1}{\alpha!} c_n^{(\alpha)} = 0 \tag{5.19}$$

for all $n \geq 0$, where

$$c_n^{(1)} = \frac{1}{(2n+3)(2n+2)} w_n \quad \text{and} \quad c_n^{(\alpha+1)} = \sum_{m=\alpha}^{n} c_{m-1}^{(\alpha)} \frac{(2m+1)!(2n-2m+1)!}{(2n+3)!} w_{n-m}$$

for all $\alpha \geq 1$. Setting $n = 0$ in (5.19) gives $w_0 = -\frac{1}{4}(1-v^2)^{-1}$; for $n > 0$, eq. (5.19) can easily be solved for w_n in terms of w_k, where $k < n$, since $c_n^{(1)}$ is the only one of the coefficients $c_n^{(\alpha)}$ to contain w_n. Thus any desired number of coefficients can be calculated in a recursive manner.

5.6 Borel summation

The series expansion (5.18) for $V(p)$ has radius of convergence k_1. This follows from the fact that the integral equation (5.15) has singularities at $p = \pm ik_n$ on the imaginary axis, where k_n are the roots, in order from smallest to largest, of (5.13). This can be seen by inspection of the integral equation – the coefficient in front of $V(p)$ on the left-hand side vanishes at these points, whereas the sum of the convolution terms will, in general, not vanish, implying that $V(p)$ must be singular. The power-series expansion cannot continue past these singularities. When this series, eq. (5.18), is Laplace-transformed, we obtain (as required) the inverse-power series (5.11) which in general will not converge for any value of ζ (since the integration path in the Laplace integral extends beyond the radius of convergence of the power series).

The next step is to attempt to re-sum the power series to an expression with no restriction on its radius of convergence; when Laplace transformed, this expression will be a Borel sum of the asymptotic series (5.11). Indeed, the method of Borel summation is what originally motivated Pomeau, Ramani and Grammaticos [133] to employ an integral transform when they pioneered the method.

The resummation of the power series (5.18) is obviously not a straightforward task as we do not even have an explicit expression for the coefficients [but rather the recurrence relation (5.19)]. We are guided by (5.12), the expression for the radiation tails of the inner solution. Whatever path of integration we pick in (5.14) will result in a solution with the same inverse-power series expansion $\hat{\varphi}(\zeta)$. However, if we pick a path in the first quadrant, the solution, which we call $\varphi_s(\zeta)$, will tend to zero as $\mathrm{Re}\,\zeta \to +\infty$ for fixed $\mathrm{Im}\,\zeta$. [This follows from (5.14).] That is, $\alpha_1^{(+)} = 0$ in (5.12). Likewise, for a path of integration in the *second* quadrant we generate a solution $\varphi_u(\zeta)$ for which $\alpha_1^{(-)} = 0$. From (5.12), the difference between the two is given by

$$\varphi_s(\zeta) - \varphi_u(\zeta) = \mp\alpha_1^{(\pm)} \left[1 - \frac{i(1-\nu^2)}{\sin k_1 - \nu^2 k_1^2}\frac{1}{\zeta} + \mathcal{O}\left(\zeta^{-2}\right)\right] e^{-ik_1\zeta} + \text{higher-wavenumber terms.} \tag{5.20}$$

To generate the first term in the square brackets, $V(p)$ must have a a simple pole at ik_1, and to generate the second term, a logarithmic singularity at ik_1. Further subdominant singularities generate the $\mathcal{O}\left(\zeta^{-2}\right)$ terms. Considering that $V(p)$ is an odd function, the expression for the singularities is therefore the following:

$$V(p) = K_1(\nu)\frac{pk_1^2}{p^2+k_1^2} + \sigma(\nu)p\ln(p^2+k_1^2) + \ldots \tag{5.21}$$

The ellipsis ('...') stands for terms which grow more slowly as $p \to ik_1$. Here,

$$\mp\alpha_1^{(\pm)} = i\pi k_1^2 K_1(\nu) \quad \text{and}$$
$$\sigma(\nu) = \frac{i(1+ik_1)(1-\nu^2)}{(\sin k_1 - \nu^2 k_1^2)(1+k_1^2)}.$$

Equation (5.21) and the expressions above are obtained by taking the difference of Laplace transforms along the paths γ_s and γ_u shown in figure 3.1 (p. 63) and comparing to eq. (5.20), as was described in section 3.2.4 for the discrete ϕ^4 equation.

We now expand the expression (5.21) in powers of p in order to match it to (5.18):

$$V(p) = (K_1(\nu) + \sigma(\nu)\ln k_1^2)p + \sum_{\ell=1}^{\infty}(-1)^\ell k_1^{-2\ell}\left[K_1(\nu) - \frac{\sigma(\nu)}{\ell} + \ldots\right] p^{2\ell+1} \tag{5.22}$$

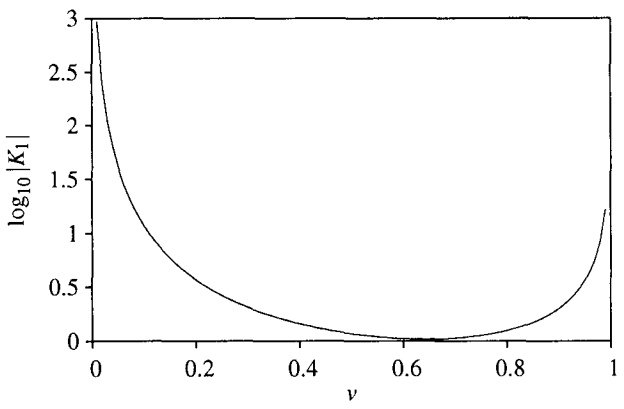

Figure 5.1: First Stokes constant as a function of velocity for the Frenkel–Kontorova equation (note the logarithmic scale).

This implies that

$$K_1(v) = \lim_{\ell \to \infty} (-1)^{\ell} k_1^{2\ell} w_{\ell}. \tag{5.23}$$

The expansions have only been matched in the limit $\ell \to \infty$ because of the unknown terms represented by '...'. Thus, (5.21) does not *fully* match the power series; it only matches the high-order coefficients – that is, it only matches close to the singularity. If we had an expression which matched everywhere, its Laplace transform would be a Borel sum of the asymptotic series, i.e. an exact solution of the inner equation. However, knowing a function which matches only near the singularities is almost as good: Taking the difference of Laplace transforms along the two paths γ_s and γ_u has given us the expression for the radiation tail in (5.12). The expression for the oscillatory tails in (5.12) is the difference between two possible Borel sums of the asymptotic series (5.11). The Borel sum, of course, is nonunique, depending on the position of the integration contour relative to singularities of the integrand. With γ_u we generate a solution with a radiation tail at the right infinity, and at the left infinity with γ_s.

5.7 Results and conclusions

Figure 5.1 shows the Stokes constant $K_1(v)$ calculated using (5.23). The coefficients w_n are evaluated numerically using the algebraic recurrence relation (5.19). It is nowhere zero, its minimum value being approximately 1.04 at $v = 0.64$.

Recall that $\varphi_s(\zeta)$ is represented by (5.12), with $\alpha^{(+)} = 0$ and $\alpha^{(-)} = i\pi k_1^2 K_1(v)$. The question still remains whether these oscillatory tails in the inner equations translate to radiation from

the original soliton. The answer is yes, as we demonstrate in the context of the discrete NLS equation in chapter 6. For now, we again restrict ourselves to arguing the nonexistence of radiationless kinks. Due to the presence of the radiation tails, the inverse-power series (5.11) does not converge. However, if a radiationless kink did exist, its asymptotic expansion, and hence inverse-power series, would be convergent. Since $K_1(v)$ is never zero, there will always be a singularity of the integral equation (5.15) at $p = ik_1$ which, as discussed, leads to the non-convergence of the inverse-power series. This argument (that nonzero Stokes constants are sufficient for nonexistence of radiationless solutions to the original, outer equation) is rigorously proved by Tovbis in [138]. We conclude that radiationless travelling kinks of unit topological charge (i.e. an amplitude of 2π) do not exist in the Frenkel–Kontorova model, at least near the continuum limit. This conclusion agrees with that of ref. [113] (which does not only apply near the continuum limit). Thus, we have confirmed that the candidate sliding solitons observed by Peyrard and Kruskal [109] are not entirely radiationless. However, aside from these $Q = 1$ kinks, Peyrard and Kruskal also observed freely-propagating multikinks of topological charge 2 and 3 (i.e. kinks of amplitude 4π and 6π) which, numerics suggest, are indeed radiation free [185].

The objective of this chapter—to find an example of a nonexceptional system which supports sliding kinks—has not been met, and so we now proceed to consider another candidate, the DNLS model.

Chapter 6

Moving solitons in the discrete nonlinear Schrödinger equation

The subject of this chapter—the discrete nonlinear Schrödinger (DNLS) equation—is very rich in physical applications (in contrast to the exceptional ϕ^4 models considered in chapter 3, which were primarily of mathematical interest), and therefore sliding solitons, if they exist, could have great practical use. Also, having found no sliding solitons in the Frenkel–Kontorova model, we aim again to find disproof of the necessity of exceptionality for the existence of sliding kinks. In this chapter our objective is no longer simply to prove or disprove the existence of sliding solitons, but to measure the radiation from travelling solitary waves and its effect on their dynamics.

6.1 Introduction

The earliest applications of the cubic DNLS equation were to the self-trapping of electrons in lattices (the polaron problem) and energy transfer in biological chains (Davydov solitons) – see the reviews [9, 122, 164] for references. Relatedly, the equation arises in the description of small-amplitude breathers in Frenkel–Kontorova chains with weak coupling [164]. In optics the equation describes light-pulse propagation in nonlinear waveguide arrays in the tight-binding limit [81, 105]. Most recently the DNLS equation has been used to model Bose–Einstein condensates in optically-induced lattices [106].

The question of the existence of moving solitons in the DNLS equation has been the subject

of debate for some time [87, 112, 113, 114, 119, 123, 124, 186, 187, 188, 189, 190, 191, 192]. Recently, Gómez-Gardeñes, Floría, Falo, Peyrard and Bishop [193, 194] have demonstrated that the stationary motion of pulses in the cubic one-site DNLS equation (the 'standard' DNLS equation) is only possible over an oscillatory background consisting of a superposition of plane waves. This result was obtained by numerical continuation of the moving Ablowitz–Ladik breather with two commensurate time scales. We should mention here that earlier studies of moving breathers in Klein–Gordon chains had numerically detected a similar background of plane waves [195]. In this chapter, we study the travelling discrete solitons analytically and independently of any reference models. Consistently with the conclusions of [193, 194], we will show that solitons cannot freely move in the cubic DNLS equation; they emit radiation, decelerate and eventually become pinned by the lattice. We shall show, however, that this radiation is exponentially small in the soliton's amplitude, so that broad, small-amplitude pulses are highly mobile and are for all practical purposes indistinguishable from freely moving solitons.

In the context of optical waveguide arrays—important not only in themselves but also as a first step to understanding more complicated optical systems such as photonic crystals—interest among experimentalists [101, 102, 142] has recently shifted away from media with pure-Kerr nonlinearity (which gives rise to a cubic term in the DNLS equation) and towards photorefractive media, which exhibit a *saturable* nonlinearity [140, 141, 196, 197, 198]. In practice such arrays may be optically induced in a photorefractive material [101, 102] or fabricated permanently – see [142], for example. The study of solitons in *continuous* optical systems with saturable nonlinearitites has a long history; interesting phenomena here include bistability [199, 200], fusion [201] and radiation effects [202] which do not arise in the cubic case. Collisions between solitons have also been investigated in the discrete saturable model [198], where fusion, soliton creation, and reflection are observed in the interaction. As far as stationary solutions go, Khare, Rasmussen, Samuelsen and Saxena's work [203] suggests that the saturable one-site DNLS equation may, after all, be exceptional in the sense defined in chapter 4 (that is, despite not being a translation-invariant system, it supports translationally invariant stationary solitons). This property is usually seen as a prerequisite for undamped motion in discrete equations (as discussed in section 1.6 and supported by the evidence of chapters 3 and 5 of this thesis), and indeed, Hadžievski, Maluckov, Stepić and Kip [140] have found vanishings of the PN barrier and numerically verified that this leads to enhanced soliton mobility in the saturable DNLS equation.

Thus, two questions to be answered are whether the saturable DNLS model is indeed exceptional, and whether it supports sliding solitons. The results will either strengthen or destroy the evidence of chapters 3 and 5 for a connection between the two. Thus, after the cubic model, the DNLS equation with a saturable nonlinearity is the second object of our analysis here; our conclusions will turn out to be in agreement with the numerical observations of enhanced mobility in refs [140, 141] (although the latter study was in the two-dimensional case). We will show that for nonlinearities which saturate at a low enough intensity, solitons can indeed slide—that is, move without radiative deceleration—at certain isolated velocities. These sliding solitons are examples of embedded solitons.

The usual saturable DNLS equation is the discrete form of the Vinetskii–Kukhtarev model [204]:

$$i\dot{\Phi}_n + \Phi_{n+1} - 2\Phi_n + \Phi_{n-1} - \gamma\frac{1}{1+|\Phi_n|^2}\Phi_n = 0. \tag{6.1}$$

In order to encompass both cubic and saturable nonlinearities in a single model, we shall instead consider the equation

$$i\dot{\phi}_n + \phi_{n+1} + \phi_{n-1} + \frac{2|\phi_n|^2}{1+\mu|\phi_n|^2}\phi_n = 0, \tag{6.2}$$

obtained from (6.1) by making the transformation $\Phi_n = \sqrt{2/\gamma}e^{-i(2+\gamma)t}\phi_n$, and letting $\mu = 2/\gamma$. In the form above, $1/\mu$ represents the saturation threshold of the medium [200], which tends to infinity as one approaches the pure Kerr (cubic) case of $\mu = 0$. The higher the value of μ, the lower is the intensity at which the nonlinearity saturates.

This chapter is structured in the following way. In section 6.2, we construct a small-amplitude, broad travelling pulse as an asymptotic series in powers of ε, its amplitude. The velocity and frequency of this soliton are obtained as explicit functions of ε and the wavenumber of its carrier wave. Then in section 6.3, the main section of this chapter, we derive an expression for the soliton's radiation tails and measure their amplitude using the method of asymptotics beyond all orders. In section 6.4, we investigate the influence of this exponentially weak radiation on the soliton's amplitude and speed. Finally, in section 6.6, we summarise our work and make comparisons with some earlier results.

6.2 Asymptotic Expansion

6.2.1 The leading order

We begin by seeking solutions of the form

$$\phi_n(t) = \psi(X)e^{ikn+i\omega t}, \tag{6.3}$$

where

$$X = \varepsilon(n - vt) \tag{6.4}$$

and ε is a parameter. By analogy with the soliton of the continuous NLS, we expect the discrete soliton to be uniquely characterised by two parameters, e.g. ε and k, while the other two (ω and v) are expected to be expressible through ε and k. Substituting the Ansatz (6.3)-(6.4) into (6.2) gives a differential advance-delay equation

$$\psi(X+\varepsilon)e^{ik} + \psi(X-\varepsilon)e^{-ik} - \omega\psi(X) - i\varepsilon v\psi'(X) + \frac{2|\psi(X)|^2}{1+\mu|\psi(X)|^2}\psi(X) = 0. \tag{6.5}$$

This can be written as an ordinary differential equation of an infinite order:

$$e^{ik}\sum_{n=0}^{\infty}\varepsilon^n\frac{1}{n!}\psi^{(n)} + e^{-ik}\sum_{n=0}^{\infty}\varepsilon^n\frac{(-1)^n}{n!}\psi^{(n)} - \omega\psi - i\varepsilon v\psi' + \frac{2|\psi|^2}{1+\mu|\psi|^2}\psi = 0, \tag{6.6}$$

where $\psi^{(n)} = d^n\psi/dX^n$.

From now on we assume that ε is small. Our aim in this section is to find an approximate solution to eq. (6.6)—and hence eq. (6.2)—with $\psi = \mathcal{O}(\varepsilon)$. (That is, we are looking for small, broad pulses which modulate a periodic carrier wave.) To this end, we expand ψ, ω and v as power series in ε:

$$\psi = \varepsilon(\psi_0 + \varepsilon\psi_1 + \ldots), \tag{6.7a}$$

$$\omega = \omega_0 + \varepsilon^2\omega_2 + \ldots, \tag{6.7b}$$

$$v = v_0 + \varepsilon^2 v_2 + \ldots. \tag{6.7c}$$

(We are not expanding k as we consider it, along with ε, as one of the two independent parameters characterising our solution.) Substituting these expansions into (6.6) gives a hierarchy of equations to be satisfied at each power of ε by choosing ω_n and v_n properly. In nonlinear oscillations, this perturbation procedure is known as Lindstedt's method [205].

At the order ε^1 we obtain

$$\omega_0 = 2\cos k, \tag{6.8}$$

while the order ε^2 gives

$$v_0 = 2\sin k. \tag{6.9}$$

These two relations correspond to the dispersion of linear waves. At the power ε^3 we obtain the following nonlinear equation for ψ_0:

$$\cos k\, \psi_0'' - \omega_2 \psi_0 + 2|\psi_0|^2 \psi_0 = 0.$$

This is the stationary form of the nonlinear Schrödinger (NLS) equation, which has the homoclinic solution

$$\psi_0 = a\sqrt{\cos k}\,\mathrm{sech}(aX)$$

with

$$a^2 = \frac{\omega_2}{\cos k}.$$

Returning to the original variable ψ, we note that the amplitude a can always be absorbed into ε, the parameter in (6.4) and in front of ψ_0 in (6.7a). That is, there is no loss of generality in setting $a = 1$ and letting ε describe the amplitude (and inverse width of the pulse) instead. This allows us to set

$$\omega_2 = \cos k. \tag{6.10}$$

Note that the coefficients in (6.5) are periodic functions of the parameter k with period 2π; therefore it is sufficient to consider k in the interval $(-\pi, \pi)$. Also, (6.5) is invariant with respect to the transformation $k \to -k$, $\varepsilon \to -\varepsilon$, $v \to -v$; hence it is sufficient to consider positive k only. Finally, our perturbative solution does not exist if $\cos k$ is negative. Thus, from now on we shall assume that $0 \le k \le \pi/2$.

6.2.2 Higher orders

At the order ε^{n+3}, where $n \ge 1$, we arrive at the following equations for the real and imaginary parts of ψ_n:

$$\mathcal{L}_1 \operatorname{Re}\psi_n = \frac{\operatorname{Re} f_{n-1}(X)}{\cos k} \tag{6.11a}$$

$$\mathcal{L}_0 \operatorname{Im}\psi_n = \frac{\operatorname{Im} f_{n-1}(X)}{\cos k}, \tag{6.11b}$$

where

$$\mathcal{L}_0 = -\partial_X^2 + 1 - 2\,\mathrm{sech}^2 X,$$
$$\mathcal{L}_1 = -\partial_X^2 + 1 - 6\,\mathrm{sech}^2 X$$

and

$$f_{n-1}(X) = \sum_{j=1}^{[n/2]} \left(\frac{2\cos k}{(2j+2)!} \psi_{n-2j}^{(2j+2)} - \omega_{2j+2} \psi_{n-2j} \right) + i \sum_{j=1}^{[\frac{n+1}{2}]} \left(\frac{2\sin k}{(2j+1)!} \psi_{n-2j+1}^{(2j+1)} - \nu_{2j} \psi_{n-2j+1}' \right)$$
$$+ \sum_{m=1}^{n-1} 2\psi_0 (\psi_m \psi_{n-m}^* - \psi_{n-m} \psi_m^*) + \sum_{m=1}^{n-1} \sum_{\ell=0}^{n-1-m} 2\psi_{n-m-\ell} \psi_m \psi_\ell^*$$
$$+ \mu \sum_{m=0}^{n-1} \sum_{\ell=0}^{n-1-m} \left[\sum_{j=1}^{[\frac{n-m-\ell}{2}]} \left(\frac{2\cos k}{(2j)!} \psi_{n-m-\ell-2j}^{(2j)} - \omega_{2j} \psi_{n-m-\ell-2j} \right) \right.$$
$$\left. + i \sum_{j=1}^{[\frac{n-m-\ell-1}{2}]} \left(\frac{2\sin k}{(2j+1)!} \psi_{n-m-\ell-2j-1}^{(2j+1)} - \nu_{2j} \psi_{n-m-\ell-2j-1}' \right) \right] \psi_m \psi_\ell^*. \quad (6.12)$$

The linear nonhomogeneous ordinary differential equations (6.11) must be solved subject to a boundedness condition.

The bounded homogeneous solutions of (6.11a) and (6.11b) ($\mathrm{sech}\, X \tanh X$ and $\mathrm{sech}\, X$, respectively) correspond to the translation- and U(1)-invariances of eq. (6.5). Including these zero modes in the full solution of eqs (6.11) would amount just to the translation of $\psi(X)$ by a constant distance in X and its multiplication by a constant phase factor. These deformations are trivial, and hence we can safely discard the homogeneous solutions at each order of ε.

As ψ_0's real part is even and its imaginary part is odd (zero), ψ_1's real and imaginary parts are also even and odd, respectively. The same holds, by induction, to all orders of the perturbation theory. Indeed, assume that $\psi_0, \psi_1, \ldots, \psi_{n-1}$ have even real parts and odd imaginary parts. Then it is not difficult to verify that the function $\mathrm{Re} f_{n-1}(X)$ is even and $\mathrm{Im} f_{n-1}(X)$ is odd. Since the operators $\mathcal{L}_0$ and $\mathcal{L}_1$ are parity-preserving, and since we have excluded the corresponding homogeneous solutions, this means that ψ_n has an even real part and an odd imaginary part. Finally, the homogeneous solution of (6.11b) being even and that of (6.11a) being odd, the corresponding solvability conditions are satisfied at any order.

Note that since the solvability conditions do not impose any constraints on ν_n and ω_n, the coefficients ν_n with $n \geq 2$ and ω_n with $n \geq 4$ can be chosen completely arbitrarily.

6.2.3 Explicit perturbative solution to order ε^3

Solving equations (6.11) successively, we can obtain the discrete soliton (6.7a) to any desired accuracy. Here, we restrict ourselves to corrections up to the cubic power in ε. The order ε^3 is the lowest order at which the saturation parameter μ appears in the solution. On the other hand, it is high enough to exemplify and motivate our choice of the coefficients in (6.7b) and (6.7c).

Letting $n = 1$ in eq. (6.12), we have

$$f_0(X) = \frac{2i}{3!}\sin k\psi_0''' - iv_2\psi_0'.$$

The corresponding solution of eq. (6.11) is

$$\psi_1 = \frac{i}{\sqrt{\cos k}}\left[\frac{1}{2}\sin k\,\mathrm{sech}\,X\tanh X + \frac{1}{2}\left(v_2 - \frac{1}{3}\sin k\right)X\,\mathrm{sech}\,X\right].$$

Here the term proportional to $X\,\mathrm{sech}\,X$ decays to zero as $|X| \to \infty$; however, it becomes greater than $\psi_0(X)$ for sufficiently large $|X|$, leading to non-uniformity of the expansion (6.7a). In order to obtain a uniform expansion, the term in question should be eliminated. Being free to choose the coefficients v_n with $n \geq 2$, we use this freedom to set

$$v_2 = \frac{1}{3}\sin k.$$

This leaves us with

$$\psi_1 = \frac{i}{2}\sqrt{\cos k}\tan k\,\mathrm{sech}\,X\tanh X.$$

After 'distilling' in a similar way the correction ψ_2, where we fix

$$\omega_4 = \frac{1}{12}\cos k$$

to eliminate a term proportional to $X\,\mathrm{sech}\,X$, we obtain:

$$\psi = \varepsilon\sqrt{\cos k}\Big\{\mathrm{sech}\,X + \frac{i}{2}\varepsilon\tan k\,\mathrm{sech}\,X\tanh X + \frac{1}{12}\varepsilon^2\big[4\,\mathrm{sech}^3 X - 3\,\mathrm{sech}\,X + \frac{1}{2}\tan^2 k(14\,\mathrm{sech}^3 X - 13\,\mathrm{sech}\,X) + 4\mu\cos k(2\,\mathrm{sech}\,X - \mathrm{sech}^3 X)\big] + \mathcal{O}(\varepsilon^3)\Big\}, \quad (6.13)$$

where

$$\omega = 2\left[1 + \frac{1}{2!}\varepsilon^2 + \frac{1}{4!}\varepsilon^4 + \mathcal{O}(\varepsilon^6)\right]\cos k, \quad (6.14a)$$

$$v = 2\left[1 + \frac{1}{3!}\varepsilon^2 + \mathcal{O}(\varepsilon^4)\right]\sin k. \quad (6.14b)$$

6.2.4 Velocity and frequency of the discrete soliton

In the previous subsection we have shown that fixing suitably the coefficients ω_n and v_n can lead to a uniform expansion of ψ to order ε^3. Our approach was based on solving for ψ_n explicitly and then setting the coefficients in front of the 'secular' terms $X\,\mathrm{sech}\,X$ to zero. Here, we show that the secular terms can be eliminated to all orders – and without appealing to explicit solutions.

Assume that the secular terms have been suppressed in all nonhomogeneous solutions ψ_m with m up to $n-1$; that is, let

$$\psi_m(X) \to C_m e^X + o(e^X) \quad \text{as } X \to -\infty \quad (m = 0, 1, ..., n-1). \tag{6.15}$$

(Since we know that the real part of ψ_m is even and the imaginary part odd, it is sufficient to consider the asymptotic behaviour at one infinity only.) The constant C_m may happen to be zero for some m in which case the decay of ψ_m will be faster than e^X. Our objective is to choose ω_n and v_n in such a way that $\psi_n(X)$ will also satisfy (6.15). To this end, we consider the function (6.12). All terms which are trilinear in $\psi_0, ..., \psi_{n-1}$ and derivatives of these functions decay as e^{3X} or faster; these terms in f_{n-1} cannot give rise to the secular terms proportional to $X\,\mathrm{sech}\,X$ in ψ_n. On the other hand, the terms making up the first line in (6.12) tend to

$$e^X \sum_{j=1}^{[n/2]} \left[\frac{2\cos k}{(2j+2)!} - \omega_{2j+2} \right] C_{n-2j} + ie^X \sum_{j=1}^{[\frac{n+1}{2}]} \left[\frac{2\sin k}{(2j+1)!} - v_{2j} \right] C_{n-2j+1}$$

as $X \to -\infty$. These are 'asymptotically resonant' terms – in the sense that their asymptotics are proportional to the asymptotics of the homogeneous solutions of (6.11a) and (6.11b). It is these terms in the right-hand sides of (6.11a) and (6.11b) that give rise to the secular terms in the solution ψ_n. The resonant terms will be suppressed if we let

$$\omega_{2j+2} = \frac{2\cos k}{(2j+2)!}, \quad v_{2j} = \frac{2\sin k}{(2j+1)!}, \quad j \geq 1. \tag{6.16}$$

After the resonant terms have been eliminated, the bounded solution to (6.11) will have the asymptotic behaviour $\psi_n \to C_n e^X$ as $X \to -\infty$. By induction, this result extends to all $n \geq 0$.

Substituting (6.16), together with (6.8)–(6.10), into eqs (6.7b) and (6.7c), and summing up the series, we obtain

$$\omega = 2\cos k \cosh \varepsilon, \quad v = 2\sin k \frac{\sinh \varepsilon}{\varepsilon}, \tag{6.17}$$

the frequency and velocity of the discrete soliton parametrised in terms of k and ε.

Equations (6.17) coincide with the expressions [23] of the Ablowitz–Ladik soliton's velocity and frequency in terms of its amplitude and wavenumber. The difference between the two sets of answers is in that eqs (6.17) pertain to small-amplitude solitons only, whereas Ablowitz and Ladik's formulas are valid for arbitrarily large amplitudes.

Note, also, that in the case $k = 0$, the solution (6.13) coincides (at least to third order) with the stationary solution of eq. (6.5) obtained by Khare, Rasmussen, Samuelson and Saxena [203]. However, the soliton of ref. [203] has its amplitude and frequency uniquely determined by the saturation parameter (μ), whereas the velocity and frequency (6.17) of our perturbative solution do not depend on μ. This restriction on the exact solution (compared to the perturbative one) is attributable to beyond-all-orders terms, to which we now turn our attention.

6.3 Terms beyond all orders of the perturbation theory

6.3.1 Dispersion relation for linear waves

As $X \to -\infty$, the series (6.7a) reduces to $\psi(X) = \sum_{n=0}^{\infty} \varepsilon^{n+1} C_n e^X$. The convergence of the series $\sum \varepsilon^{n+1} \psi_n(X)$ for all X would imply, in particular, the convergence of the series $\sum \varepsilon^{n+1} C_n$. Therefore, if the series (6.7a) converged, the solution $\psi(X)$ would be decaying to zero as $X \to -\infty$. However, although we have shown that the series $\sum \varepsilon^{n+1} \psi_n(X)$ is asymptotic to all orders, it does not have to be convergent. For instance, it is easy to see that the series cannot converge for $v = \mu = 0$ and any ε; since the advance-delay equation (6.5) is translation-invariant, this would imply that we have constructed a family of stationary solitons with an arbitrary position relative to the lattice. This, in turn, would contradict the well established fact that the 'standard' cubic DNLS solitons can only be centred on a site or midway between two adjacent sites [206] (that is, that the 'standard' discretisation of the cubic NLS is not exceptional [207]). Thus, we expect that the perturbative solution (6.7a) satisfies $\psi(X) \to 0$ as $|X| \to \infty$ only for some special choices of v, ε and μ.

Can eq. (6.5) have a bounded solution despite the divergence of the corresponding series $\sum \varepsilon^{n+1} C_n$? To gain some insight into this matter, we linearise eq. (6.5) about $\psi = 0$ and find nondecaying solutions of the form $\psi = e^{iQX/\varepsilon}$ where Q is a root of the dispersion relation

$$\omega = 2\cos(k + Q) + Qv. \tag{6.18}$$

It is easy to check that there is at least one such harmonic solution [i.e. eq. (6.18) has at least one root] if $v \neq 0$. These harmonic waves can form a radiation background over which the soliton

propagates (as suggested by the numerics of [193, 194] and the analysis of a similar problem for the ϕ^4 kinks in chapter 3). Being nonanalytic in ε, such backgrounds cannot be captured by any order of the perturbation expansion.

As we will show below, not only the wavenumbers but also the amplitudes of the harmonic waves are nonanalytic in ε. This phenomenon was first encountered in the context of the breather of the continuous ϕ^4 model, where Eleonskii, Kulagin, Novozhilova, and Silin [208] suggested that the radiation from the breather could be exponentially weak. Segur and Kruskal [52, 177] then developed the method of 'asymptotics beyond all orders' to demonstrate that, in the limit $\varepsilon \to 0$, such radiation does exist. We will use Segur and Kruskal's method to measure the magnitude of the radiation background of the travelling discrete soliton.

Qualitatively, the fact that the radiation is not excited at any order of the perturbation expansion is explained by the fact that the soliton exists on the long length scale X, whereas the radiation has the shorter scale X/ε. To all orders, the two are uncoupled.

Using the relations (6.17), we can rewrite (6.18) as

$$\frac{\cosh\varepsilon - \cos\mathcal{Q}}{(\sinh\varepsilon/\varepsilon)\mathcal{Q} - \sin\mathcal{Q}} = \tan k. \tag{6.19}$$

The left hand side is plotted in figure 6.1. For $\varepsilon = 0$ it has minima at multiples of 2π where the curve is tangent to the horizontal axis. For nonzero ε, the minima of the curve are lifted off the $\mathcal{Q}$ axis slightly. The minima with larger values of $\mathcal{Q}$ have smaller elevations above the horizontal axis, i.e., the minima come closer and closer to the $\mathcal{Q}$ axis as $\mathcal{Q}$ grows. We see from the figure that for $k > k^{(1)}_{\max}$, where $k^{(1)}_{\max} \approx 0.22$, there is only one radiation mode. Note also that the left-hand side of eq. (6.19) is negative for negative $\mathcal{Q}$; since we have assumed that $0 \le k \le \pi/2$, this implies that eq. (6.19) cannot have negative roots.

6.3.2 Radiating solitons

Although we originally constructed the expansion (6.7a) as an asymptotic approximation to a solution which is stationary in the frame of reference moving with the velocity v, it can also represent an approximation to a time-dependent solution $\psi(X,t)$. Here $\psi(X,t)$ is related to $\phi_n(t)$, the discrete variable in eq. (6.2), by the substitution (6.3):

$$\phi_n(t) = \psi(X,t)e^{ikn+i\omega t}. \tag{6.20}$$

The coefficients ψ_n in the asymptotic expansion of $\psi(X,t)$ will coincide with the coefficients in the expansion of the stationary solution $\psi(X) = \sum \varepsilon^{n+1}\psi_n$ if the time derivatives $\partial_t\psi_n$ lie

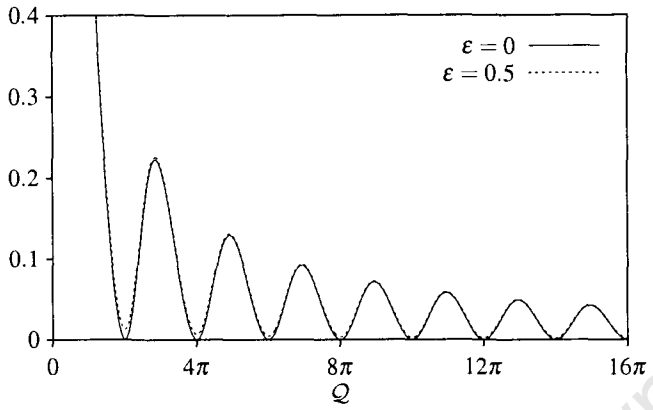

Figure 6.1: The left hand side of (6.19) for two values of ε. The root(s) $\mathcal{Q}_n$ of the dispersion relation (6.18) are located where this graph is intersected by a horizontal straight line with ordinate equal to $\tan k$.

beyond all orders of ε and hence the time evolution of the free parameters k and ε occurs on a timescale longer than any power of ε^{-1}. Physically, one such solution represents a travelling soliton slowing down and attenuating as the Cherenkov radiation left in its wake carries momentum and energy away from its core.

Substituting (6.20) in (6.2), gives

$$i\psi_t + \psi^+ e^{ik} + \psi^- e^{-ik} - \omega\psi - i\varepsilon v\psi_X + \frac{2|\psi|^2}{1+\mu|\psi|^2}\psi = 0, \tag{6.21}$$

where $\psi^\pm = \psi(X \pm \varepsilon, t)$.

We consider two solutions of this equation which both have the same asymptotic expansion (6.7a), denoted $\psi_s(X,t)$ and $\psi_u(X,t)$, such that $\psi_s(X,t) \to 0$ as $X \to +\infty$ and $\psi_u(X,t) \to 0$ as $X \to -\infty$. Since the difference $\Psi \equiv \psi_s - \psi_u$ is small (lies beyond all orders of ε), and since the solution ψ_s can be regarded as a perturbation of ψ_u, Ψ obeys the linearisation of eq. (6.21) about ψ_u to a good approximation. That is,

$$i\Psi_t + \Psi^+ e^{ik} + \Psi^- e^{-ik} - \omega\Psi - iv\varepsilon\Psi_X + \frac{4|\psi_u|^2\Psi + 2\psi_u^2\Psi^*}{1+\mu|\psi_u|^2} + \frac{2\mu|\psi_u|^2(|\psi_u|^2\Psi + \psi_u^2\Psi^*)}{(1+\mu|\psi_u|^2)^2} = 0. \tag{6.22}$$

Since $\psi_u = \mathcal{O}(\varepsilon)$, we can solve eq. (6.22) to leading order in ε by ignoring the last two terms in it; the resulting solutions are exponentials of the form $e^{i\mathcal{Q}X/\varepsilon - i\Omega t}$. We make a pre-emptive simplification by setting $\Omega = 0$. [That Ω has to be set equal to zero, follows from matching these exponentials to the far-field asymptotes of the stationary 'inner' solution; see section 6.3.4

below. Physically, $\Omega = 0$ implies that the travelling pulse will only excite the radiation with its own (zero) frequency in the comoving frame.] The leading-order solution of eq. (6.22) is therefore

$$\Psi = \sum_n A_n e^{i\mathcal{Q}_n X/\varepsilon} + \mathcal{O}\left(\varepsilon^1\right), \tag{6.23}$$

where $\mathcal{Q}_n$ ($n = 1, 2, ...$) are the roots, numbered in order from smallest to largest, of the dispersion relation (6.18). (Recall that since we have taken k in the interval $[0, \pi/2]$, all the roots $\mathcal{Q}_n$ are positive.) For $k > k_{\max}^{(1)} \approx 0.22$, there is only one root, $\mathcal{Q}_1$.

Higher-order corrections to the solution (6.23) can be found by substituting the ansatz

$$\begin{aligned}\Psi = &\sum_n A_n[1 + \varepsilon f_1^{(n)}(X) + \varepsilon^2 f_2^{(n)}(X) + \ldots]e^{i\mathcal{Q}_n X/\varepsilon} \\ &+ \sum_n A_n^*[\varepsilon^2 g_2^{(n)}(X) + \varepsilon^3 g_3^{(n)}(X) + \ldots]e^{-i\mathcal{Q}_n X/\varepsilon}\end{aligned} \tag{6.24}$$

in eq. (6.22), expanding the advance/delay terms $f_{1,2,\ldots}^{(n)}(X \pm \varepsilon)$, $g_{2,3,\ldots}^{(n)}(X \pm \varepsilon)$ in Taylor series in ε, and making use of the asymptotic expansion (6.7a), (6.13) for ψ_u. For instance, the first few corrections are found to be

$$\begin{aligned} f_1^{(n)}(X) &= \frac{4i\cos k}{2\sin(k+\mathcal{Q}_n) - v}\tanh X, \\ g_2^{(n)}(X) &= \frac{2\cos k}{\omega + vq_n - 2\cos(k - \mathcal{Q}_n)}\operatorname{sech}^2 X. \end{aligned} \tag{6.25}$$

Since $\psi_u \to 0$ as $X \to -\infty$, it follows that $\psi_s \to \Psi$ as $X \to -\infty$, and hence, once we know the amplitudes A_n, we know the asymptotic behaviour of ψ_s. We shall now employ the method of asymptotics beyond all orders to evaluate these amplitudes.

6.3.3 'Inner' equations

Segur and Kruskal's method allows one to measure the amplitude of the exponentially small radiation by continuing the solution analytically into the complex plane. The leading-order term of ψ, $\varepsilon\sqrt{\cos k}\operatorname{sech} X$, has singularities at $X = \frac{i\pi}{2} + i\pi n$, $n = 0, \pm 1, \pm 2, \ldots$. In the vicinity of these points, the radiation becomes significant; the qualitative explanation for this is that the sech function forms a sharp spike with a short length scale near the singularity point, and hence there is a strong coupling to the radiation modes, unlike on the real axis. The radiation, which is exponentially small on the real axis, becomes large enough to be measured near the singularities.

We define a new complex variable y, such that εy is small in absolute value when X is near the lowest singularity in the upper half-plane:

$$\varepsilon y = X - \frac{i\pi}{2}. \tag{6.26}$$

The variables y and X are usually referred to as the 'inner' and 'outer' variables, respectively: the transformation to y effectively 'zooms in' on the singularity at $X = \frac{i\pi}{2}$. We also define $u(y) \equiv \psi(X)$ and $w(y) \equiv \psi^*(X)$. Continuing eq. (6.5) to the complex plane, i.e. substituting $u(y)$ for $\psi(X)$ and $w(y)$ for $\psi^*(X)$, we obtain, in the limit $\varepsilon \to 0$:

$$e^{ik}u(y+1) + e^{-ik}u(y-1) - 2\cos k\, u(y) - 2i\sin k\, u'(y) + \frac{2u^2 w}{1+\mu uw} = 0, \tag{6.27a}$$

$$e^{-ik}w(y+1) + e^{ik}w(y-1) - 2\cos k\, w(y) + 2i\sin k\, w'(y) + \frac{2w^2 u}{1+\mu wu} = 0. \tag{6.27b}$$

Here we have used that $\omega \to 2\cos k$ and $v \to 2\sin k$ as $\varepsilon \to 0$. Equations (6.27) are our 'inner equations'; they are valid in the 'inner region' $-\infty < \mathrm{Re}\, y < \infty$, $\mathrm{Im}\, y < 0$. (The solution cannot be continued up from the real X axis past the singularity at $y = 0$.)

Solving the system (6.27) order-by-order, we can find solutions in the form of a series in powers of y^{-1}. Alternatively, we can make the change of variables (6.26) in the asymptotic expansions (6.7a), (6.13) and send $\varepsilon \to 0$. This gives, for the first few terms,

$$\hat{u} = \sqrt{\cos k}\left\{-\frac{i}{y} + \tan k\frac{1}{2y^2} + \left[\frac{1}{3}(1-\mu\cos k) + \frac{7}{12}\tan^2 k\right]\frac{i}{y^3} + \mathcal{O}(y^{-4})\right\}, \tag{6.28a}$$

$$\hat{w} = \sqrt{\cos k}\left\{-\frac{i}{y} - \tan k\frac{1}{2y^2} + \left[\frac{1}{3}(1-\mu\cos k) + \frac{7}{12}\tan^2 k\right]\frac{i}{y^3} + \mathcal{O}(y^{-4})\right\}. \tag{6.28b}$$

We are using hats over u and w to distinguish the series solution (6.28) from other solutions of eq. (6.27) that will appear in the next section. The asymptotic series (6.28) may or may not converge. We note a symmetry $\hat{u}(-y) = -\hat{w}(y)$ of the power-series solution.

6.3.4 Exponential expansion

In order to obtain an expression for the terms which lie beyond all orders of y^{-1}, we substitute $(u, w) = (\hat{u}, \hat{w}) + (\delta u, \delta w)$ into equations (6.27). Since $\hat{u}$ and $\hat{w}$ solve the equations to all orders in y^{-1}, then provided δu and δw are small, they will solve the linearisation of equations (6.27) about $(\hat{u}, \hat{w})$ for large $|y|$.

Formal solutions to the linearised system can be constructed as series in powers of y^{-1}. Because $\hat{u}$ and $\hat{w}$ are both $\mathcal{O}\left(y^{-1}\right)$, the leading-order expressions for δu and δw as $y \to \infty$ are

obtained by substituting zero for $\hat{u}$ and $\hat{w}$ in the linearised equations. This gives

$$\delta u \to \sum_n J_n \exp(iq_n y), \quad \delta w \to \sum_n K_n \exp(-iq_n y) \quad \text{as } y \to \infty, \tag{6.29}$$

where q_n ($n = 0, 1, 2, \ldots$) are the roots of

$$\cos(k+q) - \cos k + q \sin k = 0. \tag{6.30}$$

Note that the roots q_n with $n \geq 1$ are given by the $\varepsilon \to 0$ limits of the roots of the dispersion equation (6.19): $q_n = \lim_{\varepsilon \to 0} Q_n$. In addition, there is a root $q_0 = 0$ which does not have a Q_0 counterpart.

The full solutions (i.e. solutions including corrections to all orders in y^{-1}) will result if we use the full inverse-power series (6.28) for $\hat{u}$ and $\hat{w}$; these solutions should have the form

$$\delta u = \sum_n K_n \sum_{m=1}^{\infty} \frac{d_m^{(n)}}{y^m} \exp(-iq_n y), \tag{6.31a}$$

$$\delta w = \sum_n K_n \left[1 + \sum_{m=1}^{\infty} \frac{c_m^{(n)}}{y^m} \right] \exp(-iq_n y). \tag{6.31b}$$

Note that we have excluded the terms proportional to $e^{iq_n y}$ from this ansatz (i.e. set the amplitudes J_n to zero) as they would become exponentially large on the real X axis. [One can readily verify this by making the change of variables (6.26) in eq. (6.29).] The coefficients $c_1^{(n)}, c_2^{(n)}, \ldots$, and $d_1^{(n)}, d_2^{(n)}, \ldots$ are found recursively when the ansatz (6.31) is substituted into the linearised equations and like powers of y^{-1} collected. In particular, the first few coefficients are

$$\begin{aligned} c_1^{(n)} &= -\frac{2i \cos k}{\sin(k+q_n) - \sin k}, \\ c_2^{(n)} &= \frac{[\cos(k+q_n) - 2\cos k] \cos k}{[\sin(k+q_n) - \sin k]^2}, \end{aligned} \tag{6.32a}$$

and

$$d_1^{(n)} = 0, \quad d_2^{(n)} = \frac{\cos k}{\cos(k-q_n) - \cos k - q_n \sin k}, \tag{6.32b}$$

where $n = 1, 2, \ldots$.

Having restricted ourselves to considering the linearised equations for δu and δw, we have only taken into account the simple harmonics in (6.29) and (6.31). Writing $\delta u = \varepsilon^1 U_1 + \varepsilon^2 U_2 + \ldots$ and $\delta w = \varepsilon^1 W_1 + \varepsilon^2 W_2 + \ldots$, where ε is an auxiliary small parameter (not to be confused with our 'principal' small parameter ε); substituting $u = \hat{u} + \delta u$ and $w = \hat{w} + \delta w$

in eqs (6.27), and solving order-by-order the resulting hierarchy of nonhomogeneous linear equations, we can recover all nonlinear corrections to δu and δw. The ε^2-corrections will be proportional to $e^{-i(q_n+q_m)y}$; higher-order corrections will introduce harmonics with higher combination wavenumbers. Later in this section it will become clear that ε is actually of the order $\exp(-\pi\mathcal{Q}_1/2\varepsilon)$ [see eq. (6.36) below]; hence the amplitudes of the combination harmonics will be exponentially smaller than that of $\exp(-iq_1y)$.

Now we return to the object that is of ultimate interest to us in this work; that is, to the function Ψ of section 6.3.2 representing the radiation of the moving soliton. We need to match Ψ to the corresponding object in the inner region. To this end, we recall that $\Psi = \psi_s - \psi_u$, where ψ_s and ψ_u are two solutions of the outer equation (6.5) which share the same asymptotic expansion to all orders. In the limit $\varepsilon \to 0$, the corresponding functions

$$\begin{aligned} u_s(y,t) &\equiv \psi_s(X,t), & w_s(y,t) &\equiv \psi_s^*(X,t), \\ u_u(y,t) &\equiv \psi_u(X,t), & w_u(y,t) &\equiv \psi_u^*(X,t) \end{aligned} \tag{6.33}$$

solve the equations (6.27) and share the same inverse-power expansions. We express this fact by writing

$$\begin{aligned} u_s(y,t) &\sim \hat{u}(y), & w_s(y,t) &\sim \hat{w}(y), \\ u_u(y,t) &\sim \hat{u}(y), & w_u(y,t) &\sim \hat{w}(y). \end{aligned}$$

Therefore, the difference $u_s - u_u$ (which results from the analytic continuation of the function Ψ) can be identified with δu and $w_s - w_u$ with δw. Continuing eq. (6.24) and its complex conjugate gives, as $\varepsilon \to 0$,

$$\begin{aligned} u_s - u_u = &\sum_n \lim_{\varepsilon\to 0} A_n(\varepsilon) \exp\left(-\frac{\pi\mathcal{Q}_n}{2\varepsilon}\right)\left[1+\mathcal{O}\left(\frac{1}{y}\right)\right]\exp(iq_ny) \\ &-\sum_n \lim_{\varepsilon\to 0} A_n^*(\varepsilon)\exp\left(\frac{\pi\mathcal{Q}_n}{2\varepsilon}\right)\left[\frac{2\cos k}{\omega+vq_n-2\cos(k-q_n)}\frac{1}{y^2}+\mathcal{O}\left(\frac{1}{y^3}\right)\right]\exp(-iq_ny) \end{aligned} \tag{6.34a}$$

and

$$\begin{aligned} w_s - w_u = &\sum_n \lim_{\varepsilon\to 0} A_n^*(\varepsilon) \exp\left(\frac{\pi\mathcal{Q}_n}{2\varepsilon}\right)\left[1+\mathcal{O}\left(\frac{1}{y}\right)\right]\exp(-iq_ny) \\ &-\sum_n \lim_{\varepsilon\to 0} A_n(\varepsilon)\exp\left(-\frac{\pi\mathcal{Q}_n}{2\varepsilon}\right)\left[\frac{2\cos k}{\omega+vq_n-2\cos(k-q_n)}\frac{1}{y^2}+\mathcal{O}\left(\frac{1}{y^3}\right)\right]\exp(iq_ny). \end{aligned} \tag{6.34b}$$

[Here we have used eq. (6.25).] Matching (6.34a) to (6.31a) and (6.34b) to (6.31b) yields then $K_0 = 0$ and

$$\lim_{\varepsilon \to 0} A_n(\varepsilon) \exp\left(-\frac{\pi \mathcal{Q}_n}{2\varepsilon}\right) = 0, \tag{6.35a}$$

$$\lim_{\varepsilon \to 0} A_n^*(\varepsilon) \exp\left(\frac{\pi \mathcal{Q}_n}{2\varepsilon}\right) = K_n \tag{6.35b}$$

for $n = 1, 2, \ldots$. We note that eq. (6.35a) follows from eq. (6.35b), while the latter equation can be written, symbolically, as

$$A_n(\varepsilon) \longrightarrow K_n^* \exp\left(-\frac{\pi \mathcal{Q}_n}{2\varepsilon}\right) \quad \text{as } \varepsilon \to 0. \tag{6.36}$$

Our subsequent efforts will focus on the evaluation of the constants K_n.

For k greater than $k_{\max}^{(1)}$ (approximately 0.22), there is only one radiation mode and therefore only one pre-exponential factor, K_1. For smaller k we note that the amplitude of the n-th radiation mode, A_n, is a factor of $\exp\left\{\frac{\pi}{2\varepsilon}(\mathcal{Q}_n - \mathcal{Q}_1)\right\}$ smaller than A_1, the amplitude of the first mode. Referring to fig. 6.1, it is clear that for $n \geq 3$, the difference $\mathcal{Q}_n - \mathcal{Q}_1$ will be no smaller than π. As for the second mode, it becomes as significant as the first one only when $k = \mathcal{O}\left(\varepsilon^2\right)$ in which case $(\mathcal{Q}_2 - \mathcal{Q}_1)/\varepsilon = \mathcal{O}(1)$. But in our asymptotic expansion of section 6.2 we assumed, implicitly, that k is of order 1 and so the case of $k = \mathcal{O}\left(\varepsilon^2\right)$ is beyond the scope of our current analysis. Therefore, for our purposes all the radiation modes with $n \geq 2$ (when they exist) will have negligible amplitudes compared to that of the first mode, provided K_1 is nonzero and ε is small. For this reason, we shall only attempt to evaluate K_1.

6.3.5 Borel summability of the asymptotic series

Pomeau, Ramani, and Grammaticos [133] have shown that the radiation can be measured using the technique of Borel summation rather than by solving differential equations numerically, as in Segur and Kruskal's original approach. The method has been refined by (among others) Grimshaw and Joshi [134, 135] and Tovbis, Tsuchiya, Jaffé and Pelinovsky [136, 137, 138, 139], who have applied it to difference equations. In chapter 3 of this thesis it has been applied to differential-difference equations in the context of moving kinks in ϕ^4 models. This is the approach that we will be pursuing here.

Expressing $u(y)$ and $w(y)$ as Laplace transforms,

$$u(y) = \int_\gamma U(p) e^{-py} dp \tag{6.37a}$$

and

$$w(y) = \int_\gamma W(p) e^{-py} dp, \tag{6.37b}$$

where γ is a contour extending from the origin to infinity in the complex p-plane, the inner equations (6.27) are cast in the form of integral equations

$$f(p)U + \mu[f(p)U] * U * W + U * U * W = 0, \tag{6.38a}$$

$$f(-p)W + \mu[f(-p)W] * W * U + W * W * U = 0, \tag{6.38b}$$

where

$$f(p) = (\cosh p - 1)\cos k - i(\sinh p - p)\sin k.$$

The asterisk $*$ denotes the convolution integral,

$$U(p) * W(p) = \int_0^p U(p - p_1) W(p_1) dp_1,$$

where the integration is performed from the origin to the point p on the complex plane, along the contour γ. We have invoked (once again) the convolution theorem for a Laplace transform over a contour in the complex plane, which allows us to write

$$u(y)w(y) = \int_\gamma [U(p) * W(p)] e^{-py} dp. \tag{6.39}$$

The proof of this theorem was provided in appendix 3.A of chapter 3. It requires that the path γ be concave-up, and that $W(p)$ have no singularities between γ and the imaginary axis. Our choice of the contours of integration ensures that both these conditions are always satisfied.

Again, we choose the contour so that $\arg p \to \pi/2$ as $|p| \to \infty$ along γ. This ensures that $e^{-py} \to 0$ as $|p| \to \infty$ for all y along the line $-\infty < \mathrm{Re}\, y < \infty$, $\mathrm{Im}\, y < 0$. Therefore, the integrals in (6.37) converge for all y along this line and any bounded $U(p)$ and $W(p)$.

The function $U(p)$ will have singularities at the points where $f(p)$ vanishes while the sum of the double-convolution terms in (6.38a) does not. Similarly, $W(p)$ will have a singularity wherever $f(-p)$ vanishes [while the sum of the double-convolution terms in (6.38b) does not]. Therefore, U and W may have singularities at the points where

$$\cosh p - 1 = \pm i \tan k\, (\sinh p - p), \tag{6.40}$$

with the top and bottom signs referring to $U(p)$ and $W(p)$, respectively. The imaginary roots of eq. (6.40) with the top sign are at $p = -iq_n$ and those of eq. (6.40) with the bottom sign

at $p = iq_n$, where q_n are the real roots of (6.30). (We remind the reader that all roots q_n are positive.) The point $p = 0$ is not a singularity as both double-convolution terms in each line of (6.38) vanish here. There is always at least one pure imaginary root of (6.40) (and *only* one if $k > k^{(1)}_{\max}$, where $k^{(1)}_{\max} \approx 0.22$).

In addition, there are infinitely many complex roots. The complex singularities of U [complex roots of the top-sign equation in (6.40)] are at the intersections of the curve given by

$$q = \frac{\cosh\kappa}{\sin k}\sqrt{1-\sin^2 k\left(\frac{\kappa}{\sinh\kappa}\right)^2} - \cot k \tag{6.41a}$$

with the family of curves described by

$$q = k - \arcsin\left(\frac{\kappa}{\sinh\kappa}\sin k\right) + 2\pi n, \quad n = 1,2,\ldots, \tag{6.41b}$$

and at the intersections of the curve

$$q = -\frac{\cosh\kappa}{\sin k}\sqrt{1-\sin^2 k\left(\frac{\kappa}{\sinh\kappa}\right)^2} - \cot k \tag{6.42a}$$

with the family of curves described by

$$q = k + \arcsin\left(\frac{\kappa}{\sinh\kappa}\sin k\right) + \pi(2n+1), \quad n = -2,-3,-4,\ldots. \tag{6.42b}$$

Here κ and q are the real and imaginary part of p: $p = \kappa + iq$. The curve (6.41a) looks like a parabola opened upwards, with the vertex at $\kappa = q = 0$, and the curve (6.42a) like a parabola opened downwards, with the vertex at $\kappa = 0$, $q = -2\cot k$. The curves (6.41b) and (6.42b), on the other hand, look like parabolas for small κ but then flatten out and approach horizontal straight lines as $\kappa \to \pm\infty$. [In compiling the list of these 'flat' curves in (6.41b) and (6.42b), we have taken into account that the curve (6.41b) with $n = 0$ does not have any intersections with the parabola (6.41a), and the curve (6.42b) with $n = -1$ does not have any intersections with the parabola (6.42a).] As k is reduced, the vertex of the parabola (6.42a) moves down along the q-axis; the intersections of this parabola with the 'flat' curves (6.42b) approach, pairwise, the q-axis. After colliding on the q-axis, pairs of complex roots move away from each other along it. [The parabola (6.41a) does not move as k is reduced, but only steepens, which results in the singularities in the upper half-plane approaching the imaginary axis but not reaching it until $k = 0$.] In a similar way, the complex singularities of $W(p)$ move onto the imaginary axis as k is decreased. In section 6.3.5 below we will use the fact that the distance from any complex singularity to the origin is larger than 2π; this follows from the observation that the closest points

of the curves (6.41b) and (6.42b) to the origin are their intersections with the q-axis. These are further away than 2π from the origin.

In addition to singularities at $p = -iq_n$, the function $U(p)$ will have singularities at points $p = iq_n$, $n = 1,2,....$ These are induced by the cubic terms in eq. (6.38a); for instance, the singularity at $p = iq_1$ arises from the convolution of the term proportional to p in $U * U$ with the function W which has a singularity at $p = iq_1$. [That $U(p)$ has singularities at $p = iq_n$ can also be seen directly from eq. (6.31a).] Similarly, the function $W(p)$ will have singularities at points $p = -iq_n$, $n = 1,2,....$ By virtue of the nonlinear terms there will also be singularities at the 'combination points' $i(\pm q_n \pm q_m)$, $i(\pm q_n \pm q_m \pm q_j)$, etc.

The formal inverse-power series (6.28), which we can write as

$$\hat{u}(y) = \sum_{\ell=0}^{\infty} \rho_\ell \frac{\ell!}{y^{\ell+1}}, \quad \hat{w}(y) = \sum_{\ell=0}^{\infty} \nu_\ell \frac{\ell!}{y^{\ell+1}}, \tag{6.43}$$

result from the Laplace-transformation of power series for $U(p)$ and $W(p)$:

$$U(p) = \sum_{\ell=0}^{\infty} \rho_\ell p^\ell, \quad W(p) = \sum_{\ell=0}^{\infty} \nu_\ell p^\ell. \tag{6.44}$$

The series (6.44) converge in the disk of radius q_1, centred at the origin, and hence can be integrated term-by-term only over the portion of the contour γ which lies within that disk. However, by Watson's lemma, the remaining part of the contour makes an exponentially small contribution to the integral and the resulting series (6.43) are asymptotic as $y \to \infty$. The functions $u(y)$ and $w(y)$ defined by (6.37) give the Borel sums of the series $\hat{u}(y)$ and $\hat{w}(y)$.

Consider now some horizontal line in the inner region, that is, let $\mathrm{Im}\, y < 0$ be fixed and $\mathrm{Re}\, y$ vary from $-\infty$ to ∞. If the integration contour γ is chosen to lie in the first quadrant of the complex p-plane, the functions $u(y)$ and $w(y)$ generated by (6.37) will tend to zero as $\mathrm{Re}\, y \to +\infty$ along this line. Similarly, if it is chosen to lie in the second quadrant, they will tend to zero as $\mathrm{Re}\, y \to -\infty$. Suppose there were no singularities between two such contours: Then the one could be continuously deformed to the other without any singularity crossings, i.e. they would generate the same solution which, therefore, would decay to zero at both infinities. [That is, the oscillatory tails in (6.31) would have zero amplitudes, $K_n = 0$.] In general, however, $U(p)$ and $W(p)$ have singularities both on and away from the imaginary axis. In order to minimise the number of singularities to be crossed in the deformation of one contour to the other, we choose the contours to lie above all singularities with nonzero real part. (That this is possible, is shown in appendix 6.A at the end of this chapter.) Note also that the imaginary part of the singularity

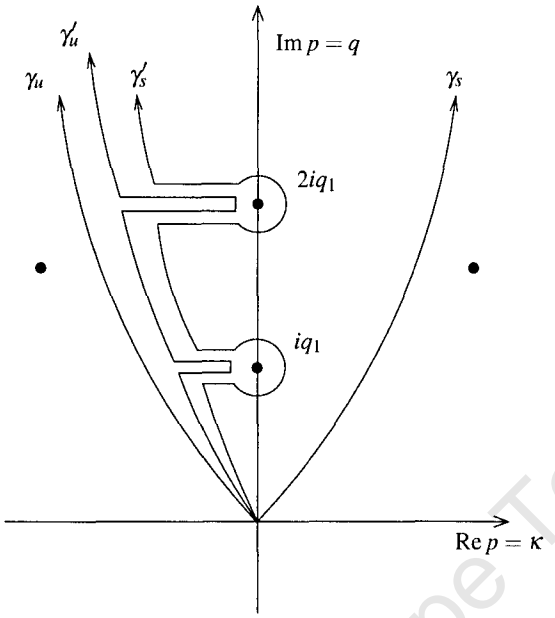

Figure 6.2: The integration contours γ_s and γ_u used to generate the solutions (u_s, w_s) and (u_u, w_u) respectively via (6.37). The dots are singularities of $W(p)$. Shown is the situation where the linear dispersion relation (6.30) has only one real root, q_1.

grows faster than its real part and hence $\arg p$ should tend to $\pi/2$ as $|p| \to \infty$ along γ; this was precisely our choice for the direction of the contours γ in the beginning of section 6.3.5.

Let γ_s and γ_u be two contours chosen in this way, with γ_s lying in the first quadrant and γ_u in the second quadrant. The solutions $u(y), w(y)$ generated by eq. (6.37) with the contour γ_s will tend to zero as $\mathrm{Re}\, y \to \infty$ (with $\mathrm{Im}\, y < 0$ fixed). Hence they can be identified with solutions u_s, w_s obtained by the continuation of the outer solution ψ_s which has the same asymptotic behaviour. Similarly, the solutions generated by eq. (6.37) with the contour γ_u coincide with solutions u_u, w_u: Like u_u, w_u, the solutions generated by eq. (6.37) tend to zero as $\mathrm{Re}\, y \to -\infty$ (with fixed $\mathrm{Im}\, y < 0$).

Consider, first, solutions w_s and w_u. Since the contours γ_s and γ_u are separated by singularities of $W(p)$ on the positive imaginary axis, they cannot be continuously deformed to each other without singularity crossings and so the solution w_s does not coincide with w_u, unless the residue at the singularity happens to be zero. If we deform γ_s to γ_s' and γ_u to γ_u' as shown in fig. 6.2, without crossing any singularities, then the only difference between the two contours is that γ_s' encircles the singularities, whereas γ_u' does not. Therefore, the difference $w_s - w_u$ can be

deduced exclusively from the leading-order behaviour of $W(p)$ near its singularities. There can be two contributions to this difference: The first arises from integrating around the poles, and is a sum of residues, while the second arises if the singularity is a branch point.

To find the singularity structure of the function $W(p)$, we equate

$$w_s - w_u = \int_{\gamma_s'} W(p)e^{-py}dp - \int_{\gamma_u'} W(p)e^{-py}dp \tag{6.45}$$

to the expansion (6.31b). The first term in (6.31b), $e^{-iq_n y}$, arises from the integration of a term $(2\pi i)^{-1}(p-iq_n)^{-1}$ in $W(p)$. For such a term, the difference of the two integrals in (6.45) reduces to an integral around a circle centred on the point $p = iq_n$:

$$\frac{1}{2\pi i}\oint \frac{1}{p-iq_n}e^{-py}dp = \operatorname{res}\left\{\frac{e^{-py}}{p-iq_n}, iq_n\right\}.$$

The term $y^{-m}e^{-iqy_n}$ in (6.31b), with $m = 1,2,...$, arises from the integration of a term

$$\frac{1}{2\pi i}\frac{(p-iq_n)^{m-1}}{(m-1)!}\ln(p-iq_n)$$

in $W(p)$. This time, $p = iq_n$ is a branch point. After going around this point along the circular part of γ_s', the logarithm increases by $2\pi i$ and the difference between the integrals in (6.45) is given by

$$\frac{1}{(m-1)!}\int_C (p-iq_n)^{m-1}e^{-py}dp = \frac{e^{-iq_n y}}{(m-1)!}\int_0^\infty z^{m-1}e^{-zy}dz,$$

where C is the part of γ_s' extending from $p = iq_n$ to infinity. This equals exactly $y^{-m}e^{-iq_n y}$.

Thus, in order to generate the full series (6.31b) we must have

$$W(p) = \frac{1}{2\pi i}\sum_n K_n\left[\frac{1}{p-iq_n} + \sum_{m=1}^{\infty}\frac{c_m^{(n)}}{(m-1)!}(p-iq_n)^{m-1}\ln(p-iq_n)\right] + W_{\text{reg}}(p), \tag{6.46}$$

where W_{reg} denotes the part of W which is regular at $p = iq_n$, $n = 1,2,....$ By the same process, matching $u_s - u_u$ to δu in (6.31a) yields

$$U(p) = \frac{1}{2\pi i}\sum_n K_n\sum_{m=1}^{\infty}\frac{d_m^{(n)}}{(m-1)!}(p-iq_n)^{m-1}\ln(p-iq_n) + U_{\text{reg}}(p). \tag{6.47}$$

The solution to eqs (6.38) is nonunique; for instance, if $\{U(p),W(p)\}$ is a solution, then so is $\{e^{py_0+\zeta_0}U(p), e^{py_0-\zeta_0}W(p)\}$ with any complex y_0 and ζ_0. Also, if $\{U(p),W(p)\}$ is a solution, $\{W(-p),U(-p)\}$ is another one. We will impose the constraint

$$U(p) = W(-p); \tag{6.48}$$

this constraint is obviously compatible with eqs (6.38). It is not difficult to see that the reduction (6.48) singles out a unique solution of eqs (6.38). The motivation for imposing the constraint (6.48) comes from the symmetry $\hat{u}(-y) = -\hat{w}(y)$ of the power-series solution of eq. (6.27). Using this symmetry in eq. (6.43), we get $\rho_\ell = (-1)^\ell \nu_\ell$ and then eq. (6.44) implies (6.48).

In view of (6.48), the singularities of $U(p)$ in the upper half-plane are singularities of $W(p)$ in the lower half-plane, which fall within $W_{\rm reg}(p)$, and vice-versa. Thus we have, finally,

$$W(p) = \frac{1}{2\pi i}\sum_n \frac{K_n}{p - iq_n} + \frac{1}{2\pi i}\sum_n K_n \sum_{m=1}^{\infty} \frac{1}{(m-1)!} \times \left[c_m^{(n)}(p-iq_n)^{m-1}\ln(p-iq_n) - (-1)^m d_m^{(n)}(p+iq_n)^{m-1}\ln(p+iq_n)\right] + \tilde{W}_{\rm reg}(p), \quad (6.49)$$

where $\tilde{W}_{\rm reg}(p)$ is regular at $p = \pm iq_n$. We also mention an equivalent representation for (6.49) which turns out to be computationally advantageous:

$$W(p) = \frac{1}{2\pi i}\sum_n K_n \sum_{m=0}^{\infty} D^{-m}\left[\frac{c_m^{(n)}}{p - iq_n} - \frac{(-1)^m d_m^{(n)}}{p + iq_n}\right] + \check{W}_{\rm reg}(p). \quad (6.50)$$

Here D^{-1} is an integral map:

$$D^{-1}f(p) \equiv \int_0^p f(p_1)dp_1;$$

the notation $D^{-m}f(p)$ should be understood as

$$D^{-m}f(p) \equiv \int_0^p dp_1 \int_0^{p_1} dp_2 \int_0^{p_2} dp_3 \ldots \int_0^{p_{m-1}} dp_m f(p_m).$$

We have also introduced $c_0^{(n)} = 1$ and $d_0^{(n)} = 0$ for economy of notation. The only difference between eqs (6.49) and (6.50) is that the double-sum term on the right-hand side of (6.50) includes some terms which are regular at $p = \pm iq_n$, whereas in eq. (6.49), all regular terms are contained in $\tilde{W}_{\rm reg}(p)$.

The residues K_n at the poles of $W(p)$ are known as the Stokes constants. The leading-order Stokes constant, K_1, can be related to the behaviour of the coefficients in the power-series expansion of $W(p)$. Indeed, the coefficients in the power series (6.44) satisfy

$$\nu_\ell \longrightarrow K_1 \sum_{m=0}^{\ell} \frac{c_m^{(1)} + (-1)^\ell d_m^{(1)}}{2\pi q_1 (iq_1)^{\ell - m}} \frac{(\ell - m)!}{\ell!} \quad \text{as } \ell \to \infty. \quad (6.51)$$

This is obtained by expanding the singular part of the expression (6.50) in powers of p. (Coefficients of the regular part become negligible in the limit $\ell \to \infty$ compared to those of the

singular part.) Note that we have ignored singularities with nonzero real part and singularities on the imaginary axis other than at $p = \pm iq_1$. The reason is that all these singularities are further away from the origin than the points $\pm iq_1$ (in particular all complex singularities are separated from the origin by a distance greater than 2π), and their contribution to v_ℓ becomes vanishingly small as $\ell \to \infty$. We have also neglected singularities at the 'combination points' because of their exponentially small residues. The coefficients v_ℓ can be calculated numerically; once they are known, it follows from (6.51) that

$$K_1 = 2\pi q_1 \lim_{\ell\to\infty} (iq_1)^\ell v_\ell \tag{6.52}$$

(where we have recalled that $c_0^{(1)} = 1$ and $d_0^{(1)} = 0$).

We now turn to the numerical calculation of the coefficients v_ℓ.

6.3.6 Recurrence relation

To make our forthcoming numerical procedure more robust, we normalise the coefficients in the power series (6.44) by writing

$$v_\ell = -i\frac{\delta_\ell}{(iq_1)^\ell}. \tag{6.53}$$

Substituting the expansion (6.44) and (6.53) as well as the constraint (6.48) into either of equations (6.38) and equating coefficients of like powers of p, yields the following recurrence relation for the numbers δ_n ($n \geq 0$):

$$\sum_{m=0}^{n} \frac{q_1^m \delta_{n-m}}{(m+2)!}\mathcal{R}_m = \frac{1}{(n+2)(n+1)} \sum_{m=0}^{n} \left[\delta_{n-m} + \mu \sum_{j=2}^{n-m} \frac{q_1^j \delta_{n-m-j}}{j!}\mathcal{R}_j\right] \times \left(\sum_{j=0}^{m} (-1)^{m-j}\delta_{m-j}\delta_j \frac{j!(m-j)!}{m!}\right) \frac{m!(n-m)!}{n!}. \tag{6.54}$$

Here

$$\mathcal{R}_m = \begin{cases} (-1)^{\frac{m}{2}} \cos k, & \text{for } m \text{ even}, \\ (-1)^{\frac{m-1}{2}} \sin k, & \text{for } m \text{ odd}. \end{cases}$$

Solving eq. (6.54) with $n = 0$ gives $\delta_0 = \sqrt{1-c^2}$. Thereafter it can be solved for each member of the sequence $\{\delta_n\}$ in terms of the preceding ones, and thus each δ_n can be calculated in turn. [Since all the coefficients in the recurrence relation (6.54) are real, the sequence $\{\delta_n\}$ turns out to be a sequence of real numbers.]

Once the sequence $\{\delta_n\}$ has been generated, expression (6.52) can be used to calculate the Stokes constant K_1:

$$K_1 = -2\pi i q_1 \delta_\ell, \tag{6.55}$$

for sufficiently large ℓ. Unfortunately, the convergence of the sequence $\{\delta_n\}$ is slow and thus the above procedure is computationally expensive. The convergence can be accelerated by expanding eq. (6.51) in powers of small $1/\ell$:

$$\delta_\ell = \frac{iK_1}{2\pi q_1}\left[1 + iq_1\frac{c_1^{(1)}}{\ell} - q_1^2\frac{c_2^{(1)} + (-1)^\ell d_2^{(1)}}{\ell^2} + \mathcal{O}\left(\frac{1}{\ell^3}\right)\right],$$

whence

$$K_1 = -2\pi i q_1 \delta_\ell\left[1 - iq_1\frac{c_1^{(1)}}{\ell} + q_1^2\frac{c_2^{(1)} - (c_1^{(1)})^2 + (-1)^\ell d_2^{(1)}}{\ell^2} + \mathcal{O}\left(\frac{1}{\ell^3}\right)\right]. \tag{6.56}$$

According to eq. (6.56), eq. (6.55) gives K_1 with a relatively large error of order $1/\ell$. On the other hand, a two-term approximation

$$K_1 = -2\pi i q_1 \delta_\ell\left(1 - iq_1\frac{c_1^{(1)}}{\ell}\right) \tag{6.57}$$

is correct to $\mathcal{O}(1/\ell^2)$. More precisely, the relative error associated with the answer (6.57) is given by

$$\frac{\mathcal{E}}{K_1} = q_1^2\frac{c_2^{(1)} - (c_1^{(1)})^2 + (-1)^\ell d_2^{(1)}}{\ell^2}. \tag{6.58}$$

In our calculations, we set $\mathcal{E}/K_1 = 10^{-5}$. Since $c_1^{(1)}$, $c_2^{(1)}$ and $d_2^{(1)}$ are known constants [given by (6.32a) and (6.32b)], eq. (6.58) tells us what ℓ we should take, i.e. how many members of the sequence $\{\delta_n\}$ we should calculate in order to achieve the set accuracy. Figure 6.3 illustrates the convergence of the approximate values of K_1 calculated using (6.55) and (6.57) as ℓ is increased. Note the drastic acceleration of convergence in the latter case.

Figure 6.4(a) shows the calculated Stokes constant as a function of k for various values of the saturation parameter μ. First of all, $K_1(k)$ does not have any zeros in the case of the cubic nonlinearity ($\mu = 0$). This means that solitons of the cubic one-site discrete NLS equation [eq. (6.2) with $\mu = 0$] cannot propagate without losing energy to radiation. For $\mu = 3$ the Stokes constant does have a zero, but at a value of k smaller than $k_{\max}^{(1)}$ (where $k_{\max}^{(1)} \approx 0.22 = 0.07\pi$). Since higher radiation modes do exist in this range of k, there will still be radiation from the soliton – unless the 'higher' Stokes constants $K_2(k)$, $K_3(k)$,..., happen to be zero at the same

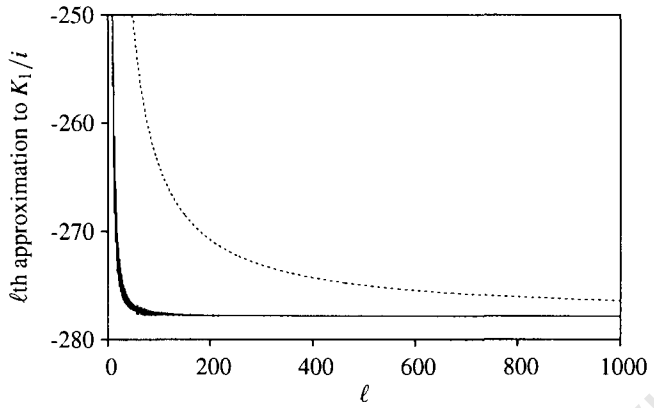

Figure 6.3: Convergence of the sequence in the right-hand side of (6.55) (dashed line) and the 'accelerated' sequence defined by the right-hand side of (6.57) (solid line). Shown are the ℓ-th approximations to the Stokes constant K_1 [the ℓ-th members of the sequences (6.55) and (6.57)] divided by i to get a real value. In this plot, $\mu = 0$ and $k = 0.5$.

value of k. Finally, for $\mu = 4$ the zero is seen to have moved just above $k_{\max}^{(1)}$ and for $\mu = 6$ it has an even higher value. There are no $\mathcal{Q}_2, \mathcal{Q}_3, \ldots$ radiations for these k; hence the zeros of $K_1(k)$ define the carrier wavenumbers at which the soliton 'slides', i.e. travels without emitting any radiation. Equation (6.17) then gives the corresponding sliding velocities, for each ε.

Figure 6.4(b) shows the Stokes constant $K_1(k)$ for higher values of the parameter μ. For $\mu = 12$ a second zero of the Stokes constant has appeared while for $\mu = 25$, the function $K_1(k)$ has three zeros. As μ is increased, the existing zeros move to larger values of k while new ones emerge at the origin of the k axis.

6.3.7 Radiation waves

For not very large $|X|$, the solution ψ_s is close to the localised pulse found by means of the perturbation expansion in section 6.2. As $X \to +\infty$, it tends to zero, by definition, while the $X \to -\infty$ asymptotic behaviour is found from $\psi_s = \psi_u + \Psi$. Here the solution ψ_u decays to zero as $X \to -\infty$ and hence ψ_s approaches the oscillatory waveform Ψ given by eqs (6.24), (6.25) and (6.36):

$$\psi_s(X) \to \sum_n K_n^* e^{-\pi \mathcal{Q}_n/2\varepsilon} \left[1 + \varepsilon \frac{4i \cos k \tan X}{2\sin(k+\mathcal{Q}_n) - \nu} + \mathcal{O}\left(\varepsilon^2\right)\right] e^{i\mathcal{Q}_n X/\varepsilon} \tag{6.59}$$

as $X \to -\infty$. Equation (6.59) describes a radiation background over which the soliton is superimposed. As we have explained, we can ignore all but the first term in the sum.

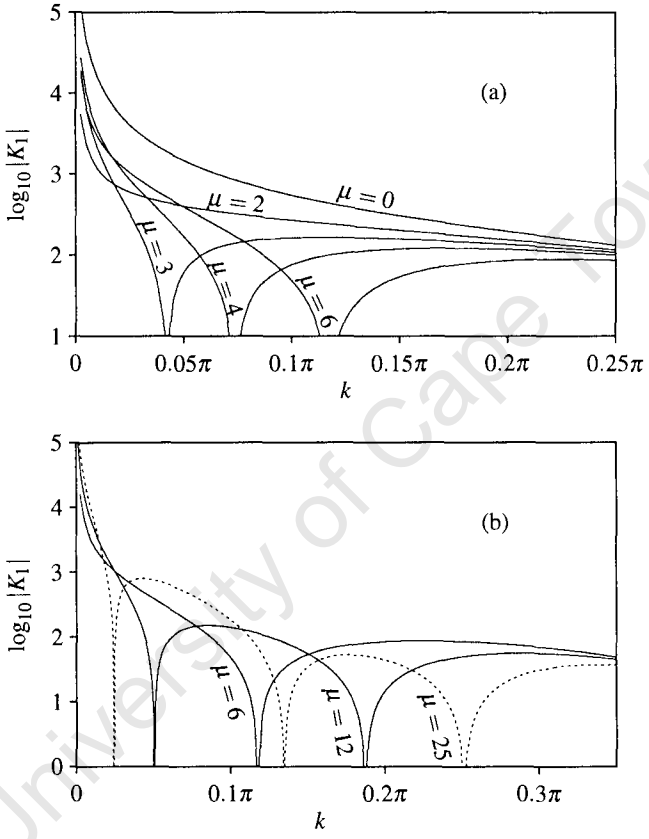

Figure 6.4: The Stokes constant K_1 for various values of μ. Note the logarithmic scale on the vertical axis. The downward spikes extend all the way to $-\infty$; hence each spike corresponds to a zero crossing. Each panel shows only a portion of the full range $0 \leq k \leq \pi/2$; there are no additional zero crossings in the part which is not shown.

Substituting (6.64) into (6.63) and evaluating the integral over the region $(a-1,a)$ in the soliton's wake, we obtain

$$\frac{dN}{dt} = |K_1|^2 e^{-\pi\mathcal{Q}_1/\varepsilon}[2\sin(k+\mathcal{Q}_1) - v], \tag{6.65}$$

where we have used eq. (6.36). Note that $[2\sin(k+\mathcal{Q}_1) - v]$ is the group velocity of the first radiation mode, $\Omega'(\mathcal{Q}_1)$, which, as we have established, is negative; hence $\dot{N} \leq 0$.

We now turn to the momentum integral,

$$P = \frac{i}{2}\int_a^b (\varphi_x^*\varphi - \varphi_x\varphi^*)dx.$$

Multiplying (6.61) by φ_x^*, adding its complex conjugate and integrating, gives the rate equation

$$\begin{aligned}\frac{dP}{dt} &= \int_{a-1}^{a}(\varphi^+\varphi_x^* + c.c.)dx - \int_b^{b+1}(\varphi^-\varphi_x^* + c.c.)dx \\ &+ \frac{i}{2}(\varphi\varphi_t{}^* - \varphi^*\varphi_t)\Big|_a^b - \quad (\varphi^+)^*\varphi\Big|_{a-1}^{b} - \quad (\varphi^-)^*\varphi\Big|_a^{b+1} - \left[\frac{2}{\mu}|\varphi|^2 - \frac{2}{\mu^2}\ln\left(1+\mu|\varphi|^2\right)\right]_a^b.\end{aligned} \tag{6.66}$$

Evaluating the right-hand side of (6.66) similarly to the way we obtained (6.65) and substituting eq. (6.18) for ω, produces

$$\frac{dP}{dt} = |K_1|^2 e^{-\pi\mathcal{Q}_1/\varepsilon}(k+\mathcal{Q}_1)[2\sin(k+\mathcal{Q}_1) - v]. \tag{6.67}$$

Using the leading order term of the perturbative solution (6.13) and eq. (6.62), we can express N and P via ε and k:

$$\begin{aligned}N &= 2\varepsilon\cos k + \mathcal{O}\left(\varepsilon^2\right), \\ P &= 2k\varepsilon\cos k + \mathcal{O}\left(\varepsilon^2\right).\end{aligned}$$

In calculating N and P we had to integrate from $X = \varepsilon a$ to $X = \varepsilon b$. Since the integrands decay exponentially, and since $a < 0$ and $b > 0$ were assumed to be much larger than ε^{-1} in absolute value, it was legitimate to replace these limits with $-\infty$ and ∞, respectively. The error introduced in this way is exponentially small in ε.

Taking time derivatives of N and P above and discarding ε^1-corrections to ε^0-terms, we deduce that

$$\begin{aligned}\dot{\varepsilon} &= \frac{\dot{N} + \tan k(\dot{P} - k\dot{N})}{2\cos k}, \\ \dot{k} &= \frac{\dot{P} - k\dot{N}}{2\varepsilon\cos k}.\end{aligned}$$

Finally, substituting for $\dot{N}$ and $\dot{P}$ from eqs (6.65) and (6.67), we arrive at the dynamical system

$$\dot{\varepsilon} = |K_1(k)|^2 e^{-\pi\mathcal{Q}_1/\varepsilon}\,\Omega'(\mathcal{Q}_1)\,\frac{1+\mathcal{Q}_1\tan k}{2\cos k}, \tag{6.68a}$$

$$\dot{k} = |K_1(k)|^2 e^{-\pi\mathcal{Q}_1/\varepsilon}\,\Omega'(\mathcal{Q}_1)\,\frac{\mathcal{Q}_1}{2\varepsilon\cos k}, \tag{6.68b}$$

where the group velocity $\Omega'(\mathcal{Q}_1) = 2\sin(k+\mathcal{Q}_1) - v$ with $v = 2(\sinh\varepsilon/\varepsilon)\sin k$, and $\mathcal{Q}_1 = \mathcal{Q}_1(\varepsilon,k)$ is the smallest root of eq. (6.19).

6.4.2 Soliton's deceleration and sliding velocities

The vector field (6.68) is defined for $k \geq k_{\min}^{(1)}$, where $k_{\min}^{(1)}$ is the value of k for which the roots $\mathcal{Q}_1$ and $\mathcal{Q}_2$ merge in fig. 6.1 (i.e. the smallest value of k for which the roots $\mathcal{Q}_1$ and $\mathcal{Q}_2$ still exist). When $k = k_{\min}^{(1)}$, the group velocity $\Omega'(\mathcal{Q}_1)$ becomes equal to zero; therefore, the equation $k = k_{\min}^{(1)}(\varepsilon)$ defines a line of (nonisolated) fixed points of the system (6.68). Assume, first, that the saturation parameter μ is such that $K_1(k)$ does not vanish for any k. For $k > k_{\min}^{(1)}$, the factor $\Omega'(\mathcal{Q}_1)$ in (6.68b) is negative; since $\mathcal{Q}_1$ and $\cos k$ are positive for all $0 < k \leq \pi/2$, the derivative $\dot{k}$ satisfies $\dot{k} \leq 0$ for all times. Hence, all trajectories are flowing towards the line $k = k_{\min}^{(1)}(\varepsilon)$ from above. It is worth noting that the derivative $\dot{\varepsilon}$ is also negative, and that the k-axis is also a line of nonisolated fixed points. However, no trajectories will end there as follows from the equation

$$\frac{d\varepsilon}{dk} = \varepsilon\left[\tan k + \frac{1}{\mathcal{Q}_1(k,\varepsilon)}\right],$$

which is a consequence of (6.68a) and (6.68b).

Representative trajectories are plotted in figure 6.5(a). Since $k_{\min}^{(1)}(\varepsilon) \approx \varepsilon^2/4\pi$ is very small for small ε, the line $k = k_{\min}^{(1)}(\varepsilon)$ is practically indistinguishable from the horizontal axis. Therefore, we can assert that, to a good accuracy, $k \to 0$ as $t \to \infty$. This means that the soliton stops moving – and stops decaying at the same time.

For k smaller than $k_{\min}^{(1)}$, the vector field (6.68) is undefined and we cannot use it to find out what happens to the soliton after k has reached $k_{\min}^{(1)}$. The reason for this is that the soliton stops radiating at the wavenumber $\mathcal{Q}_1$ as k drops below $k_{\min}^{(1)}$. In fact our analysis becomes invalid as soon as k becomes $\mathcal{O}(\varepsilon^2)$, i.e. even before k reaches $k_{\min}^{(1)}$, because we can no longer disregard the $n = 2$ radiation here. At the qualitative level it is obvious, however, that the parameter k should continue to decay all the way to zero, in a cascade way. First, the $n = 2$ radiation will become as intense as the $n = 1$ mode when $k \approx \varepsilon^2/4\pi$. Subsequently, i.e. for smaller k, the $n = 3$

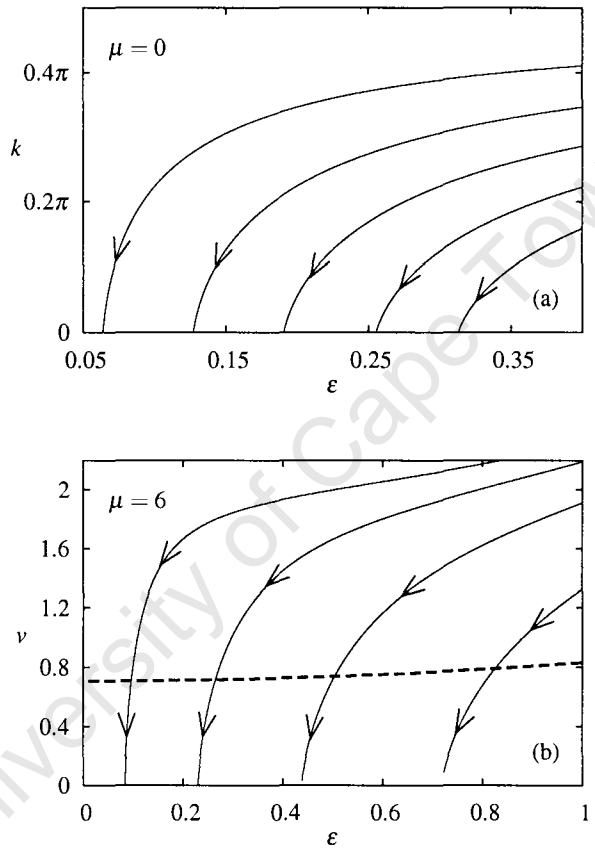

Figure 6.5: The phase portrait of the system (6.68) in the case (a) where the Stokes constant $K_1(k)$ does not have zeros, and (b) where $K_1(k)$ has one zero. In (b), the dashed line is the line of nonisolated fixed points $k = k_1$. Note that in (b), the phase portrait has been replotted on the (ε, v) plane; hence the dashed line gives the value of the sliding velocity for each value of ε. In (a), $\mu = 0$; in (b), $\mu = 6$.

harmonic will replace the radiation with the wavenumbers Q_1 and Q_2 as a dominant mode. The $n = 4$ mode will become equally intense near $k = k_{\min}^{(2)} \approx \varepsilon^2/8\pi$; as k drops below $\varepsilon^2/8\pi$, both Q_3 and Q_4 will cede to Q_5, and so on.

If μ is such that the Stokes constant $K_1(k)$ vanishes at one or more values of k, the system has one or more lines of nonisolated fixed points, $k = k_i$. The corresponding values of v, $v = v_i(\varepsilon) \equiv 2(\sinh\varepsilon/\varepsilon)\sin k_i$, define the *sliding* velocities of the soliton, i.e. velocities at which the soliton moves without radiative friction. One such velocity is shown by the dashed line in fig. 6.5(b). The fixed points (ε, k_i) are semistable; for k above k_i, the flow is towards the line $k = k_i$ but when k is below k_i, the flow is directed away from this straight line [see fig. 6.5(b)]. Since both $\dot{\varepsilon}$ and $\dot{k}$ are negative, the soliton's velocity $v = 2(\sinh\varepsilon/\varepsilon)\sin k$ will generally be decreasing – until it hits the nearest underlying sliding velocity v_i and locks on to it. The ensuing sliding motion will be unstable; a small perturbation will be sufficient to take the soliton out of the sliding regime after which it will resume its radiative deceleration. However, since $\dot{k}$ is proportional to the *square* of the Stokes constant and not to $K_1(k)$ itself, small perturbations δk will be growing linearly, not exponentially, in t. As a result, the soliton may spend a fairly long time sliding at the velocity v_i. It is therefore not unreasonable to classify this sliding motion as *metastable*.

We conclude that the soliton becomes pinned (i.e. $k \to 0$ and so $v \to 0$) before it has decayed fully (i.e. before the amplitude ε has decreased to zero). The exponential dependence of $\dot{\varepsilon}$ and $\dot{k}$ on $1/\varepsilon$ implies that tall, narrow pulses will be pinned very quickly while short, broad ones will travel for a very long time before they have slowed appreciably. Next, if μ is such that there is one or more sliding velocity available in the system, and if the soliton is initially moving faster than some of these, its deceleration will be interrupted by long periods of undamped motion at the corresponding sliding velocities.

It is worth re-emphasising here that if the amplitude ε is small, then even if the soliton is *not* sliding, its deceleration will be so slow that it will spend an exponentially long time travelling with virtually unchanged amplitude and speed. The deceleration rate $-\dot{v}/v$ is shown in fig. 6.6, as a function of the soliton's velocity v, for fixed amplitude ε. Note that the decay rate drops, exponentially, as the velocity is decreased; this drop is due to the exponential factor $e^{-\pi Q_1/\varepsilon}$ in eq. (6.68). As the velocity v (and hence the wavenumber k) decreases, the root $Q_1(\varepsilon, k)$ grows towards the limit value of approximately 2π (see fig. 6.1). This variation in Q_1 is amplified by the division by small ε and exponentiation in $e^{-\pi Q_1/\varepsilon}$.

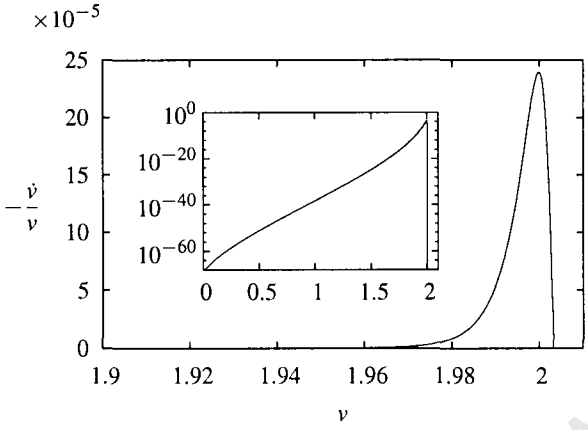

Figure 6.6: The soliton's decay rate as a function of its velocity, for fixed $\varepsilon = 0.1$. (Here $\mu = 0$.) In the inset, the same curve is replotted using a logarithmic scale on the vertical axis.

6.5 Zero eigenvalues of the stationary solutions

As mentioned in the introduction (section 1.6), we are seeking a counterexample to verify the claim [119] that it is not necessary for a discrete equation to be exceptional (i.e. to admit a continuous family of stationary kinks) in order for sliding solitons to exist in that model. None of the discrete nonlinear Klein–Gordon models we have investigated in previous chapters have provided such a rebuttal. As for the DNLS equation, we have shown that the cubic DNLS model, which is not exceptional (having only site-centred and bond-centred stationary solutions; see [124, 206]), does not admit sliding solitons. What remains is to establish whether the saturable DNLS equation, which we have shown to possess sliding velocities, is exceptional. As mentioned, the work of Khare, Rasmussen, Samuelsen and Saxena [203] suggests that this may be the case, since they have discovered translationally invariant stationary solutions of (6.2). We now look more closely at their results.

The form of our equation differs from that of Khare *et al.* by various rescalings. Written in terms of our variables and parameters, they have found the soliton solution

$$\phi_n = \frac{\sqrt{1-\mu^2}}{\mu^{3/2}} \operatorname{sech}\left[\varepsilon(n-c)\right] e^{i\omega t}. \tag{6.69}$$

Here, $\cosh\varepsilon = 1/\mu$, $\omega = 2/\mu$ and $c \in \mathbb{R}$. (Of course, the solution is also invariant with respect to time-translation, i.e. multiplication by a constant phase factor not shown.) These solutions only exist for

$$0 < \mu \leq 1, \tag{6.70}$$

with the amplitude and inverse-width (ε) tending to zero as $\mu \to 1^-$ and to infinity as $\mu \to 0^+$. Note that ε need not be small.

In view of the restriction (6.70) on μ, we cannot, in fact, claim that the equation possesses effective translational invariance for the values of μ at which sliding kinks exist, namely $\mu > 4$. Also note that for a given μ, the amplitude and inverse-width are fixed; apart from the translation parameter c there are no other free parameters. This is in contrast to the stationary kinks of the exceptional models studied in chapter 4, which existed for all values of the lattice-spacing parameter h of those models. This parameter h of the discrete ϕ^4 equations and the parameter ε of our DNLS soliton are analogous, since both reduce the model to the continuum limit when sent to zero. For a given μ, the solutions (6.69) only exist for an *isolated* value of ε. It therefore seems that we cannot class the saturable DNLS model as exceptional, unless there are stationary solutions other than (6.69) which we are unaware of.

To establish this claim—that the saturable DNLS equation is *not*, in fact, exceptional—we study the stationary equation in more detail. We are looking for solutions of (6.2) which have the form

$$\phi_n(t) = \psi_n e^{i\omega t}. \tag{6.71}$$

(Note that the variable ψ_n is defined the same as the function $\psi(X)$ of section 6.2 at the points $X = \varepsilon n$ when $k = 0$ and hence $v = 0$.) This yields the difference equation

$$\psi_{n+1} - \omega\psi_n + \psi_{n-1} + \frac{2|\psi_n|^2}{1+\mu|\psi_n|^2}\psi_n = 0. \tag{6.72}$$

By the definition of chapter 4, the equation is exceptional if this stationary second-order difference equation can be obtained from a two-point map. This implies that it has a continuous family of solutions centred at arbitrary points relative to the lattice for all parameter values sufficiently close to the continuum limit, and not just isolated ones.

To replace ω we define the more physically meaningful parameter ε (representing the inverse-width of the soliton) as

$$\omega = 2\cosh\varepsilon,$$

which agrees with its previous definition (6.17) since $v = 0$. In order to establish whether the continuous family of solitons exists only for isolated values of ω, we shall check for zero eigenvalues of (6.2) linearised about its stationary solutions, i.e. we assume a solution of the form

$$\phi_n(t) = [\psi_n + \delta\psi_n(t)]e^{i\omega t},$$

where $\delta\psi_n(t)$ is small. The stationary solutions ψ_n (both on- and off-site) are first calculated numerically from (6.72) using Newton iterations, with the first term of the perturbation expansion (6.13) as the initial guess. Because of the phase invariance of (6.72) we can clearly assume its solutions to be real without loss of generality.

We write $\delta\psi_n(t) = \tilde{u}_n(t) + i\tilde{v}_n(t)$, where $\tilde{u}_n(t)$ and $\tilde{v}_n(t)$ are real, and separate variables in the resulting linear equations, i.e. set

$$\tilde{u}_n(t) = u_n e^{\lambda t} \quad \text{and} \quad \tilde{v}_n(t) = v_n e^{\lambda t}.$$

This finally yields the eigenvalue problem

$$\begin{pmatrix} 0 & -\mathcal{L}_0 \\ \mathcal{L}_1 & 0 \end{pmatrix} \begin{pmatrix} u_n \\ v_n \end{pmatrix} = \lambda \begin{pmatrix} u_n \\ v_n \end{pmatrix} \tag{6.73}$$

for all $n \in \mathbb{Z}$. The linear operators are defined as

$$\mathcal{L}_1 = \oplus - \omega + \ominus + \frac{6\psi_n^2}{1+\mu\psi_n^2} - \frac{4\mu\psi_n^4}{(1+\mu\psi_n^2)^2} \quad \text{and}$$

$$\mathcal{L}_0 = \oplus - \omega + \ominus + \frac{2\psi_n^2}{1+\mu\psi_n^2}.$$

Here, $\oplus u_n$ is shorthand for u_{n+1} and $\ominus u_n \equiv u_{n-1}$, and similarly for v_n. Recall that ψ_n is real. It is straightforward to show that the eigenvalues come in $\pm$ pairs: If $\binom{u_n}{v_n}$ is an eigenvector with eigenvalue λ, then $\binom{-u_n}{v_n}$ is an eigenvector with eigenvalue $-\lambda$.

The eigenvalue problem (6.73) was solved numerically by restricting n to a finite but large range of values (this depended on ε and was large enough to ensure that the stationary solution ψ_n fell below 10^{-20} at the ends). The matrix was padded with rows of zeros to make it square [because of the advance and delay terms in $\mathcal{L}_0$ and $\mathcal{L}_1$, there are four more unknowns than equations in (6.73)]. This introduced spurious zero eigenvalues which were ignored. There is always a further pair of zero eigenvalues corresponding to the invariance of (6.2) with respect to multiplication by a constant phase factor. The existence of yet another pair of zero eigenvalues would indicate the translation invariance of the stationary solution. We observed that all eigenvalues are always pure real/imaginary, although the reason is not immediately obvious.

To detect this eigenvalue pair we have plotted the eigenvalue with the second-smallest modulus; see figure 6.7. Note the logarithmic scale, on which the downward spikes represent decay to zero. The numerical error in these calculations is of the order of 10^{-6}; the 'noise' on the left of the plots is a result of the modulus of the eigenvalue dropping below this value. Figure 6.7(a)

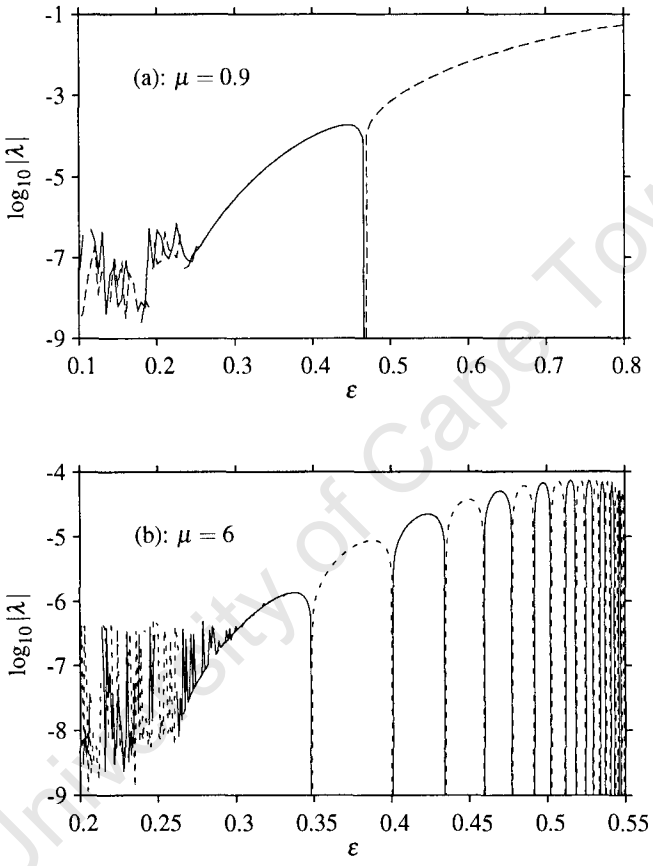

Figure 6.7: The second-smallest eigenvalue of (6.22) linearised about its stationary solutions, plotted with respect to their inverse-width for the indicated values of μ. Dashed lines: Real eigenvalue of the on-site solution and imaginary eigenvalue of the off-site solution. Solid: Imaginary eigenvalue of the on-site solution and real eigenvalue of the off-site solution. Plots for the on-site and off-site solutions are superimposed and indistinguishable.

is a plot for $\mu = 0.9$. We note a single zero of the eigenvalue in this case; this is precisely the value of ε for which the explicit solution (6.69) exists: For $\mu = 0.9$, $\varepsilon = 0.467$ in eq. (6.69). For all other values of ε (except $\varepsilon < 0.25$ where numerical inaccuracy prevents us drawing any conclusion) we see that the stationary solutions do not have a translation mode.

The case $\mu = 6$ is depicted in fig. 6.7(b). Here we know that we *do* have sliding solitons; however, the eigenvalue again only crosses through zero at certain isolated values. Thus we conclude that the saturable DNLS model is not exceptional; the stationary equation (6.72) cannot be written as a two-point map.

The cascade of zero crossings in fig. 6.7(b) is interesting because it indicates that there are other translation-invariant solutions apart from (6.69), which only exists for $\mu \leq 1$. Thus, one should be able to find further classes of solutions like (6.69), where ψ_n is given by a continuous function of $n - c$. We were unable to generate the stationary solution for $\varepsilon > 0.55$ (approximately), where the cascade of zeros appears to accumulate. As ε approaches this limit, the amplitude of the soliton tends to infinity.

As an aside, it would be wasteful not to work out the stability of the stationary solutions of eq. (6.2), since we have already set up the eigenvalue problem for the linearisation. The existence of any eigenvalue with a positive real part indicates instability of the solution. In view of paragraphs (a) and (b) above, this implies that the existence of any real eigenvalue amounts to instability. In fig. 6.7, we have plotted the imaginary eigenvalue of the on-site solution and the real eigenvalue of the off-site solution with a solid line, and the other way around with a dashed line; the two solid lines and two dashed lines match up completely. The dashed line therefore indicates instability of the on-site solution and the solid line, instability of the off-site solution. As for stability, it is of course not sufficient that a single eigenvalue is imaginary: they all need to be. We have, however, checked all eigenvalues for certain values of ε and it appears that whenever the eigenvalue plotted in fig. 6.7 is imaginary, all others are as well. Therefore the solid lines indicate stability of the on-site solution and the dashed lines, stability of the off-site solution. We see that the stability of the site-centred and bond-centred solutions is always opposite, and that where the eigenvalues pass through zero, real eigenvalues become imaginary and vice versa, and hence stability is exchanged between the two types of solution. This phenomenon has previously been noted by Melvin, Champneys, Kevrekidis and Cuevas [209].

6.6 Concluding remarks

6.6.1 Summary

In this chapter, we have constructed the moving discrete soliton of the saturable NLS equation (6.1)–(6.2) as an asymptotic expansion in powers of its amplitude. The saturable nonlinearity includes the cubic nonlinearity as a particular case (for which $\mu = 0$). Our perturbation procedure is a variant of the Lindstedt-Poincaré technique where corrections to the parameters of the solution are calculated along with the calculation of the solution itself. Although the resulting asymptotic series (6.13) for the soliton is generally not convergent, the associated expansions for its frequency and velocity sum up to exact explicit expressions (6.17).

From the divergence of the asymptotic series (6.13) it follows, in particular, that the travelling discrete soliton does not decay to zero at least at one of the two infinities. Instead, the soliton approaches, as $X \to \infty$ or $X \to -\infty$, an oscillatory resonant background (6.23) where the amplitudes A_n of its constituent harmonic waves lie beyond all orders of ε. For the soliton moving with a positive velocity and approaching zero as $X \to \infty$, the oscillatory background at the left infinity represents the Cherenkov radiation left in the soliton's wake. To evaluate the amplitudes of the harmonic waves arising as $X \to -\infty$, we have continued the radiating soliton into the complex plane, where it exhibits singularities. We then matched the asymptotic expansion (6.34) of the background near the lowest singularity on the imaginary X axis to the far-field asymptotic expansion (6.31) of the background solution of the 'inner' equation, i.e. of the advance/delay equation 'zoomed in' on this singularity. The asymptotic expansions here are in inverse powers of the zoomed variable, y. The amplitudes of the radiation waves were found to be exponentially small in ε, with the pre-exponential factors (the so-called Stokes constants) being dependent only on the wavenumber of the soliton's carrier-wave. Representing solutions to the inner equation as Borel sums of their asymptotic expansions, the Stokes constants can be related to the expansion coefficients; we have calculated these coefficients numerically, using algebraic recurrence relations.

The upshot of the calculation of the leading Stokes constant K_1 is that in the case of the cubic nonlinearity (i.e. for $\mu = 0$), $K_1(k)$ does not vanish for any k. This means that the cubic discrete soliton cannot 'slide', i.e. cannot move without radiative friction. The saturable solitons, on the other hand, *can* slide – provided the saturation parameter μ is large enough. This is because, for a sufficiently large μ, the Stokes constant $K_1(k)$ is found to have one or more zeros $k_1, k_2, \ldots$.

Since the soliton with wavenumber $k > 0.22$ can have no higher-order resonances, those zeros which satisfy $k_i > 0.22$ do define wavenumbers at which sliding motion occurs. For each value of the soliton's amplitude ε, the formula (6.17) then gives the sliding velocities $v(k_i, \varepsilon)$.

The calculation of asymptotics beyond all orders is useful not only for determining the sliding velocities. Knowing the radiation amplitudes has allowed us to derive a two-dimensional dynamical system (6.68) for the soliton's parameters. Trajectories of this dynamical system describe the evolution of the soliton travelling at a generic speed. The evolution turns out to be simple: If μ is such that the Stokes constant $K_1(k)$ does not vanish anywhere in the region $k > 0.22$, the soliton decelerates, although very slowly. Eventually it becomes pinned to the lattice with a decreased but finite amplitude. However, if μ is such that there are sliding velocities in the system, and if the soliton starts its motion with the velocity higher than some of these then, although it will finally become pinned to the lattice, its deceleration will be interrupted by long periods of metastable sliding motion at these isolated velocities.

Finally, we have numerically calculated the eigenvalues of the saturable DNLS model (6.2) linearised about its stationary solutions, and deduced that it does not admit continuous translation-invariant families of stationary solitons; that is, it is not an exceptional system.

6.6.2 Concluding remarks

It is interesting to tie up the above results with our previous work on exceptional discretisations of the ϕ^4 model in chapter 3. There we discovered that for some exceptional models (in which the stationary soliton possesses an effective translational symmetry), sliding velocities, at which the radiation disappears, do exist. The fact that all these models involve a complicated nonlocal discretisation of the nonlinearity leads one to wonder whether the nonlinearity *has* to be discretised nonlocally in order for sliding solitons to exist. This question is answered—negatively—by our present work, which gives a counterexample of a simple, local and physically motivated nonlinearity supporting sliding solitons. This confirms the negative proof already given in ref. [119].

Although the question of whether exceptionality of the system is a prerequisite for the existence of sliding solitary waves has been answered (also negatively) both in this work and in ref. [119], an interesting open question is whether the existence of sliding solitons implies the existence of translation-invariant solutions of the stationary equation at *isolated* parameter values; that is, whether the exchange of stability of the static on-site and intersite modes is a prerequisite for sliding kinks to exist. Indeed, the work of Melvin, Champneys, Kevrekidis

and Cuevas [209] suggests that the two are directly connected: If one extrapolates the parameter curves of sliding solitons to the stationary regime, one hits the precise points at which translation modes of the stationary solitons exist (termed 'transparent points' by them). This is particularly interesting given that the Stokes constants themselves are *dis*continuous as the soliton velocity tends to zero, as we found in chapter 3.

We conclude this section by placing our results in the context of earlier studies of discrete solitons.

Moving solitons in the cubic DNLS equation have previously been studied by Ablowitz, Musslimani, and Biondini [112] (among others), using a numerical technique based on discrete Fourier transforms as well as perturbation expansions for small velocities. As we have done, these authors suggest that sliding (radiationless) solitons may not exist. They also observe, with the aid of numerical simulations, that strongly localised pulses are pinned quickly to the lattice, while broader ones are more mobile – results which are in agreement with ours.

Duncan, Eilbeck, Feddersen and Wattis [113, 187] have studied the bifurcation of periodic travelling waves from constant solutions in the cubic DNLS equation, using numerical path-following techniques. They find that the paths terminate when the soliton's amplitude reaches a certain limit value, and in the light of our results it seems likely that this is the point at which the radiation becomes large enough to have an effect on the numerics.

More general DNLS equations have been studied by Flach, Zolotaryuk and Kladko though their inverse method [119]. They find that sliding solitons *cannot* occur in a DNLS equation with local nonlinearity – a contradiction of the results of this chapter. However, they make the assumption that a real envelope modulates the carrier wave, whereas eq. (6.13) shows this to be untrue in general.

Solitary waves which decay to constant values at the spatial infinities, despite the fact that the generic asymptotic behaviour in the underlying model is oscillatory, are commonly referred to as embedded solitons. An example is given by the sliding solitons reported in this chapter as well as the sliding kinks of chapter 3; both types of solitary waves propagate without exciting the resonant background oscillations. Embedded solitons have been studied for some time in continuous systems [55], but their history in lattice equations is younger. Recently, Malomed, González-Pérez-Sandi, Fujioka, Espinosa-Cerón and Rodríguez have considered certain lattice equations with next-to-nearest-neighbour couplings and shown (by means of explicit solutions) that both stationary [210] and moving [211] embedded solitons exist. Stationary embedded

solitons in discrete waveguide arrays have also been analysed by Yagasaki, Champneys and Malomed [212].

Finally, after this work was substantially completed, we learnt that Melvin, Champneys, Kevrekidis, and Cuevas had obtained results very similar to ours. Using a combination of intuitive arguments and numerical computations, they have found sliding solitons for certain values of the parameters of a saturable DNLS model [209].

Appendix 6.A Proof that singularities do not accumulate to the imaginary axis

Roots of the equation (6.40) with the top and bottom signs give singularities of $U(p)$ and $W(p)$, respectively. Our aim here is to show that the integration contours γ_u and γ_s in section 6.3.5 can be chosen to lie above all the complex singularities, i.e., that singularities of $U(p)$ and $W(p)$ do not accumulate to the imaginary axis.

Roots of eq. (6.40) are zeros of the functions $F(\pm p)$, where

$$F(p) \equiv \cosh p - 1 - i \tan k(\sinh p - p). \tag{6.74}$$

The imaginary zeros of $F(p)$ are at $p = -iq_n$, where q_n are the real roots of eq. (6.30). We let N denote the number of these imaginary zeros; for $k \neq 0$, N is finite. We recall that all q_n are positive; hence all N imaginary zeros of $F(p)$ are on the negative imaginary axis, and all N zeros of $F(-p)$ on the positive imaginary axis.

Let κ and q be the real and imaginary part of p: $p = \kappa + iq$. We let $\mathcal{D}$ denote the rectangular region in the complex-p plane bounded by the vertical lines $\kappa = \pm\varepsilon$ and horizontal lines $q = \varepsilon^{1/2}$ and $q = Q$, where ε is small and Q is large enough for the region to contain all N zeros of $F(-p)$ on the positive imaginary axis. By the argument principle, the total number of (complex) zeros of the function $F(-p)$ in the region $\mathcal{D}$ is given by $(2\pi)^{-1}$ times the variation of its argument (i.e., its phase) along the boundary of $\mathcal{D}$. In a similar way, one may count the number of zeros of the function $F(p)$ in $\mathcal{D}$.

We have

$$\tan\arg F(\pm p) = \frac{\sinh\kappa\sin q \mp \tan k(\sinh\kappa\cos q - \kappa)}{\cosh\kappa\cos q - 1 \pm \tan k(\cosh\kappa\sin q - q)}.$$

Points on the vertical line $\kappa = \varepsilon$ satisfy

$$\tan\arg F(\pm p) \approx -\varepsilon\frac{d}{dq}\ln|1 - \cos q \pm \tan k(q - \sin q)|. \tag{6.75}$$

Consider, first, the case of the bottom sign in eq. (6.75). The expression between the bars in (6.75) crosses through zero N times as the line $\kappa = \varepsilon$ is traced out. Each time zero is crossed, the logarithmic derivative in (6.75) jumps from $-\infty$ to $+\infty$, and the argument of $F(-p)$ increases by π as we move from one crossing to the next one. The net increase of the argument as the line $\kappa = \varepsilon$ is traversed from its bottom to the top, is $N\pi$. In the case of the top sign in (6.75), on the other hand, the expression in $|...|$ never crosses through zero and hence the total increment of the argument of $F(p)$ is zero.

As we move along the vertical line $\kappa = -\varepsilon$ from top to bottom, the argument of $F(-p)$ increases by another $N\pi$ while the argument of $F(p)$ does not acquire any increment. Since there are no zero crossings on the horizontal segments, the net change of the argument of $F(-p)$ along the boundary of $\mathcal{D}$ is $2N\pi$ while the total increment of $\arg F(p)$ is zero. Therefore $F(-p)$ has only N zeros in the region $\mathcal{D}$ (and they all lie on the imaginary axis) while the function $F(p)$ has no zeros in $\mathcal{D}$. This implies that complex singularities of $U(p)$ and $W(p)$ cannot accumulate to the positive imaginary axis.

Chapter 7

Cubic-quintic solitons in the square-well waveguide

We now turn our attention away from discrete equations, but stay with the topic of optical waveguides. In this chapter, we consider a single waveguide made of a medium with cubic-quintic nonlinearity. Since spatial solitons can exist in a self-focussing medium in the absence of a waveguide, one might intuitively expect its presence to enhance the stability of solitons. Indeed, the numerical study of this problem [143] has revealed soliton bistability. Our aims in this chapter are to provide analytical results to bolster the numerical analysis of ref. [143] and to understand in more detail the behaviour of light in a single waveguide as a preliminary step to a more realistic waveguide-array model.

7.1 Introduction

We shall be studying the nonlinear Schrödinger equation with a cubic-quintic nonlinearity and an additional square-well potential,

$$i\psi_t + \psi_{xx} - U(x)\psi + 2|\psi|^2\psi - |\psi|^4\psi = 0, \tag{7.1}$$

where

$$U(x) = \begin{cases} -U_0, & |x| \leq d \\ 0, & |x| > d. \end{cases} \tag{7.2}$$

We shall restrict ourselves to the case $U_0 > 0$. For $U_0 = 0$, eq. (7.1) reduces to the cubic-quintic NLS equation, which describes spatial solitons in PTS (polydiacetylene *para*-toluene sulfonate) crystals, special glasses, and organic materials (see references in [143]). The cubic-quintic nonlinearity also describes photorefractive materials when the intensity is not too great, as it comes from a Taylor expansion of the saturable nonlinearity of the Vinetskii–Kukhtarev model (described in [69]). A review of theoretical studies of solitons in cubic-quintic media is given in ref. [213]. Since (7.1) is (1+1)-dimensional, it describes light constrained within a *planar* medium. On this plane, the variable t represents the spatial coordinate parallel to propagation of the beam, with the x axis perpendicular to it. Turning on the square potential well—i.e., setting U_0 to a nonzero value—corresponds to adding a step in the index of refraction for $|x| \leq d$. The equation now describes the simplest kind of channel waveguide, which has two regions—the core and cladding—with two different indices of refraction.

Gisin, Driben, and Malomed [143] have made several interesting observations in their numerical studies of the solitons of eq. (7.1). As mentioned, one of the objectives of the present investigation is to provide mathematical foundation for the conclusions of the numerical analysis of ref. [143]. In particular, we will give an explanation of the phenomenon of the coexistence of two stationary solitons for $k > k_\infty$ and prove that $k_\infty = \frac{3}{4}$, in agreement with the numerical observations in [143]. Here k is the wavenumber of the carrier wave in the t direction. We will also provide an explanation for the soliton bistability detected through simulations in ref. [143], and reconcile this result with the Vakhitov–Kolokolov stability theory.

7.2 Soliton solutions

7.2.1 Stationary solutions

Assuming that $\psi(x,t) = R(x)e^{ikt}$ in (7.1), where $R(x)$ and k are real, yields

$$R_{xx} - kR - U(x)R + 2R^3 - R^5 = 0. \tag{7.3}$$

Integrating with the factor R_x gives

$$R_x^2 + V_{\text{int}}(R) = E_{\text{int}}, \tag{7.4a}$$

$$R_x^2 + V_{\text{ext}}(R) = E_{\text{ext}}, \tag{7.4b}$$

where the subscripts 'int' and 'ext' denote the regions $|x| \leq d$ and $|x| > d$, respectively. Here,

$$V_{\text{int}}(R) = -(k - U_0)R^2 + R^4 - \frac{1}{3}R^6 \tag{7.5}$$

and

$$V_{\text{ext}}(R) = -kR^2 + R^4 - \frac{1}{3}R^6. \tag{7.6}$$

We seek solutions to eq. (7.3) which decay to zero as $|x| \to \infty$; hence, k has to be positive. Since $V_{\text{ext}}(0) = 0$, eq. (7.4b) gives $E_{\text{ext}} = 0$. We shall restrict ourselves to even solutions of (7.3).

Equation (7.3) must be solved for $|x| \leq d$ and for $|x| > d$ and the solutions and their derivatives matched at $|x| = d$. Our strategy will be as follows. Assume the external and internal solutions have been matched at $x = d$: $R(d-0) = R(d+0)$. Then their derivatives will be matched, $R_x^2(d-0) = R_x^2(d+0)$, provided

$$E_{\text{int}} - V_{\text{int}}[R(d)] = E_{\text{ext}} - V_{\text{ext}}[R(d)].$$

Using eqs (7.5), (7.6) and the fact that $E_{\text{ext}} = 0$, this becomes

$$E = U_0 R^2(d). \tag{7.7}$$

(Here and below, E stands for E_{int}.) Thus it remains to choose E such that the internal solution satisfies eq. (7.7) and finally, match the external solution to the internal solution chosen in this way.

Note that in view of (7.7), E may not be negative.

7.2.2 The external region, $|x| > d$

It is convenient to interpret eqs (7.4) as the energy conservation laws for classical particles in the potentials $V_{\text{int}}(R)$ and $V_{\text{ext}}(R)$. The three possible shapes of the potential $V_{\text{ext}}(R)$ are shown in fig. 7.1. According to eq. (7.4b), a particle with $E_{\text{ext}} = 0$ can only move in a region where $V_{\text{ext}}(R) \leq 0$; such a region should obviously include the asymptotic value $R = 0$. Therefore, for $0 \leq k \leq \frac{3}{4}$, the only allowed region is $R \leq R_0$, where R_0 is the smaller positive root of $V_{\text{ext}}(R)$:

$$R_0^2 = \frac{3}{2}\left(1 - \sqrt{1 - 4k/3}\right). \tag{7.8}$$

As for the case $k > \frac{3}{4}$, eq. (7.4) imposes no bounds on $R(x)$.

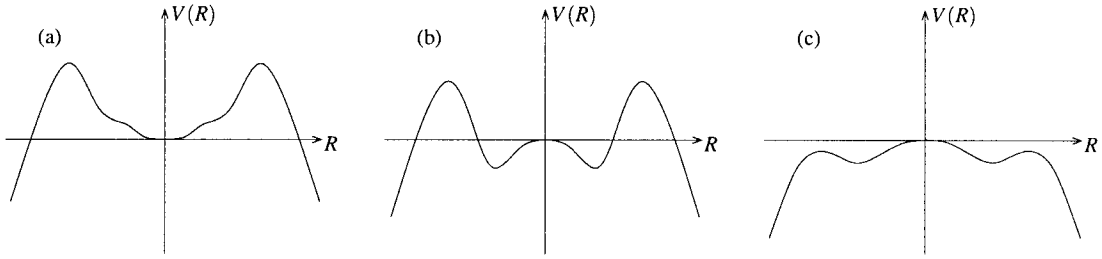

Figure 7.1: The form of $V_{\rm ext}(R)$ for: (a) $k<0$; (b) $0\le k\le\frac{3}{4}$; (c) $k>\frac{3}{4}$, and of $V_{\rm int}(R)$ for: (a) $k-U_0<0$; (b) $0\le k-U_0\le\frac{3}{4}$; (c) $k-U_0>\frac{3}{4}$.

We also note that if $k>\frac{3}{4}$, the solution $R(x)$ has to decay monotonically in the region $x>d$ (and, naturally, in the mirror-reflected region $x<-d$). Indeed, if $R(x)$ had a point of maximum at some $x_*>d$, the corresponding $R_*=R(x_*)$ would have to be a zero of the potential $V_{\rm ext}(R)$. However, $V_{\rm ext}(R)$ does not have zeros other than $R=0$ for $k>\frac{3}{4}$, and therefore the solution $R(x)$ can have no local maxima. On the other hand, in the case $0\le k\le\frac{3}{4}$, the potential $V_{\rm ext}(R)$ does have a zero in the region of allowed motion (at $R=R_0$); hence nonmonotonic solutions do exist for $0\le k\le\frac{3}{4}$. Such solutions have a local maximum with $R_*=R_0$ but no additional local minima.

The outer solution can be readily found in closed form. Separating variables in (7.4b) gives

$$x=\pm\int\frac{dR}{R\sqrt{k-R^2+\frac{1}{3}R^4}},$$

whence we have in the region $x\ge d$:

$$R_{\rm ext}^2(x)=\frac{2k}{1+\sqrt{1-4k/3}\cosh[2\sqrt{k}(x-x_0)]}\qquad\left(0\le k<\frac{3}{4}\right);\tag{7.9a}$$

$$R_{\rm ext}^2(x)=\frac{4k}{2+\exp[-2\sqrt{k}|x-x_0|]}\qquad\left(k=\frac{3}{4}\right);\tag{7.9b}$$

$$R_{\rm ext}^2(x)=\frac{2k}{1+\sqrt{4k/3-1}\sinh[2\sqrt{k}(x-x_0)]}\qquad\left(k>\frac{3}{4}\right).\tag{7.9c}$$

The corresponding solution in the region $x\le -d$ is obtained by letting $R_{\rm ext}(x)=R_{\rm ext}(-x)$. Equation (7.9a) has the form of the familiar soliton of the cubic-quintic NLS without an external potential [214, 215, 216, 217]. Equation (7.9b) has the form of a kink; it is not unknown in the literature either [218, 219]. As for eq. (7.9c), it is singular for large enough $x_0>0$ even if considered only in the region $x\ge d$. We shall, however, only need to use those values of x_0 for which the denominator in (7.9c) is positive for all $x\ge d$.

We match the inner and outer solutions by setting $R_{\rm ext}(d) = R_{\rm int}(d)$ and solving for x_0. For $k \geq \frac{3}{4}$, invoking (7.9b) and (7.9c), this gives a unique value of x_0. On the other hand, when $k < \frac{3}{4}$, there are two solutions for x_0 since the right-hand side of (7.9a) is not a monotonic function. We must select the one for which the sign of $R'_{\rm ext}(d)$ matches the sign of $R'_{\rm int}(d)$.

7.2.3 The internal region, $|x| \leq d$

The three possible forms of $V_{\rm int}(R)$ are shown in fig. 7.1. The maxima of $V_{\rm int}(R)$ are at $R = \pm R_m$ where $R_m^2 = 1 + \sqrt{1-(k-U_0)}$. At these points,

$$V_m \equiv V_{\rm int}(\pm R_m) = 2/3 - (k-U_0) + \frac{2}{3}[1-(k-U_0)]^{3/2}. \tag{7.10}$$

This value is negative for $k - U_0 > \frac{3}{4}$. It follows that for $k - U_0 > \frac{3}{4}$, $V_{\rm int}(R)$ is negative for all R except $R = 0$, where $V_{\rm int} = 0$ [see fig. 7.1(c)].

Even solutions (to which we are confining ourselves in this work) satisfy $R_x(0) = 0$. The corresponding values $R(0)$ give the turning points of the classical particle in the potential $V_{\rm int}(R)$. Since $E > 0$, turning points cannot arise if $k - U_0 > \frac{3}{4}$ [see fig. 7.1(c)]. On the other hand, assuming $k - U_0 \leq \frac{3}{4}$, there are two positive turning points if the energy is smaller than V_m, $0 \leq E \leq V_m$, and none if $E > V_m$. Denoting the turning points $R_2 = \sqrt{\rho_2}$ and $R_3 = \sqrt{\rho_3}$, where ρ_2 and ρ_3 are the smaller and larger positive roots of the equation

$$\frac{1}{3}\rho^3 - \rho^2 + (k-U_0)\rho + E = 0, \tag{7.11}$$

$0 < \rho_2 < \rho_3$, we have two allowed regions of motion of the 'internal' particle:

$$R^2 \leq \rho_2 \tag{7.12}$$

and

$$R^2 \geq \rho_3. \tag{7.13}$$

7.2.4 Matching of the solution

We now show that the motion in the region $R^2 \geq \rho_3$ cannot be matched to the outer solution, and so we shall only need to consider the region $R^2 \leq \rho_2$. Consider, first, the case $k > \frac{3}{4}$ and assume that $R(0) = \sqrt{\rho_3}$. As the particle moves away from the turning point $R = \sqrt{\rho_3}$, $R(x)$ grows and so $R_x(x) > 0$ for all x, and in particular, $R_x(d) > 0$. This is obviously inconsistent

with the requirement that the outer solution should be monotonically decaying to zero. On the other hand, if $R(0) = -\sqrt{\rho_3}$, we will have $R_x(x) < 0$ and $R(x) < 0$ for all x, and in particular for $x = d$. This is, again, incompatible with the monotonic decay in the outer region.

Now let $0 \leq k \leq \frac{3}{4}$. In this case, the value of R^2 is bounded in the outer region: $R^2(x) \leq R_0^2$. In the inner region, on the other hand, we have, by assumption, $R^2 \geq \rho_3$. Since ρ_3 is obviously greater than the point of maximum of $V_{\text{int}}(R)$, i.e. $\rho_3 \geq R_m^2$, the inner solution satisfies $R^2(x) \geq R_m^2$ for all x. As one can readily verify, R_m is greater than R_0 if $0 \leq k \leq \frac{3}{4}$ and $U > 0$, and therefore the inner solution with $R^2 \geq \rho_3$ cannot be matched to the outer one. This leaves us with only the region $R^2 \leq \rho_2$ to be considered.

When $k > \frac{3}{4}$, the outer solution $R_{\text{ext}}(x)$ is unbounded and takes on all values between 0 and ∞. Therefore, whatever the value of the inner solution $R_{\text{int}}(x)$ at $x = d$, the outer solution can always be matched to it by a suitable translation in x.

Now let $0 \leq k \leq \frac{3}{4}$. Here, the outer solution attains all values between 0 and R_0 and can therefore be matched, by a translation, to any inner value $R_{\text{int}}(d)$ which is smaller than R_0. It is easy to see that $R_{\text{int}}(d)$ is smaller than R_0 for any E and so the matching can always be achieved. Indeed, $V_{\text{ext}}(\rho)$ can be readily found if $V_{\text{int}}(\rho)$ is known:

$$V_{\text{ext}}(\rho) = V_{\text{int}}(\rho) - U_0\rho. \tag{7.14}$$

For $\rho = \rho_2$, we have $V_{\text{int}}(\rho_2) = E$ and the above equation gives

$$V_{\text{ext}}(\rho_2) = E - U_0\rho_2. \tag{7.15}$$

Since $R^2(d) \leq \rho_2$, equation (7.7) yields $E \leq U_0\rho_2$ and we conclude that $V_{\text{ext}}(\rho_2) \leq 0$. This inequality implies that $\rho_2 \leq R_0^2$, and so $R(d) \leq R_0$. Q.E.D.

A useful corollary of the inequality $R(d) \leq R_0$ (valid in the region $0 \leq k \leq \frac{3}{4}$), and eq. (7.7), is

$$E \leq U_0R_0^2. \tag{7.16}$$

Since $U_0R_0^2 = V_{\text{int}}(R_0)$, which is obviously smaller than V_m [the maximum value of $V_{\text{int}}(R)$], the inequality (7.16) provides a lower upper bound on the energy E than the inequality $E \leq V_m$.

In view of the simplicity of the matching-by-translation procedure, it is convenient to use the free parameter in the outer solution (x_0) to match the *functions*, $R_{\text{int}}(x)$ and $R_{\text{ext}}(x)$. Consequently, in order to match their *derivatives*, $R'_{\text{int}}(x)$ and $R'_{\text{ext}}(x)$ [as per (7.7)], we will have to make use of the free parameter (E) associated with the inner solution.

7.2.5 The inner solution and transcendental equation

The solution of eq. (7.4a) can be expressed as an elliptic integral:

$$\pm(\kappa x+\alpha)=F\left(\arcsin\sqrt{\frac{(\rho_2-\rho_1)R^2}{\rho_2(R^2-\rho_1)}},\mu\right). \tag{7.17}$$

Here ρ_1, ρ_2 and ρ_3 are the roots of eq. (7.11); ρ_2 and ρ_3 are the two positive roots defined above and ρ_1 is the negative root: $\rho_1<0<\rho<\rho_2<\rho_3$. The function F is the Legendre elliptic integral of the first kind, with modulus

$$\mu=\sqrt{\frac{\rho_2(\rho_3-\rho_1)}{\rho_3(\rho_2-\rho_1)}}. \tag{7.18}$$

Finally, the parameter

$$\kappa=\sqrt{\rho_3(\rho_2-\rho_1)/3} \tag{7.19}$$

has the meaning of inverse width of the inner solution, and α is an arbitrary real constant.

Inverting the relationship (7.17), we obtain a family of explicit solutions

$$R_{\rm int}(x)=\frac{\sqrt{-\rho_1}\,\mathrm{sn}\,(\kappa x+\alpha,\mu)}{\sqrt{1-\rho_1/\rho_2-\mathrm{sn}^2\,(\kappa x+\alpha,\mu)}}. \tag{7.20}$$

Equation (7.20) defines an even function of x if we choose $\alpha=K(\mu)$, where $K(\mu)$ is the complete elliptic integral. This gives

$$R_{\rm int}(x)=\frac{\sqrt{\rho_3}\,\mathrm{cn}\,(\kappa x,\mu)}{\sqrt{\rho_3/\rho_2-1+\mathrm{cn}^2\,(\kappa x,\mu)}}. \tag{7.21}$$

[We could also choose $\alpha=-K(\mu)$; this would give eq. (7.21) with a minus in front of the right-hand side.]

Substituting $R_{\rm int}(d)$ from (7.21) into (7.7) yields a transcendental equation

$$\frac{\rho_3\,\mathrm{cn}^2\,(\kappa d,\mu)}{\rho_3/\rho_2-1+\mathrm{cn}^2\,(\kappa d,\mu)}=\frac{E}{U_0}, \tag{7.22}$$

where the parameters ρ_2, ρ_3, κ and μ in the left-hand side are functions of E, k and U_0 defined by eqs (7.11), (7.18) and (7.19). Solving eq. (7.22) numerically for the given k, U_0 and d gives the value $E=E(k,U_0,d)$ for which the absolute values of the derivatives $R'_{\rm int}(x)$ and $R'_{\rm ext}(x)$ are equal at $|x|=d$. [This value may be nonunique, in which case—provided the signs of $R'_{\rm int}(d)$ and $R'_{\rm ext}(d)$ also match—there are several solutions with the same k, U_0 and d.]

For a given E, eq. (7.17) yields two sequences of the corresponding values of d:

$$d_n^{(\pm)} = \pm\frac{1}{\kappa}F\left(\arcsin\sqrt{\frac{\rho_2-\rho_1}{\rho_2}\frac{E}{E-U_0\rho_1}},\mu\right)+\frac{2n-1}{\kappa}K(\mu), \tag{7.23}$$

where $n = 1,2,3,\ldots$. The value $d_n^{(-)}$ lies in the interval

$$(2n-2)K(\mu) \le \kappa d_n^{(-)} \le (2n-1)K(\mu), \tag{7.24}$$

and the value $d_n^{(+)}$ satisfies

$$(2n-1)K(\mu) \le \kappa d_n^{(+)} \le 2nK(\mu). \tag{7.25}$$

The solution $R(x)$ with $d = d_n^{(-)}$ has $2(n-1)$ zeros (nodes) at $x = \pm x_m$, where $x_m = \frac{2m-1}{\kappa}K(\mu)$ and $m = 1,2,\ldots,n-1$. The solution with $d = d_n^{(+)}$ has $2n$ nodes, at $x = \pm x_m$ with $m = 1,2,\ldots,n$.

Finally, we need to ensure matching of the signs of the derivatives $R'_{\rm int}(d)$ and $R'_{\rm ext}(d)$ in addition to the matching of their absolute values. Assume, first, that $k \ge \frac{3}{4}$. Here, the outer solution decays to zero monotonically and so we require $\operatorname{sgn} R'_{\rm int}(d) = -\operatorname{sgn} R_{\rm int}(d)$. The cnoidal wave (7.20) changes sign at the points $\kappa x = (2n+1)K$, $n = 0,\pm1,\pm2,\ldots$, while its derivative changes sign at the points $\kappa x = 2nK$. Consequently, the sign of $R'_{\rm int}$ is opposite to the sign of $R_{\rm int}$ for κx between $2nK$ and $(2n+1)K$, and the above requirement is satisfied by choosing

$$2nK(\mu) \le \kappa d \le (2n+1)K(\mu), \quad n = 0,1,2,\ldots. \tag{7.26}$$

This range of d-values coincides with the one in (7.24); therefore, out of the two sequences $d_n^{(+)}$ and $d_n^{(-)}$ only the sequence $d_n^{(-)}$ satisfies the requirement of the derivative sign matching.

When $0 \le k < \frac{3}{4}$, the function $R_{\rm ext}(x)$ is nonmonotonic. For a given $R_{\rm ext}(d)$ and $|R'_{\rm ext}(d)|$, we can choose either the 'uphill' or 'downhill' slope of the graph of $R_{\rm ext}(x)$ depending on the sign of $R'_{\rm int}(d)$. Therefore the derivatives can be matched regardless of $\operatorname{sgn} R'_{\rm int}(d)$; accordingly, both sequences, $d_n^{(+)}$ and $d_n^{(-)}$, satisfy the sign-matching requirement in this case.

7.2.6 Summary

Given any value of $U_0 \ge 0$, even soliton solutions of eq. (7.1) may exist for $0 \le E \le U_0 R_0^2$, with R_0 given by (7.8), when $0 \le k \le \frac{3}{4}$, and for $0 \le E \le V_m$, with V_m as in (7.10), when $\frac{3}{4} < k \le U_0 + \frac{3}{4}$. Solutions exist for any such values of E which satisfy eq. (7.22), where d is any positive value for $k < \frac{3}{4}$ but must satisfy (7.26) for $k \ge \frac{3}{4}$. For these values of E, the even

soliton is given by $R(x) = R_{\text{int}}(x)$ for $|x| \leq d$ [see eq. (7.20)] and $R(x) = R_{\text{ext}}(x)$ for $|x| > d$ [see eqs (7.9)], with x_0 selected to match the values of $R_{\text{int}}(d)$ and $R_{\text{ext}}(d)$ and the signs of their derivatives.

7.3 Multiplicity of solutions

Without attempting to solve eq. (7.22) analytically, we can draw conclusions about the number of solutions through the analogy with a particle in the potential $V_{\text{int}}(R)$. Without loss of generality, we let $R(0) > 0$. For a given E, the particle starts its journey at $R(0) = \sqrt{\rho_2}$ and must reach $R(d) = \pm\sqrt{E/U_0}$ [by (7.7)] after a 'time' of $x = d$ has elapsed. We shall consider the behaviour of the function $x_f(E) = x(R_E)$, with $R_E = \pm\sqrt{E/U_0}$, which represents the 'time' the particle takes to move between these initial and final positions. Solutions of (7.22) occur for those values of E for which the horizontal line $x = d$ intersects the curve $x = x_f(E)$.

The function $x_f(E)$ arises by letting $R = R_E$ in eq. (7.17). The behaviour of this function depends on the choice of k and $k - U_0$. Before plotting $x_f(E)$ for different combinations of k and $k - U_0$, it is pertinent to consider the behaviour of the function $x_f(E)$ as E approaches its lower and upper bounds.

Firstly, as E approaches its lower bound of zero, the value R_E, the final position of the particle, tends to zero. For $k - U_0 > 0$, the origin is a point of unstable equilibrium for the 'internal' particle and hence the 'time' taken to reach this point tends to infinity: $x_f(E) \to \infty$ as $E \to 0$. For $k - U_0 \leq 0$, on the other hand, the particle moves harmonically in the neighbourhood of the origin (which is a stable equilibrium in this case):

$$R(x) = \sqrt{\frac{E}{U_0 - k}} \cos\left(\sqrt{U_0 - k}\, x\right).$$

Therefore, the 'time' taken to reach R_E approaches a finite value: $x_f(E) \to \mathcal{D}$ as $E \to 0$, where

$$\mathcal{D} = \mathcal{D}(U_0, k) = \frac{1}{\sqrt{U_0 - k}} \arccos\sqrt{\frac{U_0 - k}{U_0}}. \tag{7.27}$$

Proceeding to the upper bound of E, we recall that it equals $U_0 R_0^2$ for $0 \leq k \leq \frac{3}{4}$ and V_m for $k > \frac{3}{4}$. Assume, first, $0 \leq k \leq \frac{3}{4}$. The inequality $E \leq U R_0^2$ is saturated when $R_0^2 = \rho_2 = R^2(d)$. When this is the case, and if we restrict ourselves to solutions $R = R_{\text{int}}(x)$ which do not cross through $R = 0$, then the 'time' taken by the particle to reach the end point $R(d)$ from the identical starting point, is obviously zero, hence $x_f(E) \to 0$ as $E \to U_0 R_0^2$.

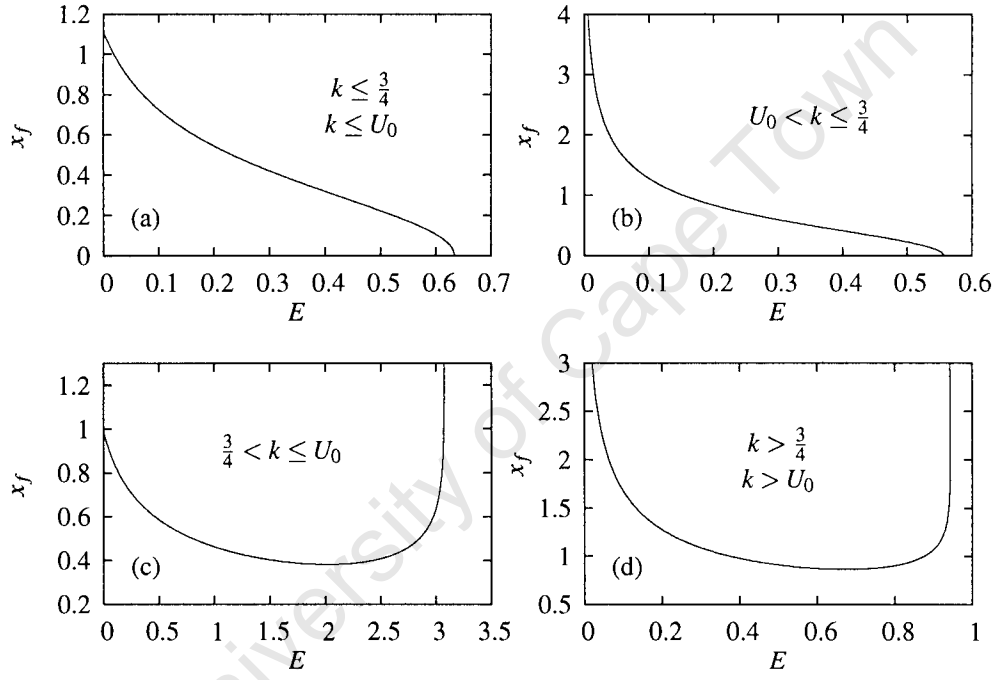

Figure 7.2: The graph of $x_f(E)$ (described in the text). There is one solution for every intersection of this graph with the horizontal line $x_f = d$. The four qualitatively different cases are shown. The parameter values used in these particular figures are: (a) $k = 0.5$, $U_0 = 1$; (b) $k = 0.7$, $U_0 = 0.5$; (c) $k = 1.2$, $U_0 = 2$ and (d) $k = 1.2$, $U_0 = 1$.

Let now $k > \frac{3}{4}$. Here, when E approaches its maximum value of V_m, the initial position of the particle approaches an unstable equilibrium point and hence the time it takes to escape this point and reach the point R_E tends to infinity: $x_f(E) \to \infty$ as $E \to V_m$.

Since the function $x_f(E)$ is continuous, knowledge of its behaviour near the boundaries of its domain of definition is sufficient to make some general conclusions about the form of the graph $x = x_f(E)$ and the number of its intersections with the horizontal line $x = d$. Namely,

(a) When $0 \le k \le \min(\frac{3}{4}, U_0)$, there is an odd number of nodeless solutions (but at least one) for any d in the interval $0 \le d \le \mathcal{D}$, with $\mathcal{D}$ as in (7.27).

(b) When $U_0 \le \frac{3}{4}$ and $U_0 < k \le \frac{3}{4}$, there is an odd number of nodeless solutions (one or more) for any $d \ge 0$.

(c) When $U_0 > \frac{3}{4}$ and $\frac{3}{4} < k \le U_0$, there is an odd number of solutions (and at least one) for $d \ge \mathcal{D}$, where $\mathcal{D}$ is as in (7.27).

(d) When $\max(\frac{3}{4}, U_0) < k \le U_0 + \frac{3}{4}$, there is an even number of solutions for any $d \ge 0$. There will be at least two solutions for sufficiently large d.

Here, by nodeless we mean solutions that do not cross zero. Note that the statements (c) and (d) are not limited to nodeless solutions.

One arrives at more precise and specific conclusions by plotting $x_f(E)$ in each of the four cases, (a)–(d). The number of extrema of the function $x_f(E)$—and hence the conclusions of the graphical analysis—remain the same over all k and U_0 in each of the four parameter regions. These can be summarised as follows.

(a) When $0 \le k \le \min(\frac{3}{4}, U_0)$, there is one nodeless solution for any $d \in (0, \mathcal{D})$ and no such solution for $d > \mathcal{D}$.

(b) When $U_0 \le \frac{3}{4}$ and $U_0 < k \le \frac{3}{4}$, there is one nodeless solution for any $d \ge 0$.

(c) When $U_0 > \frac{3}{4}$ and $\frac{3}{4} < k \le U_0$, and for any $n = 0, 1, 2, \ldots$, there is one solution with $2n$ nodes if $d \ge \mathcal{D}$, two solutions if $d_{2n} < d < \mathcal{D}$ and no solutions if $d < d_{2n}$. Here $d_{2n} = d_{2n}(U_0, k)$ is the minimum value of $x_f(E)$ over all E.

(d) When $U_0 < k \le U_0 + \frac{3}{4}$, and for any $n = 0, 1, 2, \ldots$, there are two solutions with $2n$ nodes if $d > d_{2n}$ and no solutions if $d < d_{2n}$.

We are now in a position to demonstrate that the point of bifurcation at which the second stationary solution appears, is given by $k = \frac{3}{4}$. As k is increased, continuously, through the value of $\frac{3}{4}$, the maximum value of energy accessible to the 'inner particle' jumps from $E_{\max} = U_0 R_0^2$ to $E_{\max} = V_m$. The value $U_0 R_0^2$ does not correspond to a stationary point of the potential $V_{\text{int}}(R)$, while V_m is a value at a point of local maximum. Therefore, the 'time' taken by the particle with energy $E = E_{\max}$ to escape from the point $R = \sqrt{\rho_2}$ and reach the point $R = R_E$, jumps from zero for $k = \frac{3}{4}$ to infinity for $k > \frac{3}{4}$. When k is close to $\frac{3}{4}$, no matter whether it is smaller or greater than $\frac{3}{4}$, the minimum of the function $x_f(E)$ is close to zero. For k approaching $\frac{3}{4}$ from below, this minimum occurs at $E = U_0 R_0^2$, which is the endpoint of the allowed interval of E. For k approaching $\frac{3}{4}$ from above, the minimum is still at $E = U_0 R_0^2$ but this time, this is an internal point and so the minimum is local. Therefore, for any $d > 0$ the curve $x = x_f(E)$ has one intersection by a straight line $x = d$ when $k \to \frac{3}{4}$ from below (or when $k = \frac{3}{4}$) and two intersections when $k = \frac{3}{4} + 0$. This means that for any $d > 0$, eq. (7.3) has one solution when $k \to \frac{3}{4}$, $k \leq \frac{3}{4}$, and two solutions when $k \to \frac{3}{4}$, $k > \frac{3}{4}$. One of the two solutions arising for $k = \frac{3}{4} + 0$ is close to the solution arising for $k = \frac{3}{4} - 0$ and the same value of E (and hence, the same d). The other solution with $k = \frac{3}{4} + 0$ has a different value of E (despite having the same d); here, E belongs to the interval $(U_0 R_0^2, V_m)$. Therefore, the 'arrival' value of $R_{\text{int}}(x)$, $R_E = \sqrt{E/U_0}$, is greater than R_0 for this solution. If an inner solution with $R_E > R_0$ had occurred in the region $k \leq \frac{3}{4}$, we would not have been able to match $R_{\text{int}}(d)$ to $R_{\text{ext}}(d)$ because $R_{\text{ext}}(x)$ is bounded from above by R_0. In the region $k > \frac{3}{4}$, however, the outer solution attains all values from 0 to ∞ and hence can always be matched to $R_{\text{int}}(x)$.

For convenience, the solution with the smaller value of E, i.e. with $0 \leq E \leq U_0 R_0^2$, will be called the 'narrow' solution; this is the solution which continues to exist for $k < 3/4$. The solution with the larger value of E, which only exists for $k > 3/4$, will be called the 'broad' solution. These names are motivated by the fact that $R(d)$ is greater in the case of the broad soliton, as per eq. (7.7).

As k is increased beyond $\frac{3}{4}$, the minimum value of the function $x_f(E)$ grows and, at some $k = k_{sn}$, exceeds d (fig. 7.3). This is the point of a saddle-node bifurcation; the two branches of solution merge at this point and cease to exist for $k > k_{sn}$.

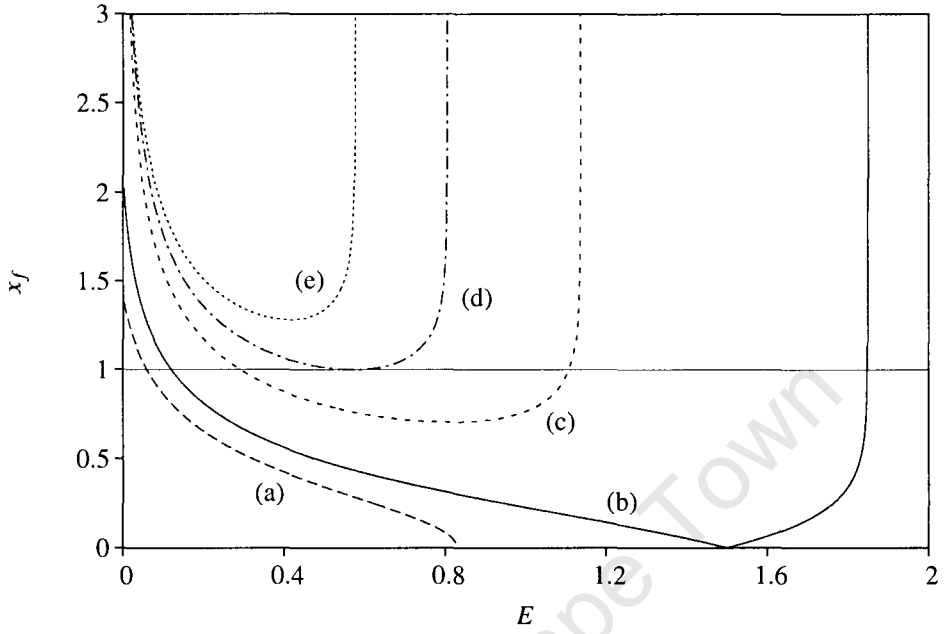

Figure 7.3: The function $x_f(E)$ for different values of k. Here, $U_0 = 1$. (a): $k < \frac{3}{4}$ (in this plot $k = 0.6$); (b): $k = \frac{3}{4} + 0$ (here $k = 0.750001$); (c): $\frac{3}{4} < k < k_{sn}$ (in this plot, $k = 1.1$); (d): $k = k_{sn}$ ($k_{sn} = 1.2743$ for this U_0 and $d = 1$); (e): $k > k_{sn}$ (here $k = 1.4$)

7.4 Stability: The nodeless solutions

Letting $\psi = R(x)e^{ikt} + \delta\psi$, we linearise eq. (7.1) in small $\delta\psi$. Writing $\delta\psi = e^{ikt}[\tilde{u}(x,t) + i\tilde{v}(x,t)]$, with real $\tilde{u}$ and $\tilde{v}$, this gives

$$\tilde{u}_t = \mathcal{L}_0\tilde{v}, \quad -\tilde{v}_t = \mathcal{L}_1\tilde{u}, \tag{7.28}$$

where the linear operators $\mathcal{L}_0$ and $\mathcal{L}_1$ are defined as

$$\mathcal{L}_0 \equiv -\frac{d^2}{dx^2} + k + U(x) - 2R^2 + R^4, \tag{7.29}$$

and

$$\mathcal{L}_1 \equiv -\frac{d^2}{dx^2} + k + U(x) - 6R^2 + 5R^4. \tag{7.30}$$

Assuming a separable solution $\tilde{u}(x,t) = e^{\lambda t}u(x)$, $\tilde{v}(x,t) = e^{\lambda t}v(x)$, eq. (7.28) reduces to an eigenvalue problem

$$\begin{pmatrix} \mathcal{L}_1 & 0 \\ 0 & \mathcal{L}_0 \end{pmatrix} \begin{pmatrix} u \\ v \end{pmatrix} = \lambda \begin{pmatrix} 0 & -1 \\ 1 & 0 \end{pmatrix} \begin{pmatrix} u \\ v \end{pmatrix}. \tag{7.31}$$

The soliton $\psi = e^{ikt}R(x)$ is unstable if there is at least one eigenvalue λ with a positive real part.

7.4.1 General formalism

We start with the case of the bell-shaped solitons, for which $R(x) > 0$ for all $x \in (-\infty, \infty)$. When $k \leq \frac{3}{4}$, there is one such soliton (irrespective of the values of U_0 and d). When $k > \frac{3}{4}$, there are one or two coexisting nodeless solitons depending on U_0 and d. In the region of coexistence, we will be denoting $R_0^{(-)}(x)$ as the soliton that is continuable to $k \leq \frac{3}{4}$. The other nodeless soliton in this region will be denoted $R_0^{(+)}(x)$.

The solution $R(x)$ satisfies $\mathcal{L}_0 R(x) = 0$; since $R(x)$ does not have any zeros, this implies that the operator $\mathcal{L}_0$ does not have negative eigenvalues. The subsequent analysis depends on how many negative eigenvalues the operator $\mathcal{L}_1$ has. The simplest situation arises where $\mathcal{L}_1$ has more than two negative eigenvalues, or no negative eigenvalues at all. We formulate the corresponding conclusions in the form of two short theorems.

Theorem 1. If the minimum eigenvalue of $\mathcal{L}_1$ is positive, then the operator (7.31) does not have real eigenvalues other than zero, and the corresponding soliton solution is stable.

The proof makes use of the invertibility of $\mathcal{L}_1$. Eliminating $u(x)$ from (7.31), we get

$$\mathcal{L}_0 v = -\lambda^2 \mathcal{L}_1^{-1} v. \tag{7.32}$$

The smallest eigenvalue of the generalised eigenvalue problem (7.32), with $\mathcal{L}_0$ symmetric and $\mathcal{L}_1^{-1}$ positive, is given by the minimum of the Rayleigh quotient:

$$-\lambda_0^2 = \min \frac{(y, \mathcal{L}_0 y)}{(y, \mathcal{L}_1^{-1} y)}, \tag{7.33}$$

where $(y,z) \equiv \int_{-\infty}^{\infty} y(x)z(x)dx$. Since $\mathcal{L}_0$ does not have negative eigenvalues, the Rayleigh quotient is obviously nonnegative. Therefore, all generalised eigenvalues $(-\lambda^2)$ satisfy $(-\lambda^2) \geq 0$, i.e. all λ are pure imaginary.

Theorem 2. If $\mathcal{L}_1$ has three or more negative eigenvalues, the stability operator (7.31) has at least one pair of nonzero real eigenvalues, and the corresponding soliton solution is unstable.

Eliminating $v(x)$ from (7.31), we get $\mathcal{L}_0 \mathcal{L}_1 u = -\lambda^2 u$. This equation has a bounded solution if the right-hand side is orthogonal to the zero mode of $\mathcal{L}_0$: $(u, R) = 0$. In this case we can write

$$\mathcal{L}_1 u = -\lambda^2 \mathcal{L}_0^{-1} u. \tag{7.34}$$

To determine whether the radiation is emitted by the soliton or being fed into it from outside sources, we consider a harmonic solution $\psi = e^{i\mathcal{Q}X/\varepsilon - i\Omega t}$ of the linearised eq. (6.21); the corresponding dispersion relation is

$$\Omega(\mathcal{Q}) = -2\cos(k+\mathcal{Q}) + \omega - \mathcal{Q}v.$$

The radiation background Ψ consists of harmonics with $\Omega = 0$ and $\mathcal{Q} = \mathcal{Q}_n$ where $\mathcal{Q}_n$ are roots of eq. (6.18). The group velocities of these harmonic waves are given by

$$\Omega'(\mathcal{Q}_n) = 2\sin(k+\mathcal{Q}_n) - v. \tag{6.60}$$

The $\mathcal{Q}_n$'s are zeros of the function $\Omega(\mathcal{Q})$ and the group velocities are the slopes of this function at its zeros; thus the group velocities $\Omega'(\mathcal{Q}_1)$, $\Omega'(\mathcal{Q}_2)$,..., have alternating signs. The first one, which is the only one that concerns us in this work, must be negative. Indeed, the value

$$\Omega(0) = -2\cos k + \omega = 2\cos k(\cosh\varepsilon - 1)$$

is positive, and hence the slope of the function $\Omega(\mathcal{Q})$ as it crosses the $\mathcal{Q}$ axis at $\mathcal{Q}_1 > 0$ is negative. Therefore, the first radiation mode, extending to $-\infty$, carries energy *away* from the soliton.

The even-numbered radiation modes (where present) in our asymptotic solution (6.59) have positive group velocities and hence describe the flux of energy fed into the system at the left infinity. A more interesting situation is obviously the one with no incoming radiation; the corresponding solution is obtained by subtracting off the required multiple of the solution to the linearised equation, e.g. $e^{i\mathcal{Q}_2 X/\varepsilon}$. One would then have a pulse leaving the odd modes in its wake and sending even modes ahead of it.

If the first Stokes constant $K_1(k)$ has a zero at some $k = k_1$ while $\mathcal{Q}_1$ is the only radiation mode available (as it happens in our saturable model with μ greater than approximately 4), then according to eq. (6.59), the radiation from the soliton with the carrier-wave wavenumber k_1 is suppressed completely. It is fitting to note here that this conclusion is based on calculating Ψ as a solution to a linearised equation (6.22); however, nonlinear corrections become negligible when the radiation disappears (i.e., when $\Psi \to 0$), so there is no loss of accuracy as a result.

6.4 Time evolution of a radiating soliton

6.4.1 Amplitude-wavenumber dynamical system

To find the radiation-induced evolution of the travelling soliton, we use conserved quantities of the advance/delay equation associated with eq. (6.2). In the reference frame moving at the soliton velocity v this equation reads

$$i\varphi_t + \varphi(x+1,t) + \varphi(x-1,t) - iv\varphi_x + \frac{2|\varphi|^2\varphi}{1+\mu|\varphi|^2} = 0. \tag{6.61}$$

The discrete variable $\phi_n(t)$ in eq. (6.2) is related to the value of the continuous variable $\varphi(x,t)$ at the point $x = n - vt$: $\phi_n(t) = \varphi(n-vt,t)$. For future use, we also mention the relation between $\varphi(x,t)$ and the corresponding solution of eq. (6.21):

$$\varphi(x,t) = \psi(X,t)e^{ik(x+vt)+i\omega t}. \tag{6.62}$$

We first consider the norm:

$$N = \int_a^b |\varphi|^2 dx.$$

Multiplying eq. (6.61) by φ^*, subtracting the complex conjugate and integrating yields the rate of change of the integral N:

$$i\frac{dN}{dt} = \int_{a-1}^{a} (\varphi^+\varphi^* - c.c.)dx + \int_b^{b+1} (\varphi^-\varphi^* - c.c.)dx + iv|\varphi|^2\Big|_a^b. \tag{6.63}$$

In eq. (6.63), $\varphi^\pm \equiv \varphi(x\pm 1,t)$ and $c.c.$ stands for the complex conjugate of the immediately preceding term. The integration limits $a < 0$ and $b > 0$ are assumed to be large ($|a|, b \gg \varepsilon^{-1}$) but finite; for example one can take $a, b = \mathcal{O}(\varepsilon^{-2})$.

Consider the soliton moving with a positive velocity and leaving the radiation in its wake. This configuration is described by the solution ψ_s of eq. (6.21); the corresponding solution of eq. (6.61) has the asymptotic behaviour $\varphi_s \to 0$ as $x \to +\infty$. Substituting the leading-order expression (6.23) for the soliton's radiation tail into eq. (6.62) yields the asymptotic behaviour at the other infinity:

$$\varphi_s(x,t) \to \sum_n A_n[1+\mathcal{O}(\varepsilon)]e^{i(k+\mathcal{Q}_n)x+i(\omega+kv)t} \quad \text{as } x \to -\infty. \tag{6.64}$$

Since, as we have explained above, the $\mathcal{Q}_1$ radiation is dominant, it is sufficient to keep only the $n = 1$ term in (6.64).

showed that the $1/n$ term (and, in principle, all other terms in the expansion in powers of $1/n$) are, in fact, known analytically. This convergence-acceleration technique could be useful to other researchers working in the field.

Lastly, in chapter 7 we studied the continuous cubic-quintic nonlinear Schrödinger equation with a square-well potential. We found explicit expressions for two coexisting branches of stationary even solutions, which represent spatial optical solitons in a single waveguide made of a photorefractive material. Therefore, our investigations in chapter 7 apply to a single element of the waveguide array studied in chapter 6. We calculated the stability of these solitons and confirmed that both branches are stable. This brought us to the primary purpose of the chapter, which was to reconcile the Vakhitov–Kolokolov stability criterion with the observation of bistability, which had previously been thought to contradict the theorem [143]. This conundrum had been the main motivation for the investigation; however we also suggested that the model could be extended to include an infinite number of neighbouring square-wells, and thus describe in more detail the waveguide array considered in chapter 6. We pointed out that possibly, the bistability observed in a single waveguide would extend to collective bistability in the array when weakly coupled.

8.2 Summary of results and conclusions

Below, we provide a brief summary of the overall conclusions and significant findings in this thesis.

1. It was shown that the wobbling ϕ^4 kink does not behave chaotically near resonance when the wobbling is small.

2. We have proved that a resonance exists when the ϕ^4 kink is directly driven near its natural frequency, which sustains translational motion of the kink. The relevant amplitude equations are (2.31).

3. It was proved that all exceptional discretisations are derivable from two-point maps.

4. We have confirmed that there is no correlation between the exceptionality of a discrete model and the existence of sliding solitons in that model; however

5. We have established that the amplitude of radiation from moving solitons is significantly reduced in exceptional models (refer to fig. 3.5).

6. Sliding solitons were shown to exist both in discrete equations whose nonlinearities are nonlocal and also in models with locally discretised nonlinearities.

7. Three classes of exceptional ϕ^4 models were identified, namely equations (4.19), (4.21) and (4.27) with (4.2) and (4.17), of which the previously known models are particular members.

8. It was demonstrated that the exceptional model of Speight and Ward has one sliding velocity, while that of Kevrekidis has three. The Bender–Tovbis model was shown to have no sliding velocities, despite being exceptional, as was the standard, nonexceptional, one-site discretisation. (See fig. 3.3.)

9. The Frenkel–Kontorova model was shown to admit no sliding kinks near to the continuum limit (see fig. 5.1).

10. We have demonstrated that the discrete nonlinear Schrödinger equation admits sliding solitons provided that the nonlinearity saturates at a low enough intensity (fig. 6.4).

11. These sliding solitons were shown to be metastable.

12. It was shown that sliding pulses in the DNLS equation are pinned to the lattice before they have decayed, and that the decay may be interrupted by a period of metastable motion at one or more sliding velocities.

13. It was proved that radiation from moving solitons in the discrete equations studied is exponentially small, and therefore that the moving solitons will be indistinguishable from lossless travelling solitons sufficiently near to the continuum limit.

14. We have shown that the expression for the radiation tails of the DNLS pulses is given by eq. (6.59), where K_1 is graphed in fig. 6.4 as a function of velocity.

15. We have proved that the stability of both branches of solitons in the cubic-quintic nonlinear Schrödinger equation with a square-well potential does not contradict the Vakhitov–Kolokolov stability theorem.

16. We have found stationary, spatially-symmetric solitons of this equation; they are given explicitly by equations (7.9) and (7.21) subject to (7.22).

8.3 Open issues and speculations for future investigation

Our search for travelling waves in chapters 3, 5 and 6 was based on perturbation expansions about the continuum limit. This is one of the few avenues along which the problem can be approached analytically; for example, the anti-continuum limit, used to find intrinsic localised modes, does not work for moving pulses. An obvious aim, then, is to extend this work beyond the vicinity of the continuum limit. For instance, it would be interesting to continue sliding solitons numerically into the highly discrete regime, where radiation is significant and hence their importance would be greatest.

One can reasonably expect our measurements of the *leading-order* radiation amplitudes to hold whenever the radiation is small, even if this is not particularly close to the continuum limit, since the calculation of Stokes constants via recurrence relations involves a very large number of terms in the perturbation expansion. Of course, the leading-order expression alone is inaccurate if one is far from the continuum limit. However, the effect of higher-order terms in the Stokes constant should generically be to shift its zeros rather than to destroy them (since they are single and not double roots), and hence would not affect our conclusions on the existence or otherwise of sliding kinks, but merely the accuracy of the calculation of their sliding velocities. Again it would be useful to find out, numerically, how far from the continuum limit our results remain valid, and how accurate or otherwise they are. Such a numerical investigation has been carried out for the continuum ϕ^4 breather by Boyd [221].

We conclude with some rather more speculative suggestions for future investigations of travelling discrete solitons.

The work of Melvin, Champneys, Kevrekidis and Cuevas [209] gives a tantalising glimpse of the structure underlying the dependence of the kink's sliding velocities on the other parameters. As mentioned in section 6.6.2, these authors show that there is a relationship between the parameter values which yield sliding solitons and those for which zero eigenvalues of the stationary solitons occur. Although a zero of the first Stokes constant is a necessary condition for both sliding solitons and translation-invariant stationary solutions to exist, this observation does not provide an explanation for the connection between them, since the calculation of Stokes constants is totally different in the stationary and moving cases (see chapter 3). If a unified explanation can be found for sliding and translationally invariant kinks, it may well help in achieving the ultimate objective of finding an analytical expression which expresses the sliding velocities in terms of the other parameters.

In pursuit of this goal, another possible line of inquiry is a study of the moving solitons in the FPU equation, to try to find out why an analytical proof has been achieved for this lattice [76] but not for lattices with an on-site potential. In the continuum limit, there is an important difference between the two: The FPU model reduces to the KdV equation for which there is a fixed amplitude-velocity relationship, whereas for models such as the discrete ϕ^4, there is no such constraint in the continuum limit. It could be enlightening to understand how this difference extends to the discrete case – in particular, to find out whether FPU solitons emit exponentially small radiation when not travelling at their prescribed velocities. From the point of view of the dispersion relations for discrete equations [see e.g. fig. 1.1(b)], it would appear that FPU solitary waves are embedded solitons. If so, one would expect them to be semistable. However, if they are in fact stable, it could be illuminating to find out how this comes about.

Keener has used an averaging method to detect exponentially small effects in the equation for wave speed as a function of lattice spacing in discrete reaction-diffusion equations [121, 222]. One could try to apply the same method to energy-conserving models in order to obtain an approximate analytical expression relating the sliding velocities to the other parameters.

Finally, the inverse method of Flach, Zolotaryuk and Kladko [119] could provide an invaluable analytical tool in the quest to better understand sliding solitons. The fact that the exact solution is known could help one to investigate its properties with a view to understanding sliding solitons better. One could perform perturbation expansions from the known solution in a parameter regime far away from the continuum limit, for example. The insights gained could then potentially be applied to systems which are commonly used in physics.

In summary, there is a great deal still to be understood about the stubborn problem of travelling solitons in lattices. The aim of this section has been to suggest some fruitful angles of attack. The principal objective of researchers in the field of lattice equations remains to find highly localised travelling structures [111] – discrete counterparts of the intrinsic localised modes described in section 1.5. Hopefully the sliding solitons discovered in this thesis, although only investigated near the continuum limit, will prove to be a useful contribution to this cause.

Bibliography

[1] J. Scott Russell, *Report on waves*, Report of the 14th Meeting of the British Association for the Advancement of Science (John Murray, London, 1844) pp. 311–390.

[2] J. Boussinesq, C. R. Acad. Sci. Paris, **72**, 755 (1871) or J. Boussinesq, J. Math. Pures Appl. (ser. 2), **17**, 55 (1872).

[3] Lord Rayleigh, Phil. Mag. (5), **1**, 257 (1876).

[4] D. J. Korteweg and H. de Vries, Phil. Mag. **39**, 422 (1895).

[5] E. Fermi, J. R. Pasta, and S. M. Ulam, Los Alamos Sci. Lab. Rep., LA-1940 (1955).

[6] N. Zabusky and M. Kruskal, Phys. Rev. Lett. **15**, 240 (1965).

[7] R. K. Dodd, J. C. Eilbeck, J. D. Gibbon, and H. C. Morris, *Solitons and Nonlinear Wave Equations* (Academic Press, London, 1984).

[8] M. Remoissenet, *Waves Called Solitons* (Springer-Verlag, Berlin, 1996).

[9] A. Scott, *Nonlinear Science: Emergence and Dynamics of Coherent Structures* (Oxford University Press, 1999).

[10] C. S. Gardner, J. M. Greene, M. D. Kruskal, and R. M. Miura, Phys. Rev. Lett. **19**, 1095 (1967).

[11] P. D. Lax, Commun. Pure Appl. Math. **21**, 467 (1968).

[12] V. E. Zakharov and A. B. Shabat, Sov. Phys. JETP **34**, 62 (1972).

[13] M. J. Ablowitz, D. J. Kaup, A. C. Newell, and H. Segur, Phys. Rev. Lett. **30**, 1262 (1973).

[14] A. Seeger, H. Donth, A. Kochendörfer, Z. Phys. **134**, 173 (1953).

[15] J. K. Perring and T. H. R. Skyrme, Nucl. Phys. **31**, 550 (1962).

[16] R. M. Miura, C. S. Gardner, and M. D. Kruskal, J. Math. Phys. **9**, 1204 (1968).

[17] M. Toda, J. Phys. Soc. Jpn. **22**, 432 (1967).

[18] M. Toda, J. Phys. Soc. Jpn. **23**, 501 (1967).

[19] H. Flaschka, Prog. Theor. Phys. **51**, 703 (1974).

[20] R. Hirota and J. Satsuma, Prog. Theor. Phys. Suppl. **59**, 64 (1976).

[21] X.-B. Hu, P. A. Clarkson, and R. Bullough, J. Phys. A: Math. Gen. **30**, L669 (1997).

[22] A. V. Bäcklund, Math. Ann. **19**, 387 (1882).

[23] M. J. Ablowitz and J. F. Ladik, Stud. Appl. Math. **55**, 213 (1976); J. Math. Phys. **17**, 10011 (1976).

[24] A. Hasegawa and F. Tappert, Appl. Phys. Lett. **23**, 142 (1973).

[25] D. J. Benney and A. C. Newell, J. Math. Phys. **46**, 133 (1967).

[26] Y. H. Ichikawa, T. Imamura, and T. Taniuti, J. Phys. Soc. Jpn. **34**, 189 (1972).

[27] B. D. Fried and Y. H. Ichikawa, J. Phys. Soc. Jpn. **34**, 1073 (1973).

[28] F. Tappert and C. M. Varma, Phys. Rev. Lett. **25**, 1108 (1970).

[29] P. L. Kelly, Phys. Rev. Lett. **15**, 1005 (1965).

[30] V. I. Talanov, JETP Lett. **2**, 138 (1965).

[31] H. Y. Zhang, P. Kabos, H. Xia, R. A. Staudinger, P. A. Kolodin, and C. E. Patton, J. Appl. Phys. **84**, 3776 (1998).

[32] H. Washimi and T. Taniuti, Phys. Rev. Lett. **17**, 399 (1966).

[33] L. van Wijngaarden, J. Fluid Mech. **33**, 465 (1968).

[34] S. Leibovich, J. Fluid Mech. **42**, 803 (1970).

[35] Y. Hashizume, J. Phys. Soc. Jpn. **54**, 3305 (1985); J. Phys. Soc. Jpn. **57**, 4160 (1988).

[36] S. Yomosa, J. Phys. Soc. Jpn. **56**, 506 (1987).

[37] J. F. Paquerot and M. Remoissenet, Phys. Lett. A **194**, 77 (1994).

[38] A. Ludu and J. P. Draayer, Phys. Rev. Lett. **80**, 2125 (1998).

[39] J. Frenkel and T. Kontorova, J. Phys. (USSR) **1**, 137 (1939).

[40] W. Döring, Z. Naturforsch. **31**, 373 (1948).

[41] A. C. Scott and W. J. Johnson, Appl. Phys. Lett. **14**, 316 (1969).

[42] J. L. Fergason and G. H. Brown, J. Am. Oil Chem. Soc. **45**, 120 (1968).

[43] G. L. Lamb, Phys. Lett. A **25**, 181 (1967).

[44] R. Hirota and K. Suzuki, Proc. IEEE **61**, 1483 (1973).

[45] M. Peyrard and M. Remoissenet, Phys. Rev. B **26**, 2886 (1982).

[46] Yu. S. Kivshar and B. A. Malomed, Rev. Mod. Phys. **61**, 763 (1989).

[47] M. J. Rice, Phys. Lett. A **71**, 152 (1979).

[48] W. P. Su, J. R. Schreiffer, and A. J. Heeger, Phys. Rev. Lett. **42**, 1698 (1979).

[49] A. R. Bishop and T. Schneider (eds), *Solitons and condensed matter physics* (Springer-Verlag, Berlin, 1978).

[50] R. Rajaraman, *Solitons and Instantons* (North-Holland, Amsterdam, 1982).

[51] S. V. Manakov, S. Novikov, L. P. Pitaevskii, and V. E. Zakharov, *Theory of Solitons: The Inverse Scattering Method* (Consultants Bureau, New York and London, 1984).

[52] H. Segur and M. D. Kruskal, Phys. Rev. Lett. **58**, 747 (1987).

[53] N. N. Akhmediev and A. Ankiewicz, *Solitons: Nonlinear pulses and beams* (Chapman & Hall, London, 1997).

[54] J. Bang, B. A. Malomed, and D. J. Kaup, Phys. Rev. Lett. **83**, 1958 (1999).

[55] J. Fujioka, A. Espinosa-Cerón, and R. F. Rodríguez, Rev. Mex. Fís. **52**, 6 (2006).

[56] J. M. Burgers, Adv. Appl. Mech. **1**, 171 (1948).

[57] A. L. Hodgkin and A. F. Huxley, J. Phisiol. **117**, 500 (1952).

[58] J. Nagumo, S. Arimoto, and S. Yoshizawa, Proc. IRE **50**, 2061 (1962).

[59] A. N. Zaikin and A. M. Zhabotinsky, Nature **225**, 535 (1970).

[60] A. F. Parker-Rhodes, Trans. Br. Mycol. Soc. **38**, 59 (1955).

[61] A. T. Winfree, Science **175**, 634 (1972).

[62] W. Jahnke, C. Henze, and A. T. Winfree, Nature **336**, 662 (1988).

[63] A. T. Winfree, *When Time Breaks Down: The Three-Dimensional Dynamics of Electrochemical Waves and Cardiac Arrhythmias* (Princeton University Press, 1987).

[64] A. Turing, Phil. Trans. R. Soc. (London) B **237**, 37 (1952).

[65] V. E. Zakharov, J. Appl. Mech. Tech. Phys. **9**, 86 (1968).

[66] L. A. Ostrovskii, Zh. Tek. Fiz. **33**, 905 (1963).

[67] R. Y. Chiao, E. Garmire, and C. H. Townes, Phys. Rev. Lett. **13**, 479 (1964).

[68] Yu. S. Kivshar and G. P. Agrawal, *Optical Solitons* (Academic Press, Amsterdam, 2003).

[69] W. Królikowski, B. Luther-Davies, and C. Denz, IEEE J. Quant. Elec. **39**, 3 (2003).

[70] D. N. Christodoulides and M. I. Carvalho, J. Opt. Soc. Am. B **12**, 1628 (1995).

[71] S. K. Turitsyn, E. G. Shapiro, S. B. Medvedev, M. P. Fedoruk, and V. K. Mezentsev, C. R. Physique **4**, 145 (2003).

[72] J. D. Ania-Castañón, T. J. Ellingham, R. Ibbotson, X. Chen, L. Zhang, and S K Turitsyn, Phys. Rev. Lett. **96**, 023902 (2006).

[73] A. Hasegawa and F. Tappert, Appl. Phys. Lett. **23**, 171 (1973).

[74] D. R. Andersen, D. E. Hooton, G. A. Swartzlander Jr., and A. E. Kaplan, Opt. Lett. **15**, 783 (1990).

[75] J. C. Eilbeck and R. Flesch, Phys. Lett. A **149**, 200 (1990).

[76] G. Friesecke and J. A. D. Wattis, Commun. Math. Phys. **161**, 391 (1994).

[77] J. Scott Russell, *The Wave of Translation in the Oceans of Water, Air and Ether* (London, 1885).

[78] J. Frenkel and T. Kontorova, J. Phys. **1**, 137 (1939).

[79] T. Holstein, Ann. Phys. (NY) **8**, 325 (1959).

[80] L. Landau, Phys. Z. Sowietunion **3**, 664 (1933).

[81] D. K. Campbell, S. Flach, and Yu. S. Kivshar, Phys. Today **57**(1), 43 (2004).

[82] A. S. Dolgov, Sov. Phys. Solid State **28**, 907 (1986).

[83] A. J. Sievers and S. Takeno, Phys. Rev. Lett. **61**, 970 (1988).

[84] J. B. Page, Phys. Rev. B **41**, 7835 (1990).

[85] S. Flach and C. R. Willis, Phys. Lett. A **181**, 232 (1993).

[86] S. Flach and C. R. Willis, Phys. Rev. E **50**, 3134 (1994).

[87] S. Flach and C. R. Willis, Phys. Rep. **295**, 181 (1998).

[88] A. S. Davydov and N. I. Kislukha, Phys. Stat. Sol. **B59**, 465 (1973).

[89] A. C. Scott, Phys. Rep. **217**, 1 (1992).

[90] H. Feddersen, Phys. Lett. A **154**, 391 (1991).

[91] S. F. Mingaleev, Y. B. Gaididei, P. L. Christiansen and Yu. S. Kivshar, Europhys. Lett. **59**, 403 (2002).

[92] L. V. Yakusevich, *Nonlinear Physics of DNA* (John Wiley, Chichester, 1998).

[93] A. C. Scott, *Neuroscience: A Mathematical Primer* (Springer-Verlag, New York, 2002).

[94] M. G. Verlade, V. I. Nekorkin, V. B. Kazantsev, and J. Ross, Proc. Natl. Acad. Sci. (USA) **94**, 5024 (1997).

[95] D. N. Christodoulides and R. I. Joseph, Opt. Lett. **13**, 794 (1988).

[96] H. S. Eisenberg, Y. Silberberg, R. Morandotti, A. R. Boyd, and J. S. Aitchison, Phys. Rev. Lett. **81**, 3383 (1998).

[97] R. Morandotti, U. Peschel, J. S. Aitchison, H. S. Eisenberg and Y. Silberberg, Phys. Rev. Lett. **83**, 2726 (1999); Phys. Rev. Lett. **83**, 4756 (1999).

[98] Yu. S. Kivshar and B. Luther-Davies, Phys. Rep. **298**, 81 (1998).

[99] A. A. Sukhorukov and Yu. S. Kivshar, J. Opt. Soc. Am. B **19**, 772 (2002).

[100] D. Mandelik, H. S. Eisenberg, Y. Silberberg, R. Morandotti, and J. S. Aitchison, Proc. Nonlinear Guided Waves and Their Applications (Optical Society of America, Washington DC, 2002).

[101] N. K. Efremidis, S. Sears, D. N. Christodoulides, J. W. Fleischer, and M. Segev, Phys. Rev. E **66**, 046602 (2002).

[102] J. W. Fleischer, T. Carmon, M. Segev, N. K. Efremidis, and D. N. Christodoulides, Phys. Rev. Lett. **90**, 023902 (2003).

[103] D. N. Chrisodoulides and E. D. Eugenieva, Phys. Rev. Lett. **87**, 233901 (2001); Opt. Lett. **26**, 1876 (2001); Opt. Lett. **27**, 369 (2002).

[104] E. D. Eugenieva, N. K. Efremidis, and D. N. Christodoulides, Opt. Photon. News **12**(12), 57 (2001).

[105] D. N. Christodoulides, F. Lederer, and Y. Silberberg, Nature **424**, 817 (2003).

[106] A. Trombettoni and A. Smerzi, Phys. Rev. Lett. **86**, 2353 (2001).

[107] F. Kh. Abdullaev, B. B. Baizakov, S. A. Darmanyan, V. V. Konotop, and M. Salerno, Phys. Rev. A **64**, 043606 (2001).

[108] D. E. Pelinovsky, A. A. Sukhorukov, and Yu. S. Kivshar, Phys. Rev. E **70**, 036618 (2004).

[109] M. Peyrard and M. D. Kruskal, Physica D **14**, 88 (1984).

[110] J. P. Hirth and J. Lothe, *Theory of Dislocations* (Wiley, New York, 1982).

[111] Ch. Claude, Yu. S. Kivshar, O. Kluth, and K. H. Spatschek, Phys. Rev. B **47**, 228 (1993).

[112] M. J. Ablowitz, Z. H. Musslimani, and G. Biondini, Phys. Rev. E **65**, 026602 (2002).

[113] D. B. Duncan, J. C. Eilbeck, H. Feddersen, and J. A. D. Wattis, Physica D **68**, 1 (1993).

[114] S. Flach and K. Kladko, Physica D **127**, 61 (1999).

[115] J. M. Speight and R. S. Ward, Nonlinearity **7**, 475 (1994).

[116] J. M. Speight, Nonlinearity **10**, 1615 (1997).

[117] J. M. Speight, Nonlinearity **12**, 1373 (1999).

[118] P. G. Kevrekidis and M. I. Weinstein, Physica D **142**, 113 (2000).

[119] S. Flach, Y. Zolotaryuk, and K. Kladko, Phys. Rev. E **59**, 6105 (1999).

[120] A. A. Sukhorukov, Phys. Rev. Lett. **96**, 113902 (2006).

[121] J. P. Keener, SIAM J. Appl. Math. **61**, 317 (2000).

[122] D. Hennig and G. P. Tsironis Phys. Rep. **307**, 333 (1999).

[123] J. C. Eilbeck and M. Johansson, "The Discrete Nonlinear Schrödinger Equation – 20 Years on", in *Localization and Energy Transfer in Nonlinear Systems. Proceedings of the Third Conference, San Lorenzo de El Escorial, Spain 17 – 21 June 2002,* eds. L. Vazquez, R. S. MacKay, and M. P. Zorzano (World Scientific, Singapore, 2003), pp. 44–67.

[124] P. G. Kevrekidis, K. Ø. Rasmussen, and A. R. Bishop, Int. J. Mod. Phys. B **15**, 2833 (2001).

[125] Yu. S. Kivshar and B. A. Malomed, Rev. Mod. Phys. **61**, 763 (1989).

[126] H. Segur, J. Math. Phys. **24**, 1439 (1983).

[127] N. Quintero, A. Sánchez, and F. Mertens, Phys. Rev. Lett. **84**, 871 (2000).

[128] N. Quintero, A. Sánchez, and F. Mertens, Phys. Rev. E. **62**, 5695 (2000).

[129] N. Quintero, A. Sánchez, and F. Mertens, Phys. Rev. E. **64**, 046601 (2001).

[130] S. Flach and C. R. Willis, Phys. Rev. Lett. **72**, 1777 (1994).

[131] P. G. Kevrekidis, Physica D **183**, 68 (2003).

[132] C. M. Bender and A. Tovbis, J. Math. Phys. **38**, 3700 (1997).

[133] Y. Pomeau, A. Ramani, and B. Grammaticos, Physica D **31**, 127 (1988).

[134] R. H. J. Grimshaw and N. Joshi, SIAM J. Appl. Math. **55**, 124 (1995).

[135] R. H. J. Grimshaw, Stud. Appl. Math. **94**, 257 (1995).

[136] A. Tovbis and D. Pelinovsky, Nonlinearity **19**, 2277 (2006).

[137] A. Tovbis, M. Tsuchiya, and C. Jaffé, Chaos **8**, 665 (1998).

[138] A. Tovbis, Contemporary Mathematics **255**, 199 (2000).

[139] A. Tovbis, Stud. Appl. Math. **104**, 353 (2000).

[140] L. Hadžievski, A. Maluckov, M. Stepić, and D. Kip, Phys. Rev. Lett. **93**, 033901 (2004).

[141] R. A. Vicencio and M. Johansson, Phys. Rev. E **73**, 046602 (2006).

[142] F. Chen, C. E. Rüter, D. Runde, D. Kip, V. Shandarov, O. Manela, and M. Segev, Opt. Exp. **13**, 4314 (2005).

[143] B. V. Gisin, R. Driben, and B. A. Malomed, J. Opt. B: Quantum Semiclass. Opt. **6**, S259 (2004).

[144] N. G. Vakhitov and A. A. Kolokolov, Radiophys. Quantum Electron. **16**, 783 (1973).

[145] N. Flytzanis, S. Crowley, and V. Celli, Phys. Rev. Lett. **39**, 891 (1977).

[146] F. Axel and S. Aubry, J. Phys. C **14**, 5433 (1981).

[147] R. A. Cowley, J. D. Axe, and M. Iizumi, Phys. Rev. Lett. **36**, 806 (1976).

[148] J. A. Krumhansl and J. R. Schrieffer, Phys. Rev. B **11**, 3535 (1975).

[149] A. R. Bishop and T. F. Lewis, J. Phys. C **12**, 3811 (1979).

[150] H. J. Mikeska, J. Phys. C **11**, L29 (1978).

[151] M. J. Rice, A. R. Bishiop, J. A. Krumhansl, and S. E. Trullinger, Phys. Rev. Lett. **36**, 432 (1976).

[152] St. Pnevmatikos, Phys. Lett. A **122**, 249 (1987).

[153] A. Gordon, Physica B **150**, 319 (1988).

[154] M. J. Rice and E. J. Mele, Solid State Comm. **35**, 487 (1980).

[155] D. K. Campbell, J. F. Schonfeld, and C. A. Wingate, Physica D **9**, 1 (1983).

[156] N. R. Quintero, A. Sánchez, and F. G. Mertens, Phys. Rev. E **62**, R60 (2000).

[157] M. Peyrard and D. K. Campbell, Physica D **9**, 33 (1983).

[158] Yu. S. Kivshar, F. Zhang, and L. Vázquez, Phys. Rev. Lett. **67**, 1177 (1991).

[159] Z. Fei, V. V. Konotop, M. Peyrard, and L. Vázquez, Phys. Rev. E **48**, 548 (1993).

[160] P. Prelovšek and I. Sega, J. Phys. C **14**, 5609 (1981).

[161] J. A. Combs and S. Yip, Phys. Rev. B **28**, 6873 (1983).

[162] S. Aubry, J. Chem. Phys. **62**, 3217 (1975).

[163] P. Bak, Rep. Prog. Phys. **45**, 587 (1982).

[164] O. M. Braun, Yu. S. Kivshar, Phys. Rep. **306**, 1 (1998).

[165] Yu. S. Kivshar, A. Sánchez and L. Vázquez, Phys. Rev. A **45**, 1207 (1992).

[166] S. Flach and C. R. Willis, Phys. Rev. E **47**, 4447 (1993).

[167] S. Flach and K. Kladko, Phys. Rev. E **54**, 2912 (1996).

[168] P. Maniadis, G. P. Tsironis, A. R. Bishop, and A. V. Zolotaryuk, Phys. Rev. E **60**, 7618 (1999).

[169] P. G. Kevrekidis, M. I. Weinstein, Physica D **142**, 113 (2000).

[170] A. B. Adib, C. A. S. Almeida, Phys. Rev. E **64**, 037701 (2001).

[171] V. F. Lazutkin, Funct. Anal. Appl. **22**, 154 (1988).

[172] J. A. Sepulchre, "Energy Barriers in Coupled Oscillators: From Discrete Kinks to Discrete Breathers", in *Localization and Energy Transfer in Nonlinear Systems. Proceedings of the Third Conference, San Lorenzo de El Escorial, Spain 17 – 21 June 2002,* eds. L. Vazquez, R. S. MacKay, and M. P. Zorzano (World Scientific, Singapore, 2003), pp. 102–129.

[173] G. Iooss and G. James, Chaos **15**, 015113 (2005).

[174] B. M. Herbst and M. J. Ablowitz, J. Comput. Phys. **105**, 122 (1993).

[175] S. V. Dmitriev, P. G. Kevrekidis, and N. Yoshikawa, arXiv:nlin.PS/0506002 (2005).

[176] S. V. Dmitriev, P. G. Kevrekidis, and N. Yoshikawa, J. Phys. A: Math. Gen. **38**, 7617 (2005).

[177] M. D. Kruskal and H. Segur, Stud. Appl. Math. **85**, 129 (1991).

[178] M. J. Ablowitz and Z. H. Musslimani, Physica D **184**, 276 (2003).

[179] J. M. Speight and Y. Zolotaryuk, Nonlinearity **19**, 1365 (2006).

[180] O. M. Braun and Yu. S. Kivshar, *The Frenkel–Kontorova model. Concepts, Methods and Applications* (Springer-Verlag, Berlin, 2004).

[181] H. S. J. van der Zant, M. Barahona, A. E. Dewell, E. Trías, T. P. Orlando, S. Watanabe, and S. Strogatz, Physica D **119**, 219 (1998).

[182] F. Fillaux, C. J. Carlile, and G. J. Kearly, Phys. Rev. B **44**, 12280 (1991).

[183] F. Fillaux, C. J. Carlile, G. J. Kearly, and M. Prager, Physica B **202**, 302 (1994).

[184] S. W. Englander, N. R. Kallenbach, A. J. Heeger, J. A. Krumhansl, and A. Litwin, Proc. Natl. Acad. Sci. USA **77**, 7222 (1980).

[185] A. A. Aigner, A. R. Champneys, and V. M. Rothos, Physica D **186**, 148 (2003).

[186] J. C. Eilbeck, "Numerical Simulations of the Dynamics of Polypeptide Chains and Proteins", in *Computer Analysis for Life Science – Progress and Challenges in Biological and Synthetic Polymer Research*, eds. C. Kawabata and A. R. Bishop (Ohmsha, Tokyo, 1986), pp. 12-21.

The smallest eigenvalue of the problem (7.34) is given by

$$-\lambda_0^2 = \min_{(y,R)=0} \frac{(y,\mathcal{L}_1 y)}{(y,\mathcal{L}_0^{-1} y)}, \tag{7.35}$$

where the minimum is evaluated over the subspace defined by the constraint $(y,R)=0$. Now let $\mu_0 < \mu_1 < \mu_2 < \ldots < 0$ be the negative eigenvalues of the operator $\mathcal{L}_1$, and let $y_n(x)$ denote the associated eigenfunctions: $\mathcal{L}_1 y_n = \mu_n y_n$. The eigenfunctions $y_0(x)$ and $y_2(x)$ are obviously even, while $y_1(x)$ is odd. A linear combination $y = C_0 y_0(x) + C_2 y_2(x)$, with coefficients chosen to satisfy $(y,R)=0$, will make the Rayleigh quotient (7.35) negative. Therefore, $-\lambda_0^2 < 0$ and eq. (7.31) has at least one pair of real eigenvalues, $\pm|\lambda_0|$.

Finally, assume that $\mathcal{L}_1$ has one or two negative eigenvalues. This is the case where Vakhitov and Kolokolov's argument [144] is applicable; it shows that the smallest generalised eigenvalue $-\lambda_0^2$ of (7.34) is positive (and hence the solution is stable) if $dQ/dk > 0$, where $Q = \int_{-\infty}^{\infty} R^2(x)dx$. This conclusion does not depend on whether $\mathcal{L}_1$ has one or two negative eigenvalues as the eigenfunction $y_1(x)$ associated with the second smallest eigenvalue μ_1 ($\mu_0 < \mu_1 < 0$), is odd. Consequently, it does not appear in the expansion of $R(x)$ over eigenfunctions of $\mathcal{L}_1$ which forms the basis of Vakhitov and Kolokolov's argument [144].

Thus, the stability diagnosis for the nodeless solitons hinges on the number of negative eigenvalues of the operator $\mathcal{L}_1$.

7.4.2 Numerical results

The eigenvalues of $\mathcal{L}_1$ were calculated numerically by using the Fourier method [220] with 256 modes to solve for λ in (7.31). In fig. 7.4, the smallest and third smallest eigenvalues are plotted as functions of k for various values of U and d. For these values of U and d we see that $\mathcal{L}_1$'s first and third eigenvalues are negative and positive respectively for the narrow branch, while for the broad branch there are no negative eigenvalues. The same was observed for every other combination of values of U and d which was tried. As discussed in section 7.4.1, this means that for the broad branch, we can immediately infer stability, while for the narrow branch we need to invoke the Vakhitov–Kolokolov stability criterion [144]. That is, we need to check whether $dQ/dk > 0$. This calculation has been done numerically in [143], and will not be repeated here. It was found that for the branch of narrow solitons (those which continue to $k < 3/4$), dQ/dk is positive, and hence the solitons are stable.

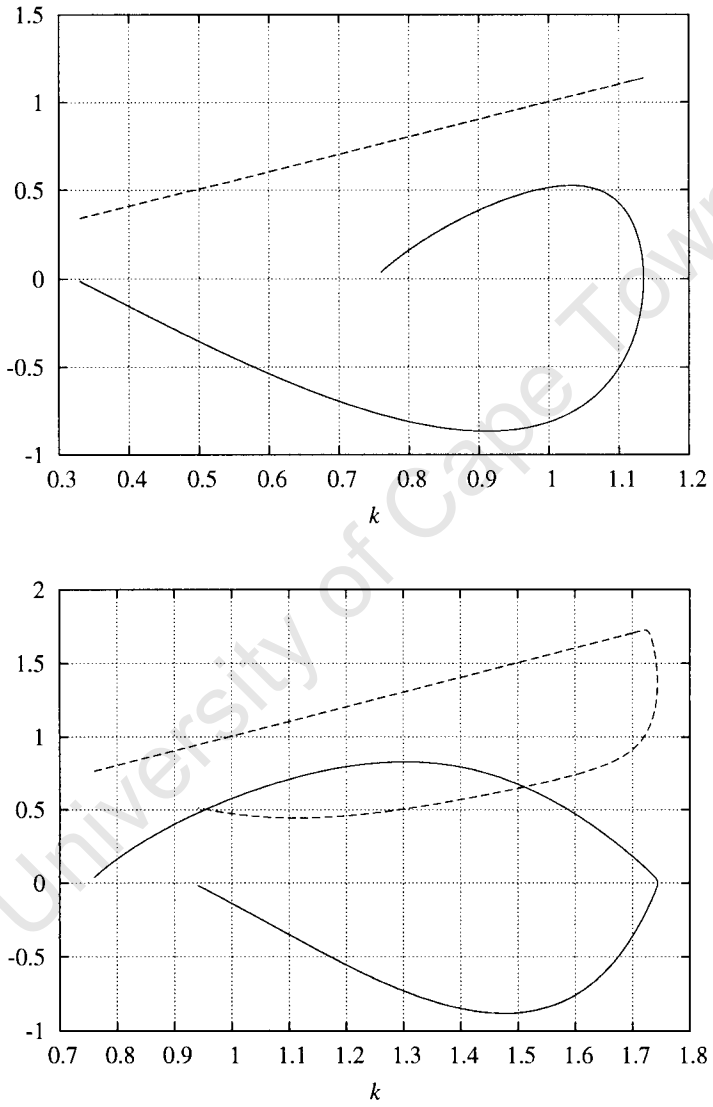

Figure 7.4: The smallest (solid) and third smallest (dashed) eigenvalues of $\mathcal{L}_1$. Top figure: $U = 0.8, d = 1.0$. Bottom figure: $U = 1, d = 5$.

7.5 Concluding remarks

In this chapter, we have found explicit stationary even solutions [(7.9), (7.21)] of eq. (7.1) with the potential well (7.2). We have shown that two branches of nodeless solutions coexist when $k \geq 3/4$. We have also studied the stability of these bell-shaped solutions and shown numerically that both branches are stable. These results are in agreement with the results presented in [143], which were obtained by direct numerical simulations of the original PDE.

On an intuitive level this bistability is not surprising, since we are studying *spatial* solitons which are self-localised even in the absence of a waveguide. Adding the potential well introduces an additional localising effect, so it is not surprising to find two families coexisting.

In [143] it is pointed out that the fact that all the nodeless solitons are stable appears to contradict the Vakhitov–Kolokolov (VK) stability criterion [144]. We have shown that this is not the case, since the VK criterion is not applicable to the broad branch of solitons (those with higher E). In order to hold, the criterion assumes exactly one negative eigenvalue of the operator $\mathcal{L}_1$ of section 7.4 in the eigenfunction-expansion of the soliton profile $R(x)$. This condition is always satisfied in a translation-invariant equation, since $R'(x)$ is then the eigenfunction corresponding to eigenvalue 0. However, when $U \neq 0$, (7.1) loses this property. Indeed, we have found that for all bell-shaped solitons, the branch of broad solitons has *no* negative eigenvalues whereas the narrow branch has exactly one negative eigenvalue (see fig. 7.4). The VK criterion is therefore applicable only in the latter case, where it correctly predicts stability. In the former case, on the other hand, we have shown that there is no call for the VK criterion at all: One can immediately infer stability from the fact that there are no negative eigenvalues.

An open question is the stability of solitons which *do* cross the x axis. In the simplest case—that of solutions with two nodes—we now mention briefly some preliminary numerical findings. These solutions fall into two classes: One which is monotonic in the external region, and thus the minima and maxima occur within the region $|x| < d$ (and are therefore symmetric), and the other in which the turning points only occur at $|x| > d$. The latter class can only occur if the external solution can be nonmonotonic, i.e. for $k < 3/4$, and appears to be always unstable. However, the solutions which are monotonic in the external region seem to be very often stable. Indeed, the broad branch appears to be always stable, while the narrow branch is stable for certain parameter values and unstable for others.

Another avenue for further work would be to obtain the odd stationary solitons of (7.1) and classify their stability; the fact that even solutions with *two* nodes can be stable provides some

hope for the unusual occurrence of odd, stable solitons.

In this chapter we have considered a single waveguide in isolation, in contrast to the waveguide array studied in chapter 6. This has allowed us to investigate in detail how light behaves in a single waveguide. It would be interesting to know how these results—the presence of bistability, in particular—would translate to a waveguide array, where it can still be reasonably expected to occur if the waveguides are weakly coupled (so that their collective behaviour shares features of their behaviour in isolation). A starting point would be to investigate whether bistability can occur in the discrete NLS equation with cubic-quintic nonlinearity. Conclusions would probably be similar to those for the saturable nonlinearity. In that case, we have found no evidence for bistability in chapter 6. However, it might only be manifest in the highly discrete limit. In any case, if no bistability is found in the discrete equation, one could investigate a more detailed model, such as (7.1) with a periodic sequence of square potential wells. Such a study would be a natural extension of this work.

Chapter 8

Conclusion

8.1 Summary and discussion

To begin with, in chapter 2 we dealt with kinks in the continuous ϕ^4 equation. Our motivation was to clarify previous results [127, 128, 129] obtained using a variational method which does not take account of radiation from the kink. We constructed a perturbation expansion for small-amplitude width-oscillations of the kink, and derived differential equations for the slowly-varying oscillation amplitude and kink velocity. This procedure was repeated with the addition of parametric and direct driving as well as damping. In each case, two different driving frequencies (which were already known to be the main resonances) were analysed. The predictions of these 'amplitude equations' were found to agree well with numerical simulations of the original partial differential equation. We confirmed that parametric driving at the natural wobbling frequency acts more strongly on the kink than at twice the natural frequency, and provided a qualitative explanation for this 'anomalous' resonance. We also showed for the first time that there is a resonance at the natural frequency in the case of direct driving. This resonance is unusual in that it generates translational motion of the kink, and we have suggested that radiation plays a role in the transfer of energy to the kink in this resonance. We have also shown that, for small-amplitude oscillations, the kink's dynamics are not chaotic. These results were obtained using the method of multiple scales. We showed that it is necessary to introduce a special 'envelope function' of the long scales when radiation functions (which are non-local and hence extend over many scales) are involved. (This function, 'B', was introduced in section 2.2—in eq. (2.13) on page 30—and its role at higher orders demonstrated in section 2.4.1 – in particular

see eqs (2.26) and (2.29), pp. 39 and 41.) This technique has not, to the author's knowledge, been described elsewhere.

The next part of this thesis—chapters 3–6—was an investigation of travelling solitons in discrete lattices. In this regard we remind the reader of two new terms which have been introduced in this thesis. Firstly, an *exceptional* discrete equation is one which admits stationary solitons centred at a continuous family of positions relative to the lattice. Secondly, a *sliding* soliton is a radiationless travelling soliton (an example of an embedded soliton). Velocities at which sliding solitons exist are termed *sliding velocities*.

In chapter 3 our intention was to apply the methods used for finding radiation in the continuous model of chapter 2 to solitary waves in corresponding discrete systems. We considered a variety of exceptional ϕ^4 models (which are free of the Peierls–Nabarro barrier [110]). As discussed in section 1.6, there were several grounds for hoping that the PN barrier would be the only obstacle to the existence of sliding kinks at arbitrary velocities. The hope that radiationless solitons may exist in exceptional models was the primary motivation behind chapter 3. The main conclusions were the following:

- In general, exceptional ϕ^4 models do *not* support moving kinks. This means, from a physical perspective, that the PN barrier is not solely responsible for soliton radiation, and from a mathematical perspective, that restoring translational symmetry is not enough to restore a velocity-boost symmetry.

- However, the radiation amplitude is much smaller in exceptional models than in generic, nonexceptional discretisations.

- For certain values of velocity, sliding solitons do exist in some of the exceptional models, but not in all of them.

- These radiationless solitons do not exist in the standard, nonexceptional ϕ^4 model.

Although our primary hope—that radiation would be absent for all velocities in the exceptional models—was not met, the discovery of sliding solitons at particular velocities was (to the author's knowledge) the first time that moving radiationless solitons had been discovered in a nonintegrable discrete lattice with a given on-site potential (i.e. not of FPU type). New nonlinear systems which support sliding solitons by construction had previously been produced, however, using the 'inverse method' of Flach, Zolotaryuk and Kladko [119].

In chapter 4 we set aside the problem of travelling kinks and concentrated on trying to unify the known exceptional models studied in chapter 3 and understand their underlying structure. We showed that these disparate models [116, 131, 132], derived in totally different ways, could all be generated from a two-point map, and generalised them to three new classes of discrete models, all supporting stationary kinks with effective translational invariance by virtue of the two point map. Additionally we showed that *all* exceptional discretisations can be generated from a two point map, thus providing a unified explanation for the phenomenon of exceptionality. We also pointed out the numerical uses of exceptional discretisations, in simulating continuous equations and calculating stationary solutions.

In chapter 5, we returned to the problem of sliding kinks and their relationship to exceptionality of the model. At this point in our investigations we had established the fact that exceptionality does not *guarantee* the existence of sliding solitons at isolated velocities (since only two of the three exceptional models studied were found to support them). This raised the converse question, of whether exceptionality is *necessary* for sliding solitons to exist. Also, we noted that all the models found to support sliding kinks had *nonlocal* discretisations of their nonlinearities – that is, nonlinear terms depending not only on u_n but also on u_{n-1} and u_{n+1}. This raised the possibility that a nonlocal nonlinearity might be another prerequisite for sliding kinks. Both these questions had, in fact, already been answered negatively by Flach, Zolotaryuk and Kladko [119], who showed that the models generated (via their inverse method) from explicit moving solitons have a nonvanishing PN barrier. Nonetheless, we aimed in chapter 5 to provide independent verification of their conclusions – i.e., to show that sliding solitons can exist in a system without effective translational invariance and whose nonlinearity is confined to a single lattice site. One such model of important physical significance is the Frenkel–Kontorova model, and indeed a previous numerical study had suggested that highly discrete moving kinks do exist in this model [109]. Unfortunately, our results showed that if these sliding kinks do exist, they do not continue to the continuum limit, and so could not be detected by our method.

In chapter 6, we searched for travelling solitons in the saturable discrete nonlinear Schrödinger equation. These were found to exist, provided that the saturation intensity of the medium is low enough. We also showed that the saturable DNLS equation is *not* an exceptional model. Thereby—and since the nonlinearity is a function of ϕ_n only, and not ϕ_{n+1} or ϕ_{n-1}—we had found the counterexample sought above. That is, we had confirmed that exceptionality and nonlocal nonlinearity-discretisations are neither sufficient *nor* necessary conditions for the ex-

istence of sliding kinks. This finding showed that the mechanism for the emission of radiation from moving solitons is more intricate than just velocity oscillations caused by the PN potential.

Though these results might appear negative, on the other hand it is very encouraging to have found sliding solitons in a physically meaningful model. It would be unfortunate if it were true that radiationless propagation is only possible in exceptional models, since such models are extremely rare and seldom physically justifiable. Indeed, of the three classes of exceptional discrete ϕ^4 models generated in chapter 4, only one model even conserves energy.

Also in chapter 6, we found explicitly the radiation amplitude of the original soliton (as opposed to the solution of the inner equations). We found that the radiation is exponentially small in the amplitude of the soliton and also—indirectly—depends exponentially on the speed of the soliton. Thus, for broad, small amplitude pulses, and for moderate-amplitude pulses moving slowly, the radiation may be so small as to be entirely undetectable for all practical purposes. We also verified that the radiation amplitude depends on the Stokes constant, a fact that was not rigorously proved in chapter 3 when considering discrete ϕ^4 equations. There, we were concentrating on existence and nonexistence of the sliding kinks, and not on the amplitude of their radiation tails. Finally, we derived ordinary differential equations for the time-evolution of the soliton's amplitude and speed as a result of the energy lost to radiation. In perturbation problems where the radiation is algebraically—rather than exponentially—small, such as in chaper 2, the method of multiple scales produces the equations for the evolution of parameters on the slow scales. The method of asymptotics beyond all orders, on the other hand, does not, and so in chapter 6 we were forced to deduce the equations for the time evolution of parameters by using conserved quantities. By analysing the resulting dynamical system, we found that the sliding states are *metastable*.

The discovery in chapter 6 of sliding solitons in the saturable DNLS model was at the time (to the author's knowledge) the first theoretical demonstration of radiationless soliton propagation in a physically realisable discrete model with a Peierls–Nabarro barrier.

In chapters 3, 5 and 6, the calculation of Stokes constants involved finding the limit of a sequence calculated recursively using the relations (3.47), (5.19) and (6.54). In sections 3.3 and 6.3.6, we explained that the convergence of these sequences to the Stokes constant is only $\mathcal{O}(1/n)$, and developed techniques to eliminate the $1/n$ terms and hence speed the convergence to $\mathcal{O}(1/n^2)$. This provided huge savings in calculation time. In section 3.3 we described an 'empirical' way of determining the $1/n$ term, and hence removing it, and in section 6.3.6 we

[187] H. Feddersen, in *Nonlinear Coherent Structures in Physics and Biology. Proceedings of the 7th Interdisciplinary Workshop Held at Dijon, France, 4-6 June 1991,* eds. M. Remoissenet and M. Peyrard. Lecture Notes in Physics vol. 393 (Springer-Verlag, Berlin, 1991), pp. 159–167.

[188] K. Kundu, J. Phys. A: Math. Gen. **35**, 8109 (2002).

[189] I. E. Papacharalampous, P. G. Kevrekidis, B. A. Malomed, and D. J. Frantzeskakis, Phys. Rev. E **68**, 046604 (2003).

[190] S. V. Dmitriev, P. G. Kevrekidis, B. A. Malomed, and D. J. Frantzeskakis, Phys. Rev. E **68**, 056603 (2003).

[191] D. E. Pelinovsky and V. M. Rothos, Physica D **202**, 16 (2005).

[192] J. Cuevas, B. A. Malomed, and P. G. Kevrekidis, Phys. Rev. E **71**, 066614 (2005).

[193] J. Gómez-Gardeñez, F. Falo, L. M. Floría, Phys. Lett. A **332**, 213 (2004).

[194] J. Gómez-Gardeñez, L. M. Floría, M. Peyrard, and A. R. Bishop, Chaos **14**, 1130 (2004).

[195] S. Aubry and T. Cretegny, Physica D **119**, 34 (1998).

[196] J. W. Fleischer, M. Segev, N. K. Efremidis, and D. N. Christodoulides, Nature **422**, 147 (2003).

[197] M. Stepić, D. Kip, L. Hadžievski, and A. Maluckov, Phys. Rev. E **69**, 066618 (2004).

[198] J. Cuevas and J. C. Eilbeck, Phys. Lett. A **358**, 15 (2006).

[199] S. Gatz and J. Herrmann, J. Opt. Soc. Am. B **8**, 2296 (1991).

[200] S. Gatz and J. Herrmann, Opt. Lett. **17**, 484 (1992).

[201] V. Tikhonenko, J. Christou, and B. Luther-Davies, Phys. Rev. Lett. **76**, 2698 (1996).

[202] F. Vidal and T. W. Johnston, Phys. Rev. E **55**, 3571 (1997).

[203] A. Khare, K. Ø. Rasmussen, M. R. Samuelsen, and A. Saxena, J. Phys. A: Math. Gen. **38**, 807 (2005).

[204] V. O. Vinetskii and N. V. Kukhtarev, Sov. Phys. Solid State **16**, 2414 (1975).

[205] See e.g. A. H. Nayfeh and D. T. Mook, *Nonlinear Oscillations* (J. Wiley, New York, 1979); D. W. Jordan and P. Smith *Nonlinear Ordinary Differential Equations* (Oxford University Press, 1999).

[206] E. W. Laedke, O. Kluth, and K. H. Spatschek, Phys. Rev. E **54** 4299 (1996).

[207] D. E. Pelinovsky, Nonlinearity **19**, 2695 (2006).

[208] V. M. Eleonksii, N. E. Kulagin, N. S. Novozhilova, and V. P. Silin, Teor. Mat. Fiz. **60**, 395 (1984).

[209] T. R. O. Melvin, A. R. Champneys, P. G. Kevrekidis, and J. Cuevas, Phys. Rev. Lett. **97**, 124101 (2006).

[210] S. González-Pérez-Sandi, J. Fujioka, and B. A. Malomed, Physica D **197**, 86 (2004).

[211] B. A. Malomed, J. Fujioka, A. Espinosa-Cerón, R. F. Rodríguez, and S. González, Chaos **16**, 013112 (2006).

[212] K. Yagasaki, A. R. Champneys, and B. A. Malomed, Nonlinearity **18**, 2591 (2005).

[213] L.-C. Crasovan, B. A. Malomed, and D. Mihalache, Pramana J. Phys. **57**, 1041 (2001).

[214] A. S. Kovalev and A. M. Kosevich, Fizika Nizkih Temperatur **2**, 913 (1976).

[215] Kh. I. Pushkarov, J. Low-Temp. Phys. **32**, 803 (1978).

[216] D. I. Pushkarov and Zl. Kojnov, Sov. Phys. JETP **47**, 962 (1978).

[217] P. B. Burt, Phys. Lett. A **71**, 19 (1979).

[218] A. Khare, Lett. Math. Phys. **3**, 475 (1979).

[219] M. A. Lohe, Phys. Rev. D **20**, 3120 (1979).

[220] See e.g. J. P. Boyd, *Chebyshev and Fourier spectral methods* (Dover, New York, 2001).

[221] J. P. Boyd, Nonlinearity **3**, 177 (1990).

[222] J. P. Keener, Physica D **136**, 1 (2000).